INVESTIGATION INTO THE USE OF MOLECULARLY IMPRINTED POLYMER NANOPARTICLES FOR THE DELIVERY OF THERAPEUTIC COMPOUNDS.

Thesis submitted for the degree of

Doctor of Philosophy

At the University of Leicester

By

Adam Smith, MChem (Hull)

Department of Chemistry

University of Leicester

September 2018

Abstract

Due to the increasing popularity of the use of molecularly imprinted polymer (MIP) nanoparticles as diagnostic tools, recently, interest has been directed to the use of MIP nanoparticles for use as a drug delivery system. MIPs are ideal as they are cheap to manufacture, highly stable and robust. Nanoparticles used for drug delivery work either by a triggered release of a payload under certain conditions or by controlled release out of the nanoparticles. The use of controlled release reduces the dosage of drug required to be effective on an illness or disease; it also reduces unwanted side effects caused by medication as a smaller dosage is needed compared to drugs administered by a conventional route. Initially, methods of nanoparticle sterilisation were investigated, due to the development of contamination in liquid solutions. This can cause complications when injected into live tissues. Testing found that the use of trehalose at 10mg/mL demonstrated the smallest change in nanoparticle properties, while sterilisation was found to have minimal effect on the nanoparticle properties (Chapter 2). To determine the ability of polymer nanoparticles to enter into cells, siRNA transfection studies utilising caspase-3 siRNA were carried out with the siRNA loaded onto the nanoparticles employing a charge-based interaction. The results showed that the optimal nanoparticle species was as efficient as the control transfection agent (Chapter 3). Subsequently, molecularly imprinted nanoparticles were tested for the controlled release of doxorubicin over time from different types of nanoparticles. Initially, doxorubicin imprinted magnetic core nanoparticles were tested and compared to non-imprinted nanoparticles. The results showed that the use of 2-hydroxymethyl acrylate as the functional monomer demonstrated the lowest rate of release of doxorubicin over time (Chapter 4). Solid phase synthesised were then tested with both vancomycin and EGFR binding peptide as the primary templates, the nanoparticles produced with 1mg of doxorubicin in the polymerisation mixture of the vancomycin templated nanoparticles demonstrated the lowest rate of release. With the EGFR binding peptide nanoparticles, the nanoparticles produced in aqueous solvent demonstrated the lowest rate of doxorubicin release in comparison to the organic solvent synthesised nanoparticles (Chapter 5). The effect of the primary template presence on the nanoparticles was tested and demonstrated that the presence increases the rate and amount of doxorubicin release compared to no template being present (Chapter 6). The final stage was to test the effect of different levels of cross-linking by increasing the amount of cross-linking monomer in the polymerisation mixture and found that increasing the amount of cross-linking monomer by 25 x decreased the rate and amount of doxorubicin released over time. When the effect of template presence was tested against the amount of cross-linking monomer, it was found that the presence of vancomycin caused a small increase in the rate and amount of doxorubicin released (Chapter 7). Overall the nanoparticles demonstrated significant potential for use as a delivery vessel for doxorubicin for a controlled release into the cells.

Acknowledgements

Firstly, I would like to thank my supervisor, professor Sergey A. Piletsky, for his support and guidance throughout my research. A thank you to my examiners for reviewing the entirety of my thesis. Special thanks go to Dr Abeer Safaryan for the support and assistance in completing the research into the lyophilisation and sterilisation of nanoparticles. Thanks to Noor Siksek and Samira Warsame who assisted in the synthesis and testing of the magnetic core nanoparticles for doxorubicin delivery and Dr Bin Yang from the department of infection, immunity and inflammation at the University of Leicester for her assistance in the testing of the charged nanoparticles for the transfection of siRNA. I would also like to thank my laboratory colleagues, in particular, Francesco Canfarotta for his aid in understanding molecularly imprinted nanoparticles, including the synthesis and design. Thanks also go to, Todd, Tom, Alvaro, Bashar, Omar, Eman, Asma, Julie and Asia for their insight and help in the laboratory. I want to also thank, the support of my family and friends during my studies and research. I also submit this PhD thesis in memory of my grandparents, Pauline and Anthony Taylor who sadly passed away during my final year.

Aims and Objectives

Aims:

- Optimisation and testing of sterile storage methods to maintain the sterility of nanoparticles for use in biological systems.
- Optimisation and testing of charged polymer nanoparticles for the transfection of Caspase-3 siRNA to kidney cells to reduce the expression of caspase-3.
- Optimisation and testing of molecularly imprinted polymer nanoparticles with doxorubicin for controlled release.

Objectives:

- Nanoparticles imprinted for trypsin will undergo sterilisation via both lyophilisation and autoclaving with fundamental properties being tested before and after the process to observe changes.
- Nanoparticles produced with different charges and compositions will undergo incubation with siRNA to facilitate a charge based interaction before application to cells to test transfection efficiency.
- Nanoparticles synthesised using a magnetic iron oxide core will be imprinted with doxorubicin internally to test release efficiency of the nanoparticles.
- Nanoparticles synthesised using solid phase synthesis with vancomycin initially as a template will be imprinted with doxorubicin internally to test release efficiency of doxorubicin from the nanoparticles.
- Nanoparticles synthesised using solid phase synthesis with EGFR binding site peptide subsequently as a template will be imprinted with doxorubicin internally to test release efficiency of doxorubicin from the nanoparticles.
- The solid phase synthesised nanoparticles will be tested in the presence of the primary template to determine the effect of template presence and interaction on the efficiency of doxorubicin release from the nanoparticles.
- Nanoparticles will be subsequently synthesised with an increasing amount of cross-linking monomer to determine the effect on doxorubicin release from the nanoparticles.

Table of Contents

List of tables

Tables found in Chapter 2

Tables found in Chapter 3

Tables found in Chapter 4

Tables found in Chapter 5

Tables found in Chapter 6

Tables found in Chapter 7

List of figures

Figures found in Chapter 1

Figures found in Chapter 2

Figures found in Chapter 3

Figures found in Chapter 4

Figures found in Chapter 5

Figures found in Chapter 6

Figures found in Chapter 7

Abbreviations

TPP = Triphenyl phosphonium

SLN = Solid lipid nanoparticles

TPP-PEG-PE = Triphenyl phosphonium-polyethylene glycol-phosphatidylethanolamine

TEOS = Tetra-ethoxy-silane

BTSE = Bis-1, 2-(trimethoxysilyl) ethane

PDMS = Polydimethylsiloxane

PEG = Polyethylene glycol

MSN = Mesoporous silica nanoparticles

APTMS = 3-aminopropyl trimethoxysilane

CPTMS = 3-chloropropyltriethoxysilane

CTAB = Cetrimonium bromide

NDC = Nanoparticle drug conjugate

PBS = Phosphate buffer saline

EDTA = Ethylenediaminetetraacetic acid

EGFR = Epidermal growth factor receptor

MIP = Molecularly Imprinted Polymers

MN = Magnetic Nanoparticles

CS = Chitosan

APS = Ammonium Persulfate

TEMED = Tetramethylethylenediamine

SIA = Succinimidyl Iodoacetate

UV = Ultraviolet Light

RNA = Ribonucleic acid

DNA = Deoxyribonucleic acid

DLS = Dynamic Light Scattering

PCR = Polymerase chain reaction

GADPH = Glyceraldehyde 3-phosphate dehydrogenase

NMR = Nuclear Magnetic Resonance

MRI = Magnetic Resonance Imaging

TNF = Tumor necrosis factor

RISC = RNA-induced silencing complex

Chapter 1: A review: nanotechnology and the delivery of therapeutic agents

1.1. Introduction

In recent years there has been a significant increase in interest in the development of nanotechnology for medical purposes.[1] Nanotechnology is designed to act on objects on a nanometre scale. Technology on this scale is ideal for use in nano-scale environments such as cells or reaction mixtures. In chemistry, nanotechnology involves the development of nanoscale particles to perform a specific function, ranging from catalysis to separation systems. There are many different types of nanoparticles available; however, not every type is suited for drug delivery. By considering current therapeutics, improvements in their effects are produced by modification of the chemical structure to fine-tune their properties. These alterations change the solubility, dispersion, cellular uptake, renal clearage, cell toxicity and influence the interactions between the body and therapeutic agent.[2]

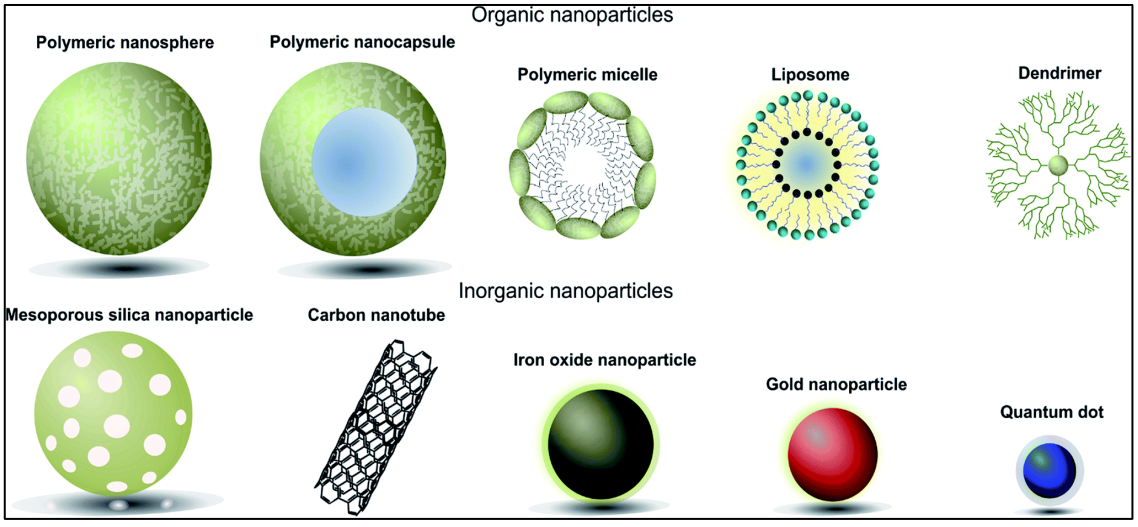

Figure 1 - 1: Diagram of the different types of nanoparticle species that can be used for the delivery of therapeutic agents.[3]

Alternatively, current therapeutics can undergo augmentations with the use of a delivery vessel. With a suitable delivery vessel, the side effects of therapeutic agents can be reduced due to their containment within the delivery vessel. Depending on the entrapment conditions, the agent will remain inside the vessel until it reaches its target. Entrapment

of a therapeutic agent is beneficial as it reduces the side effects on the initial administration and allows a higher concentration of the therapeutic agent to reach the afflicted cells. This section will consider the most promising nanoparticle types for drug delivery and recent developments in this field.

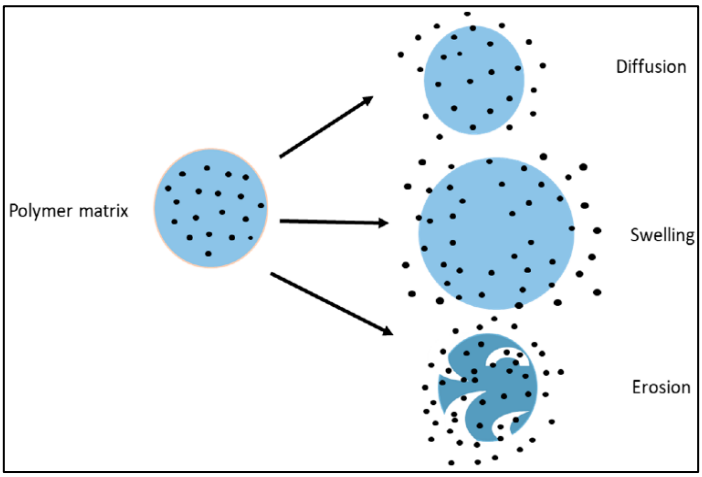

Figure 1 - 2: Diagram of drug release methods from nanoparticles.[4]

Nanoparticles can be used to augment the delivery of therapeutic agents in several ways. Firstly, nanoparticles can be used to control the release of the therapeutic agent in biological systems. There are two methods to achieve this, triggered release and release at a controlled rate.[5, 6] For triggered release to occur, the nanoparticles require exposure to specific conditions found within certain cellular environments. For example, hydrazone based linkers require a mildly acidic environment to break down and trigger the release of the therapeutic payload. In acidic conditions the hydrazone is reduced on the nitrogen-nitrogen double bond cleaving in two, separating the payload and targeting vector. In contrast peptide-based linkers require the presence of a suitable enzyme to cleave the peptide bond, the enzyme binds onto the molecule around the bond holding it in place for hydration of the bond via a water molecule causing the payload and targeting vector to separate.[7] For control release, however, nanoparticles are reliant on the diffusion of the therapeutic, delivering the dosage over time instead of one initial burst.

Secondly, nanoparticles can be used to increase the solubility of water-insoluble drugs. Drug solubility can be improved *via* incorporation into the structure of the nanoparticles during synthesis when produced using a suitable solvent. The nanoparticles can then be transferred into the water, removing the starting solvent. These nanoparticles can then be

administered to biological systems without issues of solvent compatibility or poor drug uptake.

Finally, nanoparticles can be modified to target a specific cell species through one of two methods, imprinting a surface protein or molecule that is specific to the target species of cell into the structure of the nanoparticle, alternatively a targeting vector such as an antibody or magnetic nanoparticle can be attached to the particle via a covalent linker. Using a targeting vector is advantageous as the nanoparticles will deliver the drug to the target cell, instead of being taken up by the surrounding healthy cells. Currently, drugs are administered systematically, requiring a larger dose to kill unhealthy cells in the body. However, with the use of the nanoparticles, a lower dosage of the drug is needed, reducing the risk and severity of the side effects.

1.2. Non-polymeric nanoparticles

Firstly, consideration of non-polymeric nanoparticles is necessary as significant research into their use for drug delivery has been carried out.

1.2.1. Liposomes

A liposome is a spherical particle containing a liquid zone comprised of water or aqueous solution which is surrounded by phospholipid bi-layer. A liposome is formed via the dispersion of a lipid bilayer in an aqueous solvent causing the particles to be aggregated together. These particles have a hollow core on the inside and can be used to transport water-insoluble drug molecules.[8] The use of these has been demonstrated to improve the therapeutic index of drug molecules, the rate of drug metabolism in the body and a reduction in the harmful side effects.[9] The release of the drug from inside the liposome is reliant on the conditions of the liposome such as pH and osmosis gradients. Additionally, the surrounding environment affects the release of the internal payload.[9]

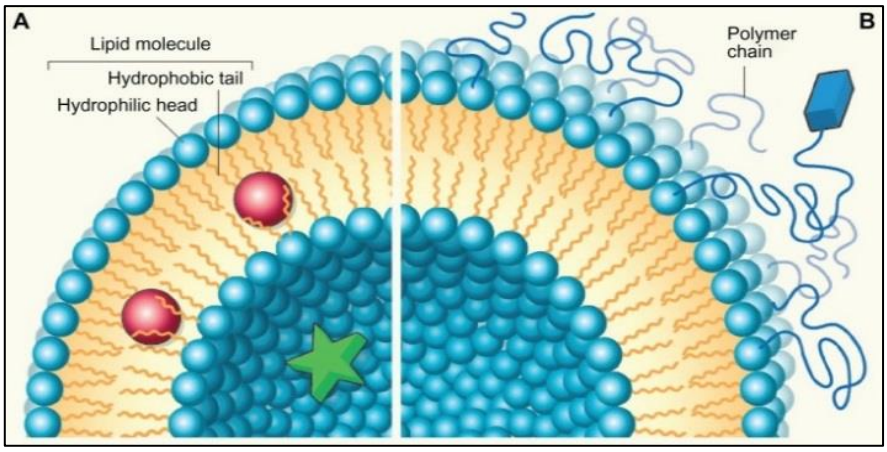

Figure 1 - 3: Schematic of a liposomal nanoparticle for drug delivery[10]

An *et al.* used a liposomal formation to deliver a reduced dose of 5-aminolevulinic acid in combination with photodynamic therapy to treat severe acne. Typically, 5-aminolevulinic acid is used in a topical cream at a concentration of 20% before being subjected to light irradiation. However, this can usually result in a large amount of discomfort and pain for the patient. An et al. used a 0.5% concentration of drug encapsulated within a liposomal system, the study produced a significant decrease in acne severity with a reduction of the usually observed side effects.[11]

Giubert *et al.* developed pH-sensitive liposomes for the controlled delivery of cisplatin to cancerous tumours and improving the long-term stability of cisplatin. Cisplatin is a highly potent anti-cancer drug used for the treatment of various cancers. However, it has limited use clinically due to the numerous side effects and resistivity that can develop. To counter this Giubert et al. encapsulated the cisplatin inside freeze-dried liposomes, the study found that the liposomal formulated cisplatin was stable for longer than their non-liposomal counterparts.[9]

Diswas *et al.* developed liposomal formulations loaded with paclitaxel modified with Phosphonium groups for treatment of cancerous tumours. Using stearyl triphenylphosphonium (TPP) modified liposomes for targeting mitochondria, a modification was developed to make these less cytotoxic to human cells. The group added polyethene glycol-phosphatidylethanolamine with TPP attached (TPP-PEG-PE) to the liposomes. Paclitaxel incorporation into the modified liposomes was carried out before being tested *in vitro* and *in vivo*. The liposomes demonstrated a higher level of anti-tumour activity compared to paclitaxel alone.[12]

1.2.2. Solid lipid nanoparticles

A solid lipid nanoparticle (SLN) requires the use of a lipid which is solid at physiological temperatures. These types of nanoparticles have shown potential by demonstrating excellent physical stability, the ability to protect the payload from damage, and is capable of facilitating a controlled release of the payload. However, there are some limitations, primarily in that the SLNs demonstrate low levels of drug loading. The drug loading is dependent on the solubility of the drug and the composition of the lipid matrix. The drug is released from the lipid via crystallisation of the lipid to its solid form; the drug is expelled out of the SLN. The SLNs are loaded by heating the lipids until they turn into a semi-solid state, before combining this with a lipid-soluble drug. The SLNs are taken up into the lipid micelle surrounding the site of administration releasing the drug.

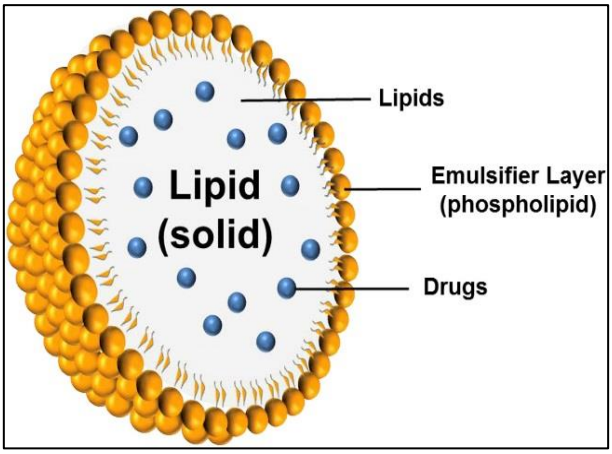

Figure 1 - 4: Cross-section of a solid lipid nanoparticle for drug delivery[13]

Liu *et al.* developed a lipid nanoparticles for the pulmonary delivery of insulin. The amount of sodium cholate and soybean phosphatidylcholine were modified to determine their effect on the distribution of insulin. As a comparison to conventional methods, a subcutaneous injection yielded a 22% bioavailability rate for the insulin. In contrast, the optimal SLN composition displayed an entrapment efficiency of 96.5%; the SLNs also possessed a respirable fraction of 82%. When administered, the nanoparticles were found to have a nebulization efficiency of 63% with the SLNs remaining stable during nebulization. When using fluorescently labelled insulin, the SLNs were found to be distributed homogeneously amongst the lung alveoli. The study demonstrated that SLNs have a significant potential for the delivery of insulin *via* a pulmonary route.[14]

Abdel-Mottaleb *et al.* developed lipid nanocapsules for transdermal delivery of ibuprofen and compared its effectiveness to polymeric based nanoparticles. From the study, the polymeric nanoparticles doubled the permeability of ibuprofen. However, the lipid composition of the nanoparticles quadrupled the permeability of ibuprofen, in comparison with free ibuprofen. Moreover, the lipid nanoparticles were found to have a significantly lower accumulation in the skin than the polymeric nanoparticles, and the group, therefore, summarised that polymeric nanoparticles are more suited to site-specific delivery to the skin as opposed to the lipid nanoparticles which were more capable of transportation across the skin and into the underlying layers.[15]

Nayak *et al.* developed lipid nanoparticles for the treatment of malaria using curcuminoids as a payload for administration using parenteral methods.[16] Parenteral administration involves the delivery of a drug to a patient *via* any route which does not involve the digestive tract.[17] The study investigated the use of three different species of solid lipids in combination with a liquid lipid species. The nanoparticles produced ranged in size between 120 and 250 nm with a different zeta potential dependent upon the species used in the nanoparticles. The lipid nanoparticles were found to be highly efficient in encapsulating the curcuminoid payload. However, they demonstrated a low drug loading capacity, and this again was affected by composition. Based on experiments in vivo, the anti-malarial properties of the curcuminoids was found to possess a 2-fold increase in the antimalarial activity in comparison to the free curcuminoids tested at an equivalent dosage level.[16]

1.2.3. Nanoparticle-drug conjugates

Recently, development into the use of nanoparticle-drug conjugates as a method of drug delivery has been carried out. The nanoparticle-drug conjugates are designed to target a specific cell type for drug delivery to a target cell without affecting the surrounding tissue. Nanoparticle-drug conjugates (NDCs) are a combination of a drug payload and either a synthetic nanoparticle or an antibody. Using an antibody requires a naturally occurring antibody or synthetically created analogue complementary to a target protein to be produced or isolated. The antibody is then coated with cleavable linkers on the surface which are designed to cleave under certain conditions located within cellular environments. The antibodies must be complementary to a surface protein on the target cell to work effectively. The target chosen on the target cell species is an overexpressed

protein, ensuring a more substantial amount of the drug reaches the target species of the cell compared to healthy cells. When the NDC binds to the target protein, the cell reacts by engulfing the NDC by closing up the section of cell membrane around the bound protein causing the drug to be released.[18] However, due to the fragile nature of antibodies and their complexity in synthesis, NDCs can be expensive to produce, with significant costs involved to produce small quantities.[19,20]

The mechanism for the release of the drug is dependent upon the type of linker used. If the linker used is dependent upon the conditions in the target cell, then the linker will break when internalised into the target cell. For example: if the target cell possesses an acidic internal environment, then a pH-sensitive linker such as a hydrazone is used. When the NDC becomes internalised, the linker breaks due to the acidic conditions, releasing the drug into the cell.[21] If the target cell possesses a reducing environment, then a disulphide bridge is used. When the NDC becomes internalised, then the reducing conditions of the cell cleaves the disulphide bond and releases the drug into the cell.[22]

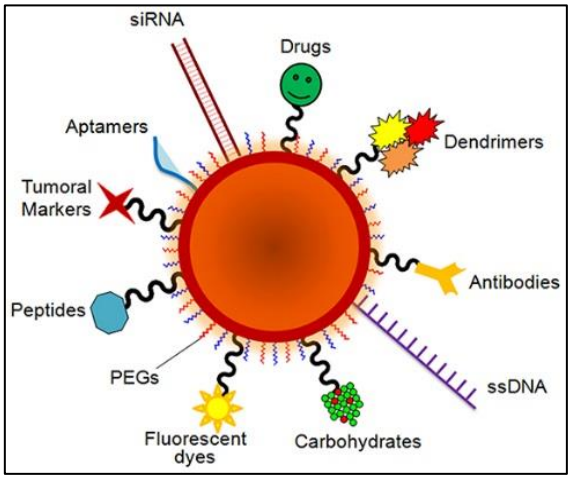

Figure 1 - 5: Diagram of a nanoparticle conjugated to various potential functional groups.[23]

If the linker is susceptible to enzyme cleavage, then when the NDC becomes internalised, it can be cleaved by an enzyme. There are two main enzymes which can be used to cleave the peptide-based linkers, cathepsin-B and β-glucuronidase.[24, 25] When the NDC becomes internalised by the cell, the enzyme cleaves the linker, this causes the drug to release into the cell. This method of drug delivery is advantageous over nanoparticles which rely on internally loaded drug payloads; this is due to the drug remaining bound until the NDC encounters specific release conditions.

Raucher *et al.* developed a polypeptide based nanoparticle coupled *via* a hydrazone linker to the chemotherapeutic drug paclitaxel.[26] Due to cancer cells undergoing a high amount of anaerobic respiration the cells possess an increased level of lactic acid, this causes the internal pH to become 4.5 – 5.5.[27] These conditions can be used to break a hydrazone based linker to release a drug payload. The group used a hydrazone derivative of paclitaxel. The nanoparticles were found to be effective on breast cancer cells; the nanoparticles inhibited cell proliferation, which leads to apoptosis occurring in a similar method the original paclitaxel drug. The group demonstrated the potential of the nanoparticle conjugate as a delivery system for paclitaxel.[26]

Kong *et al.* developed silica nanoparticles tethered *via* a pH-sensitive linker for the controlled delivery of doxorubicin. The group utilised a pH-sensitive hydrazone linker for acid responsive delivery of doxorubicin into cancer cells. The group attached the doxorubicin *via* the linker to the silica nanoparticles; the nanoparticles were coated with a fluorescent dye to monitor the internalisation of the nanoparticles. Testing of the release from the nanoparticles showed the doxorubicin accumulated in the cell nucleus with a significant uptake into a line of HeLa cells.[28]

1.2.4. Silica materials

Silica materials used in drug delivery come in two primary forms, xerogels and mesoporous nanoparticles. These nanoparticles are used mainly due to their high biocompatibility, and the relative easiness of their functionalization and modification.[29] Silica nanoparticles are the most commonly used type of inorganic nanoparticles, other examples include metallic and polymeric nanoparticles.[30]

1.2.4.1. Xerogels

A xerogel is a silica-based gel with a high level of porosity and surface area; these gels also possess an amorphous structure with no fixed shape or size. However, all of these factors are dependent on the method of synthesis used to produce the xerogel.[31] Xerogels are most commonly produced *via* the use of a sol-gel method as this allows greater control over the properties of the material for drug release.[32]

Maver *et al.* produced a hybrid xerogel complex for the controlled release of nifedipine using a combination of two different silica materials, tetraethoxysilane (TEOS) and bis-1,2-(trimethoxysilyl)ethane (BTSE).[33] Nifedipine itself is used to reduce blood pressure

in the body in patients who suffer from hypertension and angina.[34] The production of the gels was carried out at 60 ºC *via* a combination of acid hydrolysis and polycondensation; the reaction was carried out in the dark due to the light-sensitive nature of one of the reagents. The gel species produced were found to hold the nifedipine in an amorphous state as characterised using various analytical methods. The TEOS only composite was found to possess the lowest rate of drug release from the gel, this is due to the rigidity of the structure, with the addition of BTSE to loosen the structure the release rate was found to increase, however, this increase had little effect on the amorphicity of the drug. The group found that these type of delivery vessels would be suitable for treatments which require a high initial dose followed by a sustained release of the remaining dosage.[33]

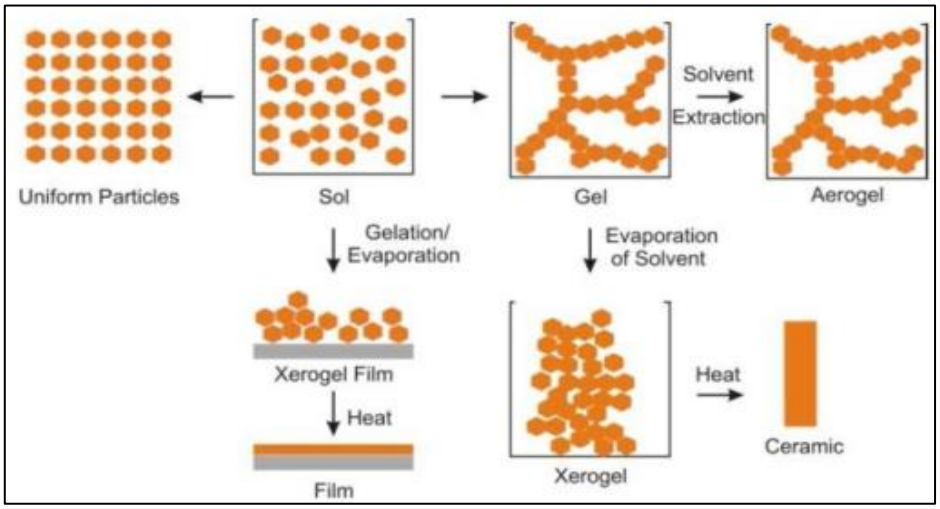

Figure 1 - 6: Schematic of the synthesis of silica-based gel nanoparticles[35]

Czarnobaj *et al.* developed silica-based xerogels for the sustained delivery of cisplatin. The group investigated three main compositions, TEOS, TEOS/PEG and TEOS/PDMS. The group used a sol-gel process formed the xerogels. The group prepared the three species by the same method, resulting in the following loading amounts, Silica: 7.2mg g^{-1}, Silica/PEG: 5.08mg g^{-1} and Silica/PDMS: 3.07mg g^{-1}. The group also investigated the effect of different drying temperatures on the xerogels, 25ºC, 40ºC, 80ºC and 120ºC. Through in vitro testing, the group found that the organically doped silica matrices released a more considerable amount of cisplatin over time compared to the silica only matrices. This release is due to the doping making the pore size of the matrix larger, facilitating a more significant release, during the first 3 hours over 50% of the payload was released. However, due to the hydrophobic nature of the PDMS, the release rate of

the cisplatin was lower during the extended duration of the experiment. The effect of drying temperature demonstrated that increased temperature facilitated a higher release of cisplatin from the xerogel up to 80ºC. However, the 120ºC drying decreased the rate of release of the cisplatin, and this is due to the temperature causing the pores to shrink in size.[36]

Prokopowicz *et al.* investigated the use of a xerogel formed *via* the sol-gel method for the encapsulation and delivery of doxorubicin. The sol gel matrix was formed first with incubation with doxorubicin at low temperature in the dark to prevent doxorubicin degradation. The silica particles underwent vacuum drying followed by freeze drying. During the initial 24 hours of the release studies, around 55% of the loaded doxorubicin was released, over the next 216 hours (9 days), the cumulative amount of doxorubicin released increased by 35%. The xerogel demonstrated a rapid initial release over the first 24 hours followed by a slower controlled release over the following nine days. This release profile is useful as it reduces the toxicity of doxorubicin delivery to the body while delivering a significant initial dose.[37]

1.2.4.2. Mesoporous silica nanoparticles

Mesoporous silica nanoparticles (MSN) are silica nanoparticles formed with adjustable size pores. This material contains a highly ordered system of hexagonal pores ideal for drug loading *via* physical or chemical adsorption.[38] In comparison to xerogels, MSNs have a more homogeneous structure along with a lower polydispersity index. MSNs also possess a larger surface area for adsorption of drugs and imaging agents facilitating a more substantial payload in a small volume.[39] However, recent studies have shown that larger MSNs, possess acute toxicological effects on cells.[40] The level of toxicity is dependent upon the size of the nanoparticles. When the size of the MSN is 100+ nm, then the toxicity increased as size increases. When MSNs are less than 100nm, the toxicological effects decrease.[41]

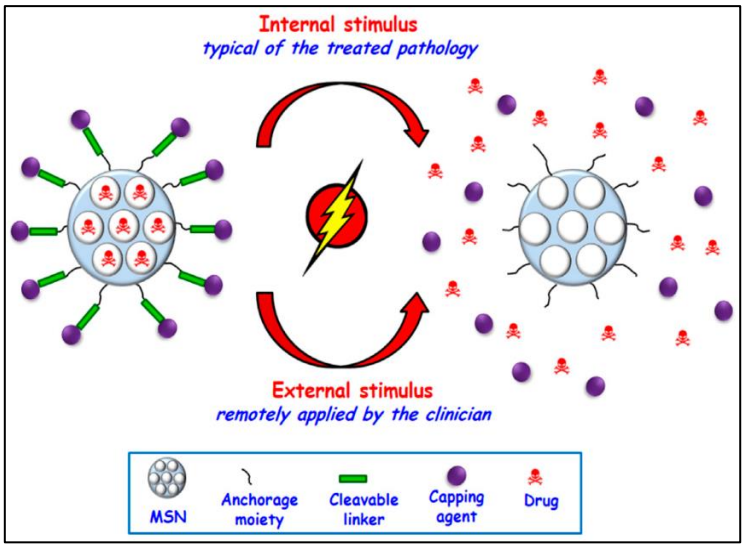

Figure 1 - 7: Schematic of triggered release from a mesoporous silica nanoparticle[42]

Zhenhuan *et al*. developed MSN for the controlled delivery of amoxicillin.[43] Amoxicillin is an antibiotic compound used for the treatment of bacterial infections such as pneumonia.[44] The group prepared an MSN based upon MCM-41 and combined this with APTMS and CPTMS. The group demonstrated that the MSNs could be used to deliver a sustained dose of amoxicillin over time. As a further test, the group immobilised L-tryptophan onto the surface of the MSNs to improve the physiochemical properties of the MSNs with the release of amoxicillin undergoing a small increase.[43]

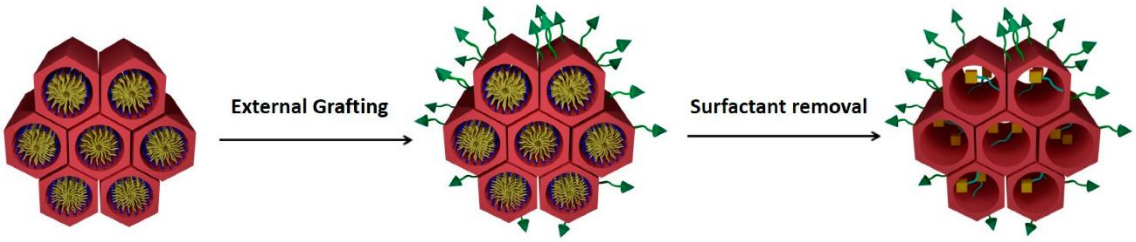

Figure 1 - 8: Functionalization of MCM-41 with external payload[45]

Qianjun et al. developed an MSN for a pH-responsive multi-drug delivery system designed to help overcome drug resistance.[46] Drug resistance develops in cancer cells due to the poor solubility of most cancer drugs preventing sufficient uptake into cancer cells.[47] The group developed a combined nanoparticle structure of CTAB surfactant micelles with a silicon species to form a combined drug delivery system. Unlike conventional MSN formation with the CTAB micelles used to create pores in the nanoparticle before being removed and loaded with a drug, the group used an alternative method. The group

combined the water-insoluble drug inside the CTAB surfactant micelles comprised of Cetrimonium bromide before incorporating them into the MSN structure. Testing of the MSNs against drug resistant MCF-7/ADR cells resulted in the MSNs displaying a significant effect on the drug resistant MCF-7/ADR cells.[46]

Popovici *et al.* developed an MSM for the controlled delivery of captopril.[48] Captopril is an angiotensin-converting enzyme (ACE) inhibitor used in the treatment of hypertension, and congestive heart failure.[49] Functionalization of the silica surface can modify the release of captopril from the nanoparticles. In vivo studies of the release demonstrated a 60% release within the first 6 hours, the surface interaction between the MSNs and the captopril likely caused a slower rate of release. Subsequently, over the following 56 hours, a slower rate of captopril release was observed. The group concluded that the MSNs show potential in delivering captopril over a prolonged period reducing the dosage intervals required for captopril.[48]

1.2.5. Carbon nano-carriers

Carbon-based nano-carriers are carbon-based materials in the form of nanotubes or graphene composites designed for drug delivery.[50] Traditional carbon nanotubes have been observed to possess toxicity to specific cells and organelles within the body.[51] However, consideration of graphene has become a new area of research. Graphene is a single-layered sheet of carbon hexagonal layers.[52]

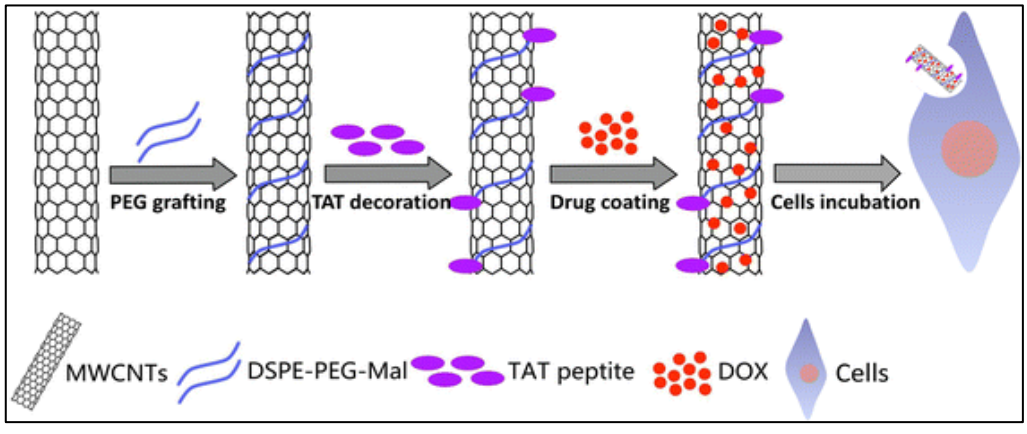

Figure 1 - 9: Schematic of a carbon nanotube being loaded with doxorubicin for drug delivery[53]

Luan *et al.* developed a reduced graphene oxide nano-carriers for the delivery of doxorubicin. The graphene was reduced using riboflavin-5'-phosphate sodium salt

dehydrates in the presence of a stabilising compound. Upon initial testing of the hemolytic properties of the nanoparticle, the nanoparticles were found to have minimal effect on the cells. This demonstrates the suitability of the nanoparticles for drug delivery. Doxorubicin underwent incorporation into the nano-carrier *via* π- π stacking interactions. The nano-carriers were found to have a high loading efficiency and were very pH-stable. The nano-carriers were found to demonstrate a sufficient level of cytoxicity of against MCF-7 and A549 cells and worked *via* non-specific endocytosis, showing potential for drug delivery applications.[54]

Faghihi *et al.* investigated octaarginine functionalized graphene oxide based nano-carriers for use as a delivery system for gene-therapy treatments. The group loaded the nano-carriers with different concentrations of octaarginine *via* a two-step amidation process. The group found that at higher concentrations of octaarginine, the nanoparticles were found to possess an increase in cytoxicity. The group determined that one μmol of peptide per mg of graphene oxide was the most effective for loading. This concentration demonstrated the best delivery of fluorescent proteins to target cells.[55]

1.2.6. Magnetic nanoparticles

Magnetic nanoparticles (MN) have been investigated for their potential use as a drug delivery vector in recent years. Magnetic nanoparticles have two methods for use as a therapeutic agent. Firstly, magnetic nanoparticles can undergo exposure to a magnetic field generated by an alternating current, this causes the nanoparticles to generate a localised increase in temperature, overheating the cell leading to cell death *via* hyperthermia, the metal nanoparticles heat up due to an increase in the energy of the metal atoms in the nanoparticles causing a greater amount of vibrations generating more heat in the area surrounding the metal. The second method is to use the magnetic nanoparticle as a targeting vector. The magnetic core is guided by the use of a magnetic field placed near to a target cell or organ *via* a magnet or localised magnetic field facilitating delivery to that cell.[56]

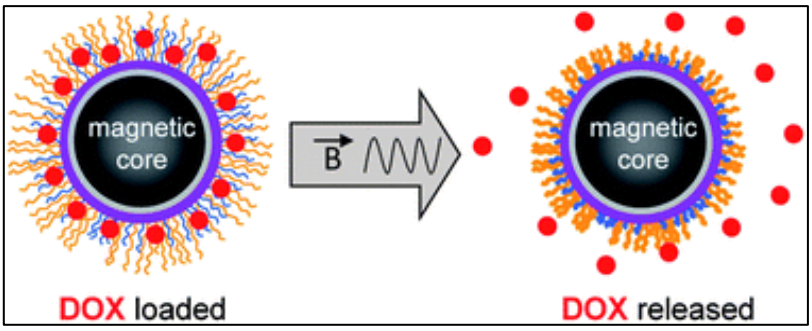

Figure 1 - 10: Diagram of a drug release from doxorubicin loaded magnetic core nanoparticle[57]

Xing *et al.* developed biocompatible iron oxide nanoparticles for drug delivery of gentamicin sulphate.[58] Gentamicin sulphate is an antibiotic used in the treatment of a variety of infections within the human body, including pneumonia.[59] The group modified iron oxide nanoparticles with PEG dicarboxylic acid and chitosan (CS) to enhance the dispersity of the nanoparticles; the addition of the PEG also increased the amount of carboxyl binding sites. When exposed to acidic conditions, the CS/PEG layer on the cell protonated to facilitate better uptake in bacterial cells. The nanoparticles were found to move deeper into the cell when exposed to a magnetic field. The delivery of the gentamicin sulphate was found to be increased especially in acidic conditions; the nanoparticles also demonstrated a considerable effect on the biofilm that is produced by the bacterium S. aureus which the nanoparticles were tested.[58]

Liu *et al.* developed iron oxide nanoparticles coated with a macrophage membrane based shell.[60] A macrophage is a species of white blood cell which engulf anything within the blood that does not contain surface proteins, these cells form part of the human body's immune system.[61] The group investigated the use of photodynamic therapy to convert a pulse of light into a dynamic temperature increase inside a cell to cause the cell to over-heat, leading to cell death. The nanoparticles displayed an increase in biocompatibility, immune evasion and cancer cell targeting compared to traditional iron oxide nanoparticles. The nanoparticles exhibited a rise in photodynamic activity when tested in breast cancer cells *via* mouse studies.[60]

1.3. Polymers in drug delivery

A polymer nanoparticle contains many polymer chains in repeating units with a variety of different monomers. Polymeric based nanoparticles are becoming more widespread due to the cheap cost and simplistic synthesis in comparison to metallic or biological

nanoparticles. Synthesis of polymer nanoparticles is carried out through a variety of polymerisation methods. Nanoparticles produced *via* these methods usually are solids immersed in the solution and are stable in extremes of temperature and pH.[61] Due to this, polymer nanoparticles have shown potential for use as a drug delivery system. Incorporation of the drug is achieved *via* internalisation into the nanoparticles.

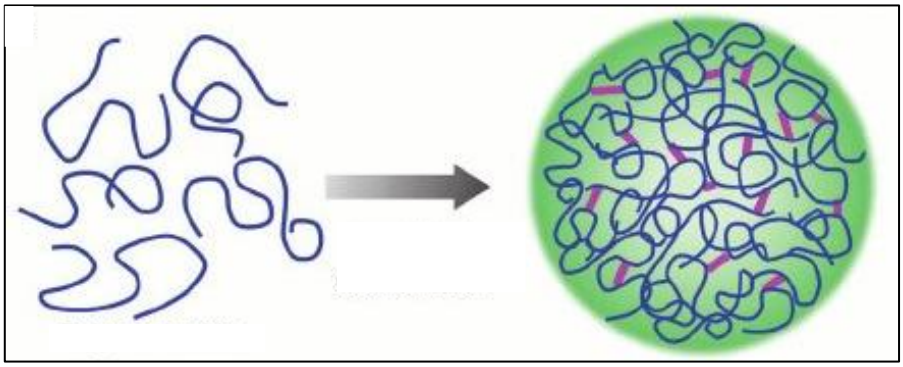

Figure 1 - 11: Schematic of polymer cross-linking to form nanoparticles[62]

Usually, loading of a drug utilises large groups attached to the surface such as PEG. The PEG groups undergo grafting onto the surface of the nanoparticles in the presence of a drug to create loading cavities to store the drug. When injection of the nanoparticles into a clean solution without the drug present occurs, the diffusion gradient generated between the inside and outside of the nanoparticle causes the drug to diffuse out of the nanoparticles, into the surrounding solution. The release of the drug is dependent on the species of the drug being used and its interaction, along with the composition of the polymer and surrounding solution. The main issue with this method of loading the nanoparticles is that the release is entirely dependent on diffusion. Therefore, as soon as the nanoparticles enter into a clean (drug-free) solution, the drug begins to diffuse from the nanoparticles.

Zhang *et al.* developed a magnetic drug carrier based around iron oxide nanoparticle core, to this doxorubicin were conjugated before encapsulation with a dextran-based thermally responsive polymer. The magnetite nanoparticles were functionalized using a sulphur bond coupled to anticancer agent doxorubicin through a hydrazone linker. The nanoparticles were found to possess a low level of doxorubicin release in normal cellular conditions, however, in the acidic conditions found in cancer cells, a significant amount of the doxorubicin was found to be released. This nanoparticle system was found to show potential as a systematic delivery system for doxorubicin.[63]

Yang *et al.* developed a multifunctional polymer vesicle for targeted delivery of doxorubicin and iron oxide nanoparticles. The nanoparticles formed vesicles with an acrylic inner layer along with a PEG outer shell. A hydrazone linker attached to doxorubicin anchored the doxorubicin to the iron core. The nanoparticles were able to increase the relaxivity of MRI images of a tumour, alongside a controlled release of doxorubicin inside cancerous cells only, as compared to other cells.[64]

Gu *et al.* developed a multi-functional nano-carrier for the delivery of doxorubicin to cancer cells.[65] The group developed a nanoparticle designed to decompose when exposed to intense light utilising 2-nitroimidazole which undergoes redox reaction inside hypoxic conditions.[66] The outer layer of the nanoparticle breaks when exposed to light releasing doxorubicin free into the cells. When the nanoparticle breaks down and releases the 2-nitroimidazole into the cells, it undergoes decomposition to form toxic fragments leading to cell death. The combination of these effects can successfully eliminate cancer cells.[65]

1.4. Molecularly imprinted polymers for drug delivery

Molecularly imprinted nanoparticles are polymer nanoparticles which possess a cross-linking network of different polymer chains around a template molecule incorporating specialised monomers called functional monomers. The functional monomers create a three-dimensional imprint of the template held in place *via* cross-linking monomers in the polymer chains. This structure creates a complementary binding site to the template. Molecularly imprinted polymer nanoparticles demonstrate significant potential as a replacement for biological antibodies including use as, sensors, assays, cellular labelling and drug delivery.

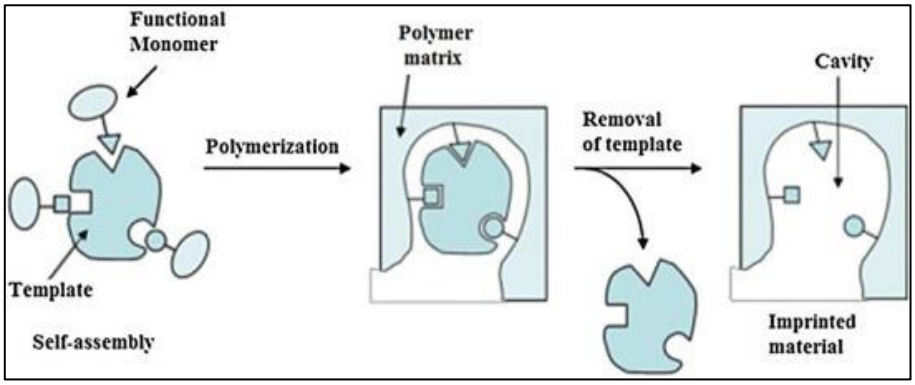

Figure 1 - 12: Schematic of molecularly imprinted polymer synthesis[3]

Recently, molecularly imprinted nanoparticles for use as a drug delivery system is becoming an increasingly significant area of research.[67] Due to the synthesis of molecularly imprinted nanoparticles possessing a large number of binding sites for any chosen drug. Incorporation of a drug inside the nanoparticle creates binding sites *via* the addition of the drug to the polymerisation mixture before initiation. The template molecules and functional monomers form a 3D complex in solution immobilising the template into place *via* the formation of the cross-linking chains.

Denizli *et al.* developed a molecularly imprinted nanoparticle drug delivery system with a magnetic core based on iron oxide.[68] The group designed nanoparticles for the delivery of mitomycin C, a chemotherapeutic agent used in the treatment of different cancers.[69] The group utilised magnetic fields to cause the nanoparticles to swell; this leads to a slight increase in the size of the nanoparticles causing the mitomycin C to be released. The group demonstrated a near complete delivery of mitomycin C from the nanoparticles when heated to physiological conditions.[68]

Atyabi *et al.* developed molecularly imprinted nanoparticles for the delivery of paclitaxel *via* mini-emulsion polymerisation. Paclitaxel is a chemotherapeutic agent used for the treatment of lung and other primary organ cancers.[70] The group used different degrees of cross-linking to improve paclitaxel retention for extended release of paclitaxel. The nanoparticles were found to retain the paclitaxel at neutral pH 7.0, however, when the conditions changed to those found within cancer cells the paclitaxel is released.[71]

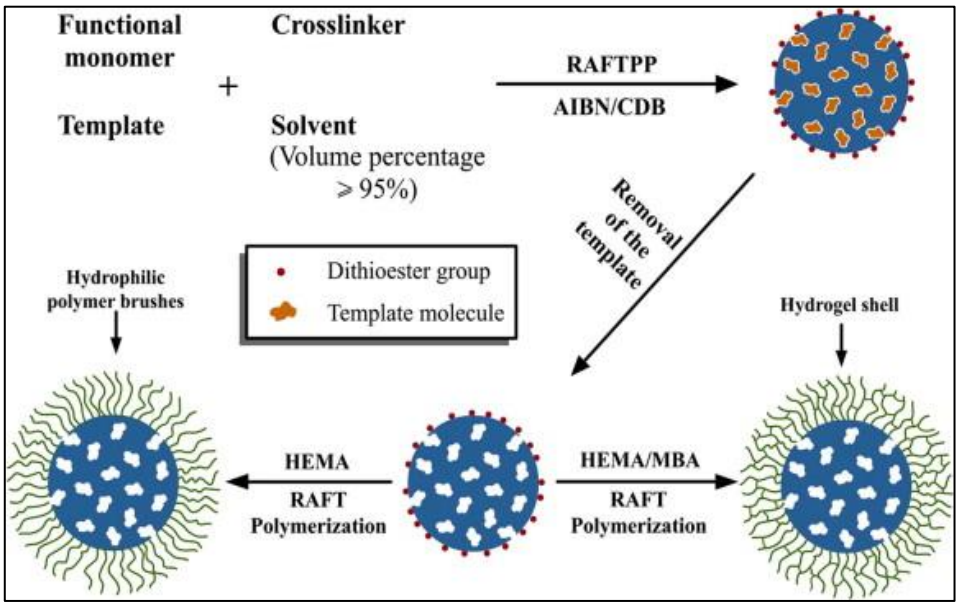

Figure 1 - 13: Schematic of dual layer polymer nanoparticle synthesis for both hydrophobic and hydrophilic nanoparticles.[72]

Denizli *et al.* prepared copper infused nanogels developed for the delivery of 5-fluorouracil to cancer cells.[73] 5-fluorouracil is a chemotherapeutic agent used for the treatment of various cancers.[74] The group used copper as the metal centre for a complex with N-methacryloyl-L-histidine and 5-fluorouracil polymerised together. When increasing the level of cross-linking degree, the rate of release decreased. The pH of the nanoparticle and its surroundings mediates the release rate of 5-fluorouracil, as the copper ions behave as a Lewis acid in solution, there is a decrease in the rate of release.[73]

Denizli *et al.* produced degradable cryogel discs for the pH-responsive delivery of doxorubicin to cancer cells. The cryogel discs utilised an amino-acid based functional monomer in combination with hydroxyethyl methacrylate and gelatin as a cross-linker. The discs were found to be stable in biological systems for over 56 days by which time only 84% had degraded. The initial release of doxorubicin occurred over a short burst over the first 12 hours followed by a steady release over the subsequent 100 hours. A combination of diffusion and erosion of the discs causes the doxorubicin to be released. As the conditions become more acidic, the rate of release of doxorubicin increases in comparison to the neutral pH found in healthy cells.[75]

1.5. Biocompatibility and suitability

With the increasing requirement for more effective therapeutics and fewer side effects, specific requirements need to be met by nanoparticles for use in drug delivery. The nanoparticles need to be biologically compatible and stable within biological systems. Also, these nanoparticles should only target unhealthy cells instead of all cells.

The nanoparticles used for drug delivery need to be stable in the conditions found within the blood as this is the primary method of transport around the body to the target cells. Non-biological nanoparticles display a high tolerance to acidic conditions and physiological temperatures, making them suitable for drug delivery. To this end, nanoparticles are a better alternative to using biological-based drug delivery systems which can break down under adverse conditions; this makes nanoparticles an ideal mechanism for drug delivery.

However, like all new technology, there are drawbacks. Nanoparticles tend to aggregate, leading to an accumulation of nanoparticles and drug molecules in cells and organs. The optimal size for nanoparticles is to be smaller than 100nm in size as larger sizes can affect cellular uptake, alongside this the charge of the nanoparticles can affect the uptake of

nanoparticles as certain cellular surfaces are charged and can interact with surfaces of the opposite charge. The accumulation of the nanoparticles may occur in the healthy cells surrounding the target cell; this can lead to these cells being adversely affected. Aggregation can also lead to issues with nanoparticle distribution around the body, preventing the clearance of the nanoparticles. This build-up can lead to cell death causing complications from the treatment.

Secondly, if the nanoparticles being used are not fully bio-compatible due to the use of monomers that are potentially toxic if they become separated from the nanoparticle, to overcome this, the nanoparticles need to be thoroughly purified and washed before use.

In conclusion, synthetic nanoparticles have been shown to demonstrate a suitably high level of biocompatibility and stability for use within biological systems. These properties make nanoparticles ideal for use in biological systems, due to the greater stability compared to biological nanoparticles.

1.6. Future of nanotechnology within drug delivery

Nanotechnology, like any technology, has the potential for improvement. There are several methods for the enhancement of nanoparticles. One method for improvement would be the development of biocompatible nanoparticles comprised of non-toxic, biocompatible monomers to prevent unwanted cell death. The second method for improvement is the development of multifunctional nanoparticles; these nanoparticles would possess multiple functional components. The third method of improvement is the development of nanoparticles which do not undergo aggregation and are capable of remaining free in solution, as mentioned previously, nanoparticles can aggregate together. If these aggregates were to form within the body, then there is a risk of accumulation occurring inside the healthy cell. To prevent aggregation from occurring, the nanoparticles need to be modified to avoid this from happening. Preventing aggregation can be achieved by using surfactants as a shell coating the nanoparticle or the modification of the nanoparticle surface to decrease particle interaction.[76]

Nanoparticles have the potential to replace biological drug delivery systems since there are many advantages. Firstly, the cost of the nanoparticles is significantly lower than the cost of their biological counterparts. Nanoparticles are cheaper to synthesise due to the ease of manufacturing the monomers, whereas, their biological counterpart proteins are expensive to synthesise. Secondly, proteins can break down when exposed to adverse

conditions such as non-physiological pHs, temperatures and chemical conditions. Protein extraction is complicated and requires optimal conditions to ensure that the proteins do not degrade before usage. Also, the synthesis of proteins is complex and involves the use of protecting groups to ensure the correct functionality of the protein; this complicates the synthesis making it more expensive.

In contrast, nanoparticle synthesis is less complicated; it usually requires a one-pot mixture of monomers combined with an initiating agent, followed by purification. Thirdly, nanoparticles are stable in extreme conditions, including high and low pH and temperature. Meaning, the nanoparticles can be sterilised *via* autoclave without concern of degradation. Nanoparticles can be stored in non-physiological conditions without decomposition occurring. Nanoparticles can undergo long-term storage without decomposition occurring. Nanoparticles have demonstrated significant potential for use as therapeutic agents and drug delivery systems. While further improvements are needed, they show greater resilience to adverse conditions, are cheaper to synthesise, and they have become the ideal candidate to replace current therapeutic administration such as the intravenous injection of drugs and use of antibody-based delivery systems.

In biological testing, nanoparticles have been observed to reduce the amount of drug required to eliminate unhealthy cells. Problems which need to be addressed include the issue of nanoparticle aggregation, incorporation of targeting and drug into the same nanoparticle.

1.7. Conclusions

Based on current research and developments, nanoparticles are becoming the new method of delivering therapeutic agents to cancer cells. With further development of targeting mechanisms, more effective drug delivery systems can be produced to minimise the side effects while maintaining the desired effect. With the development of molecularly imprinted nanoparticles, the creation of synthetic targeting vectors has become easier, with the imprinting of any cellular target possible for drug delivery.

Chapter 2: Nanoparticle preparation for drug delivery

2.1. Introduction

After the synthesis of a drug or protein, preparation is required before use in live cells to ensure they will not bring any unwanted biological contaminants into the cell.[77] The method of preparation depends on the how soon after synthesis the product is required. If a product is needed immediately or within a short time frame, then the optimal procedure is sterilisation by autoclaving.[78] In contrast, if a product requires storage for an extended period, then the optimal procedure is to lyophilise the product and store until needed.[79]

Sterilisation is usually carried out by use of an autoclave. It is a pressure cooker like device that contains a small amount of deionised water which is heated up to approximately 121^{o}C for a predetermined period. As the water is heated, it increases the pressure inside the device. At this temperature and pressure, all the biological contaminants are killed, making the sample clean for use in live cells. Provided the sample is in a sealed vessel it will remain sterilised until opening. However, this is only for short-term storage or immediate use.[80]

Lyophilisation is a process in which a sample containing water is freeze-dried to help prevent biological contamination *via* the removal of water. The sample is frozen using liquid nitrogen before being placed under a high vacuum to remove all moisture from the sample. When required, this sample can then be re-dispersed in water. To improve lyophilisation, a cryoprotectant can be added to the sample to protect the sample from degradation. The compounds normally used are sugar based molecules or carbohydrates as these are resistant to changes in temperature and pressure experienced within the lyophilisation process.[81]

Glucose is a naturally occurring sugar molecule that can polymerise to form starch or cellulose.[82] In theory, this should form a sugar-based shell to protect the nanoparticles. Whereas, glycine is an amino acid found in most biological systems. In neutral pH the glycine forms a zwitterion, with a positive and negative end, these ends can loosely interact with each other to create a protective mesh surrounding the nanoparticles.[83]

Sorbitol is sugar-based alcohol, which is produced by the reduction of glucose. Sorbitol is used as a cryoprotectant for the preservation of certain foods and belongs to a group called glycols (alcohols with 2 or more alcohol groups). The sorbitol likely uses

intermolecular bonding such as hydrogen bonding to form a protective matrix around the nanoparticles due to the presence of six hydroxyl groups.[84] Trehalose is a naturally occurring disaccharide formed of 2 α-glucose monomers. When cells undergo significant dehydration, trehalose forms into a gel, this gel is used to keep the organelles within a cell in place preventing cellular damage when the cell is re-dispersed into the water.[85]

The nanoparticles were analysed using dynamic light scattering (DLS) facilitated via the use of a Zetasizer Nano (Nano-S) particle-size analyser from Malvern Instruments Ltd (UK). Dynamic light scattering is a process used to analyse the size distribution of polymer nanoparticles in solution.

Dynamic light scattering works by emitting a beam of light from a laser or other monochromatic light source into a polariser into the sample. The molecule then scatters the light and collected by a second polarizer where it amplified via the use of a photomultiplier and used to create a speckle pattern. These readings are recorded over multiple scans to create an average of the size readings. These readings can fluctuate; however, due to small molecules and particles under 250nm in size undergo Brownian motion in solution. This causes the readings to fluctuate altering the averages and causing anomalies to develop.[86]

In this study, the effect of sterilisation and lyophilisation on the aggregation of molecularly imprinted nanoparticles was carried out in collaboration with Dr Abeer Safaryan, a visiting academic to the research group.

2.1.1. Aim and objectives

Aim of the chapter:

- Optimisation and testing of sterilisation techniques for storage of nanoparticles for use in biological systems.

Objectives for this chapter:

- Test and observe the effects of lyophilisation on the nanoparticle properties.
- Test and identify the optimal cryoprotectant species to be used in lyophilisation to minimise changes in the nanoparticle properties.
- Identify the optimal amount of the ideal cryoprotectant for use in lyophilisation to minimise changes in the nanoparticle properties.
- Test and observe the effects of autoclaving on the nanoparticle properties.

2.2. Chemicals

Glass beads SPHERIGLASS® A-Glass 2429 (70 – 100 µm diameter) obtained from Potters Industries LLC. Acrylic acid, ammonium persulfate, 1,2-bis(trimethoxysilyl)ethane, glutaraldehyde, phosphate buffered saline tablets, N-isopropylacrylamide, N′-methylene-bisacrylamide, N-tert-butylacrylamide, N, N, N′, N′-tetramethylethylenediamine, trypsin from bovine pancreas, glucose, glycine, sorbitol, trehalose, acetone, ethanol, methanol and toluene were purchased from Sigma-Aldrich, UK. (3-Aminopropyl)triethoxysilane and sodium cyanoborohydride were obtained from Acros Organics. *N*-(3-Aminopropyl) methacrylamide hydrochloride was purchased from PolySciences Inc., UK. Amicon Ultra-15 Centrifugal Filter Units (MWCO 30 kDa), Acetonitrile, sodium hydroxide and sulphuric acid were obtained from Fisher Scientific (UK). Ultrapure water was produced by a Millipore Milli-Q system (Millipore, Bedford, MA, USA), Double-distilled ultrapure water (Millipore) was used for analysis. All chemicals and solvents were analytical or HPLC grade and were used without further purification. Phosphate buffered saline was prepared as directed from PBS buffer tablets (Sigma-Aldrich, Gillingham, UK).

2.3. Methods

2.3.1. Nanoparticle Preparation

Nanoparticle synthesis by solid phase requires two main stages. The first stage is the preparation of the solid phase for the templated nanoparticle synthesis. Initially, this is achieved by activation of glass beads in sodium hydroxide solution to coat the surface of the glass beads in hydroxyl groups. These nanoparticles undergo attachment of the template for the binding site. Initially, a silane group is attached to the hydroxyl groups before coupling a linker molecule to the amine end of the silane molecule. Amine-based templates require glutaraldehyde to be used, whereas, molecules containing a thiol or cysteine residue require the use of succinimidyl iodoacetate (SIA) for coupling. The second stage is the synthesis of the nanoparticles using polymerisation. For water-soluble templates then a free radical initiated polymerisation is carried out to form the nanoparticles. In this work, we use an APS-TEMED free radical initiation for the polymerisation. However, for organic solvent soluble templates, UV light is used to generate the radicals to initiate the polymerisation.

2.3.1.1. Trypsin Solid Phase preparation

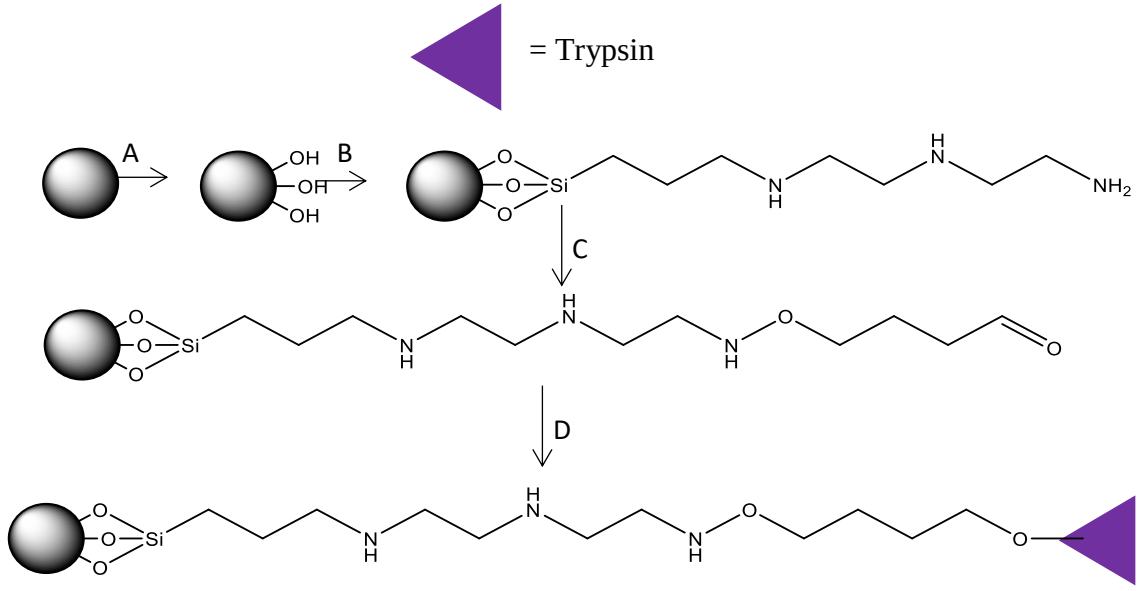

A = Hydroxylation step (Reflux, 30 minute) *B = Salinization step (Overnight, 70°C)*

C = Glutaraldehyde addition (R.T., 2 Hours) *D = Template Coupling step (R.T., Overnight)*

Figure 2 - 1: Schematic of the synthesis of the solid phase

Glass beads (100 g) were boiled in sodium hydroxide (4 M, 200 mL) for 30 minutes, after cooling, the nanoparticles were filtered and then washed with distilled water (600 mL). The beads were incubated with sulphuric acid (9 M, 200 mL), for 30 minutes, the beads were washed with distilled water to achieve a pH of 7.0. The beads were washed with acetone (200 mL), dried under vacuum then collected. The activated beads were then incubated at 150^{o}C for 30 minutes before being cooled. The activated beads were incubated in anhydrous toluene (160 mL) containing N-[3-(trimethoxysilyl) propyl] ethylenediamine (3.2 mL) and 1, 2-bis (trimethoxysilyl) ethane (528 µL) overnight under nitrogen at 70^{o}C. The beads were cooled, washed with methanol (900 mL), acetone (1.5 L) and then dried. The beads were then incubated at 150^{o}C for 1 hour before being cooled. The beads were incubated in a phosphate-buffered saline solution (PBS, 160 mL, 0.1 M) containing glutaraldehyde (11.2 mL) for 2 hours. The beads were collected, washed with distilled water (900 mL) and dried. The beads were incubated overnight in PBS (160mL, 0.1 M) containing trypsin (10mg, 429.9 nmol). Sodium cyanoborohydride (160 mg, 2.56 mmol) was added and left to react for 30 minutes. The trypsin-templated beads were washed with distilled water (900 mL), dried and collected under vacuum.

2.3.1.2. Nanoparticle Synthesis

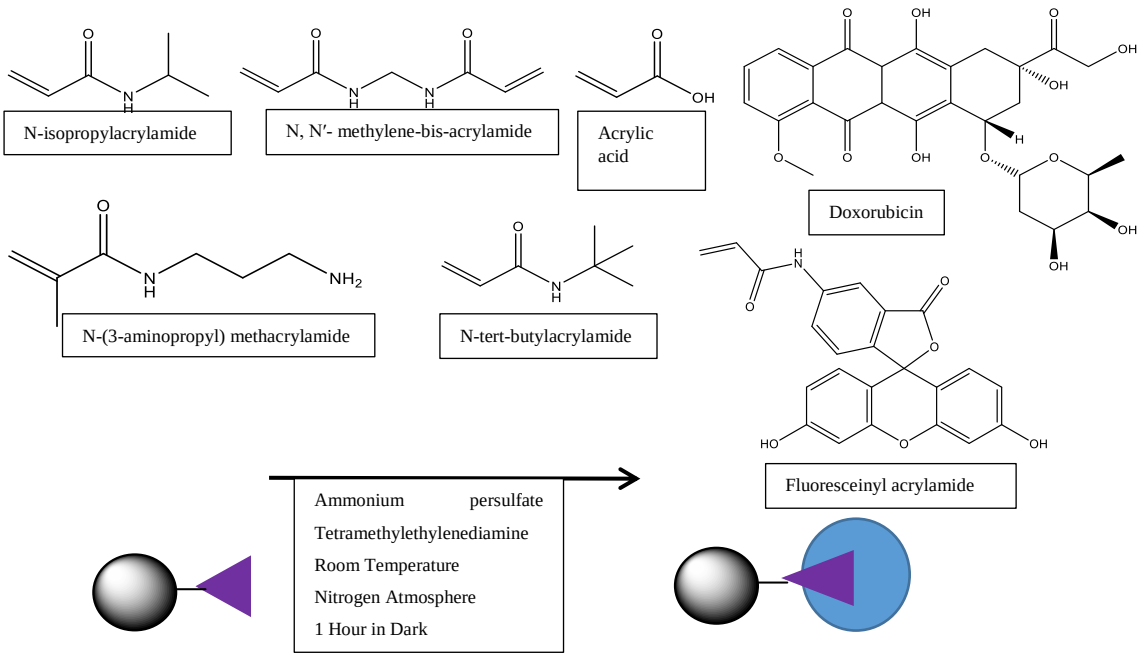

Figure 2 - 2: Schematic of the nanoparticle synthesis

A solution of N-isopropylacrylamide (39 mg, 344.6 µmol), N, N′- methylene-bis-acrylamide (2 mg, 12.9 µmol), N-(3-aminopropyl) methacrylamide (5.8 mg, 32.5 µmol), fluoresceinyl acrylamide (3 mg, 7.5 µmol) and acrylic acid (2.2 µL) in PBS solution (100 mL) was prepared. To this a solution of N-tert-butylacrylamide (33 mg, 259.5 µmol) in ethanol (0.5 mL) was added. The monomer mixture was purged with N_2 gas for 30 minutes, to this solution, trypsin-templated glass beads (60 g) were added.

A mixture of ammonium persulfate (30 mg, 131.5 µmol) and tetramethylethylenediamine (30 µL) in distilled water (1 mL) was prepared. This solution was added to the polymerisation mixture, after which the solution was re-purged with N_2. The reaction vessel was sealed and left in the dark for 1 hour. To stop the reaction, the vessel was unsealed, allowing oxygen to enter. This procedure was completed with ten repetitions to utilise all the glass beads.

2.3.1.3. Nanoparticle Collection

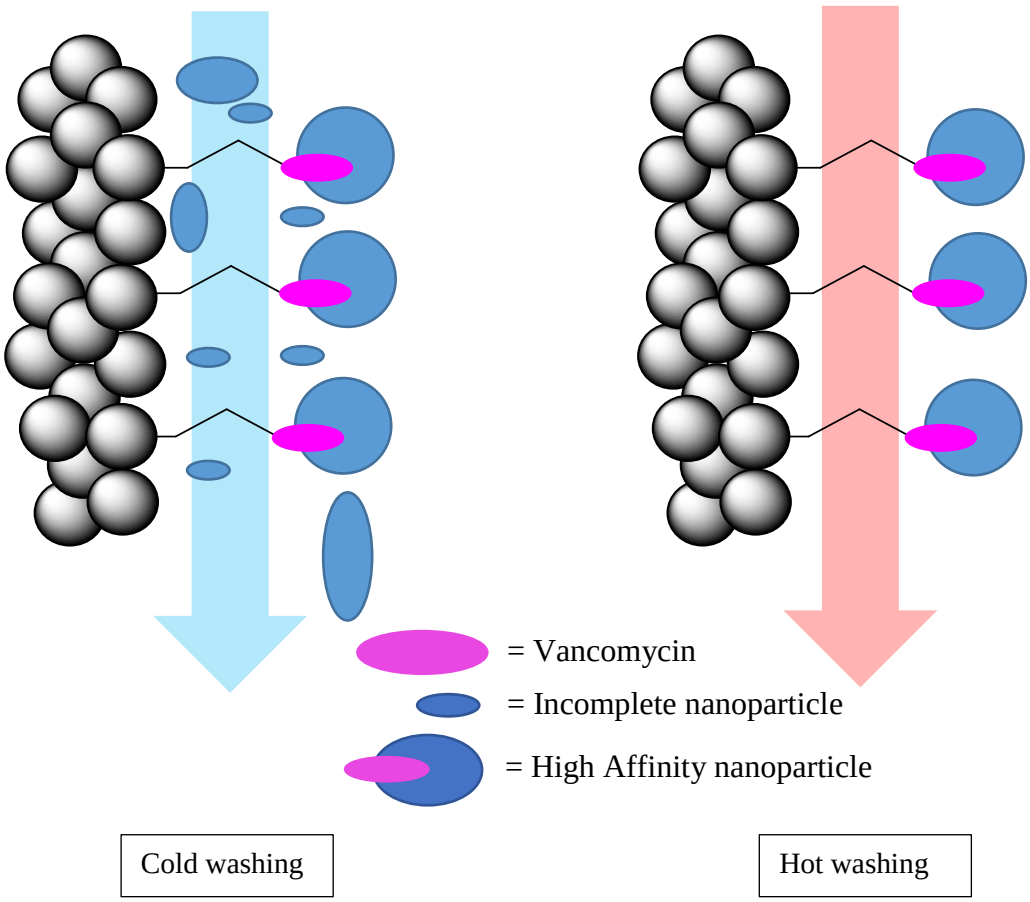

Figure 2 - 3: Schematic of nanoparticle collection

The trypsin-templated bead mixture was transferred to a 60mL solid phase extraction cartridge fitted with a polystyrene frit and washed with distilled water (600mL). Each batch of the trypsin-templated beads was heated to 65^{o}C, then washed with ethanol (65^{o}C, 120mL) with the 'hot' washings being collected. The ethanol was then evaporated off at 50^{o}C and replaced with distilled water (60mL). This procedure was completed with ten repetitions to utilise all the glass beads.

2.3.1.4. Nanoparticle Purification

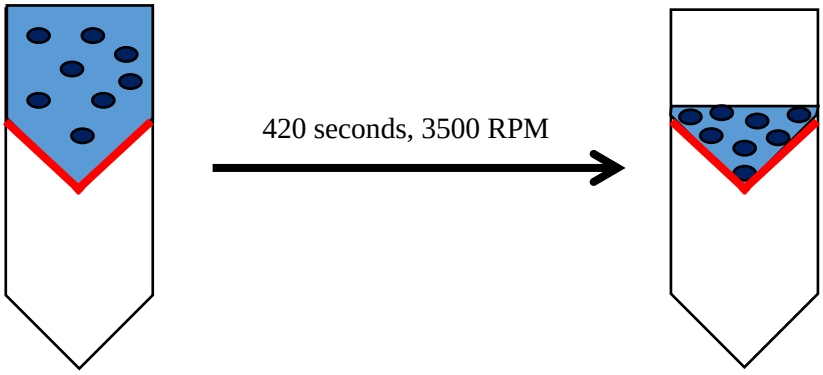

Figure 2 - 4: Schematic of the nanoparticle purification

The imprinted nanoparticle solution (15mL) was centrifuged using a dialysis cartridge (30000 MWCO, 50mL, 7 minutes, 3500 rpm). The nanoparticles solution was washed with distilled water (6 x 15mL), then concentrated (2mL). The nanoparticle solution was then collected and stored in the dark in a storage bottle (Fisherbrand™ Borosilicate Glass Narrow Neck Laboratory Bottle). This process was repeated until all the nanoparticle solution had been washed and concentrated. The concentrated solution of nanoparticles was then placed in storage at 4^{o}C until required. The nanoparticle synthesis process produced a 1% yield of the nanoparticles.

2.3.2. Lyophilisation of molecularly imprinted nanoparticles.

2.3.2.1. Cryoprotectant screening for lyophilisation.

Initially to determine the most suitable cryoprotectant to use with the nanoparticles, a comparison of glucose, glycine, sorbitol, trehalose and a control sample in a solution with nanoparticles and their effect on size before and after lyophilisation. Nine samples of concentrated nanoparticles (1mL) were placed in a pre-weighed Falcon tube (15mL). To four of these samples, each cryoprotectant (25mg of each) was added. To another four of these samples, each cryoprotectant (50mg of each) was added. All of these samples underwent DLS analysis before lyophilisation. All the samples were then immersed in liquid nitrogen (5 minutes), then placed under vacuum using a Labconco Freezone freeze dry system. The samples were placed under low pressure (0.22 bar) overnight. The samples were then collected and immersed in deionised water (1mL) then ultra-sonicated (5 minutes). The nanoparticles were reanalysed via DLS analysis after immersion.

2.3.2.2. Optimisation of the nanoparticle lyophilisation.

After identifying trehalose as the most suitable cryoprotectant, the optimal amount of trehalose required needed to be determined. This was done by analysing a range of trehalose amounts for differences in size, absorbance and fluorescence. Eight samples of concentrated nanoparticles (1mL each) were placed in a pre-weighed Falcon tube (15mL) to which different concentrations of trehalose (0mg, 5mg, 10mg, 15mg, 20mg, 25mg, 50mg and 100mg) were added. The samples were then analysed *via* DLS, UV-Vis and Fluorescence. All the samples were then immersed in liquid nitrogen (5 minutes), then placed under vacuum using a Labconco Freezone freeze dry system. The samples were placed under low pressure (0.22 bar) overnight. The samples were then collected and immersed in deionised water (1mL) then ultra-sonicated (5 minutes). The nanoparticles were reanalysed via DLS analysis after immersion.

2.3.2.3. Optimisation of post-lyophilisation sonication time

To determine the ideal process to disperse the nanoparticles in solution after lyophilisation. Four samples of concentrated nanoparticles (1mL) were placed in a pre-weighted Falcon tube (15mL) to which trehalose (10mg) was added. DLS analysed all the samples before undergoing lyophilisation as previous; the samples were then

sonicated for different amounts of time (0, 5, 10 and 15 minutes) using a Fischer Brand 15094 Ultrasound Bath). The samples were then analysed by DLS.

2.4.2.4. Effect of filtering on the concentration of lyophilisation nanoparticles

To determine the effect of filtering on the nanoparticles solution after lyophilisation, two samples of the concentrated nanoparticles were prepared. The nanoparticles were lyophilised and collected as previous. The second set of un-lyophilised samples was also prepared. All four samples were then transferred into a disposable syringe (5mL) attached to a micro-filter (Polytetrafluoroethylene, 0.4µm pore) before injection into a glass *via*l (4mL). The filtered solutions were then analysed by DLS and UV-Vis to determine the concentration.

2.3.3. Sterilisation of molecularly imprinted nanoparticles.

A sample of concentrated nanoparticles (1mL) underwent sterilisation *via* the use of a prestige classic medical Autoclave. The sample was heated to 128ºC at 30 PSI for a sustained period of 60 minutes before being cooled. The sample underwent DLS, UV-Vis and Fluorescence analysis before and after sterilisation.

2.4. Analysis and discussion.

2.4.1. Nanoparticle preparation

The glass beads from the hydroxylation step were successfully coated with OH binding sites and dried. The silanisation step was carried out successfully with the presence of the silane confirmed using dansyl chloride to label the amine end of the silane molecule. Under UV-Vis exposure, the glass beads glowed green, indicating the presence of the primary amine of the silane. The glutaraldehyde and trypsin coupling steps were completed, as shown in the method for 2.3.1. Overall this resulted in a solid phase suitable for nanoparticle synthesis. The nanoparticles were successfully synthesised by APS-TEMED initiation as described in 2.3.2. The nanoparticles were successfully purified and washed as is described in 2.3.3 with a concentrated sample (2mL) being produced. The particles were determined to be 120nm in size *via* DLS analysis.

2.4.2. Lyophilisation of molecularly imprinted nanoparticles.

2.4.2.1. Cryoprotectant screening for lyophilisation.

The initial screening utilised two concentrations of each protectant, 25 and 50mg. As a control, lyophilisation was carried out on nanoparticles with no cryoprotectant present; this was to get an idea of the overall effect of lyophilisation on the nanoparticles. The results are shown in Table 2 – 1, (Appendix 1.1 – 1.2)

Table 2 - 1: Table showing the size changes from lyophilisation without cryoprotectant present

Nanoparticle Types		Size	Standard de*via*tion
Control nanoparticles	Pre-lyophilisation	207.62 nm	± 7.39 nm
	Post-lyophilisation	281.68 nm	± 15.58 nm

Without the use of a cryoprotectant, the nanoparticle solution demonstrated an increase in the size of 74nm, indicating an increase in nanoparticle aggregation due to the removal and immersion of the nanoparticles in solution.

Glucose was then tested as a cryoprotectant at both 25mg and 50mg being added to samples of concentrated nanoparticles (1mL). The results are shown in Table 2 – 2 and Figure 2 – 5. (Appendix 1.3 – 1.6)

Table 2 - 2: Table showing the size changes from lyophilisation with glucose present

Sample	State	Size	Standard deviation
Control	Pre-lyophilisation	207.62 nm	± 11.48 nm
	Post-lyophilisation	281.68 nm	± 10.02 nm
Glucose = 25mg	Pre-lyophilisation	159.04 nm	± 11.76 nm
	Post-lyophilisation	268.74 nm	± 12.54 nm
Glucose = 50mg	Pre-lyophilisation	164.34 nm	± 10.43 nm
	Post-lyophilisation	287.84 nm	± 10.48 nm

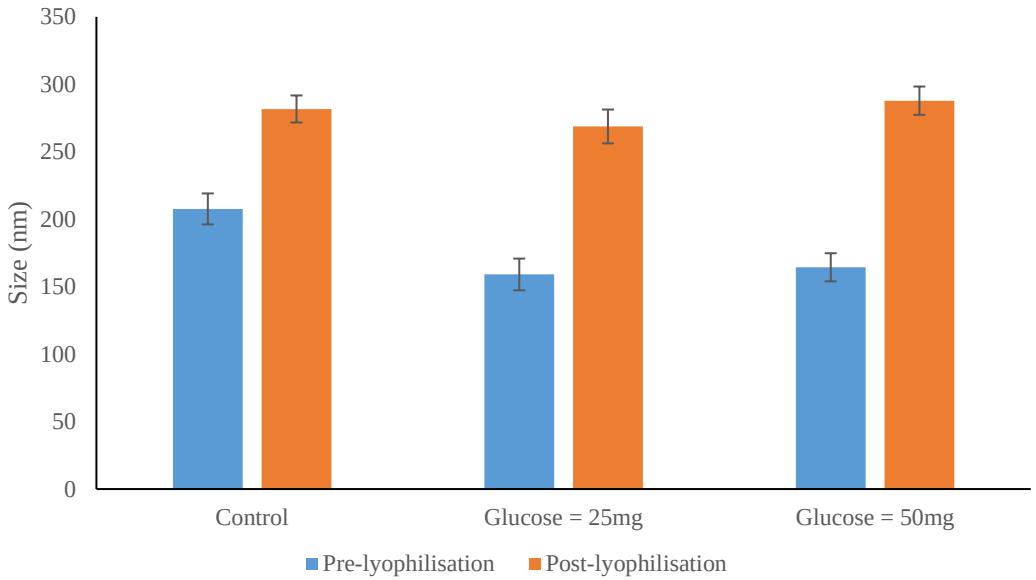

Figure 2 - 5: Graph showing the size changes from lyophilisation in the presence of glucose

When the glucose was added to the solution, a decrease in size is observed, this is likely due to the glucose altering the aggregation of the nanoparticles. After lyophilisation, the nanoparticles were found to undergo an increase in aggregation resulting in larger size readings similar to the results without cryoprotectant used.

Glycine was then tested as a cryoprotectant at both 25mg and 50mg being added to samples of concentrated nanoparticles (1mL). The results are shown in Table 2 – 3 and Figure 2 – 6. (Appendix 1.7 – 1.10).

Table 2 - 3: Table showing the size changes from lyophilisation with glycine present

Sample	State	Size	Standard deviation
Control	Pre-lyophilisation	207.62 nm	± 11.48 nm
	Post-lyophilisation	281.68 nm	± 10.02 nm
Glycine = 25mg	Pre-lyophilisation	181.22 nm	± 7.80 nm
	Post-lyophilisation	210.02 nm	± 9.32 nm
Glycine = 50mg	Pre-lyophilisation	157.96 nm	± 6.56 nm
	Post-lyophilisation	198.30 nm	± 9.56 nm

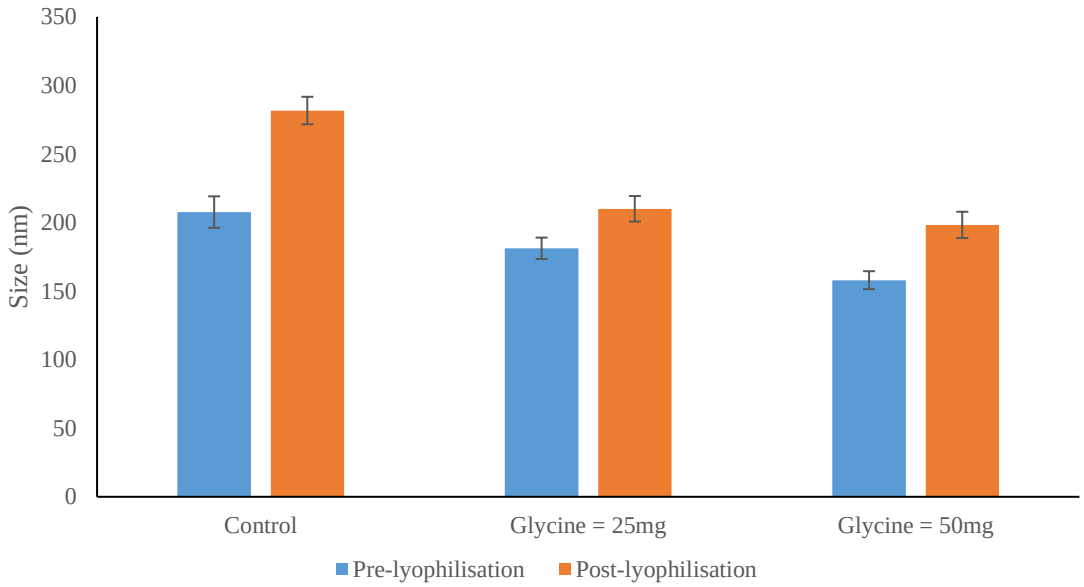

Figure 2 - 6: Graph showing the size changes from lyophilisation in the presence of glycine

When the glycine was added to the solution, a decrease in size is observed, this is likely due to the glycine altering the aggregation of the nanoparticles. After lyophilisation, the nanoparticles were found to undergo a small increase in aggregation resulting in a slight increase in size readings.

Sorbitol was then tested as a cryoprotectant at both 25mg and 50mg being added to samples of concentrated nanoparticles (1mL) The results are shown in Table 2 – 4 and Figure 2 – 7. (Appendix 1.11 – 1.14).

Table 2 - 4: Table showing the size changes from lyophilisation with sorbitol present

Sample	State	Size	Standard deviation
Control	Pre-lyophilisation	207.62 nm	± 11.48 nm
	Post-lyophilisation	281.68 nm	± 10.02 nm
Sorbitol = 25mg	Pre-lyophilisation	192.28 nm	± 8.36 nm
	Post-lyophilisation	277.94 nm	± 18.17 nm
Sorbitol = 50mg	Pre-lyophilisation	211.12 nm	± 19.79 nm
	Post-lyophilisation	262.35 nm	± 19.33 nm

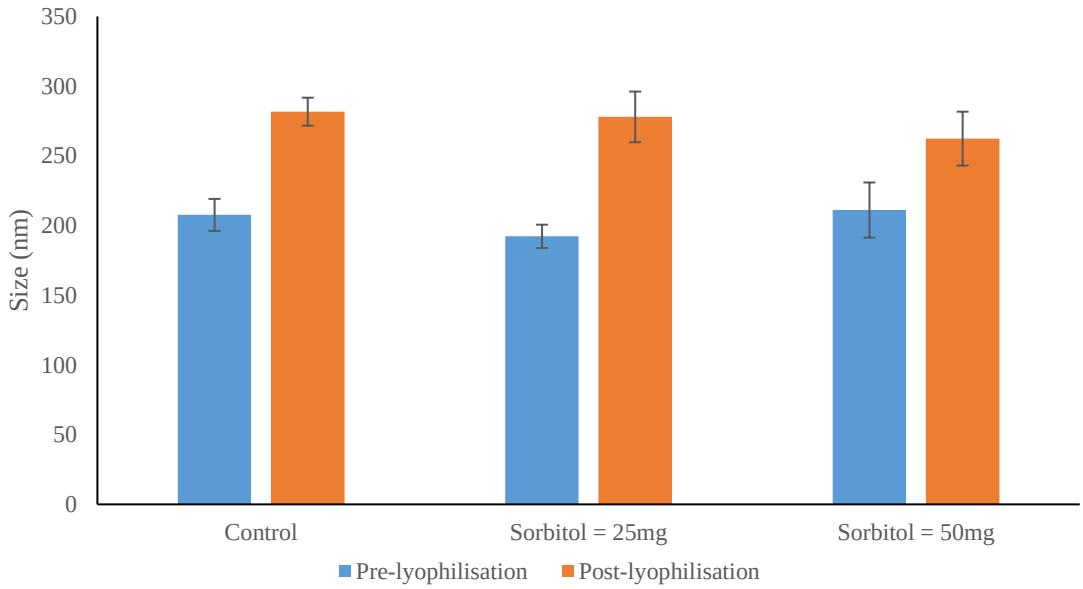

Figure 2 - 7: Graph showing the size changes from lyophilisation in the presence of sorbitol

When the sorbitol was added to the solution, a decrease in size is observed, this is likely due to the sorbitol altering the aggregation of the nanoparticles. After lyophilisation, the nanoparticles were found to undergo an increase in aggregation resulting in a slight increase in size readings.

Trehalose was then tested as a cryoprotectant at both 25mg and 50mg being added to samples of concentrated nanoparticles (1mL). The results are shown in Table 2 – 5 and Figure 2 – 8. (Appendix 1.15 – 1.18)

Table 2 - 5: Table showing the size changes from lyophilisation with trehalose present

Sample	State	Size	Standard deviation
Control	Pre-lyophilisation	207.62 nm	± 11.48 nm
	Post-lyophilisation	281.68 nm	± 10.02 nm
Trehalose = 25mg	Pre-lyophilisation	182.38 nm	± 4.21 nm
	Post-lyophilisation	208.95 nm	± 4.82 nm
Trehalose = 50mg	Pre-lyophilisation	174.46 nm	± 5.61 nm
	Post-lyophilisation	199.48 nm	± 5.13 nm

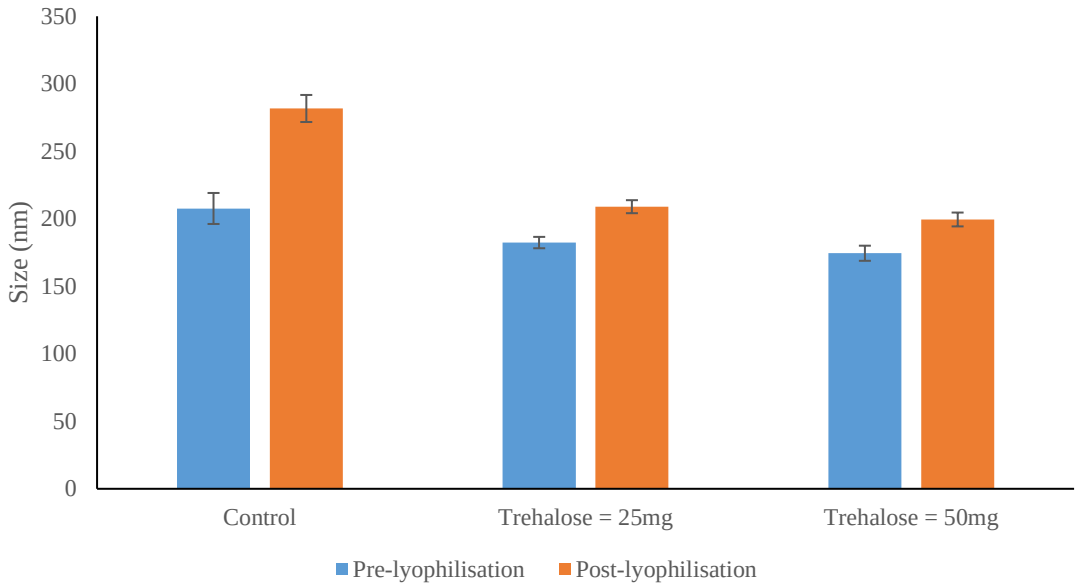

Figure 2 - 8: Graph showing the size changes from lyophilisation in the presence of trehalose

When the trehalose was added to the solution, there was a decrease in the amount of nanoparticle aggregation. After lyophilisation, there is a small increase in nanoparticle aggregation. However, this is smaller than the aggregation of the other three cryoprotectants.

2.4.2.2. Determination of the optimal amount of trehalose for nanoMIPs during lyophilisation.

From the initial screening, trehalose demonstrated the most significant effect as a cryoprotectant *via* its effect on nanoparticle size, absorbance and fluorescence. Therefore, a range of trehalose concentrations was tested to determine the minimal effective amount of trehalose required. The concentrations range tested 0 - 100mg.

Testing the effect of different concentrations of trehalose on the size of the nanoparticles and degree of aggregation occurring during lyophilisation and dispersion. The results are shown in Table 2 – 6 and Figure 2 – 9. (Appendix 2.1 – 2.16)

Table 2 - 6: Table showing the size changes from lyophilisation with different amounts of trehalose present

Sample	State	Size	Standard deviation
Control (0mg)	Pre-lyophilisation	166.62 nm	± 7.24 nm
	Post-lyophilisation	229.92 nm	± 9.59 nm
5mg	Pre-lyophilisation	157.06 nm	± 9.96 nm
	Post-lyophilisation	186.38 nm	± 6.25 nm
10mg	Pre-lyophilisation	159.24 nm	± 4.88 nm
	Post-lyophilisation	157.89 nm	± 4.63 nm
15mg	Pre-lyophilisation	154.62 nm	± 6.00 nm
	Post-lyophilisation	156.95 nm	± 7.72 nm
20mg	Pre-lyophilisation	153.52 nm	± 9.84 nm
	Post-lyophilisation	176.02 nm	± 9.15 nm
25mg	Pre-lyophilisation	182.38 nm	± 4.21 nm
	Post-lyophilisation	158.95 nm	± 4.82 nm
50mg	Pre-lyophilisation	174.46 nm	± 5.61 nm
	Post-lyophilisation	149.48 nm	± 5.13 nm
100mg	Pre-lyophilisation	198.76 nm	± 7.61 nm
	Post-lyophilisation	164.17 nm	± 6.55 nm

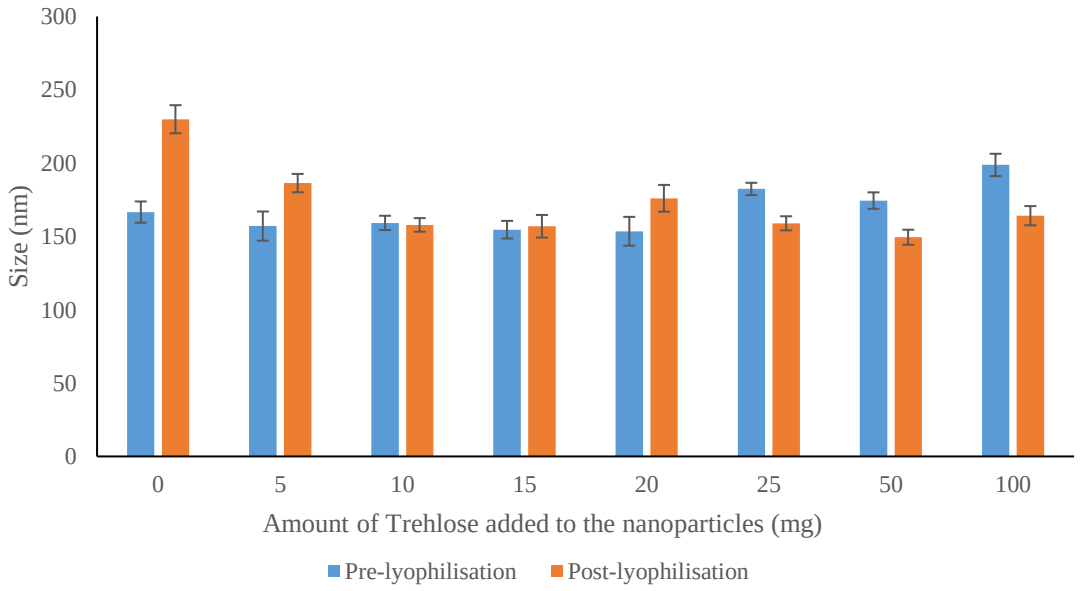

Figure 2 - 9: Graph showing the size changes from lyophilisation in the presence of different trehalose concentrations

When trehalose was added at 20mg or more to the nanoparticles, there was an interaction between the nanoparticles and trehalose altering the level of aggregation, while this is beneficial the high amount of trehalose may affect the functionality of the nanoparticles. However, when 10mg of trehalose is used, there is a minimal change in the aggregation and size readings of the nanoparticles.

Testing the effect of different concentrations of trehalose on the absorbance of the nanoparticles at 197nm as this is the standard wavelength for measuring the absorbance of molecularly imprinted nanoparticles. The results are shown in Table 2 – 7 and Figure 2 – 10.

Table 2 - 7: Table showing the absorbance changes from lyophilisation with different amounts of trehalose present

Sample	State	Absorbance at 197nm	Standard deviation
Control (0mg)	Pre-lyophilisation	0.146	± 0.009
	Post-lyophilisation	0.218	± 0.009
5mg	Pre-lyophilisation	0.642	± 0.051
	Post-lyophilisation	0.805	± 0.027
10mg	Pre-lyophilisation	0.992	± 0.031
	Post-lyophilisation	1.014	± 0.030
15mg	Pre-lyophilisation	1.181	± 0.047
	Post-lyophilisation	1.214	± 0.060
20mg	Pre-lyophilisation	1.217	± 0.088
	Post-lyophilisation	1.369	± 0.071
25mg	Pre-lyophilisation	1.253	± 0.033
	Post-lyophilisation	1.422	± 0.043
50mg	Pre-lyophilisation	1.375	± 0.048
	Post-lyophilisation	1.507	± 0.052
100mg	Pre-lyophilisation	1.517	± 0.059
	Post-lyophilisation	1.549	± 0.062

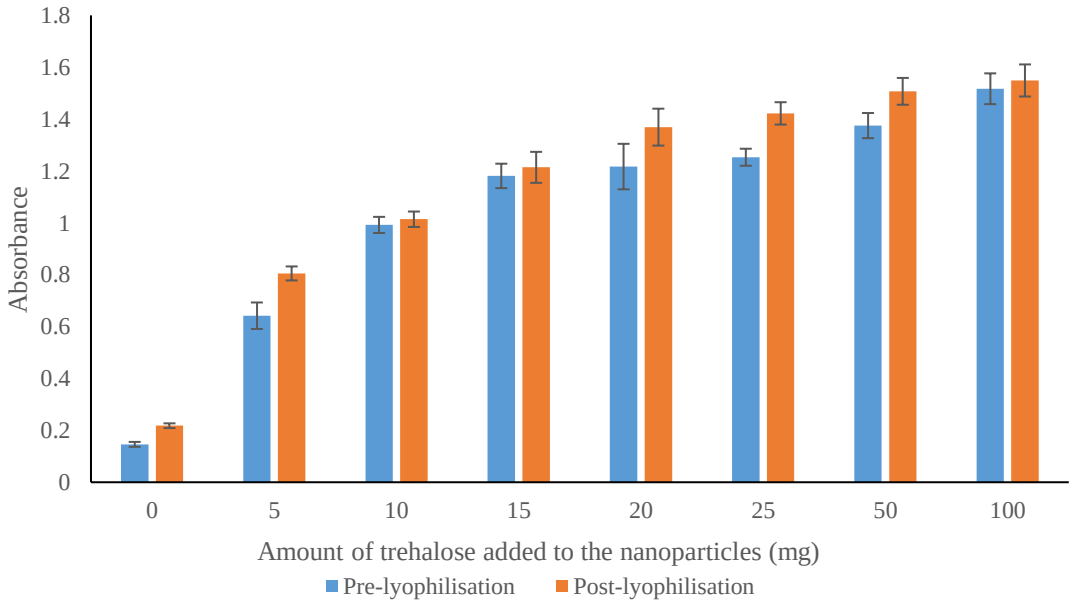

Figure 2 - 10: Graph showing the absorbance changes from lyophilisation in the presence of different trehalose concentrations

Lyophilization itself has minimal effect on the absorbance properties of the nanoparticles in solution; the most significant change in absorbance comes from the addition of

trehalose to the nanoparticle solutions. Initially, this causes a substantial increase but begins to plateau at the higher concentrations tested. This increase is likely due to the presence of an increasing number of Trehalose molecules being present in the solution.

Testing the effect of different concentrations of trehalose on the fluorescence of the nanoparticles at 514nm as this is the emission wavelength of the fluorescein component of the nanoparticles when excited at 490nm. The results are shown in Table 2 – 8 and Figure 2 – 11.

Table 2 - 8: Table showing the fluorescent intensity changes from lyophilisation with different amounts of trehalose present

Sample	State	Fluorescence Intensity ($x10^6$)	Standard de*via*tion ($x10^4$)
Control (0mg)	Pre-lyophilisation	1.50	± 6.50
	Post-lyophilisation	1.63	± 6.70
5mg	Pre-lyophilisation	1.63	± 10.3
	Post-lyophilisation	1.59	± 5.30
10mg	Pre-lyophilisation	1.82	± 5.50
	Post-lyophilisation	1.91	± 5.60
15mg	Pre-lyophilisation	1.76	± 6.80
	Post-lyophilisation	1.75	± 8.60
20mg	Pre-lyophilisation	1.67	± 10.7
	Post-lyophilisation	1.85	± 9.60
25mg	Pre-lyophilisation	1.80	± 4.10
	Post-lyophilisation	1.82	± 5.50
50mg	Pre-lyophilisation	1.83	± 5.80
	Post-lyophilisation	1.78	± 6.10
100mg	Pre-lyophilisation	1.85	± 7.10
	Post-lyophilisation	1.68	± 6.70

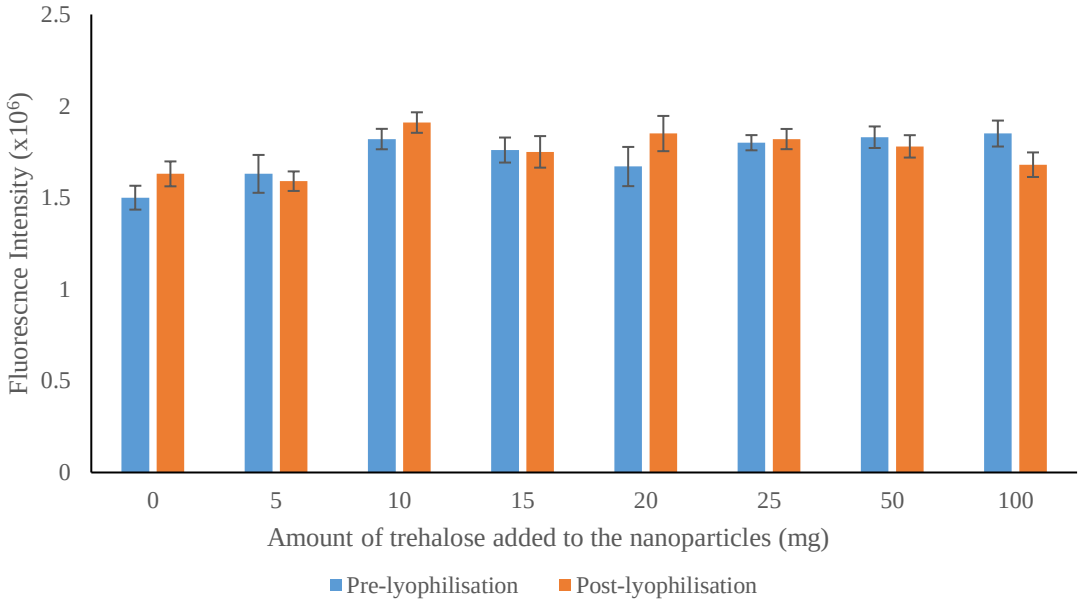

Figure 2 - 11: Graph showing the fluorescence changes from lyophilisation in the presence of different trehalose concentrations

The process of lyophilisation has minimal effect on the fluorescence properties of the nanoparticles as there is only a small change for all amounts of trehalose. The only exception is the 100mg of trehalose, where there is a slightly more significant decrease in fluorescence. This is likely due to the fluorophores in the nanoparticles undergoing quenching due to the trehalose holding the nanoparticles closer together.

2.4.2.3. Effect of sonication time on nanoparticles size after re-immersion post-lyophilisation

After determination of the optimal amount of trehalose (10mg), the post-lyophilisation sonication time to immerse the nanoparticles back into the solution. Four different sonication times were tested; 0, 5, 10 and 15 minutes. The bath used was a Fischer Brand 15094 Ultrasound Bath utilising a 37-kHz sonication frequency with a 1000w power unit. The results are shown in Table 2 – 9 and Figure 2 – 12.

Table 2 - 9: Table showing the size changes from post-lyophilisation sonication time

Sample	State	Size	Standard deviation
0 Mins – Control	Pre-lyophilisation	107.80 nm	± 7.24 nm
	Post-lyophilisation	129.40 nm	± 9.59 nm
0 Mins – With trehalose	Pre-lyophilisation	118.80 nm	± 9.96 nm
	Post-lyophilisation	149.20 nm	± 6.25 nm
5 Mins – Control	Pre-lyophilisation	100.70 nm	± 6.00 nm
	Post-lyophilisation	119.30 nm	± 7.72 nm
5 Mins – With trehalose	Pre-lyophilisation	118.80 nm	± 9.84 nm
	Post-lyophilisation	135.20 nm	± 9.15 nm
10 Mins – Control	Pre-lyophilisation	122.50 nm	± 5.61 nm
	Post-lyophilisation	127.50 nm	± 5.13 nm
10 Mins – With trehalose	Pre-lyophilisation	124.40 nm	± 7.61 nm
	Post-lyophilisation	128.10 nm	± 6.55 nm
15 Mins – Control	Pre-lyophilisation	112.70 nm	± 7.29 nm
	Post-lyophilisation	117.70 nm	± 6.23 nm
15 Mins – With trehalose	Pre-lyophilisation	118.80 nm	± 5.51 nm
	Post-lyophilisation	119.30 nm	± 8.81 nm

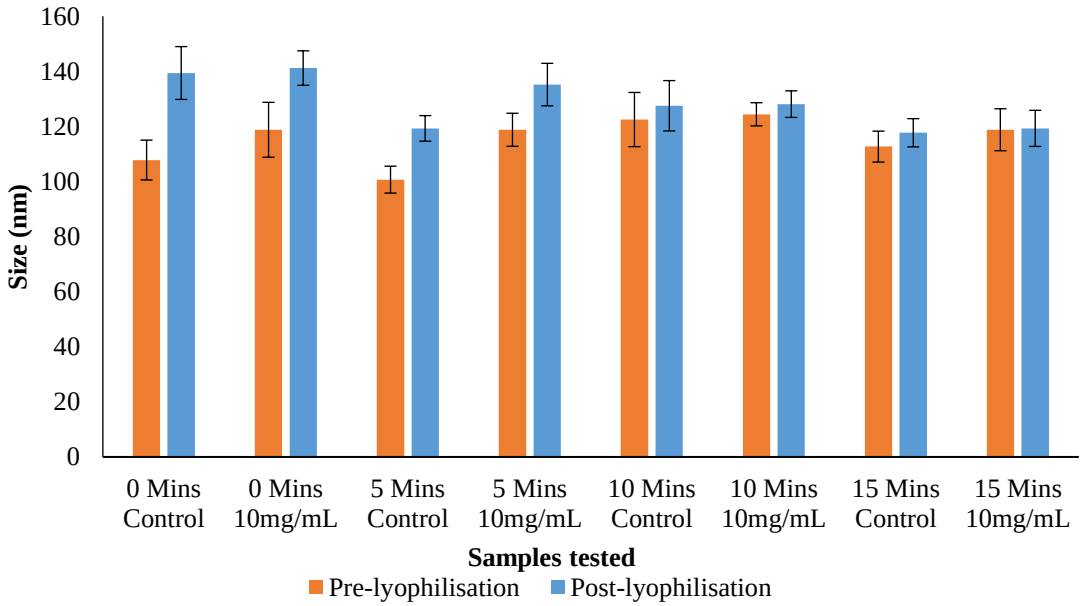

Figure 2 - 12: Graph showing the size changes from lyophilisation in the presence of different sonication times with and without trehalose

When the samples were not sonicated after lyophilisation, the control nanoparticles demonstrated a 32nm increase in size compared to the nanoparticles lyophilised with trehalose where the size increased by 23nm. However, when the samples were sonicated for 5 minutes, the control nanoparticles demonstrated a 19nm increase in nanoparticles size compared to the nanoparticles lyophilised with trehalose where the size increased by 17nm. When the samples were sonicated for 10 minutes, the control nanoparticles demonstrated a 5nm increase in nanoparticles size compared to the nanoparticles

lyophilised with trehalose where the size increased by 4nm. In contrast, when the samples were sonicated for 15 minutes, the control nanoparticles demonstrated a 5nm increase in nanoparticles size compared to the nanoparticles lyophilised with trehalose where the size increased by 1nm. Overall it showed that when the nanoparticles are sonicated for 10 minutes the difference in nanoparticle size, decreases to less than 5nm compared to shorter durations where there was a more significant increase, however, due to the imprecise nature of DLS measurements the changes in size are likely to be very small.

2.4.2.4. Effect of filtering on the concentration of nanoparticles.

To determine the effect of filtering the nanoparticles samples underwent filtering before and after lyophilisation to determine the effect on concentration. The concentration of the nanoparticles was determined by use of a calibration plot utilising the UV-Vis and DLS readings. The results are shown in Table 2 – 10 and Figure 2 – 13.

Table 2 - 10: Table showing the size changes from filtering before and after lyophilisation

Sample	State	Concentration	Standard deviation
Control pre-lyophilization	Pre-filtering	0.302 nM	0.031 nM
	Post-filtering	0.268 nM	0.018 nM
Control post-lyophilization	Pre-filtering	0.290 nM	0.015 nM
	Post-filtering	0.125 nM	0.019 nM
Trehalose (10mg) pre-lyophilization	Pre-filtering	0.289 nM	0.023 nM
	Post-filtering	0.258 nM	0.017 nM
Trehalose (10mg) post-lyophilization	Pre-filtering	0.375 nM	0.019 nM
	Post-filtering	0.275 nM	0.017 nM

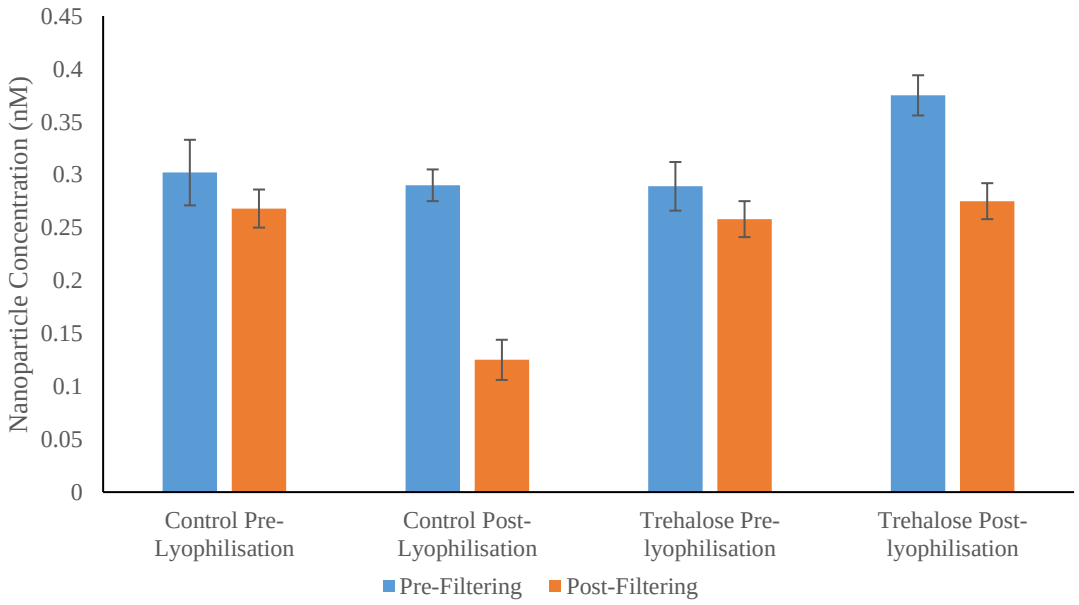

Figure 2 - 13: Graph showing the size changes from filtering before and after lyophilisation in the with and without the presence of trehalose

When both the control nanoparticles and nanoparticles in the presence of trehalose were filtered before lyophilisation, the change in concentration observed is small, indicating minimal loss of nanoparticles. However, the lyophilised control nanoparticles demonstrate a significant decrease in concentration; this shows that many nanoparticles were retained by the filter, indicating that aggregation of the nanoparticles occurred. Whereas the trehalose-treated nanoparticles showed a smaller reduction indicating some aggregation is happening, however, it is not as significant as the control nanoparticles without the protecting agent.

2.4.3. Sterilisation of molecularly imprinted nanoparticles.

The nanoparticles were sterilised *via* the use of an autoclave as described in 2.3.3 since no protecting agents are required, only the nanoparticles in solution were tested to determine the effects of sterilisation. The properties investigated were: size, absorbance and fluorescence of the nanoparticles, measured in the same way as the lyophilised nanoparticles. Testing the effect of sterilisation on the size of the nanoparticles and degree of aggregation occurring during the sterilisation. The results are shown in Table 2 – 11 and Figure 2 – 14.

Table 2 - 11: Table showing the size changes from sterilisation

Nanoparticle types		Size	Standard deviation
Trypsin nanoparticles	Pre-sterilisation	207.62 nm	± 7.39 nm
	Post-sterilisation	261.68 nm	± 11.58 nm

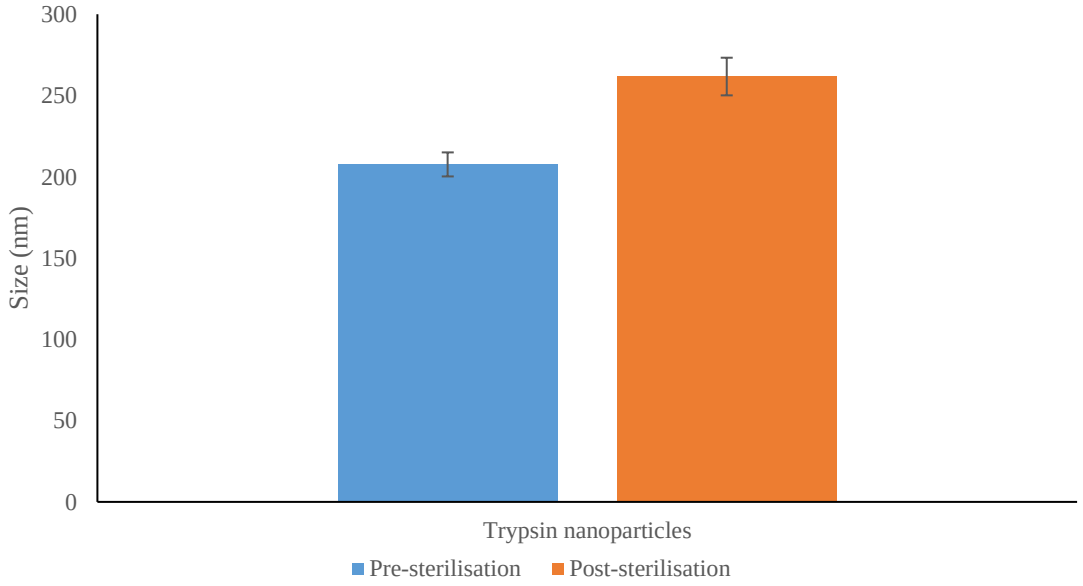

Figure 2 - 14: Graph showing the size changes from sterilisation

The nanoparticles demonstrate an increase in the size of 54nm. This increase is due to the nanoparticles' natural tendency to aggregate in solution. This tendency, in combination with the increased heating and pressure, the nanoparticles, were exposed to cause the nanoparticles to increase in size.

Testing the effect of sterilisation on the absorbance of the nanoparticles and degree of aggregation occurring during the sterilisation. The results are shown in Table 2 – 12 and Figure 2 – 15.

Table 2 - 12: Table showing the absorbance changes from sterilisation

Nanoparticle types		Absorbance	Standard deviation
Trypsin nanoparticles	Pre-sterilisation	0.149	± 0.0022
	Post-sterilisation	0.163	± 0.0024

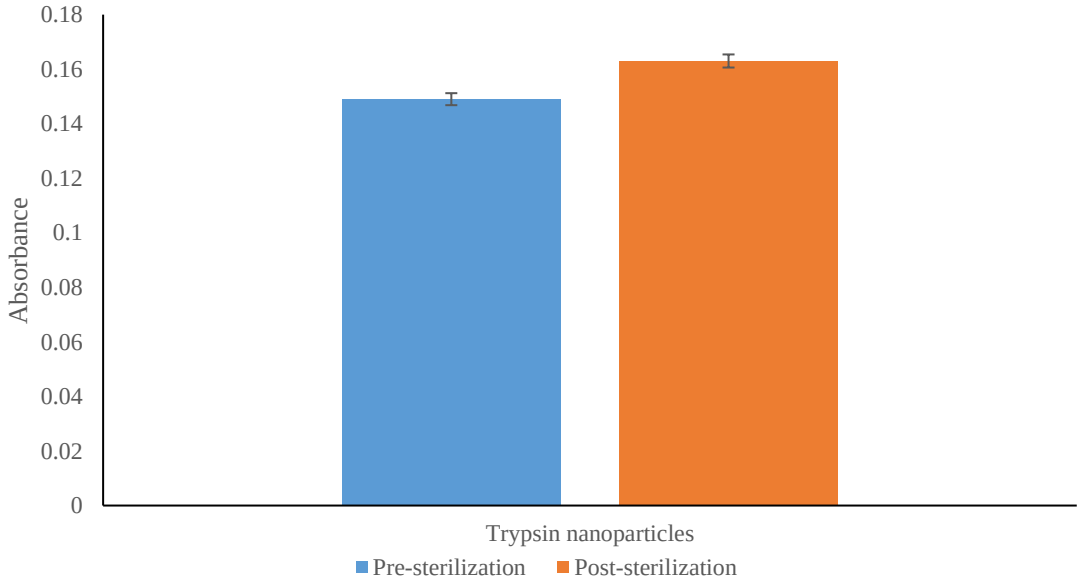

Figure 2 - 15: Graph showing the absorbance changes from sterilisation

The nanoparticles demonstrate a small increase in absorbance of 0.15nm. This increase is due to the nanoparticles natural tendency to aggregate in solution. This tendency, in combination with the increased heating and pressure, the nanoparticles, were exposed to cause the nanoparticles to increase in size.

Testing the effect of sterilisation on the fluorescence of the nanoparticles and degree of aggregation occurring during the sterilisation. The results are shown in Table 2 – 13 and Figure 2 – 16.

Table 2 - 13: Table showing the fluorescent intensity changes from sterilisation

Nanoparticle types		Fluorescent Intensity	Standard deviation
Trypsin nanoparticles	Pre-sterilisation	$1.53x10^6$	$3.06x10^4$
	Post-sterilisation	$1.56x10^6$	$3.12x10^4$

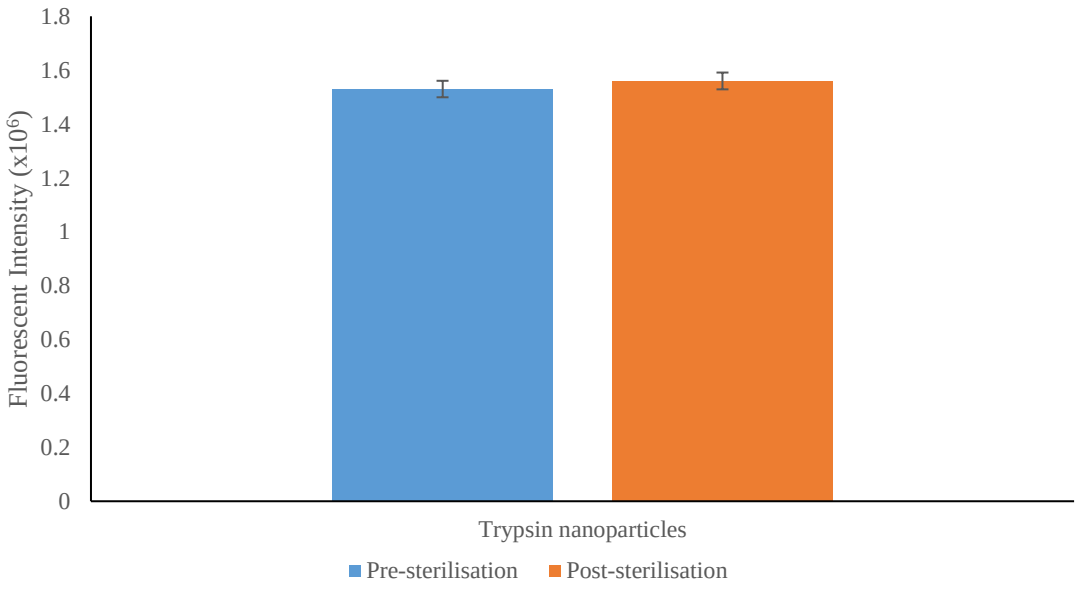

Figure 2 - 16: Graph showing the fluorescence changes from sterilisation

The nanoparticles demonstrate a small increase in the fluorescence intensity of $4x10^4$. This increase is due to the nanoparticle solution undergoing heating to 121°C during the autoclaving process. The increase in fluorescence of a molecule or particles is highly dependent on temperature as small variances in temperature can cause changes in fluorescence.

2.5 Conclusions

In this study, consideration of methods for the long-term storage of nanoparticles was carried out. As mentioned previously, with nanoparticles being stored in water or other aqueous solvents, they can develop biological contamination. This contamination is due to the growth of bacteria and other unwanted organisms; this is a common issue in biological testing if sterilisation procedures are not in place. This bacterial growth can cause problems when dealing with nanoparticles for use in biological systems such as cell cultures or in-vivo testing. In this section, we tested two different types of nanoparticle storage to prevent biological contamination, lyophilisation and sterilisation.

The first process tested was lyophilisation, where the sample undergoes immersion in liquid nitrogen before being exposed to high vacuum to remove the water. To prevent damage to the nanoparticles in this process, the use of a sugar protecting group can avert degradation. Initially, four sugar molecules were tested and compared for their potential use as cryoprotectants, glucose, glycine, sorbitol and trehalose. Of these molecules, trehalose was found to have the best protective effect for the nanoparticles, as observed by a reduction in the amount of nanoparticle aggregation after immersion of the lyophilised nanoparticles in water. From this, the concentration of trehalose was optimised to determine the appropriate amount of trehalose to use in lyophilisation. The size, absorbance and fluorescence of the nanoparticles were compared to determine the optimal amount to use, 10mg mL^{-1}.

To reduce aggregation in the nanoparticles in solution after lyophilisation, the nanoparticles were filtered through a micropore syringe filter. The control nanoparticles which did not undergo lyophilisation demonstrated a 10% decrease in concentration after filtering, whereas the control nanoparticles which underwent lyophilisation demonstrated a 50% decrease in concentration after filtering. The nanoparticles with trehalose present which did not undergo lyophilisation demonstrated a 10% decrease in concentration after filtering, whereas the nanoparticles with trehalose present which underwent lyophilisation demonstrated a 25% decrease in concentration after filtering.

The second process tested was sterilisation, where the nanoparticle sample is heated to 121^{o}C and maintained at a pressure of 30 PSI using an autoclave. This process is commonly used for the preparation of molecules and biological materials to prevent biological contamination. To determine the effect of autoclaving on the nanoparticles. The size, absorbance and fluorescence of the nanoparticles were compared before and

after autoclaving. The properties of the nanoparticles were found to have undergone small, insignificant changes in absorbance and fluorescence, in contrast, there was a slight increase in nanoparticle size likely caused by aggregation of the nanoparticles in solution. Both methods of nanoparticle preparation and storage demonstrate a significant advantage over storing the nanoparticles in solution. The only drawback of lyophilisation is that the use of trehalose or other cryoprotectants may affect how the nanoparticles function in biological systems as the cryoprotectants may negatively affect cells. In contrast, there is the minimal effect of autoclaving on nanoparticle properties as evidenced during the study, demonstrating a potential method for enhancing the storage of nanoparticles for later use.

Chapter 3: NanoMIPs as potential carriers for siRNA transfection in renal cells.

3.1. Introduction

Caspase-3 is a protein found in human cells, and part of the caspase group of proteins.[87] Caspase-3 is part of the apoptosis triggering mechanism used to eliminate cells by controlled cell death.[88] There are two pathways for the triggering of apoptosis. The first is *via* an extrinsic pathway involving the attachment of the 'death ligand' to the tumour necrosis factor (TNF) surface protein. Whereas, the second is *via* an intrinsic pathway involving signals generated by the mitochondria. These routes activate the proteins caspase-9 (extrinsic) and caspase-8 (intrinsic) which then activate the caspase-3 protein.[89] The activation of caspase-3 triggers the process of apoptosis to occur, causing the cell to undergo controlled cell death. Caspase-3 is the primary caspase protein involved in the breakdown of the amyloid-beta 4A precursor protein, a protein highly expressed in neuron synapses.[90] The breakdown of this protein leads to the development of Alzheimer's disease.[91]

One method of inhibiting the production of proteins is using small interfering RNA sequences (siRNA). SiRNA is a short, double chain RNA. Usually, 20 – 24 nucleotide bases long which are designed to interfere with the expression of messenger RNA (mRNA).[92] mRNA is used to transcribe the nucleotide sequence of the DNA stored in the chromosomes *via* matching complementary base pairs.[93] This RNA fragment is then converted into a functional protein *via* translation in the ribosomes using transfer RNA (tRNA) to form the correct protein sequence.[94]

SiRNA works by using an anti-sense strand to target a key sequence of nucleotides on the DNA chain in the nucleus. When the siRNA enters the cell, it becomes incorporated into other proteins involved in DNA transcription; this forms an RNA-induced silencing complex (RISC).[95] The siRNA unwinds and the separated into two single strands, the thermodynamically less stable stand remains incorporated in the RISC.[96] This integrated strand locates and binds to a complementary mRNA. Once the mRNA binds to the immobilised siRNA stand, the mRNA undergoes cleavage into small fragments.[97] The cell recognises these fragments and identifies them as abnormal, which is then degraded, preventing the coding of a target protein. This cause the silencing of the gene as the mRNA is unable to trigger the production of the target protein.[98]

The siRNA effectiveness was monitored by the use of quantitive polymerase chain reaction (qPCR). QPCR is a version of polymerase chain reaction (PCR) used to monitor in real time the growth of DNA chain during the process of PCR instead of at the end of the process as in conventional. PCR is a process where a DNA fragment is replicated via a series of 25 – 50 temperature change cycles depending on the amount of DNA required. A PCR cycle consists of three stages; initially, the sample is heated to 95^{o}C to separate the double helix structure of the DNA into singular strands. The sample is then cooled to between 50 and 60^{o}C, allowing the DNA primers contained within the DNA template to be activated and facilitate binding to DNA fragments. The sample is then heated to between 68 – 72^{o}C to facilitate polymerisation via the use of DNA polymerase. This process is facilitated by use of a thermal cycler which possesses the capability to generate fluorescent readings by use of a fluorescent dye exciting the sample at the absorption wavelength and detecting the emission wavelength of the excited fluorophore within the molecule.[99]

In this study, the effect of caspase-3 siRNA transfection was investigated on renal cells taken from mice. These were then grown using microplate wells to host the cell cultures. The study compared a liposomal transfection reagent currently used in liver cell transfection to a series of 6 different nanoparticle species. Three of these species were produced in aqueous media *via* persulfate-initiated polymerisation, whereas the other three were produced in organic solvents *via* UV initiated polymerisation. Of each of these two types of nanoparticles, three different species were synthesised with different net charges, negative, positive or neutral.

The transfection studies were carried out on lab-grown TCMK1 cells to determine the transfection efficiency of Caspase-3 siRNA to these cells. The TCMK1 cells originate from the kidney of the Mus Musculus (Mouse) organism. This work was carried out in collaboration with Dr Bin Yang's group in the Department of Infection, Immunity and Inflammation at the University of Leicester.

3.1.1. Aim and objectives

Aim of the chapter:

- Synthesis, characterisation and testing of charged nanoparticles for the transfection of siRNA to cells.

Objectives for this chapter:

- Synthesis charged nanoparticles using both aqueous and organic solvent based nanoparticle synthesis.
- Characterisation of the nanoparticles to determine their properties.
- Testing of the nanoparticles in transfection studies for Caspase-3 siRNA to identify the ideal nanoparticle species for siRNA transfection.

3.2. Chemicals

Acrylamide, N, N′-Methylenebisacrylamide, Ammonium Persulfate, N, N, N′, N′-Tetramethylethylenediamine, Acrylic Acid, Pentaerythritol tetrakis (3-mercaptopropionate), Diethylaminoethyl methacrylate, Ethylene glycol dimethacrylate, Trimethylolpropane trimethacrylate, Benzyl Chloride, Sodium Diethylcarbamodithioate, phosphate buffered saline tablets, were purchased from Sigma-Aldrich Methacrylic Acid, UK. Amicon Ultra-15 Centrifugal Filter Units (MWCO 30 kDa), Acetonitrile was obtained from Fisher Scientific (UK). N-(3-aminopropyl) methacrylamide were purchased from PolySciences Inc., UK. Caspase-3 siRNA and a negative control version were obtained from Cell Signaling Technology Inc., United States. TCMK1 cell lines were purchased from LGC standards, UK. Ultrapure water was produced by a Millipore Milli-Q system (Millipore, Bedford, MA, USA), Double-distilled ultrapure water (Millipore) was used for analysis. All chemicals and solvents were analytical or HPLC grade and were used without further purification. Phosphate buffered saline was prepared as directed from PBS buffer tablets (Sigma-Aldrich, Gillingham, UK).

3.3. Methods

3.3.1. Synthesis of N, N-diethyldithiocarbamic acid benzyl ester

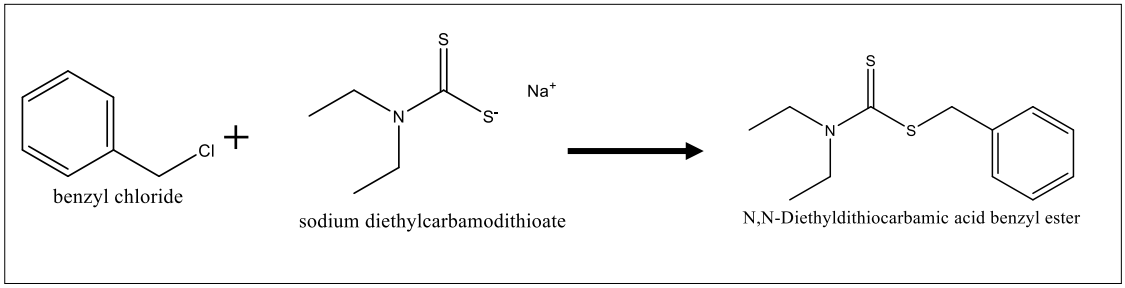

Figure 3 - 1: Schematic for the synthesis of N,N-diethyldithiocarbamic acid benzyl ester

Benzyl chloride (25.32g, 0.2mol) was dissolved in ethanol (200mL), to this sodium diethyldithiocarbamate trihydrate (48.78g, 0.22mol) was added. The solution was stirred (4 hours) at R.T. The sodium chloride residue was filtered off, and the filtrate concentrated under vacuum. The residue was then dissolved in chloroform (200mL) and washed with deionised water (3 x 200mL). The organic layer was collected and dried (sodium sulphate), filtered then concentrated under vacuum. This produced a dark yellow oil, 33.52g (70% yield). 1H NMR (DMSO), δ: 1.06 (t, 6H, 2 X CH3), 1.38 (t, 2H, SCH2), 2.35 (t, 2H, CH2), 2.68 (q, 2H, CH2), 7.23 (s, 5H, C5H5). 13C NMR (CDCl3), δ: 10.6 (2 X CH3), 31.9 (CH2), 45.1 (2 X NCH2), 47.3 (SCH2), 125.9 (CH), 127.7 (2 X CH), 129.6 (2 X CH), 139.4 (C(CH2) (2 X CH). Mass spectrum: found 241.41 (M + 1)

3.3.2. Nanoparticles preparation

The organic nanoparticles species were synthesised in acetonitrile containing the monomer mixture which underwent UV irradiation. The polymerisation required the use of a UV-sensitive initiator compound called an intifertier produced in 3.3.1. Methacrylic acid was used as it forms a negatively charged ion in solution, while Diethylaminoethyl methacrylate forms a positively charged ion in solution and Acrylamide remains neutral in solution.

The aqueous nanoparticles were synthesised in deionised water containing monomer mixture; the polymerisation was carried out using the decomposition of ammonium persulfate in solution to produce radicals. The polymerisation was carried out under a nitrogen atmosphere. Acrylic Acid was used as it forms a negatively charged ion in

solution, while (N-(3-Aminopropyl) methacrylamide) forms positive ions and N,N′-Methylenebisacrylamide remains neutral in solution.

3.3.2.1. Positively charged organic nanoparticles preparation

A mixture of pentaerythritol tetrakis(3-mercaptopropionate) (1.8mg, 0.003 mmol), N-(3-aminopropyl)methacrylamide (5.9mg, 0.033 mmol), diethylaminoethyl methacrylate (47.3mg, 0.301 mmol), ethylene glycol dimethacrylate (32.4mg, 0.163 mmol), trimethylolpropane trimethacrylate (32.4mg, 0.095 mmol) and N,N-diethyldithiocarbamic acid benzyl ester (50mg, 0.208 mmol) in acetonitrile (30mL) was placed in glass bottle and the solution was irradiated using UV light (Philips HB/171/A, 4×15 W lamps) for 60 seconds. The solution was then concentrated down to 2mL in a rotary evaporator and mixed with 18 ml of PBS solution. The nanoparticles solution was washed *via* centrifugation (3500rpm, 6 minutes) using PBS and then water. These were then collected with a yield of 0.89%.

3.3.2.2. Negatively charged organic nanoparticle preparation

A mixture of pentaerythritol tetrakis(3-mercaptopropionate) (1.8mg, 0.003 mmol), methacrylic acid (28.8mg, 0.334 mmol), ethylene glycol dimethacrylate (32.4mg, 0.163 mmol), trimethylolpropane trimethacrylate (32.4mg, 0.095 mmol) and N,N-diethyldithiocarbamic acid benzyl ester (50mg, 0.208 mmol) in acetonitrile (30mL) was placed in glass bottle and the solution was irradiated using UV light (Philips HB/171/A, 4×15 W lamps) for 60 seconds. The solution was then concentrated down to 2mL in rotor evaporator and mixed with 18 ml PBS solution. The nanoparticle solution was washed *via* centrifugation (3500rpm, 6 minutes) using PBS and then water. These were then collected with a yield of 0.92%.

3.3.2.3. Neutral organic nanoparticle preparation

A mixture of pentaerythritol tetrakis(3-mercaptopropionate) (1.8mg, 0.003 mmol), acrylamide (23.7mg, 0.333 mmol), ethylene glycol dimethacrylate (32.4mg, 0.163 mmol), trimethylolpropane trimethacrylate (32.4mg, 0.095 mmol) and N, N-diethyldithiocarbamic acid benzyl ester (50mg, 0.208 mmol) in acetonitrile (30mL) was placed in glass bottle and the solution was then irradiated using UV light (Philips HB/171/A, 4×15 W lamps) for 60 seconds. The solution was then concentrated down to

2mL and mixed with 18 ml of PBS solution. The nanoparticle solution was washed *via* centrifugation (3500rpm, 6 minutes) using PBS and then water. These were then collected with a yield of 0.68%.

3.3.2.4. Positively charged aqueous nanoparticle preparation

A mixture of acrylamide (9 mg, 0.126 mmol), N-(3-aminopropyl) methacrylamide (71.4 mg, 0.4 mmol) and N, N′-methylenebisacrylamide (5 mg, 0.032 mmol) in water (50 mL) was prepared, the solution was then flushed under nitrogen gas. The second solution of ammonium persulfate (10 mg, 0.043 mmol) and N, N,N′,N′-tetramethylethylenediamine (7.75 mg, 0.066 mmol) in water (300 µL) was prepared then added to the original solution before being re-flushed under nitrogen. The polymerisation was carried out for 15 minutes before being purged using oxygen. The nanoparticle solution was washed *via* centrifugation (3500 rpm, 6 minutes) using PBS then water. These were then collected with a yield of 0.75%.

3.3.2.5. Negatively charged aqueous nanoparticle preparation

A mixture of acrylamide (9 mg, 0.126 mmol), acrylic acid (28.82 mg, 0.4 mmol) and N, N′-methylenebisacrylamide (5 mg, 0.032 mmol) in water (50 mL) was prepared, the solution was then flushed under nitrogen gas. The second solution of ammonium persulfate (10 mg, 0.043 mmol) and N, N, N′, N′-tetramethylethylenediamine (7.75 mg, 0.066 mmol) in water (300 µL) was prepared then added to the original solution before being re-flushed under nitrogen. The polymerisation was carried out for 15 minutes before being purged using oxygen. The nanoparticle solution was washed *via* centrifugation (3500 rpm, 6 minutes) using PBS then water. These were then collected with a yield of 0.92%.

3.3.2.6. Neutral aqueous nanoparticles preparation

A mixture of acrylamide (35.54mg, 0.5 mmol) and N, N′-methylenebisacrylamide (5mg, 0.032 mmol) in water (50mL) was prepared, the solution was then flushed with nitrogen gas. The second solution of ammonium persulfate (10mg, 0.043 mmol) and N, N, N′, N′-tetramethylethylenediamine (7.75mg, 0.066 mmol) in water (300µL) was prepared then added to the original solution before being re-flushed under nitrogen. The polymerisation was carried out for 15 minutes before being purged using oxygen. The nanoparticle

solution was washed *via* centrifugation (3500rpm, 6 minutes) using PBS then water. These were then collected with a yield of 1.01%.

3.3.3. Nanoparticles analysis:

3.3.3.1. Dynamic light scattering

Nanoparticles sizes were measured using a Zetasizer Nano (Nano-S) particle-size analyser from Malvern Instruments Ltd (UK). A sample of the nanoparticles (1mL) was sonicated for 2 min. DLS analysed the dispersion at 25 °C in a 3 cm3 disposable polystyrene cuvette. Attenuator position, measurement duration and some runs were automatically chosen by the instrument. The values are reported as an average of 8 measurements.

3.3.3.2. UV-Vis spectroscopy

The absorbance of the nanoparticles was measured using a UV-1800 Scanning Spectrophotometer from Shimadzu UK LTD. A sample of the nanoparticles (1mL) was analysed at 25ºC in $1cm^3$ UV-visible cuvette between 190 and 300nm. The software predetermined the scanning speed.

3.3.3.3. RNA-nanoparticle complex sizing

The nanoparticles were analysed by DLS as detailed in part 3.3.3.1. To the nanoparticles, siRNA (25nM in 100µl) was added to each of the nanoparticle solutions, sonicated for 30 seconds. The difference in size was compared between the nanoparticles and nanoparticle-RNA conjugate.

3.3.4. RNA transfection testing

3.3.4.1. Initial screening test.

Initially, all six species of nanoparticles were tested to observe the effects of the nanoparticles on the cells. The nanoparticles were compared against the liposomal delivery vessel used as a transfection reagent used for the delivery of caspase-3 siRNA. The caspase-3 siRNA is designed to prevent the expression of caspase-3 from cells; it was compared to a negative control siRNA, which is a random sequence of nucleotides designed to be similar in mass to the caspase-3 siRNA to act as a non-binding control

species. The TCMK1 cells were seeded in a 48 well plate overnight in cell medium at 37°C with a 5% CO_2 atmosphere. The nanoparticle species underwent sonication for 5 minutes in RNA-free water. All samples were then made up to volume (200µL) with cell media solution before addition to the wells. The cells were incubated at 37°C with a 5% CO_2 atmosphere, the media was then replaced with fresh nutrient solution DMEM/F 12, which was supplemented with 10% Fetal Bovine Solution, 2mM L-glutamine. 100µg/mL penicillin and 100mg mL-1 streptomycin. The caspase-3 was then extracted from the cells *via* digestion of the cells, followed by analysis using UV-Vis (Nanodrop One) to determine the quantity and quality of the RNA. The level of caspase-3 was determined using quantitative PCR. The PCR was carried out using TaqMan expression assay of caspase-3 and GADPH primer utilising a Fast 7500-system. The GADPH level was used for comparison as this protein is present in all cells at a constant level due to its involvement in respiration. Both the caspase-3 and GADPH were amplified in the same well. The caspase-3 was normalised against the GADPH using the $2^{-\Delta\Delta Ct}$ method. The samples were laid out, as shown in Figure 3 – 2.

	1	2	3	4	5	6	7	8
A B C D E	**Non**	**MIP 1**	**MIP 2**	**MIP 3**	**MIP 4**	**MIP 5**	**MIP 6**	**TR**
F	**C3**				**NC**			

Key:

Non = Non-treated cells
MIP X = Nanoparticle species X only
NC = Negative control siRNA only
C3 = Caspase-3 siRNA only
TR = Transfection reagent only

Figure 3 - 2: Microplate layout for nanoparticle screening

3.3.4.2. Optimising of the siRNA loading.

Following the initial work, the amount of siRNA being loaded into the nanoparticles needed to be optimised. The transfection reagent was tested against three different concentrations of caspase-3 siRNA, 20, 30 and 40 µM. The cells were incubated, prepared and analysed as in 3.3.4.1. The samples were laid out, as shown in Figure 3 – 3.

	1	2	3	4	5	6	7	8
A								
B C D E		**Non**	**TR + 20µM C3 siRNA**	**TR + 30µM C3 siRNA**	**TR + 40µM C3 siRNA**	**TR + 30µM NC siRNA**	**TR Only**	
F								

Key:

Non = Non – treated cells **TR =** Transfection Reagent only
TR + 20 µM C3 siRNA = Liposomal transfection reagent with caspase-3 siRNA (20µM)
TR + 30 µM C3 siRNA = Liposomal transfection reagent with caspase-3 siRNA (30µM)
TR + 40 µM C3 siRNA = Liposomal transfection reagent with caspase-3 siRNA (40µM)
TR + 30 µM NC siRNA = Liposomal transfection reagent with negative control siRNA (30µM)

Figure 3 - 3: Microplate layout for optimisation of siRNA concentration

3.3.4.3. Testing organic synthesised nanoparticles.

Based on the results of 3.3.4.2, the organic nanoparticles were incubated with 30 µM C3 siRNA as this was deemed to be the most suitable amount. The cells were incubated, prepared and analysed as in 3.3.4.1. The samples were laid out, as shown in Figure 3 – 4.

	1	2	3	4	5	6	7	8
A B	**MIP 4 + 30 µM C3 siRNA**		**MIP 5 + 30 µM C3 siRNA**		**MIP 6 + 30 µM C3 siRNA**		**TR + 30 µM C3 siRNA**	
C D	**Non**		**C3 Only**		**NC Only**		**TR Only**	
E F	**MIP 4 + 30 µM NC siRNA**		**MIP 5 + 30 µM NC siRNA**		**MIP 6 + 30 µM NC siRNA**		**TR + 30 µM NC siRNA**	

Key:

Non = Non – treated cells **C3 =** Caspase-3 siRNA only
TR = Transfection reagent only (25µM) **NC =** Negative Control siRNA only
MIP X + 30 µM C3 siRNA = Nanoparticle species X with caspase-3 siRNA
MIP X + 30 µM NC siRNA = Nanoparticle species X with negative control siRNA
TR + 30 µM C3 siRNA = Liposomal transfection reagent with caspase-3 siRNA
TR + 30 µM NC siRNA = Liposomal transfection reagent with negative control siRNA

Figure 3 - 4: Microplate layout for testing of the organic nanoparticles

3.3.4.4. Testing aqueous synthesised nanoparticles.

Based on the results of 3.3.4.2, the aqueous nanoparticles were incubated with 30 µM C3 siRNA as this was deemed to be the most suitable amount. The cells were incubated, prepared and analysed as in 3.3.4.1. The samples were laid out, as shown in Figure 3 – 5.

	1	2	3	4	5	6	7	8
A B	**MIP 1 + 30 µM C3 siRNA**		**MIP 2 + 30 µM C3 siRNA**		**MIP 3 + 30 µM C3 siRNA**		**TR + 30 µM C3 siRNA**	
C D	**Non**		**C3 Only**		**NC Only**		**TR Only**	
E F	**MIP 1 + 30 µM NC siRNA**		**MIP 2 + 30 µM NC siRNA**		**MIP 3 + 30 µM NC siRNA**		**TR + 30 µM NC siRNA**	

Key:

Non = Non – treated cells **C3 =** Caspase-3 siRNA only
TR = Transfection reagent only (25µM) **NC =** Negative control siRNA only
MIP X + 30 µM C3 siRNA = Nanoparticle species X with caspase-3 siRNA
MIP X + 30 µM NC siRNA = Nanoparticle species X with negative control siRNA
TR + 30 µM C3 siRNA = Liposomal transfection reagent with caspase-3 siRNA
TR + 30 µM NC siRNA = Liposomal transfection reagent with negative control siRNA

Figure 3 - 5: Microplate layout for testing of the aqueous nanoparticles

3.3.4.5. Testing optimal nanoparticles species.

Based on the results of 3.3.4.3 and 3.3.4.4, the MIP 6 nanoparticles were incubated with 30 µM C3 siRNA as previous. The cells were incubated, prepared and analysed as in 3.3.4.1. The samples were laid out, as shown in Figure 3 – 6.

	1	2	3	4	5	6	7	8
A B C D E F	**Non**	**MIP6 + 30 µM C3 siRNA**	**MIP6 + 30 µM NC siRNA**	**TR + 30 µM NC siRNA**	**TR + 30 µM C3 siRNA**	**C3 Only**	**NC Only**	**MIP 6 Only**

Key:

Non = Non – treated cells **C3 =** Caspase-3 siRNA only
TR = Transfection reagent only (25µM) **NC =** Negative control siRNA only
MIP X + 30 µM C3 siRNA = Nanoparticle species X with caspase-3 siRNA
MIP X + 30 µM NC siRNA = Nanoparticle species X with negative control siRNA
TR + 30 µM C3 siRNA = Liposomal transfection reagent with caspase-3 siRNA
TR + 30 µM NC siRNA = Liposomal transfection reagent with negative control siRNA

Figure 3 - 6: Microplate layout for testing of the optimal nanoparticle species

3.4. Analysis and discussion.

3.4.1. N, N-diethyldithiocarbamic acid benzyl ester

Upon synthesis and analysis of the N, N-diethyldithiocarbamic acid benzyl ester the resultant oil was found to be pure and free from solvent via NMR analysis showing no residual solvent peaks for chloroform. The compound is a photosensitive initiator for UV light-initiated polymerisation. Until exposed to UV light the molecule remains unreactive; however, upon UV irradiation, the molecule produces free radicals allowing polymerisation to occur. These properties can also be used to perform a secondary polymerisation to graft a second polymer layer to a polymer nanoparticle.

3.4.2. Nanoparticles synthesis

The nanoparticles were successfully synthesised as described in 3.3.2. The nanoparticles were successfully washed *via* centrifugation resulting in a concentrated solution of nanoparticles in phosphate buffer saline (4mL). The collected nanoparticles were stored at 4^{o}C until needed.

3.4.3. Nanoparticles analysis

3.4.3.1. Dynamic light scattering

The nanoparticle size was determined using DLS to see the size of the nanoparticles in solution. Testing of the nanoparticles occurred without the presence of any additional chemicals or RNA present. The results are shown in Table 3 – 1 (Appendix 3).

Table 3 - 1: Table showing the size of the nanoparticles used for the siRNA transfection

Species	Size	Standard De*via*tion
MIP 1 – Positive Aqueous	124.55 nm	± 7.05 nm
MIP 2 – Negative Aqueous	124.13 nm	± 13.87 nm
MIP 3 – Neutral Aqueous	119.43 nm	± 18.75 nm
MIP 4 – Positive Organic	133.07 nm	± 21.29 nm
MIP 5 – Negative Organic	145.16 nm	± 24.08 nm
MIP 6 – Neutral Organics	162.59 nm	± 15.43 nm

All six species of nanoparticle demonstrated a size between 120 and 165nm, small enough to enter cells for delivery of siRNA and drug molecules.

3.4.3.2. The concentration of the nanoparticles

UV-Vis spectroscopy is used to determine the absorbance and concentration of the nanoparticles. The UV-Vis reading is taken from the measurement at 197nm before being used to calculate the concentration. The results are shown in Table 3 – 2.

Table 3 - 2: Table showing the concentration of the nanoparticles used for the siRNA transfection

Species	Concentration	Standard de*via*tion
MIP 1 – Positive aqueous	0.406 nM	± 0.02 nm
MIP 2 – Negative aqueous	0.814 nM	± 0.09 nm
MIP 3 – Neutral aqueous	0.737 nM	± 0.12 nm
MIP 4 – Positive organic	1.862 nM	± 0.30 nm
MIP 5 – Negative organic	1.741 nM	± 0.29 nm
MIP 6 – Neutral organics	1.987 nM	± 0.19 nm

The concentration of the nanoparticles is similar between the species, with the aqueous being between 0.4 and 0.8nM. Whereas, the organic nanoparticles have a slightly higher concentration between 1.7 and 2.0nM. These concentrations show that the nanoparticles produced in organic solvents had a higher yield than the aqueous.

3.4.3.3. Nanoparticle-RNA complex size.

To determine the change in nanoparticles size when incubated in solution with the siRNA, DLS was used to analyse the mixture. The results are shown in Table 3 – 3 and figure 3 – 7 (Appendix 4).

Table 3 - 3: Table showing the size of the nanoparticles used for the siRNA transfection before and after incubation with RNA

Species	Pre-RNA incubation size	Standard de*via*tion	Post-RNA incubation size	Standard de*via*tion
MIP 1	124.55 nm	± 7.05 nm	239.35 nm	± 20.10 nm
MIP 2	124.13 nm	± 13.87 nm	232.65 nm	± 18.68 nm
MIP 3	119.43 nm	± 18.75 nm	253.83 nm	± 16.30 nm
MIP 4	133.07 nm	± 21.29 nm	235.76 nm	± 12.12 nm
MIP 5	145.16 nm	± 24.08 nm	235.11 nm	± 13.57 nm
MIP 6	162.59 nm	± 15.43 nm	233.42 nm	± 12.53 nm

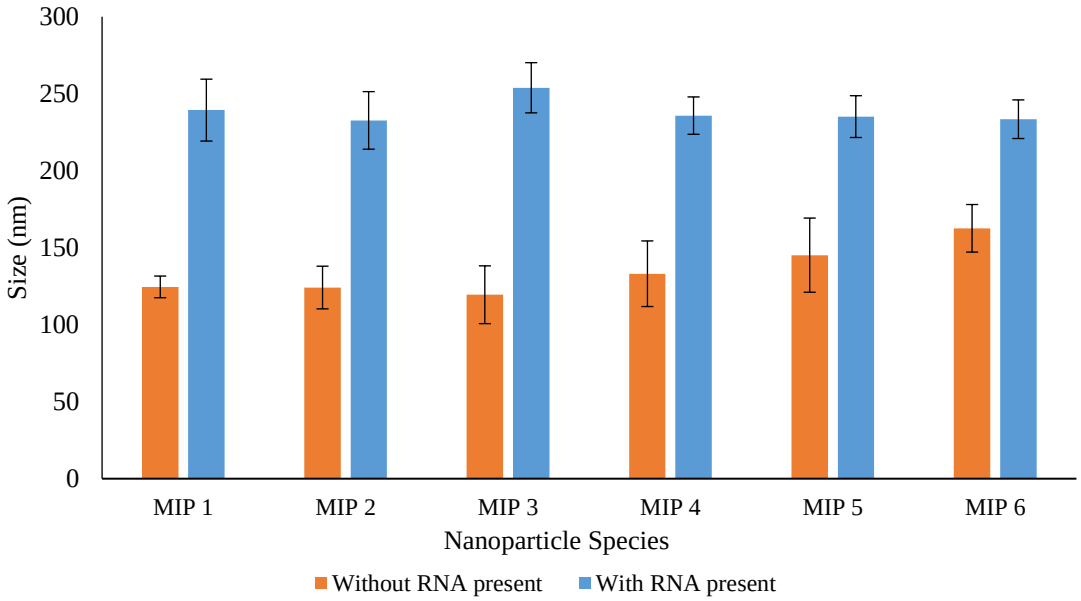

Figure 3 - 7: Graph showing the size of the nanoparticles with and without siRNA

When the nanoparticles undergo incubation with the siRNA, the nanoparticles undergo a size increase. The size increases by approximately 130nm. This increase is likely due to a combination of the RNA forming a shell around the nanoparticle, and the nanoparticles undergo aggregation in solution in the presence of siRNA. Unusually, the negatively charged nanoparticles were expected to repulse the siRNA, which is has a negative charge. However, the size of the complex was the same as the other nanoparticle species.

3.4.4. siRNA transfection testing

To assess the *via*bility of the nanoparticle as a transfection agent for caspase-3 siRNA, a series of transfection studies were carried out to identify the species with the highest potential. The cell testing was carried out in collaboration with Dr Bin Yang from the Department of Infection, Inflammation and Immunity.

3.4.4.1. Initial screening test.

Cells initially underwent incubation with each of the different nanoparticle species without siRNA present. This experiment was carried out to observe the effect of nanoparticles on the levels of caspase-3 in the cells. For comparison, some of the cells underwent incubation with the liposomal delivery vector (TR), Caspase-3 siRNA (C3) and Negative Control siRNA (NC). The caspase-3 levels were averaged from all the corresponding wells then compared against the levels of the protein GADPH, which is

present at constant levels in cells due to its use in cellular metabolism. The results are shown in Table 3 – 4 and figure 3 – 8.

Table 3 - 4: Table showing the ratio of Caspase-3 to GADPH after nanoparticle screening study

Species	The ratio of C3 to GADPH	Standard de*via*tion
Non-treated cells	1.000	± 0.001
MIP 1 – nanoparticles only	1.722	± 0.010
MIP 2 – nanoparticles only	1.468	± 0.006
MIP 3 – nanoparticles only	1.331	± 0.022
MIP 4 – nanoparticles only	0.000	-
MIP 5 – nanoparticles only	0.000	-
MIP 6 – nanoparticles only	0.945	± 0.018
Transfection reagent only	1.182	± 0.034
Negative control siRNA only	1.037	± 0.022
Caspase-3 siRNA only	0.852	± 0.005

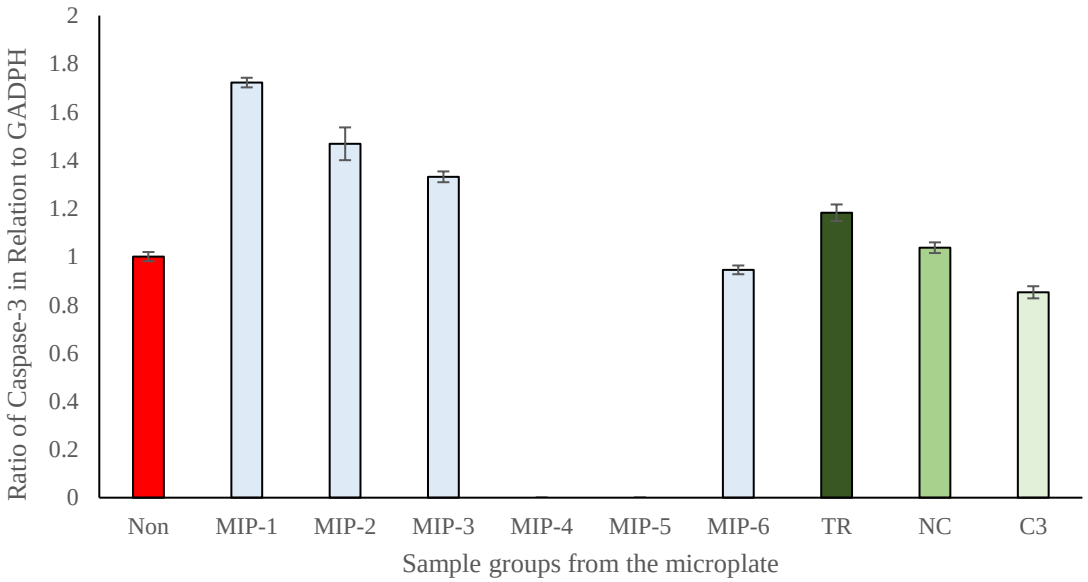

Figure 3 - 8: Graph showing the ratio of C-3 displayed for each of the nanoparticles during the initial nanoparticle screening

In the wells treated with the aqueous nanoparticles (MIP 1, 2 and 3) an increase in caspase-3 expression was observed in comparison to the untreated cells (non) it was expected that there would be no significant change in the caspase-3 levels when incubated with the nanoparticles. The wells treated with two charged species of the organic nanoparticles (MIP 4 and 5) had no measurable levels of caspase-3 due to the death of the cells during the incubation. The wells treated with the neutral organic nanoparticle species (MIP 6), showed a small decrease in the level of caspase-3 which is unexpected considering the cells treated with the charged organic nanoparticles (MIP 4 and 5) perished during incubation. The liposomal transfection agent (TR) showed a slight

increase in caspase-3 level. The negative control (NC) siRNA sequence had the expected effect with a minimal increase in caspase-3 level observed. The caspase-3 (C3) siRNA had the anticipated effect of a decrease in caspase-3 level observed.

3.4.4.2. Optimising of the siRNA loading.

Secondly, the optimal amount of siRNA was identified, using the liposomal transfection agent (TR). The transfection agent underwent incubation with three different concentrations of caspase-3 siRNA (C3) and a standard concentration of the negative control siRNA (NC). As in the previous experiments, the levels of caspase-3 are compared to the levels of GADPH. The results are shown in Table 3 – 5 and figure 3 – 9.

Table 3 - 5: Table showing the ratio of Caspase-3 to GADPH after siRNA concentration screening study

Species	The ratio of C3 to GADPH	Standard deviation
Non-treated cells	1.000	± 0.019
Transfection reagent only	0.952	± 0.027
Transfection reagent with C3 siRNA @ 20nM	0.641	± 0.010
Transfection reagent with C3 siRNA @ 30nM	0.577	± 0.009
Transfection reagent with C3 siRNA @ 40nM	0.707	± 0.008
Transfection reagent with NC siRNA @ 30nM	1.247	± 0.008

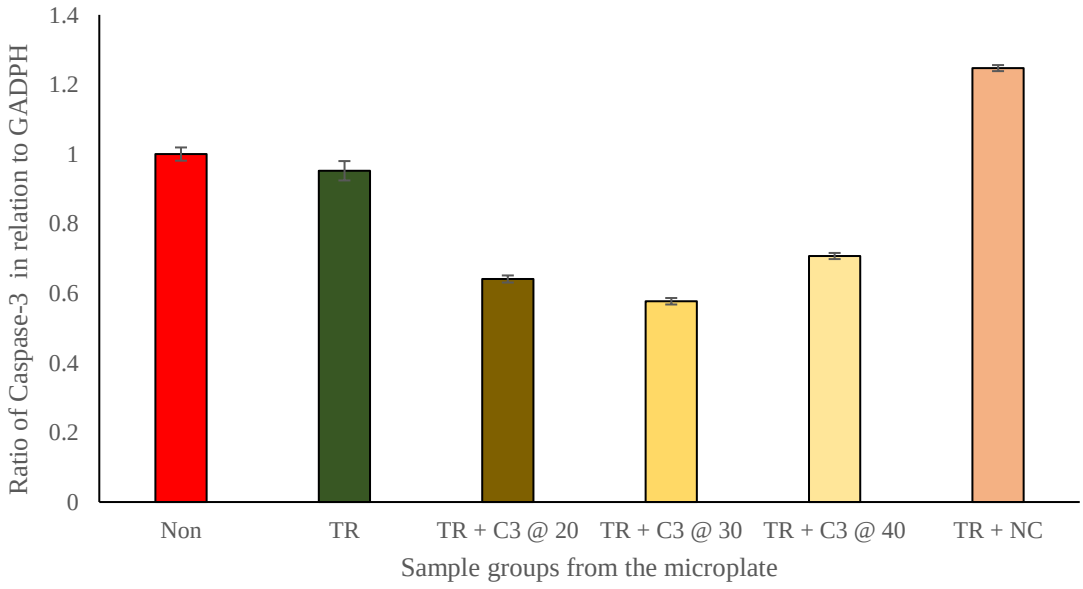

Figure 3 - 9: Graph showing the ratio of C-3 displayed for each of the siRNA concentrations during optimisation

In the wells treated with only the liposomal transfection agent (TR) a small decrease in caspase-3 levels was observed in comparison to the untreated cells (non), the expectation was that there would be no significant change in the caspase-3 levels when incubated with

the liposomes. The wells treated with transfection reagent loaded with the caspase-3 siRNA displayed a significant decrease in the level of caspase-3 expressed by the cells, with the transfection reagent loaded with 30 µM of caspase-3 siRNA demonstrating the most significant reduction in expression. The level of caspase-3 expression was expected to decrease with the delivery of caspase-3 siRNA to the cells. However, the expectation was that a more significant change in caspase-3 expression would occur with the highest concentration of caspase-3 siRNA administered. The transfection agent loaded with the negative control siRNA displayed a substantial increase in the expression of caspase-3; this was unexpected as the negative control siRNA should not affect the caspase-3 levels.

3.4.4.3. Testing the organic synthesised nanoparticles.

Thirdly, the nanoparticle synthesised in organic solvents underwent incubation with the optimal amount of caspase-3 and negative control siRNA (30uM). The levels of caspase-3 recorded from the nanoparticles loaded with siRNA were compared to the caspase-3 level from the incubation with the TR with and without siRNA along with the free siRNAs. As in previous experiments, the levels of caspase-3 is compared to the level of GADPH. The results are shown in Table 3 – 6 and figure 3 – 10.

Table 3 - 6: Table showing the ratio of Caspase-3 to GADPH after the organic nanoparticle study

Species	The ratio of C3 to GADPH	Standard de*via*tion
Non-treated cells	1.000	± 0.019
MIP 4 loaded with C3-siRNA	0.000	-
MIP 5 loaded with C3-siRNA	0.000	-
MIP 6 loaded with C3-siRNA	0.975	± 0.037
MIP 4 loaded with NC-siRNA	0.000	-
MIP 5 loaded with NC-siRNA	0.000	-
MIP 6 loaded with NC-siRNA	1.102	± 0.015
Transfection reagent with C3 siRNA	0.612	± 0.015
Transfection reagent with NC siRNA	1.189	± 0.015
Transfection reagent only	1.012	± 0.029
Negative control siRNA only	1.044	± 0.022
Caspase-3 siRNA only	0.952	± 0.009

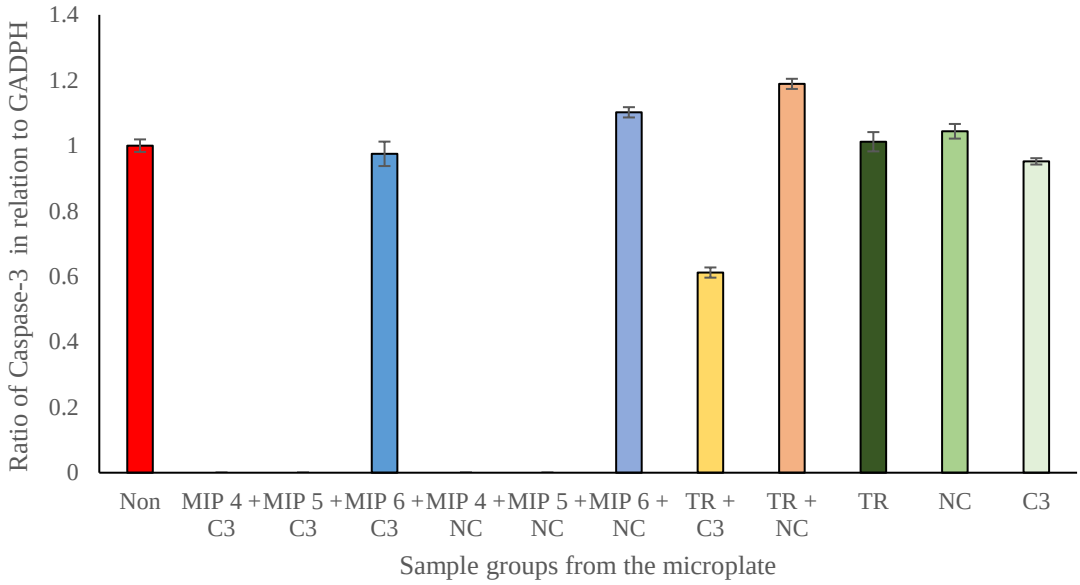

Figure 3 - 10: Graph showing the ratio of C-3 displayed for each of the nanoparticles during the organic nanoparticle testing

In the wells treated with charged species of the organic nanoparticles (MIP 4 and 5) when loaded with both the caspase-3 siRNA and the negative control, siRNA had no measurable level of caspase-3 due to the death of the cells during incubation. The wells treated with the neutral organic nanoparticle species (MIP 6) loaded with caspase-3 siRNA showed a marginal decrease in caspase-3 levels compared to the untreated cells (non), whereas, MIP 6 loaded with the negative control siRNA showed a marginal increase in the level of caspase-3 expression. The level of caspase-3 was expected to decrease with the delivery of caspase-3 siRNA *via* the MIP 6 along with there being no effect on the level of caspase-3 expression when treated with MIP 6 loaded with the negative control siRNA.

In contrast, the liposomal transfection agent (TR) showed a slight increase in caspase-3 levels. The negative control (NC) RNA sequence had the expected effect with a minimal increase in caspase-3 levels observed. The caspase-3 (C3) siRNA had the anticipated effect of a decrease in caspase-3 levels observed. The transfection agent loaded with caspase-3 siRNA demonstrated a significant reduction in the level of caspase-3 expression compared to the untreated cells (Non), whereas, the transfection agent loaded with the negative control siRNA caused a slight increase in the level of caspase-3 expression. These results were as expected due to their similarity to the last experiment.

3.4.4.4. Testing the aqueous synthesised nanoparticles.

Thirdly, the nanoparticle synthesised in aqueous solvents underwent incubation with the optimal amount of caspase-3 and negative control siRNA (30uM). The levels of caspase-3 recorded from the nanoparticles loaded with siRNA were compared to the caspase-3 level from the incubation with the TR with and without siRNA along with the free siRNAs. As in previous experiments, the levels of caspase-3 is compared to the level of GADPH. The results are shown in Table 3 – 7 and figure 3 – 11.

Table 3 - 7: Table showing the ratio of Caspase-3 to GADPH after the aqueous nanoparticle study

Species	The ratio of C3 to GADPH	Standard deviation
Non-treated cells	1.000	± 0.019
MIP 4 loaded with C3-siRNA	1.567	± 0.028
MIP 5 loaded with C3-siRNA	1.492	± 0.021
MIP 6 loaded with C3-siRNA	1.999	± 0.027
MIP 4 loaded with NC-siRNA	0.772	± 0.018
MIP 5 loaded with NC-siRNA	0.996	± 0.089
MIP 6 loaded with NC-siRNA	1.114	± 0.015
Transfection reagent with C3 siRNA	0.598	± 0.015
Transfection reagent with NC siRNA	1.099	± 0.015
Transfection reagent only	0.984	± 0.028
Negative control siRNA only	1.181	± 0.025
Caspase-3 siRNA only	0.891	± 0.015

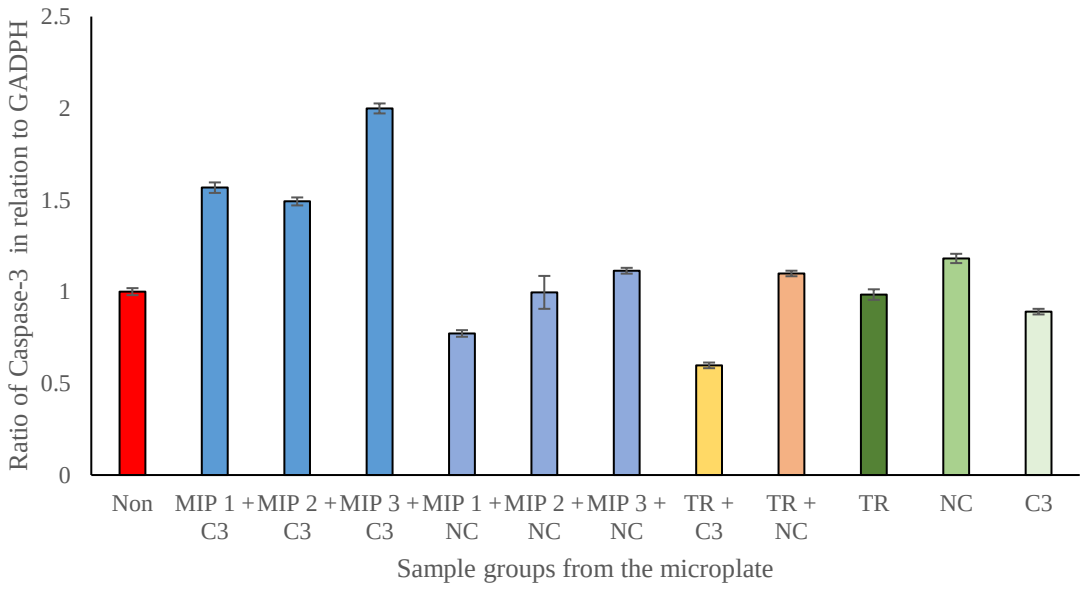

Figure 3 - 11: Graph showing the ratio of C-3 displayed for each of the nanoparticles during the aqueous nanoparticle testing

All the wells treated with the aqueous nanoparticle species (MIPs 1, 2 and 3) loaded with the caspase-3 siRNA demonstrated a significant increase in the levels of expression of

caspase-3 with neutral species (MIP 3) displaying a level of caspase-3 almost double the untreated cell (Non). This increase is unexpected as the delivery of caspase-3 siRNA should have demonstrated a decrease or marginal change in caspase-3 expression. However, the change in caspase-3 expression is quite significant. Whereas the wells treated with the positively charged nanoparticle species (MIP 1) loaded with the negative control demonstrated a decrease in the level of caspase-3 expression, this was unexpected as the negative control siRNA should not have any effect on the expression of caspase-3 expression. However, the negative and neutral species of nanoparticle (MIP 2 and 3) demonstrated marginal changes in the level of caspase-3 expression; this was as expected as the negative control siRNA should not have any effect on the expression of caspase-3. The wells treated with the loaded and unloaded transfection reagent (TR) demonstrated similar results to the previous experiment as expected. The wells treated with both free siRNA species demonstrated a similar effect to the earlier experiments.

All the nanoparticle species, when loaded with the caspase-3 siRNA, demonstrate a significant increase in the levels of caspase-3, species 3 demonstrates a 99% increase in caspase-3 levels. However, this is the opposite of the desired effect. Nanoparticles species 1 and 2 demonstrate an increase of 56% and 49% of the levels of caspase-3 respectively, while this is not as significant as species three it is the inverse of the expected result. Interestingly the negative control loading nanoparticles of species 1 and 2 demonstrated a decrease in caspase-3 levels, which is unusual considering the negative control siRNA should not affect the levels of caspase-3. However, nanoparticle species three loaded with negative control siRNA showed a slight increase in the caspase-3 level. The control samples demonstrate similar levels to the previous results. The liposomal transfection agent with the caspase-3 loaded displayed a significant effect with a decrease of 41%.

3.4.4.5. Testing the optimal nanoparticle species.

Finally, based on the results from 3.4.4.3 and 3.4.4.4, nanoparticle species six were retested to determine the effect on caspase-3 levels. The nanoparticles were incubated with the caspase-3 siRNA and NC siRNA (30uM) and compared to the liposomal transfection agent incubated with the siRNA and the free siRNA without a delivery agent. The results are shown in Table 3 – 8 and figure 3 – 12.

Table 3 - 8: Table showing the ratio of Caspase-3 to GADPH after the optimal nanoparticle species testing

Species	The ratio of C3 to GADPH	Standard deviation
Non-treated cells	1.000	± 0.0191
MIP 6 – Nanoparticles only	1.192	± 0.0230
MIP 6 loaded with C3-siRNA	0.987	± 0.0379
MIP 6 loaded with NC-siRNA	1.351	± 0.0170
Transfection reagent only	0.991	± 0.0289
Negative control siRNA only	0.984	± 0.0211
Caspase-3 siRNA only	0.906	± 0.0154
Transfection reagent with C3 siRNA	0.604	± 0.0155
Transfection reagent with NC siRNA	1.345	± 0.0162

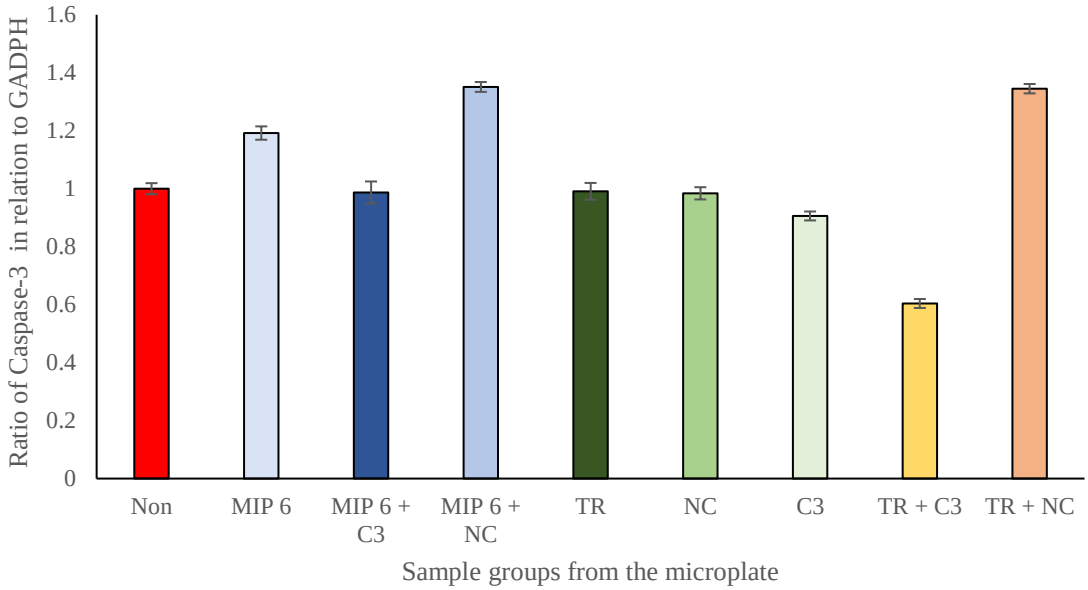

Figure 3 - 12: Graph showing the ratio of C-3 displayed for the nanoparticles during the ideal nanoparticle testing

The wells treated with the unloaded MIP 6 species nanoparticle demonstrated a small increase in the level of caspase-3 expression, this was unusual as there should be a negligible effect of the nanoparticles on the level of caspase-3 expression. It was observed that in the wells treated with MIP 6 loaded with the negative control siRNA there was an

increase in the level of caspase-3 expression, this was unexpected as the negative control siRNA should have minimal effect on the levels of caspase-3 expression. Whereas, the wells treated with MIP 6 species loaded with the caspase-3 siRNA demonstrated a negligible change in the level of caspase-3 expression. This result was unexpected as the caspase-3 siRNA should decrease the level of caspase-3 expression within cells. The liposomal transfection agent and negative control siRNA both displayed a negligible change in the levels of caspase-3 expression as expected. The caspase-3 siRNA on its own demonstrated a small decrease in the level of caspase-3 as expected. The wells treated with the transfection agent loaded with the negative control siRNA demonstrated a slight increase in the levels of caspase-3 expression, this is unusual as the negative control siRNA should not affect the level of caspase-3 expression. However, the transfection agent loaded with the caspase-3 siRNA demonstrated a significant decrease in the level of caspase-3 expression as was expected.

3.5 Conclusions

In this study, we investigated the potential use of MIP nanoparticles for the transfection of siRNA into renal cells from mice. The nanoparticles were synthesised *via* two different methods to see if there were any advantages between the aqueous or organic solvent synthesised nanoparticles. Initially, the nanoparticles were characterised, followed by observation of size changes of the nanoparticle in the presence of the RNA *via* dynamic light scattering analysis. The results from this showed that a significant increase in the size of the nanoparticles occurred, this is due to one of two causes, the nanoparticles undergoing aggregation or the formation of an RNA shell around some of the charged nanoparticle species as a result of electrostatic interactions. Results from this were not conclusive; however, as they all showed a similar change in size compared to the original nanoparticle readings.

The next stage of this study was to investigate the effect of nanoparticles only on the expression of caspase-3 in cells without the presence of caspase-3 siRNA. The results were unexpected as the nanoparticles themselves should not have had any effect on the levels of caspase-3 expression. The most significant effect of the nanoparticles was seen with charged species produced in organics (MIP 4 and 5) where no results were obtainable. This could be due to the nanoparticles affecting the cells or due to complications in the incubation process.

When the aqueous synthesised nanoparticles underwent loading with both the caspase-3 and negative control siRNA, the results obtained were unusual. The nanoparticles loaded with the caspase-3 siRNA demonstrated a significant increase in caspase-3 expression; this is unusual as the siRNA should reduce the level of caspase-3 expression. This indicates that the siRNA is not being delivered to the cell or that the nanoparticles are having an adverse effect. However, when the nanoparticles underwent loading with the negative control siRNA, two of the species (MIP 2 and 3) displayed a minimal change in caspase-3 expression. However, MIP 1 displayed a significant decrease in caspase-3 expression; this is unusual as the negative control siRNA should not have any effect on the level of caspase-3 expression.

When the organic solvent synthesised nanoparticles underwent loading with both the caspase-3 and negative control siRNA species, unexpected results were obtained. With the two-charged species (MIP 4 and 5) loaded with both types of siRNA, no results were obtainable due to cell death. This is likely due to interference from the nanoparticles or

due to complications in the incubation process. However, the neutral species (MIP 6) demonstrated the results expected. With the negative control siRNA there was a small increase in the level of caspase-3 expression which is likely caused by the presence of the negative control siRNA, whereas when loaded with the caspase-3 siRNA a small decrease in caspase-3 expression, this is a good result however the effect is negligible compared to the effect seen with the transfection reagent loaded with caspase-3 siRNA. Based on this study, the nanoparticles demonstrate a potential for transfection of siRNA into cells. However, the nanoparticles require further testing, with different compositions being tested to determine the ideal charge for transfection of the RNA. Also, the transfection should be tested on a broader range of cells to determine the effects in other cells.

Chapter 4: Magnetic core nanoparticles as a delivery vector for doxorubicin

4.1. Introduction

4.1.1. Background of doxorubicin

Doxorubicin is an anthracycline-based antitumor antibiotic compound used for the treatment of several types of cancer *via* chemotherapy including, leukaemias, Hodgkin's lymphoma, multiple myeloma, soft tissue sarcoma and cancers of the following areas, bladder, breast, stomach, lung, ovaries and the thyroid.[100]

Doxorubicin is one of the most potent anticancer drugs currently used in chemotherapy. Unfortunately, it must be administered in small doses over several treatments due to severe side effects. Doxorubicin is dissolved into saline or water at a nominal concentration of 30mg/kg, before injection. The doxorubicin solution is then administered *via* intravenous injection (IV) into a vein located near to a tumour. The dose of doxorubicin undergoes injection over several minutes, with attention being given to the injection site, as adverse reactions such as phlebosclerosis and extravasation tissue necrosis can develop.[101] The primary issue with anthracycline-based drugs is that they possess a high level of cardio-toxicity compared to the other types of anticancer drugs. To prevent permanent cardiological damage occurring a lifetime dosage limit of doxorubicin has been set to 500–550 mg/kg based on the size of the patient.[102] The second issue with doxorubicin can also cause the development of neutropenic enterocolitis, also known as typhlitis. This condition is an acute life-threatening infection which occurs within the cecum section of the bowel. This condition results from a decrease in the level of neutrophil granulocytes, the most common type of white blood cells. This condition is treatable, however, if untreated can spread through the gut and be fatal.[103] The third issue is that doxorubicin can cause chemotherapy-induced acral erythema, also referred to as the hand-foot syndrome. This condition causes the skin on a patient's hands and feet to become numb to touch, leading to severe pain and swelling. This condition is reversible and usually recedes after treatment. These conditions alongside doxorubicin's colour are why the drug is known as 'the red devil'.[104]

4.1.2. Chemistry of doxorubicin

Doxorubicin is semi-synthesised from the bacterium, Streptomyces peucetius. Streptomyces peucetius produces a naturally occurring daunorubicin. This is then artificially modified to form doxorubicin *via* the hydroxylation of the carbons in the 4 and 14 positions on the tetracyclic ring. Doxorubicin consists of two main components, an Aglyconic tetracycle backbone and a Daunosamine sugar group.

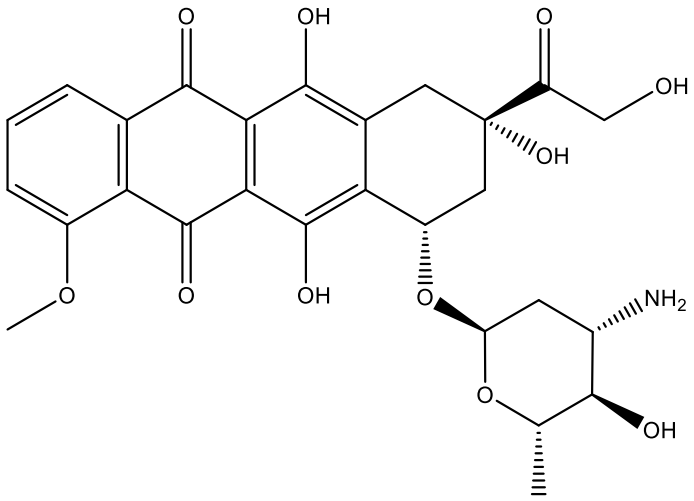

Figure 4 - 1: Structure of Doxorubicin

The aglyconic tetracycle is composed of four hexacyclic rings sharing intermediary bonds. The 1st and 3rd ring (starting from the left Figure 4-1) are aromatic, with each of the hexacyclic rings possesses a different functional moiety. On the first ring is a methoxy group attached in the 4-position, on the second ring is a quinone group, on the third ring, is a hydroquinone group and the last is a hexane ring with a carbonyl and a hydroxyl group in the 2-position. In the 4-position on the 4th ring of the tetracyclic group, a glycosidic group couples a daunosamine sugar group to the molecule. The tetracyclic part of the molecule functions as the fluorophore for the molecule, generating two peaks on a fluorescence spectrum, with the primary one at 580nm and a secondary one at 550nm.

4.1.3. Mechanism of doxorubicin action

Doxorubicin works *via* two methods when it reaches a cancer cell, intercalation of the DNA and inhibition of the biosynthesis of macromolecules. Doxorubicin intercalates into the DNA strands using the tetracyclic part to link the two DNA strands together *via* interaction with two opposing base pairs. The daunosamine sugar then fits into a small

groove in the DNA strand to interact with the base pairs adjacent to the intercalation site.[105]

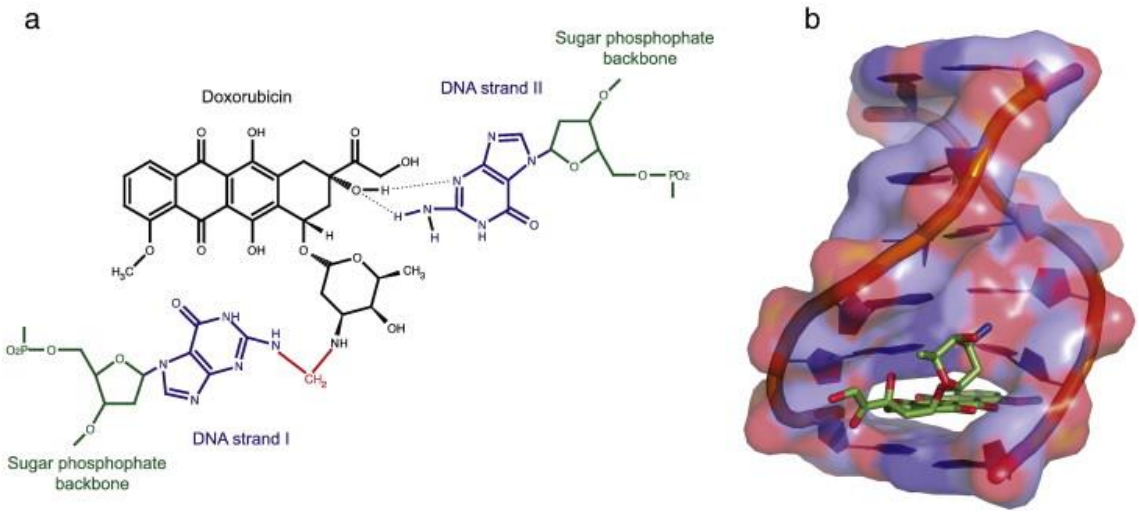

Figure 4 - 2: A) Diagram of Doxorubicin – Nucleotide interactions[106] B) Schematic of doxorubicin intercalation[106]

Doxorubicin inhibits the biosynthesis of macromolecules *via* blocking the progression of the enzyme topoisomerase II. Topoisomerase II is used to cut the DNA double strands *via* ATP hydrolysis, allowing DNA transcription to take place.[107]

4.1.4. Detection methods of doxorubicin

Typically, there are two main methods for detecting and determining the concentration of doxorubicin in solution, UV-Vis and fluorescent spectroscopies.

4.1.4.1. UV-Vis to determine drug concentration

Typically, UV-Vis absorbance spectrometry is used to determine drug concentration and absorbance properties. UV-Vis spectroscopy works by shining a light at a specific wavelength through a sample and determining how much light is absorbed by the solution. The amount of light absorbed is proportional to the number of molecules present in the solution. This absorbance reading is compared to a series of absorbance readings for a series of known concentration for doxorubicin; from this, the concentration can be determined. The main issue with using UV-Vis to determine the concentration is that only millimolar concentrations of small molecules can be detected.[108]

4.1.4.2. Fluorescence to determine drug concentration

Molecules which possess conjugation can generate a fluorescent emission, the strength of this fluorescence is highly dependent on the stability of the conjugated system within a molecule. Fluorescence is generated *via* irradiation of a conjugated system with a specific wavelength of light. Usually, this wavelength is the same as the absorption wavelength for a molecule. The electrons in the conjugated system become excited and move into higher energy states.[109]

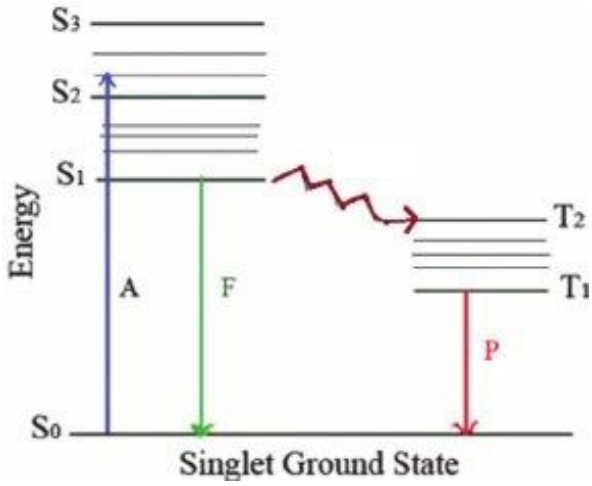

Figure 4 - 3: Jablonksi diagram of a fluorescence[110]

Some of the energy is then released from the electrons causing them to drop to a lower excited state, however, to return to the original ground state, the electron releases the remaining energy as a photon. Due to this light possessing less energy than the original excitation light, the emission is generated using a lower amount of energy, resulting in the light being emitted at a longer wavelength. Fluorescence is far more sensitive compared to UV-Vis as the fluorescence is proportional to the number of fluorophores in a molecule. The temperature of a molecule also affects the fluorescent emission of the molecule. As the temperature increases, more electrons are excited to higher electron energy levels resulting in a stronger light emission being generated.[111] As fluorescence readings are concentration dependent; they can be compared against a series of known concentrations to determine an unknown in a similar way to UV. Like all methods of measurement, fluorescence has its advantages and disadvantages. The main advantage is that fluorescence can be used to detect concentrations at the nanomolar range, unlike UV. However, fluorescence cannot be used on high concentrations as the solution can undergo fluorescent quenching; this is where the light emitted from the molecules is absorbed by the surrounding molecules, which reduces the reading.[112]

Initially, doxorubicin was incorporated into magnetic core nanoparticles synthesised utilising an organic solvent-based polymerisation. These nanoparticles were then used as a targeting vector. Magnetic core nanoparticles were synthesised utilising iron oxide nanoparticles as the magnetic component in the core of the nanoparticle with a polymer shell containing doxorubicin. The magnetic nanoparticles are based on the nanoparticles previously developed by the Piletsky group for the controlled delivery of curcumin.[113] Curcumin is a naturally occurring phenol from the curcuminoid group of molecules extracted from the *Curcuma longa* plant.[114] Using the research carried out by the group, the loading and retention of doxorubicin inside the magnetic nanoparticles was investigated.

The nanoparticles were synthesised using an organic solvent to reduce the risk or biological contamination and facilitate an easier rate of nanoparticle extraction. The nanoparticles were then dispersed into a fresh solution containing doxorubicin to reload the nanoparticles. The nanoparticles then underwent release testing to determine the release profile of the nanoparticles over time in solution to determine their suitability as a drug delivery system.

4.1.5. Aim and objectives

Aim of the chapter:

- Synthesis and testing of magnetic core nanoparticles for the controlled release of doxorubicin over time.

Objectives for this chapter:

- Synthesis of magnetic core nanoparticles using organic solvent-based solution phase nanoparticle synthesis using different functional monomers.
- Testing of the release of doxorubicin from the nanoparticles with the different functional monomer
- Comparing the doxorubicin imprinted nanoparticles against the non-imprinted nanoparticles.

4.2. Chemicals

N, N-Diethyldithiocarbamic acid benzyl ester was synthesised as described in chapter 3. A dialysis membrane (Spectra/Por, MWCO = 10 kDa) was purchased from Spectrum Laboratories Inc. Amicon Ultra-15 Centrifugal Filter Units (MWCO 30 kDa) and Acetonitrile were obtained from Fisher Scientific (UK). Ethanol, Trimethylolpropane trimethacrylate, Tetraethyl thiuram disulphide, Iron oxide particles, 2-Hydroxymethyl acrylate, Methacrylic acid, Itaconic acid, Ethylene glycol dimethacrylate, EDTA, Methanol were all purchased from Sigma Aldrich (Dorset UK). Doxorubicin Hydrochloride was purchased from Cambridge Bioscience, UK. Ultrapure water was produced by a Millipore Milli-Q system (Millipore, Bedford, MA, USA), Double-distilled ultrapure water (Millipore) was used for analysis. All chemicals and solvents were analytical or HPLC grade and were used without further purification. Phosphate buffered saline was prepared as directed from PBS buffer tablets (Sigma-Aldrich, Gillingham, UK).

4.3. Methods

4.3.1. Preparation of organic synthesised nanoparticles in solution

A stock solution of the initiator and cross-linking monomer was prepared. To one-half, doxorubicin was added while the other half contained no doxorubicin. A series of ten different nanoparticle species were produced using five different functional monomers with one of each containing doxorubicin and one of each containing no doxorubicin.

4.3.1.1. Synthesis of molecularly imprinted nanoparticles in the presence of doxorubicin

A stock solution is containing trimethylolpropane trimethacrylate (29.1 g, 85 mmol), Doxorubicin (5 mg, 9.2 µmol), tetraethyl thiuram disulphide (300 mg, 1.1 mmol) and diethyldithiocarbamic acid benzyl ester (15ug, 62.6nmol) in acetonitrile (38 mL). This solution was ultra-sonicated for 10 minutes (using a Fischer brand 15094 ultrasound Bath). Iron oxide particles (100 mg) and Functional monomer (See table) were added to a portion of the stock solution (10 g). The solution was ultra-sonicated for 15 minutes (using a Fischer Brand 15094 Ultrasound Bath). The solution was purged with nitrogen for 10 minutes. The solution was then irradiated using Ultra-Violet light for 150 minutes (using 4 x Philips HB/171/A lamps) with occasional mixing. The nanoparticles were collected using a magnet before being washed with acetonitrile (3 x 10 mL) and water (2 x 10 mL) before resuspension in water (15 mL). List of species produced listed in Table 4 – 1.

Table 4 - 1: Table showing the list of nanoparticle species and their corresponding functional monomer to be tested

Nanoparticle species	**Functional monomer species**	**Mass**	**Moles**
MIP-MD-1	2-Hydroxy methyl acrylate	46 mg	448 µmol
MIP-MD-2	Methacrylic acid	34.4 mg	400 µmol
MIP-MD-3	Itaconic acid	52 mg	400 µmol
MIP-MD-4	Ethylene glycol methacrylate	84 mg	400 µmol
MIP-MD-5	None	-	-

4.3.1.2. Synthesis of non-imprinted nanoparticles without doxorubicin

A stock solution containing trimethylolpropane trimethacrylate (29.1 g, 85 mmol), tetraethyl thiuram disulphide (300 mg, 1.1 mmol) and diethyldithiocarbamic acid benzyl ester (15 µg, 62.6 nmol) in acetonitrile (38 mL). This solution was ultra-sonicated for 10

minutes (using a Fischer brand 15094 ultrasound bath). Iron oxide particles (100 mg) and functional monomer (See table) were added to a portion of the stock solution (10 g). The solution was ultra-sonicated for 15 minutes (using a Fischer brand 15094 ultrasound bath). The solution was purged with nitrogen for 10 minutes. The solution was then irradiated using Ultra-Violet light for 150 minutes (using 4 x Philips HB/171/A lamps) with occasional mixing. The nanoparticles were collected using a magnet before being washed with acetonitrile (3 x 10 mL) and water (2 x 10 mL) before resuspension in water (15 mL). List of species produced listed in Table 4 – 2.

Table 4 - 2: Table showing the list of nanoparticle species and the amount of functional monomer required

Nanoparticle species	**Functional monomer species**	**Mass**	**Moles**
MIP-MN-1	2-Hydroxy methyl acrylate	52 mg	448 µmol
MIP-MN-2	Methacrylic acid	34.4 mg	400 µmol
MIP-MN-3	Itaconic acid	52 mg	400 µmol
MIP-MN-4	Ethylene glycol methacrylate	84 mg	400 µmol
MIP-MN-5	None	-	-

4.3.2. The release profile of doxorubicin from nanoparticles

To determine the effect of the functional monomer on the release profile of the nanoparticles, release testing was carried out with concentration monitored by fluorescence. To determine the effect of doxorubicin incorporation in the polymerisation mixture, the imprinted and non-imprinted species were compared.

4.3.2.1. The release profile of doxorubicin loaded into the molecularly imprinted nanoparticles solution phase

A solution of doxorubicin (1 mg, 1.84 µmol) in distilled water (5 mL) was prepared, an aliquot (1 mL) was prepared. To this aliquot, molecularly imprinted magnetic nanoparticles (100mg) were added. The solution was then stored at 4^{o}C overnight. The magnetic particles were removed from the solution using a magnet with the doxorubicin solution decanted away. The nanoparticles were dried using nitrogen for 1 minute then placed in the buffer (phosphate buffered saline, 2 mL, 1 M). After 5 minutes, the magnetic particles were removed then and placed in the fresh buffer. This process was repeated for the following time intervals, 5, 15, 30, 45, 60, 90, 120 and 150 minutes. The fluorescence of each solution was recorded (Fluoromax-2, excitation 480 nm, and emission 580 nm).

4.3.2.2. The release profile of doxorubicin-loaded into the non-imprinted solution phase nanoparticles

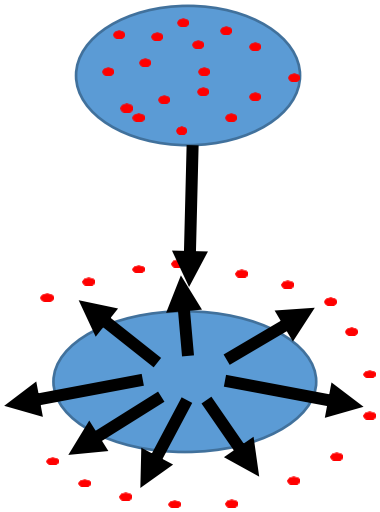

Figure 4 - 4: Diagram of release from the nanoparticles

A solution of doxorubicin (1mg, 1.84µmol) in distilled water (5mL) was prepared, separated into a 1mL aliquots. To this aliquot, molecularly imprinted magnetic nanoparticles (100mg) were added. The solution was then stored at 4^{o}C overnight. The magnetic particles were removed from the solution using a magnet with the doxorubicin solution decanted away. The nanoparticles were dried using nitrogen for 1 minute then placed in the buffer (phosphate buffered saline, 2mL, 1M). After 5 minutes, the magnetic particles were removed then and placed in the fresh buffer. This process was repeated for the following time intervals, 5, 15, 30, 45, 60, 90, 120 and 150 minutes. The fluorescence of each solution was recorded (Fluoromax-2, excitation 480nm, and emission 580nm). However, nanoparticles species, MIP-MN-2 and MIP-MN-4 were unable to be tested due to gelation of the polymer mixtures.

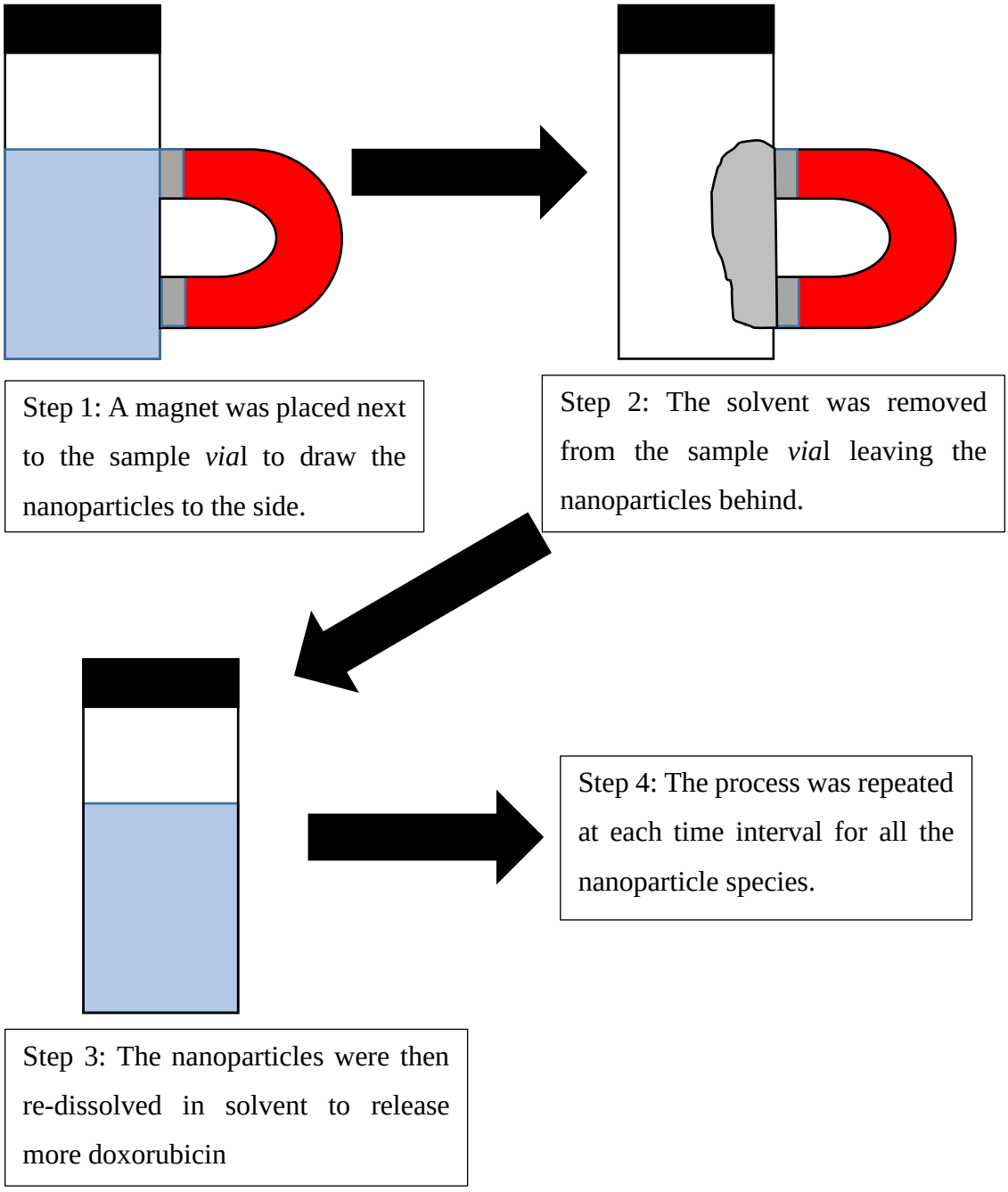

Figure 4 - 5: Diagram of release testing from the nanoparticles

4.4. Analysis and discussion.

4.4.1. Solution phase nanoparticles preparation

All the species of molecularly imprinted nanoparticles (MIP-MD series) were successfully synthesised as described in 5.3.1.1. However, only MIP-MN-1, MIP-MN-3 and MIP-MN-5 were successfully produced, yet, MIP-MN-2 and MIP-MN-4 gelated under UV irradiation, this is likely due to the cross-linking nature of the methacrylic acid and ethylene glycol methacrylate monomers.

4.4.2. The release profile of doxorubicin loaded into the solution phase molecularly imprinted nanoparticles

To determine the effect of different functional monomers on the imprinting and release profile of doxorubicin, the four monomers and a control with no functional monomer were tested alongside a control solution of doxorubicin. The results are shown in Table 4 – 3 and figure 4 – 6.

Table 4 - 3: Table showing the release of doxorubicin from the imprinted nanoparticles in comparison to a control solution of doxorubicin

Time (Mins)	Amount of doxorubicin released (mg mL^{-1}) Standard deviation = ± 0.002mg mL^{-1}					
	MIP-MD-1	MIP-MD-2	MIP-MD-3	MIP-MD-4	MIP-MD-5	Doxorubicin Control Solution
0	0.000	0.000	0.000	0.000	0.000	0.000
5	0.077	0.159	0.082	0.297	0.083	0.592
10	0.119	0.327	0.191	0.505	0.196	0.904
15	0.174	0.440	0.266	0.621	0.279	1.123
30	0.299	0.634	0.421	0.778	0.473	1.421
45	0.401	0.797	0.535	0.863	0.621	1.653
60	0.483	0.934	0.638	0.940	0.729	1.784
90	0.641	1.186	0.848	1.107	0.927	1.902
120	0.785	1.456	1.035	1.254	1.145	1.949
150	0.969	1.724	1.211	1.396	1.418	1.987

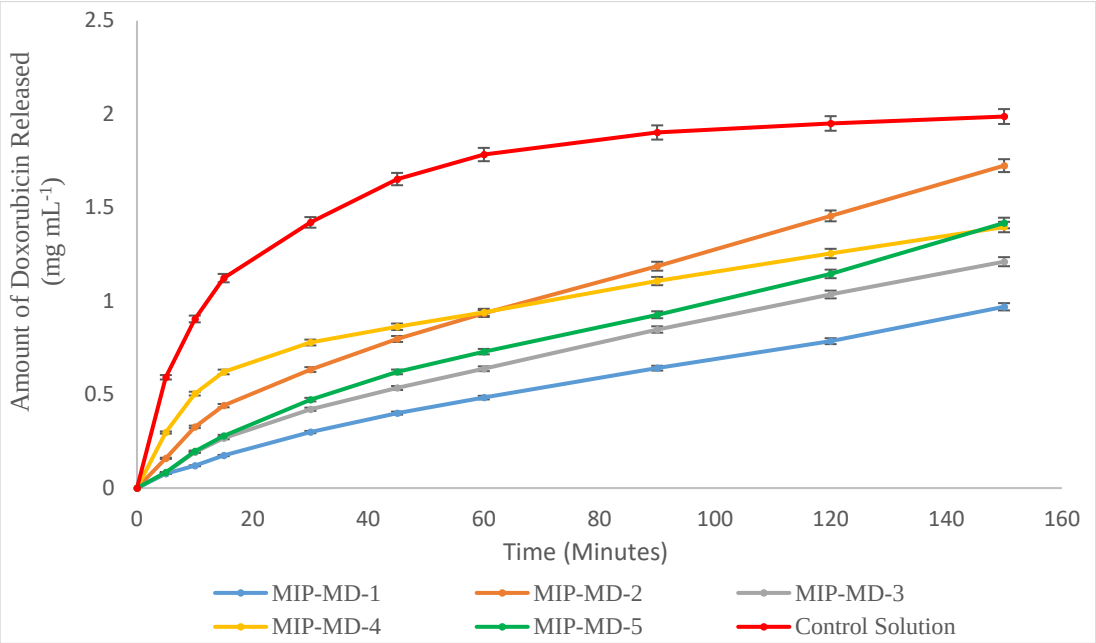

Figure 4 - 6: Graph showing the release of doxorubicin from the doxorubicin imprinted nanoparticles against time

During the initial 5 minutes of the experiments the control solution of doxorubicin demonstrated an initial release of doxorubicin at a rate of 0.118 mg mL^{-1} min^{-1} this is fairly fast compared to the fastest rate of doxorubicin from a nanoparticle species with MIP-MD-4 possessing an initial release rate of 0.059 mg mL^{-1} min^{-1} which is half the rate of the initial doxorubicin release in contrast the slowest rate of initial release was seen from the MIP-MD-1 species with a release rate of 0.015 mg mL^{-1} min^{-1} which is almost a quarter of the rate of MIP-MD-4 release. MIP-MD-2 had the second highest release of the nanoparticles with a rate of 0.031 mg mL^{-1} min^{-1} which is almost half the initial release rate of the MIP-MD-4 nanoparticles. MIP-MD-3 and 5 demonstrated a similar initial rate of release with 0.015 and 0.016 mg mL^{-1} $min^{-1,}$ respectively.

The rate of release all the species decreased after 15 minutes with the control doxorubicin solution decreasing to 0.019 mg mL^{-1} min^{-1} before decreasing to 0.003 mg mL^{-1} min^{-1} at the 60-minute mark decreasing gradually over the remaining 90 minutes. The rate of release from MIP-MD-4 decreased to 0.011 mg mL^{-1} min^{-1} before decreasing gradually for the remainder of the experiment. The rate of release from MIP-MD-2 decreased to 0.013 mg mL^{-1} min^{-1} and remained fairly constant for the remainder of the experiment. The rate of release from MIP-MD-5 decreases to 0.129 mg mL^{-1} min^{-1} before gradually decreasing for the remainder of the experiment. The rate of release from MIP-MD-3 decreased to 0.011 mg mL^{-1} min^{-1} before gradually decreasing over the remainder of the

experiment. The rate of release from MIP-MD-1 decreased to 0.008 0.011 mg mL^{-1} min^{-1} before gradually decreasing over the remainder of the experiment.

Overall the free doxorubicin solution demonstrated the highest release of doxorubicin compared to all 5 of the nanoparticle species, whereas MIP-MD-1 demonstrated the lowest amount of doxorubicin release with less than half the amount of free doxorubicin being released.

4.4.3. The release profile of doxorubicin loaded into the solution phase non-imprinted nanoparticles

To determine the effect of different functional monomers on the release profile of doxorubicin, the non-imprinted nanoparticles were compared. The two successfully polymerised monomers and a control with no functional monomer were tested and compared to a control solution of doxorubicin. The nanoparticle species, MIP-MN-2 and MIP-MN-4, were not tested due to gelation. The results are shown in Table 4 – 4 and figure 4 – 7.

Table 4 - 4: Table showing the release of doxorubicin from the non-imprinted nanoparticles in comparison to a control solution of doxorubicin

Time (min)	Amount of doxorubicin released (mg mL^{-1}) Standard deviation = ± 0.002 mg mL^{-1}					
	MIP-MN-1	MIP-MN-2	MIP-MN-3	MIP-MN-4	MIP-MN-5	Doxorubicin Control Solution
0	0.000	No Results due to Gelation	0.000	No Results due to Gelation	0.000	0.000
5	0.231		0.259		0.299	0.533
10	0.414		0.440		0.461	0.814
15	0.568		0.584		0.621	1.018
30	0.767		0.811		0.778	1.279
45	0.922		0.989		0.863	1.487
60	1.077		1.132		0.941	1.605
90	1.337		1.386		1.107	1.807
120	1.578		1.637		1.254	1.911
150	1.821		1.882		1.396	1.955

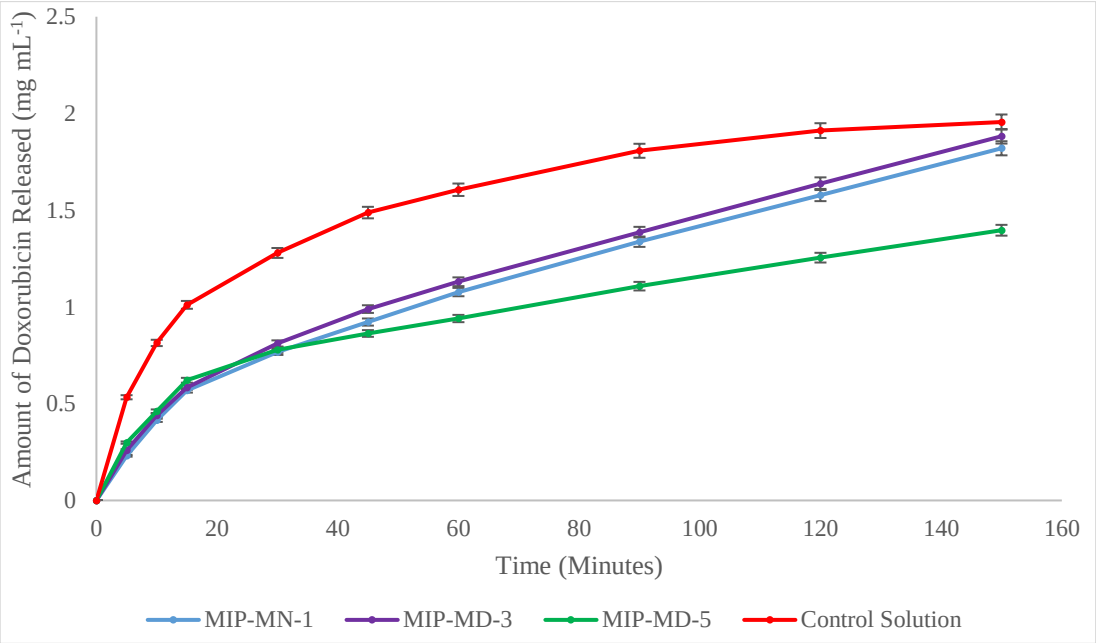

Figure 4 - 7: Graph showing the release of doxorubicin from the non-imprinted nanoparticles against time

During the initial 5 minutes of the experiments the control solution of doxorubicin demonstrated an initial release of doxorubicin at a rate of 0.106 mg mL^{-1} min^{-1} this is fairly fast compared to the rate of doxorubicin from the nanoparticle species with MIP-MN-1, 3 and 5 which demonstrated a similar initial rate of release with 0.059, 0.051 and 0.046 mg mL^{-1} min^{-1} respectively.

The rate of release all the species decreased after 15 minutes with the control doxorubicin solution decreasing to 0.017 mg mL^{-1} min^{-1} before decreasing to 0.007 mg mL^{-1} min^{-1} at 45 minutes and 0.003 mg mL^{-1} min^{-1} at 90 minutes. The rate of release from MIP-MN-3 decreased to 0.015 mg mL^{-1} min^{-1} at 15 minutes and gradually decreased over the remainder of the experiment. The rate of release from MIP-MN-1 decreased to 0.013 mg mL^{-1} min^{-1} at 15 minutes and gradually decreased over the remainder of the experiment. The rate of release from MIP-MN-5 decreased to 0.011 mg mL^{-1} min^{-1} at 15 minutes and gradually decreased over the remainder of the experiment.

Overall the free doxorubicin solution demonstrated the highest release of doxorubicin compared to all 3 of the nanoparticle species, whereas MIP-MN-5 demonstrated the lowest amount of doxorubicin release with 71.4% of the amount of doxorubicin from the control solution being released.

4.4.3. Comparison of the release profiles for each monomer of the nanoparticles

The nanoparticles were then compared by composition to determine if doxorubicin in the initial polymerisation influences the release from each nanoparticle species.

4.4.3.1. Functional monomer: 2-Hydroxymethyl acrylate

Firstly, the nanoparticle species containing 2-hydroxymethyl acrylate with and without doxorubicin in the polymerisation compared alongside a control solution of doxorubicin. The results are shown in Table 4 – 5 and figure 4 – 8.

Table 4 - 5: Table showing the release of doxorubicin from MIP-MD-1 and MIP-MN-1 in comparison to a control solution of doxorubicin

Time (Mins)	Amount of doxorubicin released (mg mL^{-1}) Standard deviation = ± 0.002mg mL^{-1}		
	MIP-MD-1	MIP-MN-1	Doxorubicin Control Solution
0	0.000	0.000	0.000
5	0.108	0.147	0.388
10	0.191	0.303	0.587
15	0.262	0.399	0.748
30	0.412	0.554	0.947
45	0.546	0.668	1.102
60	0.662	0.771	1.257
90	0.903	1.024	1.517
120	1.139	1.243	1.758
150	1.352	1.477	1.955

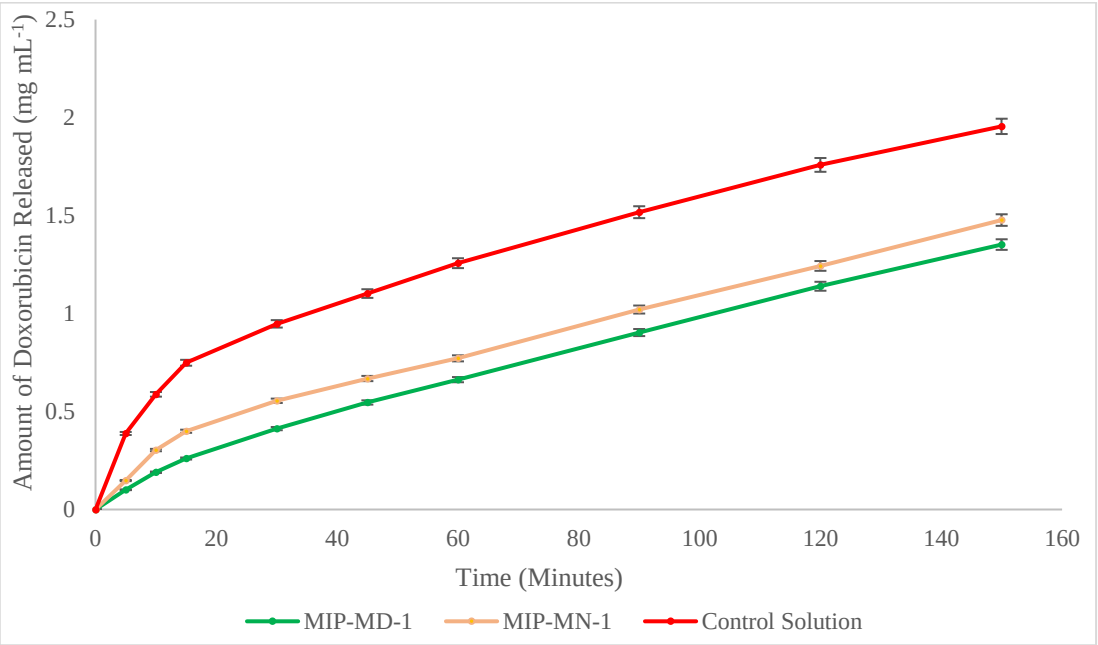

Figure 4 - 8: Graph showing the release of doxorubicin from the 2-hydroxymethyl acrylate functionalized nanoparticles against time

During the initial 5 minutes of the experiments the control solution of doxorubicin demonstrated an initial release of doxorubicin at a rate of 0.077 mg mL^{-1} min^{-1} this is fast compared to the rate of doxorubicin from the nanoparticle species with MIP-MN-1 which demonstrated an initial rate of release of 0.029 mg mL^{-1} min^{-1}, whereas, MIP-MD-1 demonstrated an initial rate release of 0.021 mg mL^{-1} min^{-1}.

The rate of release all the species decreased after 15 minutes with the control doxorubicin solution decreasing to 0.013 mg mL^{-1} min^{-1} before gradually decreasing over the remainder of the experiment. The rate of release from MIP-MN-1 decreased to 0.011 mg mL^{-1} min^{-1} at 15 minutes and gradually decreased over the remainder of the experiment. The rate of release from MIP-MN-1 decreased to 0.009 mg mL^{-1} min^{-1} at 15 minutes and gradually decreased over the remainder of the experiment.

Overall the free doxorubicin solution demonstrated the highest release of doxorubicin compared to all 3 of the nanoparticle species, whereas MIP-MN-1 demonstrated the lowest amount of doxorubicin release with 69.1% of the amount of doxorubicin from the control solution being released.

4.4.3.2. Functional monomer: Methacrylic acid

Secondly, the nanoparticles containing methacrylic acid as the functional monomer were unable to be compared, due to the gelation of the control nanoparticles.

4.4.3.3. Functional monomer: Itaconic acid

Thirdly, the nanoparticle species without any additional functional monomer used with and without doxorubicin in the polymerisation mixture were compared alongside a control solution of doxorubicin. The results are shown in Table 4 – 6 and figure 4 – 9.

Table 4 - 6: Table showing the release of doxorubicin from MIP-MD-3 and MIP-MN-3 in comparison to a control solution of doxorubicin

Time (Mins)	Amount of doxorubicin released (mg mL^{-1}) Standard deviation = ± 0.002mg mL^{-1}		
	MIP-MD-3	MIP-MN-3	Doxorubicin Control Solution
0	0.000	0.000	0.000
5	0.082	0.216	0.388
10	0.186	0.416	0.587
15	0.261	0.584	0.748
30	0.386	0.811	0.947
45	0.488	0.989	1.102
60	0.571	1.131	1.257
90	0.728	1.334	1.517
120	0.872	1.514	1.758
150	1.056	1.707	1.899

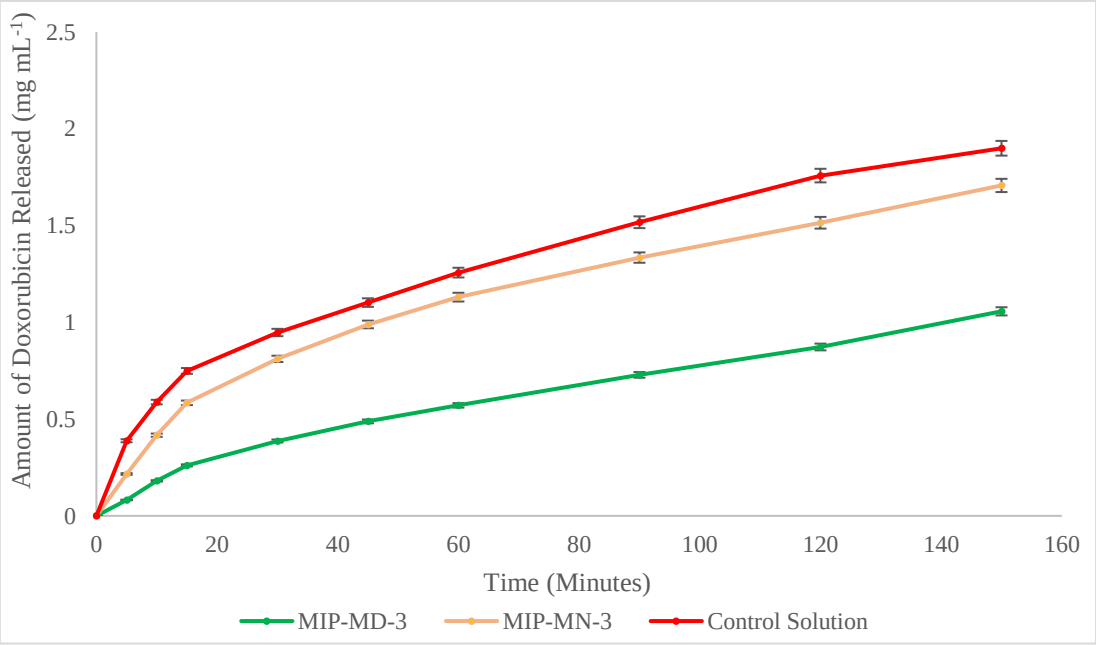

Figure 4 - 9: Graph showing the release of doxorubicin from the Itaconic acid functionalized nanoparticles against time

During the initial 5 minutes of the experiments the control solution of doxorubicin demonstrated an initial release of doxorubicin at a rate of 0.077 mg mL^{-1} min^{-1} this is fast compared to the rate of doxorubicin from the nanoparticle species with MIP-MN-3 which demonstrated an initial rate of release of 0.043 mg mL^{-1} min^{-1}, whereas, MIP-MD-3 demonstrated an initial rate release of 0.016 mg mL^{-1} min^{-1}.

The rate of release all the species decreased after 15 minutes with the control doxorubicin solution decreasing to 0.013 mg mL^{-1} min^{-1} before gradually decreasing over the

remainder of the experiment. The rate of release from MIP-MN-3 decreased to 0.015 mg mL^{-1} min^{-1} at 15 minutes and gradually decreased over the remainder of the experiment. The rate of release from MIP-MN-3 decreased to 0.008 mg mL^{-1} min^{-1} at 15 minutes and gradually decreased over the remainder of the experiment.

Overall the free doxorubicin solution demonstrated the highest release of doxorubicin compared to all 3 of the nanoparticle species, whereas MIP-MD-3 demonstrated the lowest amount of doxorubicin release with 55.6% of the amount of doxorubicin from the control solution being released.

4.4.3.4. Functional monomer: Ethylene glycol methacrylate

Secondly, the nanoparticles containing ethylene glycol methacrylate as the functional monomer were unable to be compared, due to the gelation of the control nanoparticles.

4.4.3.5. Functional monomer: No functional monomer used.

Finally, the nanoparticle species without any additional functional monomer used were tested. The presence of doxorubicin in the polymerisation mixture was investigated with the release profiles being compared alongside a control solution of doxorubicin. The results are shown in Table 4 – 7 and figure 4 – 10.

Table 4 - 7: Table showing the release of doxorubicin from MIP-MD-5 and MIP-MN-5 in comparison to a control solution of doxorubicin

Time (Mins)	Amount of doxorubicin released (mg $mL^{-1)}$ Standard deviation = ± 0.002mg mL^{-1}		
	MIP-MD-5	MIP-MN-5	Doxorubicin Control Solution
0	0.000	0.000	0.000
5	0.171	0.208	0.388
10	0.335	0.359	0.587
15	0.418	0.440	0.748
30	0.612	0.634	0.947
45	0.761	0.797	1.102
60	0.869	0.934	1.257
90	1.066	1.186	1.517
120	1.249	1.456	1.758
150	1.421	1.688	1.955

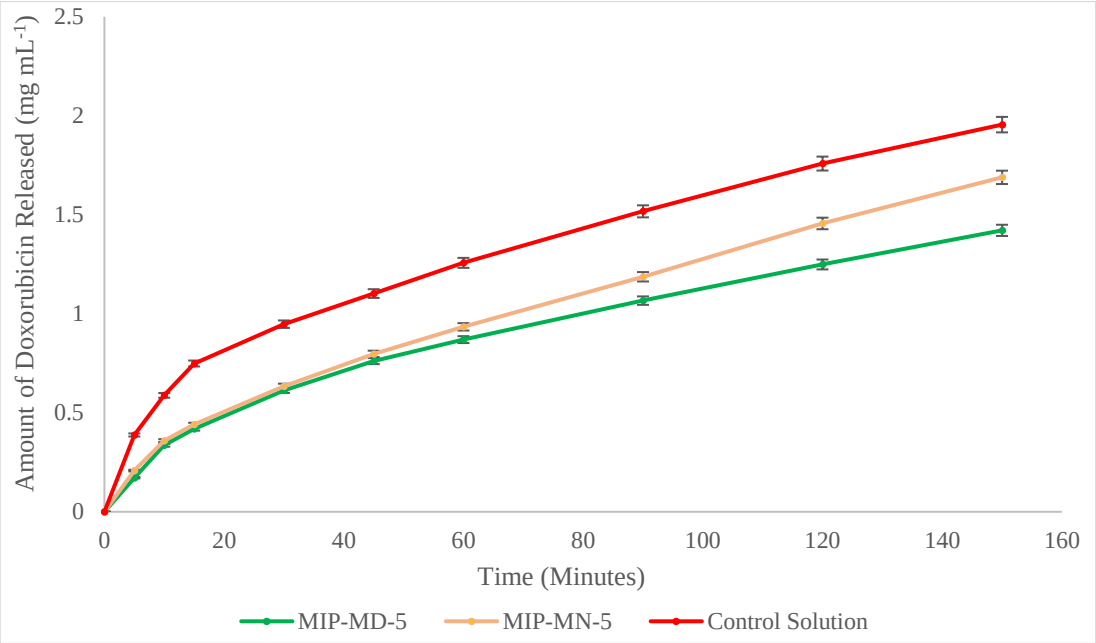

Figure 4 - 10: Graph showing the release of doxorubicin from the non-functionalized nanoparticles against time

During the initial 5 minutes of the experiments the control solution of doxorubicin demonstrated an initial release of doxorubicin at a rate of 0.077 mg mL^{-1} min^{-1} this is fast compared to the rate of doxorubicin from the nanoparticle species with MIP-MN-3 which demonstrated an initial rate of release of 0.041 mg mL^{-1} min^{-1}, whereas, MIP-MD-3 demonstrated an initial rate release of 0.035 mg mL^{-1} min^{-1}.

The rate of release all the species decreased after 15 minutes with the control doxorubicin solution decreasing to 0.013 mg mL^{-1} min^{-1} before gradually decreasing over the remainder of the experiment. The rate of release from MIP-MN-5 decreased to 0.012 mg mL^{-1} min^{-1} at 15 minutes and gradually decreased over the remainder of the experiment. The rate of release from MIP-MN-5 decreased to 0.012 mg mL^{-1} min^{-1} at 15 minutes and 0.007 mg mL^{-1} min^{-1} at 45 minutes before gradually decreased over the remainder of the experiment.

Overall the free doxorubicin solution demonstrated the highest release of doxorubicin compared to all 3 of the nanoparticle species, whereas MIP-MD-3 demonstrated the lowest amount of doxorubicin release with 72.7% of the amount of doxorubicin from the control solution being released.

4.5 Conclusions

In conclusion, the concept of using magnetic core nanoparticles for the delivery of doxorubicin is ideal. However, the composition of these nanoparticles can affect the retention of the doxorubicin and the release.

From the experiments, the MIP-MD-1 nanoparticles were observed to release the lowest amount of doxorubicin with the slowest rate of release compared to the other doxorubicin imprinted nanoparticle species. The MIP-MD-1 nanoparticles demonstrated a lower rate of release in comparison to its non-imprinted counterpart MIP-MN-1 nanoparticles, this indicating a degree of doxorubicin retention by the imprinted nanoparticles compared to the non-imprinted nanoparticles.

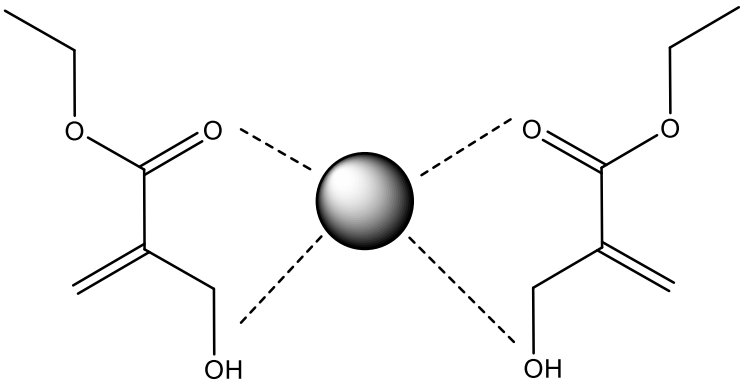

Figure 4 - 11: Binding schematic of 2-hydroxymethyl acrylate in the nanoparticles

The MIP-MD-3 nanoparticles demonstrated the second lowest release of the nanoparticles with the second lowest rate of release compared to the other doxorubicin nanoparticle species. MIP-MD-3 demonstrated a lower rate of release in comparison to the non-imprinted nanoparticles MIP-MN-3, indicating a degree of doxorubicin imprinting compared to the non-imprinted nanoparticles.

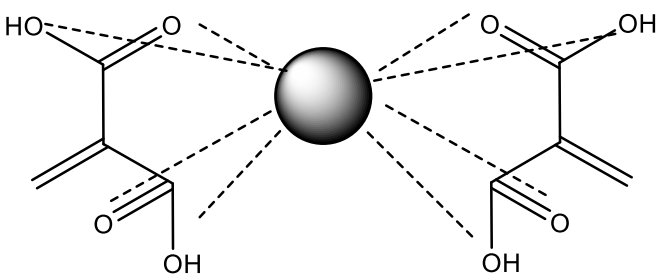

Figure 4 - 12: Binding schematic of Itaconic acid in the nanoparticles

The MIP-MD-5 nanoparticles demonstrated the third lowest release of the nanoparticles with the second lowest rate of release compared to the other doxorubicin nanoparticle species. MIP-MD-5 demonstrated a lower rate of release in comparison to the non-imprinted nanoparticles MIP-MN-5, indicating a degree of doxorubicin imprinting compared to the non-imprinted nanoparticles.

The MIP-MD-2 nanoparticles demonstrated the second highest rate of doxorubicin release overall, while the MIP-MD-4 nanoparticles demonstrated the highest rate of doxorubicin release. MIP-MD-2 and MIP-MD-4 could not be compared to their non-imprinted counterparts due to these species undergoing gelation when irradiated with UV light.

The low release seen from the MIP-MD-1 nanoparticles is likely due to the 2-hydroxymethyl acrylate functional monomer. The 2-hydroxymethyl acrylate monomer contains an alcohol group several carbons away from the alkene group used in the polymerisation. In comparison, the MIP-MD-3 nanoparticles contained itaconic acid functional monomer; the itaconic acid monomer contains three alcohol groups spaced either side of the alkene group used in polymerisation. In comparison, the Itaconic acid binding groups are more sterically hindered than the 2-hydroxymethyl acrylate reducing the interaction between the doxorubicin and the functional monomer.

As the methacrylic acid is the smallest functional monomer used, with the highest density of functional groups on the smallest molecule size, it is likely that when the polymerisation took place, the monomers cross-linked causing gelation of the nanoparticles. In contrast, the ethylene glycol methacrylate is a cross-linking monomer used in organic nanoparticles; the monomer has alcohol groups near to the alkene group used in polymerisation this also reduces the potential binding interaction with the template. With the non-imprinted nanoparticles, the ethylene glycol methacrylate likely cross-linked the polymer chains together, causing the nanoparticles to undergo gelation.

Overall, nanoparticle species MIP-MD-1 demonstrated the best characteristics for doxorubicin release due to the slower release rate, further testing of different nanoparticle compositions would be beneficial to determine the optimal nanoparticles for the delivery of doxorubicin. Testing would also need to be carried out on the magnetic core of the nanoparticles undergoing use as a secondary function such as a targeting vector guided by magnetic fields. The magnetic core also has the potential to be used in hyperthermic therapy to overheat target cells by the use of magnetic fields to increase the temperature of the cell.

Chapter 5: Solid-phase synthesised nanoparticles loaded with doxorubicin.

5.1. Introduction

Following on from chapter 5 synthesis of solid phase nanoparticles with doxorubicin incorporated into the nanoparticle structure were synthesised. Three types of imprinted nanoparticles were tested, vancomycin imprinted and epidermal growth factor receptor (EGFR) binding protein imprinted nanoparticles produced in both aqueous and organic solvents. Firstly, vancomycin imprinted nanoparticles were produced for initial loading studies; these were based on previous research by the Piletsky group on the use of molecularly imprinted nanoparticles as a replacement for enzymes in ELIZA assays.[115] Vancomycin was also used as it is a glycoprotein and similar in size to the EGFR binding peptide, which is used to target cancer cells. The synthesis was modified to include the incorporation of doxorubicin into the nanoparticle structure for drug delivery purposes.
Secondly, an EGFR binding peptide used as the template for the nanoparticles. Epidermal growth factor receptor (EGFR) is a membrane-bound protein. The nanoparticles are imprinted to an external part of the EGFR peptide which was duplicated using a short sequence of amino acids. EGFR is over-expressed in cancer cells, which makes it an ideal target for doxorubicin-loaded nanoparticles. Initially, an aqueous solvent was used as peptides and proteins dissolve into aqueous-based solvents better than their organic solvents. However, to determine if organic solvent synthesised nanoparticles possessed similar doxorubicin retention properties to their aqueous counterparts. The EGFR binding peptide nanoparticles were synthesised using acetonitrile as a solvent.

5.1.1. Aim and objectives

Aim of the chapter:

- Synthesis and testing of solid phase synthesised nanoparticles for different templates and the controlled release of doxorubicin over time.

Objectives for this chapter:

- Synthesis of solid phase nanoparticles using aqueous solvent templated to vancomycin as the primary template with and without doxorubicin imprinted.
- Synthesis of solid phase nanoparticles using aqueous solvent templated to EGFR binding peptide as the primary template with and without doxorubicin imprinted.
- Synthesis of solid phase nanoparticles using organic solvent templated to EGFR binding peptide as the primary template with and without doxorubicin imprinted.
- Testing of the release of doxorubicin from the nanoparticles with different primary templates
- Comparing the doxorubicin imprinted nanoparticles against the non-imprinted nanoparticles.

5.2. Chemicals

Glass beads SPHERIGLASS® A-Glass 2429 (70 – 100 µm diameter) obtained from Potters Industries LLC. A dialysis membrane (Spectra/Por, MWCO = 10 kDa) was purchased from Spectrum Laboratories Inc. Acrylic acid, ammonium persulfate, 1,2-bis(trimethoxysilyl)ethane, glutaraldehyde, phosphate buffered saline tablets, N-isopropylacrylamide, N′-methylene-bisacrylamide, N-tert-butylacrylamide, N, N, N′, N′-tetramethylethylenediamine, Iodoacetic acid N-hydroxysuccinimide ester, vancomycin hydrochloride, acetone, ethanol, methanol and toluene were purchased from Sigma-Aldrich, UK. (3-Aminopropyl) trimethoxysilane and sodium cyanoborohydride were obtained from Acros Organics. N-(3-Aminopropyl) methacrylamide hydrochloride was purchased from PolySciences Inc., UK. Amicon Ultra-15 Centrifugal Filter Units (MWCO 30 kDa), Acetonitrile, sodium hydroxide and sulphuric acid were obtained from Fisher Scientific (UK). Doxorubicin Hydrochloride was purchased from Cambridge Bioscience, UK. Ultrapure water was produced by a Millipore Milli-Q system (Millipore, Bedford, MA, USA), Double-distilled ultrapure water (Millipore) was used for analysis. All chemicals and solvents were analytical or HPLC grade and were used without further purification. Phosphate buffered saline was prepared as directed from PBS buffer tablets (Sigma-Aldrich, Gillingham, UK).

5.3. Methods

The nanoparticle synthesis requires two sets of procedures, preparation of the solid phase bearing the target molecule template and solid phase synthesis of the nanoparticles. Two different templates were used, vancomycin and EGFR binding peptide.

5.3.1. Solid phase preparation of nanoparticles

5.3.1.1. Templated solid phase glass beads.

Two variants of the solid phase beads were synthesised, one using vancomycin, the other using a binding epitope of an EGFR protein simulated by a peptide chain. For the vancomycin templated beads, the procedure was carried out as described in 2.3.1.1. For the EGFR beads: the beads were incubated in acetonitrile (24mL) containing succinimidyl Iodoacetate (4.8mg, 16.95µmol) for 2 hours in a dark environment. The beads were collected, washed with acetonitrile (300mL) and dried. The beads were incubated in PBS (30mL, 0.01M) containing EDTA (43.86mg, 0.15mmol) at pH 8.2 for 4 hours. The beads were collected, washed with acetonitrile (90mL) followed by deionised water (500mL) and dried.

5.3.1.2. Vancomycin templated nanoparticle synthesis

Nanoparticles imprinted with for vancomycin were synthesised *via* the method described in 2.3.1.2 using vancomycin templated glass beads. Half of the polymerisations utilised the standard composition used in 2.3.1.2 to form the MIP-SN nanoparticles, whereas, the other half incorporated different amounts of doxorubicin to produce the MIP-SD series of nanoparticles. List of species produced listed in Table 5 – 1.

Table 5 - 1: Table showing the vancomycin imprinted nanoparticle species and amount of doxorubicin used

Species	**Doxorubicin present in the synthesis**	**Mass of doxorubicin**	**Moles of doxorubicin**
MIP-SD-A	Yes	3.5 mg	6.440 µmol
MIP-SD-B	Yes	1.0 mg	1.840 µmol
MIP-SD-C	Yes	0.1 mg	0.184 µmol
MIP-SN-A	No	-	-

5.3.1.3. Aqueous synthesis of EGFR binding peptide templated nanoparticle synthesis

Nanoparticles imprinted with for EGFR were synthesised *via* the method described in 2.3.1.2 using EGFR peptide templated glass beads. Half of the polymerisations utilised the standard composition used in 2.3.1.2 to form the MIP-SN-B nanoparticles, whereas, the other half incorporated doxorubicin (1 mg, 1.84 µmol) to produce the MIP-SD-D nanoparticles.

5.3.1.4. Organic synthesis of EGFR binding peptide nanoparticles

A solution of (hydroxyethyl) methacrylate (2.18 g, 16.75 mmol), methacrylic acid (1.45 g, 16.85 mmol), trimethylolpropane trimethacrylate (3.24 g, 10.95 mmol), ethylene glycol dimethacrylate (3.24 g, 16.35 mmol), N, N-diethyldithiocarbamic acid benzyl ester (0.75 g, 3.13 mmol) in acetonitrile (13 mL) was prepared. N-(3-aminopropyl) methacrylamide (11 mg, 77.36 µmol) was dissolved in water (1 mL) and added to the initial solution; the mixture was then purged under nitrogen gas for 5 minutes. To this solution, EGFR, peptide coated beads (60 g) was added before purging under nitrogen for 5 minutes. The polymerisation mixture was then irradiated for 90 seconds under UV light (using 4 x Philips HB/171/A lamps). The process was repeated with doxorubicin (1 mg, 1.84 µmol) present in the initial polymerisation mixture.

5.3.1.5. Nanoparticle collection

The aqueous nanoparticle species were all collected *via* the procedure described in 2.3.1.3. However, the organic solvent synthesised EGFR peptide-templated bead mixture was transferred to a 60-mL solid phase extraction cartridge fitted with a polystyrene frit and washed with chilled acetonitrile (500 mL, 0^{o}C). The EGFR peptide-templated beads were heated to 65^{o}C, then washed with acetonitrile (65 ^{o}C, 120 mL) with the 'hot' washings being collected. The acetonitrile was then evaporated off at 50 ^{o}C and replaced with distilled water (60 mL).

5.3.1.6. Nanoparticle purification

All nanoparticle species were purified *via* the procedure described in 2.3.1.4.

5.3.2. The release profile of doxorubicin from solid phase nanoparticles

5.3.2.1. Doxorubicin release from vancomycin imprinted nanoparticles

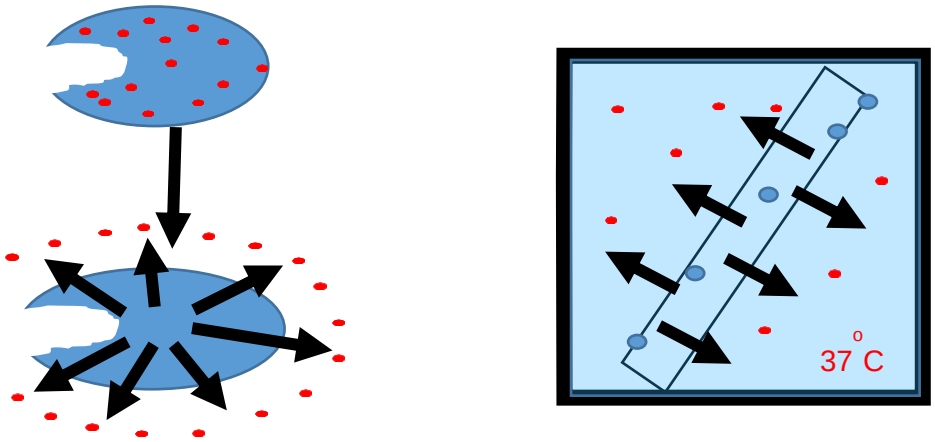

Figure 5 - 1: Schematic of doxorubicin release from the nanoparticles

The concentrated solution of the nanoparticle species was incubated in water containing doxorubicin (the polymerisation amount) at R.T. for 24 hours in a dark environment. The solution was then placed into a dialysis tube (reverse cellulose, 10000 MWCO, 12mm) and placed in a dialysis gradient (200x) incubated at 37°C in a dark environment. The concentration is monitored *via* fluorescence taken from samples collected from the inside of the tubing at different time intervals to monitor the release profile. The following nanoparticle species were tested, MIP-SD-A, MIP-SD-B and MIP-SD-C against MIP-SN-A (control nanoparticles) and free doxorubicin solution at the following doxorubicin amounts: 3.5mg (6.44µmol), 1mg (1.84µmol) and 0.1mg (0.184µmol).

5.3.2.2. Doxorubicin release from aqueous synthesised EGFR imprinted nanoparticles.

It is carried out as in 5.3.2.1 with the MIP-SD-D being tested against MIP-SD-B.

5.3.2.3. Doxorubicin release from organic synthesised EGFR imprinted nanoparticles.

Carried out as in 5.3.2.1 with the MIP-OSD being tested against MIP-OSN.

5.4. Analysis and discussion

5.4.1. Nanoparticle synthesis

5.4.1.1. Templated solid phase preparation

The glass beads from the hydroxylation step were successfully coated with OH and dried. The silanisation step was successfully carried out. The presence of the silane was confirmed using dansyl chloride to label the amine end of the silane molecule. Under UV-Vis exposure, the glass beads glowed green, indicating the presence of the primary amine of the silane. The glutaraldehyde, vancomycin and EGFR binding peptide coupling steps were completed as in 2.3.1.1 and 5.3.1.1 respectively. Overall this resulted in a solid phase suitable for nanoparticle synthesis.

5.4.1.2. Aqueous nanoparticle synthesis

APS-TEMED initiated polymerisation successfully synthesised all the nanoparticles as described in 2.3.1.2 with the modifications outlined in 5.3.1.1., 5.3.1.2. And 5.3.1.3. The nanoparticles were successfully collected and washed as described in 2.3.1.3 and 2.3.1.4.

5.4.1.3. Organic nanoparticle synthesis

All the nanoparticles were synthesised by UV light-initiated polymerisation as described in 5.3.1.4. The nanoparticles were collected as described in 5.3.1.5. And washed as described in 2.3.1.4.

5.4.2. Doxorubicin release from vancomycin imprinted nanoparticles

The concentration was measured on the inside of the membrane cell. By this method, the change in concentration is monitored by determining the decrease in doxorubicin fluorescence detected. From this, the rate of release of doxorubicin is determined. The amount of doxorubicin release was calculated as a cumulative % of the overall experiment its comparison to the free doxorubicin solution. The nanoparticles imprinted for vancomycin were tested first as this template was used previously in the design and testing of solid-phase nanoparticles. With the vancomycin imprinted nanoparticles, three different concentrations of doxorubicin added into the polymerisation mixture were

tested, 3.5mg, 1mg and 0.1mg. These compositions were examined to determine how the nanoparticles would release their payload and identify which would be best for testing with peptide imprinted nanoparticles.

5.4.2.1. The doxorubicin release profile of MIP-SD-A

MIP-SD-A was tested first, after washing the nanoparticles to remove unreacted monomers and doxorubicin. The nanoparticles were pre-incubated with doxorubicin (3.5 mg, 6.44 µmol) for the release testing. The release of doxorubicin was monitored as described in 6.3.2. The MIP-SD-A nanoparticles were tested against the control MIP-SN-A nanoparticles incubated with doxorubicin and a control solution of doxorubicin. The results are shown in Table 5 – 2 and figure 5 – 2.

Table 5 - 2: Table showing the release of doxorubicin from MIP-SD-A and MIP-SN-A in comparison to a control solution of doxorubicin

Time (Mins)	Amount of doxorubicin released (mg mL^{-1}) Standard deviation = ± 0.002mg mL^{-1}		
	MIP-SD-A	MIP-SN-A	Doxorubicin Control Solution
0	0.000	0.000	0.000
5	0.389	0.474	0.488
10	0.627	0.703	0.735
15	0.793	0.861	0.901
20	0.929	0.994	1.022
25	1.047	1.121	1.115
30	1.146	1.194	1.246
45	1.395	1.417	1.529
60	1.608	1.621	1.799
120	2.294	2.324	2.794
180	2.799	2.829	3.445

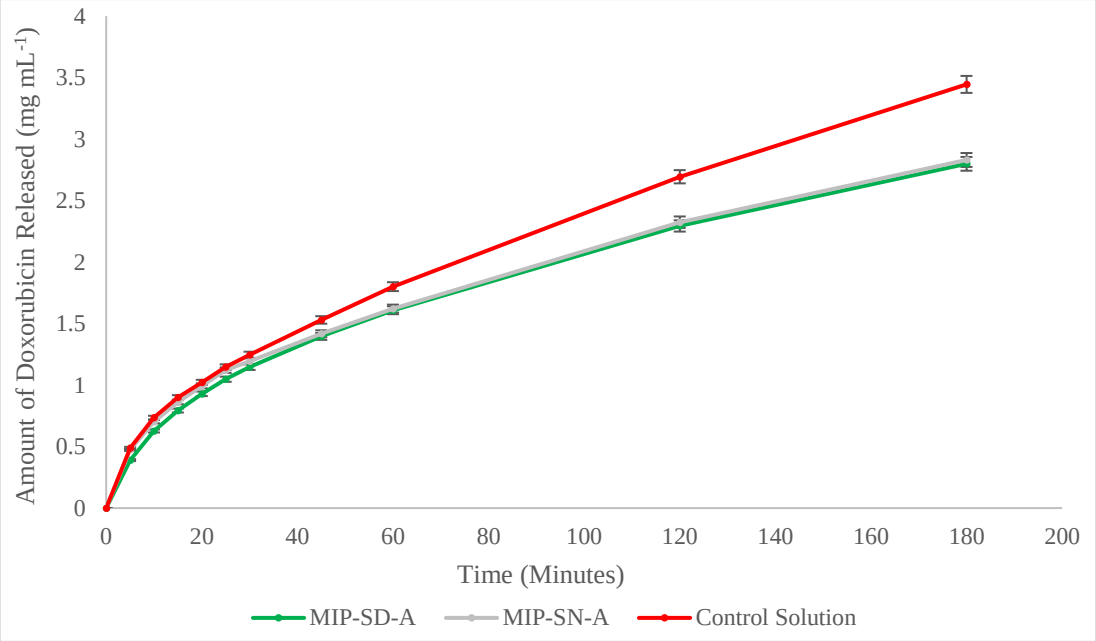

Figure 5 - 2: Graph showing a comparison of the release of doxorubicin from MIP-SD-A, MIP-SN-A and a doxorubicin control solution

During the initial 5 minutes of the experiments, the control solution of doxorubicin demonstrated an initial release of doxorubicin at a rate of 0.097 mg mL^{-1} min^{-1} whereas the MIP-SD-A and MIP-SN-A demonstrated a rate of 0.078 mg mL^{-1} min^{-1} and 0.095 mg mL^{-1} min^{-1} respectively. All species demonstrated very similar rates of the initial release. The rate of release of the doxorubicin from the doxorubicin control solution decreased to 0.049 mg mL^{-1} min^{-1} at the 5-minute mark before decreasing to 0.026 mg mL^{-1} min^{-1} at the 20-minute mark. At the 30-minute mark, the rate decreased to 0.018 mg mL^{-1} min^{-1} before gradually decreasing over the remainder of the experiment.

The rate of release of the doxorubicin from the MIP-SN-A species of nanoparticles decreased to 0.045 mg mL^{-1} min^{-1} at the 5-minute mark before decreasing to 0.026 mg mL^{-1} min^{-1} at the 20-minute mark. At the 30-minute mark, the rate decreased to 0.015 mg mL^{-1} min^{-1} before gradually decreasing over the remainder of the experiment.

The rate of release of the doxorubicin from the MIP-SD-A species of nanoparticles decreased to 0.048 mg mL^{-1} min^{-1} at the 5-minute mark before decreasing to 0.023 mg mL^{-1} min^{-1} at the 20-minute mark. At the 30-minute mark, the rate decreased to 0.016 mg mL^{-1} min^{-1} before gradually decreasing over the remainder of the experiment.

Overall the doxorubicin control solution demonstrated the highest release of doxorubicin compared to both of the nanoparticle species, whereas MIP-SD-A demonstrated the lowest amount of doxorubicin release with 81.2% of the amount of doxorubicin from the control solution being released.

5.4.2.2. The doxorubicin release profile of MIP-SD-B

MIP-SD-B was tested second, after washing the nanoparticles to remove unreacted monomers and doxorubicin. The nanoparticles were pre-incubated with doxorubicin (1 mg, 1.84 µmol) for the release testing. The release of doxorubicin was monitored as described in 6.3.2. The MIP-SD-B nanoparticles were tested against the control MIP-SN-A nanoparticles incubated with doxorubicin and a control solution of doxorubicin. The results are shown in Table 5 – 3 and figure 5 – 3.

Table 5 - 3: Table showing the release of doxorubicin from MIP-SD-B and MIP-SN-A in comparison to a control solution of doxorubicin

Time (Mins)	Amount of doxorubicin released (mg mL^{-1}) Standard deviation = ± 0.002mg mL^{-1}		
	MIP-SD-B	MIP-SN-A	Doxorubicin Control Solution
0	0.000	0.000	0.000
5	0.213	0.251	0.242
10	0.334	0.412	0.389
15	0.423	0.527	0.485
20	0.501	0.616	0.560
25	0.569	0.681	0.634
30	0.626	0.729	0.701
45	0.769	0.877	0.868
60	0.891	1.012	1.024
120	1.285	1.451	1.594
180	1.593	1.745	1.985

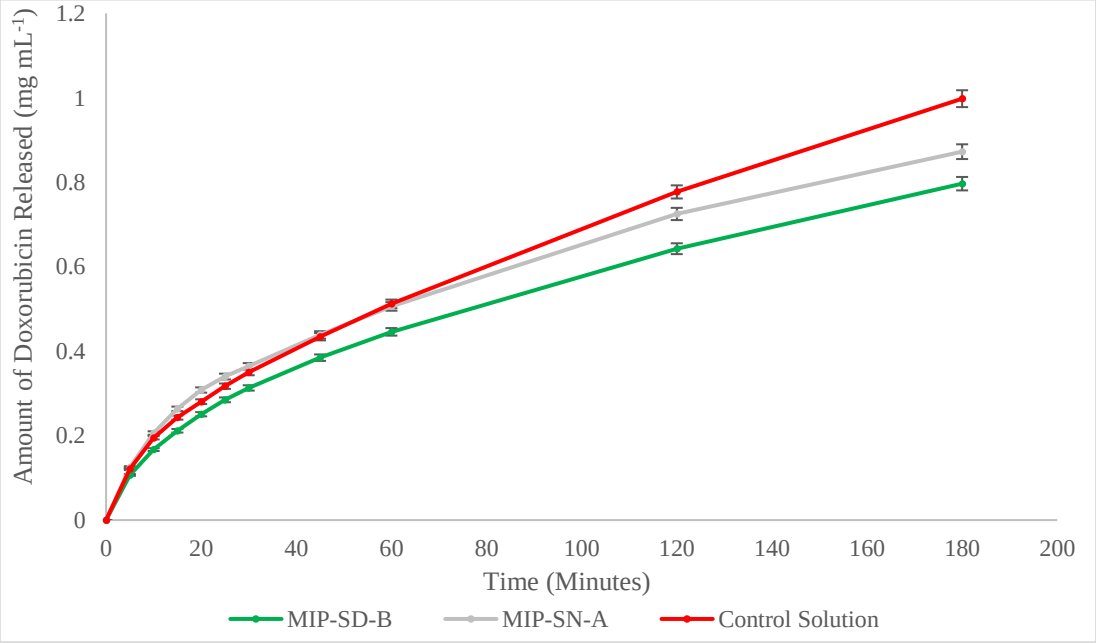

Figure 5 - 3: Graph showing a comparison of the release of doxorubicin from MIP-SD-B, MIP-SN-A and a doxorubicin control solution

During the initial 5 minutes of the experiments, the control solution of doxorubicin demonstrated an initial release of doxorubicin at a rate of 0.024 mg mL^{-1} min^{-1} whereas the MIP-SD-B and MIP-SN-A demonstrated a rate of 0.021 mg mL^{-1} min^{-1} and 0.025 mg mL^{-1} min^{-1} respectively. All species demonstrated very similar rates of the initial release. The rate of release of the doxorubicin from the doxorubicin control solution decreased to 0.015 mg mL^{-1} min^{-1} at the 5-minute mark before decreasing to 0.007 mg mL^{-1} min^{-1} at the 20-minute mark. At the 30-minute mark, the rate decreased to 0.005 mg mL^{-1} min^{-1} before gradually decreasing over the remainder of the experiment.

The rate of release of the doxorubicin from the MIP-SN-A species of nanoparticles decreased to 0.016 mg mL^{-1} min^{-1} at the 5-minute mark before decreasing to 0.006 mg mL^{-1} min^{-1} at the 20-minute mark. At the 30-minute mark, the rate decreased to 0.005 mg mL^{-1} min^{-1} before gradually decreasing over the remainder of the experiment.

The rate of release of the doxorubicin from the MIP-SD-B species of nanoparticles decreased to 0.006 mg mL^{-1} min^{-1} at the 5-minute mark before decreasing to 0.023 mg mL^{-1} min^{-1} at the 20-minute mark. At the 30-minute mark, the rate decreased to 0.004 mg mL^{-1} min^{-1} before gradually decreasing over the remainder of the experiment.

Overall the doxorubicin control solution demonstrated the highest release of doxorubicin compared to both of the nanoparticle species, whereas MIP-SD-B demonstrated the lowest amount of doxorubicin release with 79.8% of the amount of doxorubicin from the control solution being released.

5.4.2.3. The doxorubicin release profile of MIP-SD-C

MIP-SD-C was tested first, after washing the nanoparticles to remove unreacted monomers and doxorubicin. The nanoparticles were pre-incubated with doxorubicin (0.1 mg, 0.184 µmol) for the release testing. The release of doxorubicin was monitored as described in 6.3.2. The molecularly imprinted nanoparticles were tested against the control MIP-SN-A nanoparticles incubated with doxorubicin and a control solution of doxorubicin. The results are shown in Table 5 – 4 and figure 5 – 4.

Table 5 - 4: Table showing the release of doxorubicin from MIP-SD-C and MIP-SN-A in comparison to a control solution of doxorubicin

Time (Mins)	Amount of doxorubicin released (mg mL^{-1}) Standard deviation = ± 0.0001mg mL^{-1}		
	MIP-SD-C	MIP-SN-A	Doxorubicin Control Solution
0	0.0000	0.0000	0.0000
5	0.0098	0.0103	0.0107
10	0.0159	0.0183	0.0182
15	0.0204	0.0243	0.0231
20	0.0244	0.0290	0.0269
25	0.0279	0.0326	0.0306
30	0.0307	0.0354	0.0340
45	0.0381	0.0423	0.0425
60	0.0442	0.0484	0.0504
120	0.0642	0.0696	0.0754
180	0.0798	0.0841	0.0975

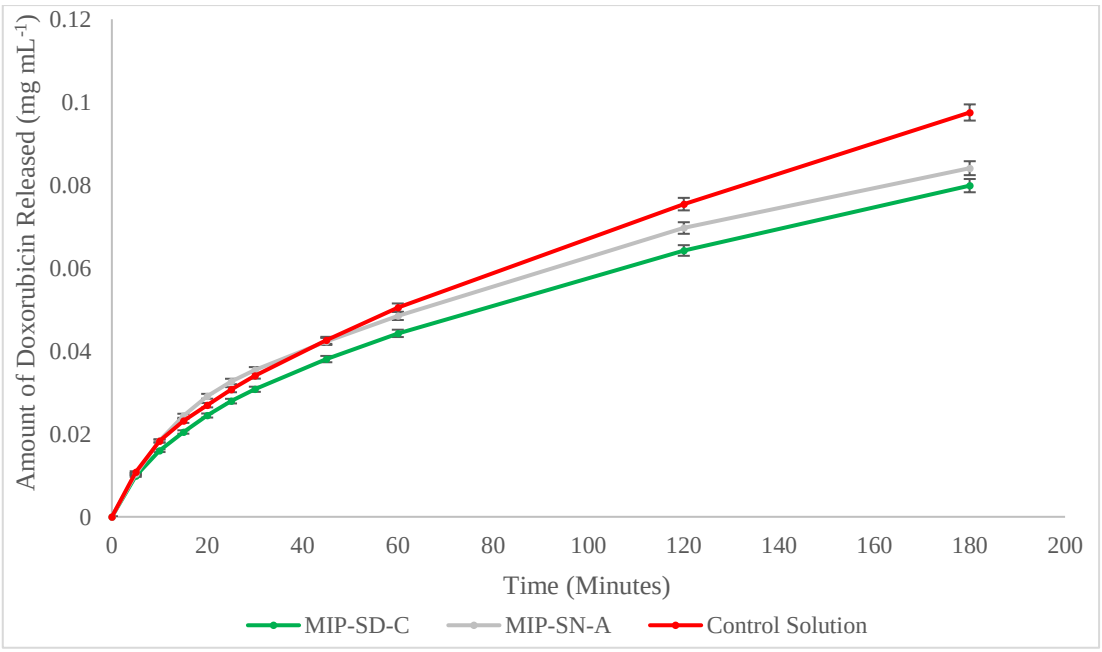

Figure 5 - 4: Graph showing a comparison of the release of doxorubicin from MIP-SD-C, MIP-SN-A and a doxorubicin control solution

During the initial 5 minutes of the experiments, the control solution of doxorubicin demonstrated an initial release of doxorubicin at a rate of 0.0022 mg mL^{-1} min^{-1} whereas the MIP-SD-C and MIP-SN-A demonstrated a rate of 0.0019 mg mL^{-1} min^{-1} and 0.0021 mg mL^{-1} min^{-1} respectively. All species demonstrated very similar rates of the initial release.

The rate of release of the doxorubicin from the doxorubicin control solution decreased to 0.0015 mg mL^{-1} min^{-1} at the 5-minute mark before decreasing to 0.0007 mg mL^{-1} min^{-1} at the 20-minute mark. At the 30-minute mark, the rate decreased to 0.0006 mg mL^{-1} min^{-1} before gradually decreasing over the remainder of the experiment.

The rate of release of the doxorubicin from the MIP-SN-A species of nanoparticles decreased to 0.0016 mg mL^{-1} min^{-1} at the 5-minute mark before decreasing to 0.0007 mg mL^{-1} min^{-1} at the 20-minute mark. At the 30-minute mark, the rate decreased to 0.0005 mg mL^{-1} min^{-1} before gradually decreasing over the remainder of the experiment.

The rate of release of the doxorubicin from the MIP-SD-C species of nanoparticles decreased to 0.0012 mg mL^{-1} min^{-1} at the 5-minute mark before decreasing to 0.0007 mg mL^{-1} min^{-1} at the 20-minute mark. At the 30-minute mark, the rate decreased to 0.0005 mg mL^{-1} min^{-1} before gradually decreasing over the remainder of the experiment.

Overall the doxorubicin control solution demonstrated the highest release of doxorubicin compared to both of the nanoparticle species, whereas MIP-SD-C demonstrated the lowest amount of doxorubicin release with 81.9% of the amount of doxorubicin from the control solution being released.

5.4.3. Doxorubicin release from EGFR imprinted nanoparticles

The nanoparticles imprinted for the EGFR binding peptide were tested second. The nanoparticles were synthesised using 1mg of doxorubicin in the polymerisation. Unlike the vancomycin nanoparticles, the EGFR nanoparticles were synthesised using the aqueous synthesis similar to the vancomycin nanoparticles. The EGFR nanoparticles were also synthesised using an organic solvent, as organic solvent synthesised nanoparticles can be modified with a second polymer layer to add alternate functionality.

5.4.3.1. Doxorubicin release from EGFR imprinted aqueous nanoparticles

MIP-SD-D was tested next, after washing the nanoparticles to remove unreacted monomers and doxorubicin. The nanoparticles were pre-incubated with doxorubicin (1 mg, 1.84 µmol) for the release testing. The release of doxorubicin was monitored as described in 6.3.2. The molecularly imprinted nanoparticles were tested against the control MIP-SN-B nanoparticles incubated with doxorubicin and a control solution of doxorubicin. The results are shown in Table 5 – 5 and figure 5 – 5.

Table 5 - 5: Table showing the release of doxorubicin from MIP-SD-D and MIP-SN-B in comparison to a control solution of doxorubicin

Time (Mins)	Amount of doxorubicin released (mg mL^{-1}) Standard deviation = ± 0.001mg mL^{-1}		
	MIP-SD-D	MIP-SN-B	Doxorubicin Control Solution
0	0.000	0.000	0.000
5	0.106	0.106	0.144
10	0.165	0.165	0.236
15	0.209	0.209	0.301
20	0.248	0.248	0.352
25	0.282	0.282	0.401
30	0.311	0.311	0.444
35	0.334	0.335	0.483
40	0.356	0.358	0.521
45	0.377	0.381	0.553
50	0.398	0.401	0.583
55	0.417	0.421	0.609
60	0.437	0.441	0.633
90	0.534	0.547	0.754
120	0.610	0.645	0.852
180	0.748	0.811	0.989

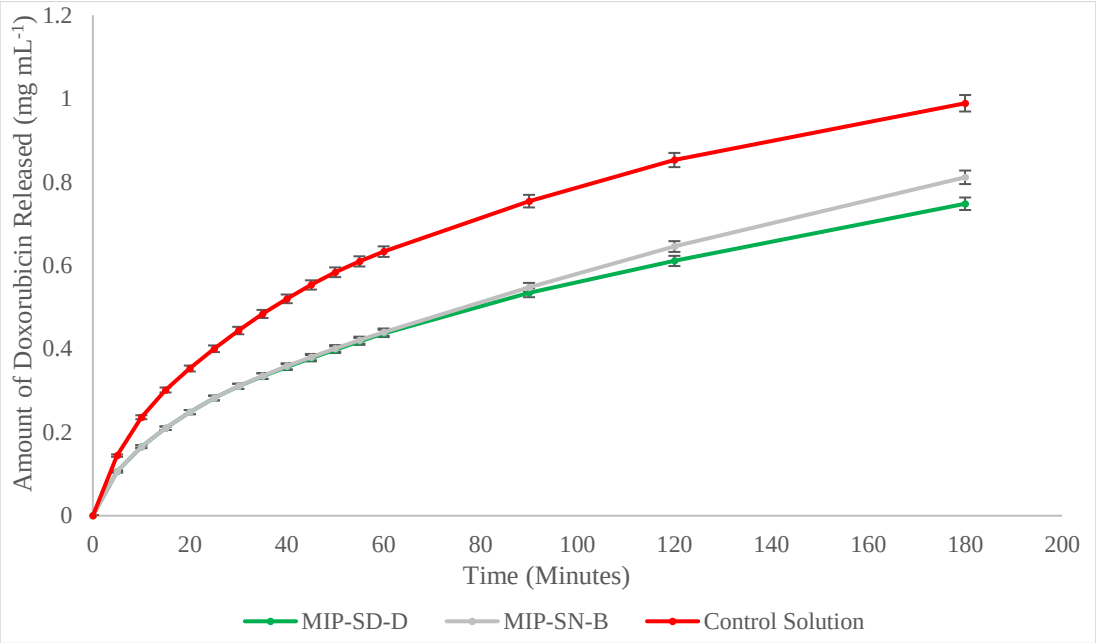

Figure 5 - 5: Graph showing a comparison of the release of doxorubicin from MIP-SD-D, MIP-SN-B and a doxorubicin control solution

During the initial 5 minutes of the experiments, the control solution of doxorubicin demonstrated an initial release of doxorubicin at a rate of 0.028 mg mL^{-1} min^{-1} whereas the MIP-SD-D and MIP-SN-B demonstrated a rate of 0.021 mg mL^{-1} min^{-1} and 0.021 mg mL^{-1} min^{-1} respectively. All species demonstrated very similar rates of the initial release. The rate of release of the doxorubicin from the doxorubicin control solution decreased to 0.019 mg mL^{-1} min^{-1} at the 5-minute mark before decreasing to 0.009 mg mL^{-1} min^{-1} at the 20-minute mark. At the 30-minute mark, the rate decreased to 0.008 mg mL^{-1} min^{-1} before gradually decreasing over the remainder of the experiment.

The rate of release of the doxorubicin from the MIP-SN-B species of nanoparticles decreased to 0.019 mg mL^{-1} min^{-1} at the 5-minute mark before decreasing to 0.006 mg mL^{-1} min^{-1} at the 20-minute mark. At the 30-minute mark, the rate decreased to 0.005 mg mL^{-1} min^{-1} before gradually decreasing over the remainder of the experiment.

The rate of release of the doxorubicin from the MIP-SD-D species of nanoparticles decreased to 0.019 mg mL^{-1} min^{-1} at the 5-minute mark before decreasing to 0.006 mg mL^{-1} min^{-1} at the 20-minute mark. At the 30-minute mark, the rate decreased to 0.004 mg mL^{-1} min^{-1} before gradually decreasing over the remainder of the experiment.

Overall the doxorubicin control solution demonstrated the highest release of doxorubicin compared to both of the nanoparticle species, whereas MIP-SD-D demonstrated the lowest amount of doxorubicin release with 75.6% of the amount of doxorubicin from the control solution being released.

5.4.3.2. Doxorubicin release from EGFR imprinted organic nanoparticles

MIP-OSD was tested after washing the nanoparticles to remove unreacted monomers and doxorubicin. The nanoparticles were pre-incubated with doxorubicin (1.mg, 1.84µmol) for the release testing. The release of doxorubicin was monitored as described in 6.3.2. The molecularly imprinted nanoparticles were tested against the control MIP-OSN nanoparticles incubated with doxorubicin and a control solution of doxorubicin. The results are shown in Table 5 – 6 and figure 5 – 6.

Table 5 - 6: Table showing the release of doxorubicin from MIP-OSD and MIP-OSN in comparison to a control solution of doxorubicin

Time (Mins)	Amount of doxorubicin released (mg mL^{-1}) Standard deviation = ± 0.001mg mL^{-1}		
	MIP-OSD	MIP-OSN	Doxorubicin Control Solution
0	0.000	0.000	0.000
5	0.072	0.073	0.109
10	0.127	0.124	0.193
15	0.168	0.164	0.261
20	0.204	0.198	0.318
25	0.235	0.229	0.369
30	0.261	0.257	0.414
35	0.284	0.284	0.455
40	0.306	0.309	0.494
45	0.327	0.334	0.531
50	0.346	0.358	0.564
55	0.364	0.382	0.596
60	0.382	0.405	0.624
90	0.482	0.539	0.754
120	0.573	0.647	0.847
180	0.727	0.793	0.993

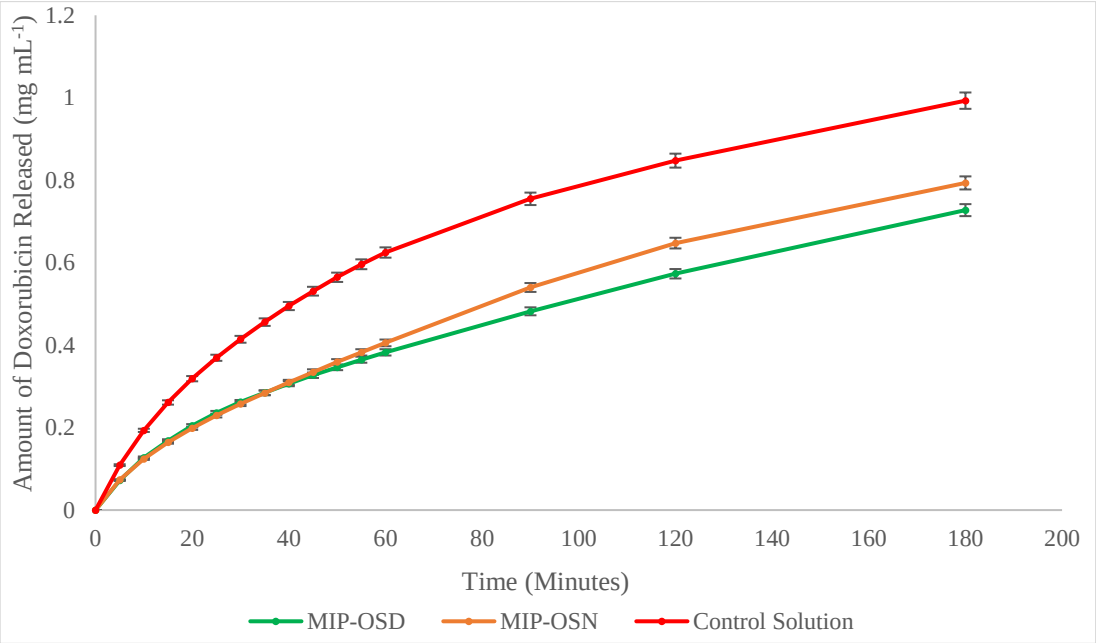

Figure 5 - 6: Graph showing a comparison of the release of doxorubicin from MIP-OSD, MIP-OSN and a doxorubicin control solution

During the initial 5 minutes of the experiments, the control solution of doxorubicin demonstrated an initial release of doxorubicin at a rate of 0.022 mg mL^{-1} min^{-1} whereas the MIP-OSD and MIP-OSN-A demonstrated a rate of 0.014 mg mL^{-1} min^{-1} and 0.015 mg mL^{-1} min^{-1} respectively. All species demonstrated very similar rates of the initial release.

The rate of release of the doxorubicin from the doxorubicin control solution decreased to 0.017 mg mL^{-1} min^{-1} at the 5-minute mark before decreasing to 0.011 mg mL^{-1} min^{-1} at the 20-minute mark. At the 30-minute mark, the rate decreased to 0.008 mg mL^{-1} min^{-1} before gradually decreasing over the remainder of the experiment.

The rate of release of the doxorubicin from the MIP-OSN species of nanoparticles decreased to 0.010 mg mL^{-1} min^{-1} at the 5-minute mark before decreasing to 0.006 mg mL^{-1} min^{-1} at the 20-minute mark. At the 30-minute mark, the rate decreased to 0.005 mg mL^{-1} min^{-1} before gradually decreasing over the remainder of the experiment.

The rate of release of the doxorubicin from the MIP-OSD species of nanoparticles decreased to 0.011 mg mL^{-1} min^{-1} at the 5-minute mark before decreasing to 0.006 mg mL^{-1} min^{-1} at the 20-minute mark. At the 30-minute mark, the rate decreased to 0.004 mg mL^{-1} min^{-1} before gradually decreasing over the remainder of the experiment.

Overall the doxorubicin control solution demonstrated the highest release of doxorubicin compared to both of the nanoparticle species, whereas MIP-OSD demonstrated the lowest

amount of doxorubicin release with 73.2% of the amount of doxorubicin from the control solution being released.

5.4.4. Comparison of the release profiles of vancomycin and aqueous and organic EGFR imprinted nanoparticles

To determine which nanoparticle composition was most useful for the retention and controlled release of doxorubicin, MIP-SD-B (vancomycin imprinted nanoparticles), MIP-SD-D (aqueous EGFR imprinted nanoparticles) and MIP-OSD (organic EGFR imprinted nanoparticles) were compared alongside a control solution of doxorubicin. The results are shown in Table 5 – 7 and figure 5 – 7.

Table 5 - 7: Table showing the release of doxorubicin from MIP-SD-B, MIP-SD-D and MIP-OSD in comparison to a control solution of doxorubicin

Time (Mins)	Amount of doxorubicin released (mg mL^{-1}) Standard deviation = ± 0.002mg mL^{-1}			
	MIP-SD-B	MIP-SD-D	MIP-OSD	Doxorubicin Control Solution
0	0.000	0.000	0.000	0.000
5	0.096	0.071	0.113	0.107
10	0.151	0.125	0.186	0.191
15	0.191	0.165	0.238	0.256
20	0.226	0.201	0.278	0.313
25	0.257	0.231	0.307	0.363
30	0.283	0.257	0.329	0.407
45	0.347	0.322	0.396	0.521
60	0.402	0.367	0.457	0.611
120	0.571	0.527	0.636	0.815
180	0.695	0.629	0.789	0.998

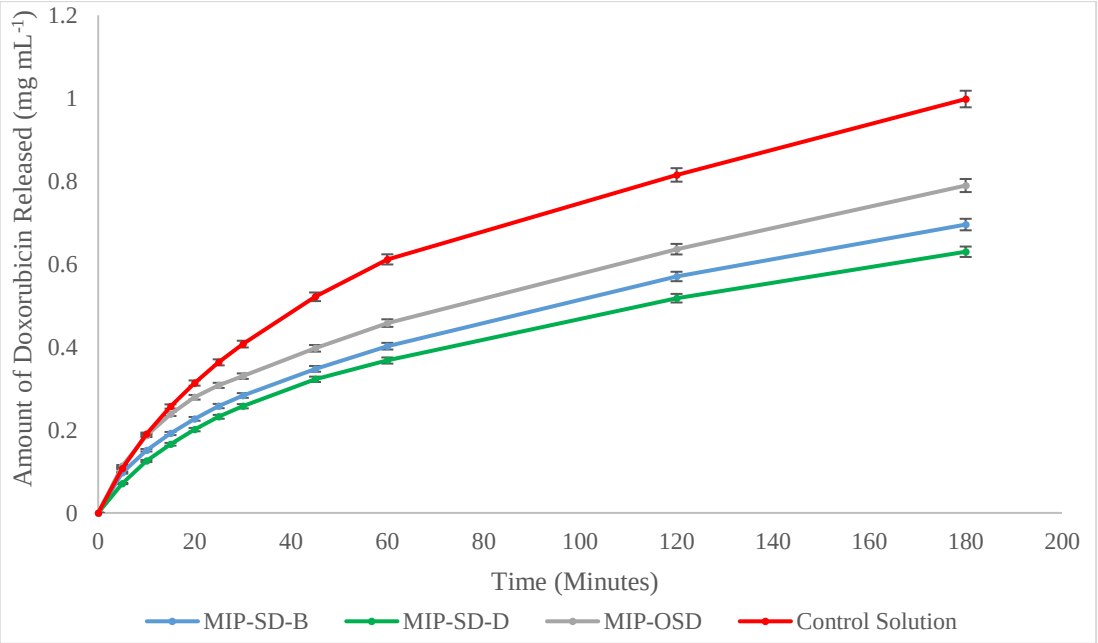

Figure 5 - 7: Graph showing a comparison of the release of doxorubicin from MIP-SD-B, MIP-SD-D, MIP-OSD and a doxorubicin control solution

During the initial 5 minutes of the experiments, the control solution of doxorubicin demonstrated an initial release of doxorubicin at a rate of 0.021 mg mL^{-1} min^{-1} whereas the MIP-SD-B, MIP-SD-D and MIP-OSD demonstrated a rate of 0.019 mg mL^{-1} min^{-1}, 0.014 mg mL^{-1} min^{-1} and 0.022 mg mL^{-1} min^{-1} respectively. All species demonstrated very similar rates of the initial release.

The rate of release of the doxorubicin from the doxorubicin control solution decreased to 0.016 mg mL^{-1} min^{-1} at the 5-minute mark before decreasing to 0.010 mg mL^{-1} min^{-1} at the 20-minute mark. At the 30-minute mark, the rate decreased to 0.007 mg mL^{-1} min^{-1} and 0.003 mg mL^{-1} min^{-1} at the 60-minute mark before gradually decreasing over the remainder of the experiment.

The rate of release of the doxorubicin from the MIP-SD-B species of nanoparticles decreased to 0.011 mg mL^{-1} min^{-1} at the 5-minute mark before decreasing to 0.006 mg mL^{-1} min^{-1} at the 20-minute mark. At the 30-minute mark, the rate decreased to 0.004 mg mL^{-1} min^{-1} before gradually decreasing over the remainder of the experiment.

The rate of release of the doxorubicin from the MIP-SD-D species of nanoparticles decreased to 0.011 mg mL^{-1} min^{-1} at the 5-minute mark before decreasing to 0.006 mg mL^{-1} min^{-1} at the 20-minute mark. At the 30-minute mark, the rate decreased to 0.004 mg mL^{-1} min^{-1} before gradually decreasing over the remainder of the experiment.

The rate of release of the doxorubicin from the MIP-OSD species of nanoparticles decreased to 0.014 mg mL^{-1} min^{-1} at the 5-minute mark before decreasing to 0.006 mg

mL^{-1} min^{-1} at the 20-minute mark. At the 30-minute mark, the rate decreased to 0.004 mg mL^{-1} min^{-1} before gradually decreasing over the remainder of the experiment.

Overall the doxorubicin control solution demonstrated the highest release of doxorubicin compared to both of the nanoparticle species, whereas MIP-SD-D demonstrated the lowest amount of doxorubicin release with 63.1% of the amount of doxorubicin from the control solution being released.

5.5 Conclusions

The solid phase synthesis of nanoparticles has been demonstrated to be an innovative technique for producing nanoparticles designed to bind to a specific target. These nanoparticles can be modified to incorporate a secondary internal template into the structure of the nanoparticles. These nanoparticles can be used to deliver a payload to a target cell or system and where the payload undergoes a controlled release over time. In these experiments, doxorubicin was used as the secondary template for controlled delivery to cancer cells. Initially, the nanoparticles were synthesised using vancomycin as the primary template to determine the retention properties of the nanoparticles in the presence of doxorubicin in the polymerisation mixture for use as a secondary template.

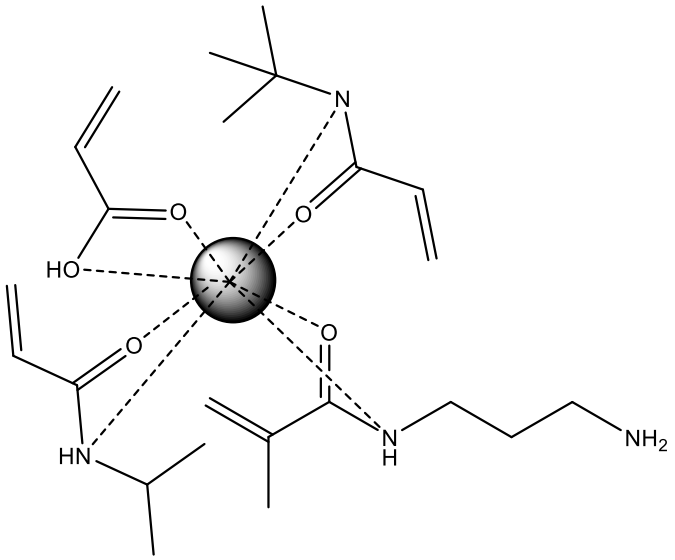

Figure 5 - 8: Binding schematic of the aqueous solvent synthesised nanoparticles

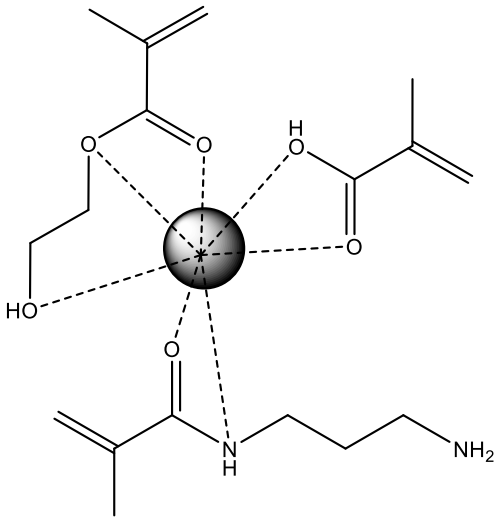

Figure 5 - 9: Binding schematic of the organic solvent synthesised nanoparticles

Three different doxorubicin amounts were used to determine a suitable quantity of doxorubicin to incorporate with MIP-SD-B utilising 1mg of doxorubicin in the polymerisation mixture producing the best results, with the lowest amount of release observed from this species in comparison to the free doxorubicin solution. This amount of doxorubicin in the polymerisation was used for subsequent testing in later experiments. The nanoparticles were then synthesised using a different primary template at the same doxorubicin concentration used. The second template used was an EGFR binding peptide binding target for the delivery of doxorubicin to cancer cells. The aqueous synthesised nanoparticles were tested first, followed by the organic nanoparticles with both types showing a lower rate of release compared to the free doxorubicin solution. All the solid phase synthesised doxorubicin imprinted nanoparticles demonstrated a lower release amount than the solid phase synthesised non-doxorubicin nanoparticles, this indicates that some of the doxorubicin was being retained by the nanoparticles internal binding sites located within the nanoparticles. When the MIP-SD-B, MIP-SD-D and MIP-OSD nanoparticle release profiles were compared, the organic nanoparticles were found to have the highest amount of doxorubicin release during the experiment with the release being 21% less than the free doxorubicin solution. In contrast, both the vancomycin templated and EGFR templated nanoparticles displayed a lower amount of doxorubicin release compared to both the free doxorubicin solution and organic solvent synthesised nanoparticles with the aqueous, EGFR peptide templated nanoparticles demonstrating the lowest overall doxorubicin release.

Chapter 6: Effect of the primary template on the release of doxorubicin from internally loaded nanoparticles.

6.1. Introduction

Following on from chapter 5, the effect of primary template presence on the release profile of doxorubicin was investigated. The presence of the primary template was tested with both the vancomycin and EGFR binding peptide imprinted nanoparticles to determine whether this would have any effect on the release of doxorubicin. The template was added at the start of the experiment on both sides of the membrane to prevent the generation of a dialysis gradient. The presence of the template in solution was to simulate a binding interaction between the nanoparticles and the template as binding usually occurs 2 hours after admission to cells.[116]

6.1.1. Aim and objectives

Aim of the chapter:

- Testing the effect of primary template presence on the release of doxorubicin from solid phase synthesised imprinted nanoparticles with different templates.

Objectives for this chapter:

- Testing of the release of doxorubicin from the nanoparticles with the primary template present in solution.
- Comparing the doxorubicin imprinted nanoparticles against the non-imprinted nanoparticles with the primary template present in solution.

6.2. Chemicals

Glass beads SPHERIGLASS® A-Glass 2429 (70 – 100 µm diameter) obtained from Potters Industries LLC. A dialysis membrane (Spectra/Por, MWCO = 10 kDa) was purchased from Spectrum Laboratories Inc. Acrylic acid, ammonium persulfate, 1,2-bis(trimethoxysilyl)ethane, glutaraldehyde, phosphate buffered saline tablets, N-isopropylacrylamide, N′-methylene-bisacrylamide, N-tert-butylacrylamide, N, N, N′, N′-tetramethylethylenediamine, Iodoacetic acid N-hydroxysuccinimide ester, vancomycin hydrochloride, acetone, ethanol, methanol and toluene were purchased from Sigma-Aldrich, UK. (3-Aminopropyl) trimethoxysilane and sodium cyanoborohydride were obtained from Acros Organics. N-(3-Aminopropyl) methacrylamide hydrochloride was purchased from PolySciences Inc., UK. Amicon Ultra-15 Centrifugal Filter Units (MWCO 30 kDa), Acetonitrile, sodium hydroxide and sulphuric acid were obtained from Fisher Scientific (UK). Doxorubicin Hydrochloride was purchased from Cambridge Bioscience, UK. Ultrapure water was produced by a Millipore Milli-Q system (Millipore, Bedford, MA, USA), Double-distilled ultrapure water (Millipore) was used for analysis. All chemicals and solvents were analytical or HPLC grade and were used without further purification. Phosphate buffered saline was prepared as directed from PBS buffer tablets (Sigma-Aldrich, Gillingham, UK).

6.3. Methods

6.3.1. Solid phase preparation of nanoparticles

The preparation of the glass beads and nanoparticles was carried out as described in 5.3.2 as the same nanoparticle compositions were used. List of species used listed in Table 6 – 1.

Table 6 - 1: Table showing a list of all nanoparticle species to be tested

Species	**Doxorubicin present**	**Previous purpose of the nanoparticles**
Vancomycin imprinted aqueous nanoparticles		
MIP-SD-B	Yes	Determining the release profile of doxorubicin-loaded aqueous nanoparticles imprinted for vancomycin
MIP-SN-A	No	
EGFR peptide imprinted aqueous nanoparticles		
MIP-SD-D	Yes	Determining the release profile of doxorubicin-loaded aqueous nanoparticles imprinted for EGFR targeting
MIP-SN-B	No	
EGFR peptide imprinted organic nanoparticles		
MIP-OSD	Yes	Determining the release profile of doxorubicin-loaded organic nanoparticles
MIP-OSN	No	

6.3.2. Effect of the primary template on the release profile of doxorubicin.

Carried out as in 5.3.2, however, to determine if template presence influences doxorubicin release it was added at the beginning of the experiment to simulate the presence of the target template.

6.3.4.1. Effect of vancomycin as a template

The experiments were carried out as described in 5.3.2. on the MIP-SD-B and MIP-SN-A nanoparticles. However, vancomycin (10 mg) was added at the start of the experiment to the solution on the outside of the dialysis membrane and 0.01 mg to the inside.

6.3.4.2. Effect of EGFR peptide as a template on aqueous nanoparticles

These experiments were carried out as described in 5.3.2. on the MIP-SD-D and MIP-SN-B nanoparticles. However, EGFR peptide (1 mg) was added at the start of the experiment to the solution on the outside of the dialysis membrane and 0.001 mg on the inside.

6.3.4.3. Effect of EGFR peptide as a template on organic nanoparticles

These experiments were carried out as described in 5.3.2. on the MIP-OSD and MIP-OSN nanoparticles. However, EGFR peptide (1mg) was added at the start of the experiment to the solution on both the inside and outside of the dialysis membrane.

6.4. Analysis and discussion.

6.4.1. Nanoparticle preparation

The solid phase and all the nanoparticles were successfully synthesised as described in 5.3.1. List of species used listed in Table 6 – 2.

Table 6 - 2: Table showing a list of all nanoparticle species to be tested

Species	**Doxorubicin present**	**Previous purpose of the nanoparticles**
EGFR peptide imprinted organic nanoparticles		
MIP-OSD	Yes	Determining the release profile of doxorubicin-loaded organic nanoparticles
MIP-OSN	No	
Vancomycin imprinted aqueous nanoparticles		
MIP-SD-B	Yes	Determining the release profile of doxorubicin-loaded aqueous nanoparticles imprinted for vancomycin
MIP-SN-A	No	
EGFR peptide imprinted aqueous nanoparticles		
MIP-SD-D	Yes	Determining the release profile of doxorubicin-loaded aqueous nanoparticles imprinted for EGFR targeting
MIP-SN-B	No	

6.4.2. Effect of vancomycin presence on doxorubicin release

To determine if the presence and binding of the vancomycin affect the release profile of doxorubicin from the nanoparticles, vancomycin was added to the nanoparticle solution at the beginning of the experiment. As described in 5.4.2, the nanoparticles were tested by measuring the concentration on the inside of the membrane cell. By this method, the change in concentration is monitored by determining the decrease in doxorubicin fluorescence detected. From this, the rate of release of doxorubicin is determined. The amount of doxorubicin release was calculated as a cumulative % of the overall experiment its comparison to the free doxorubicin solution.

Initially, the vancomycin templated species, MIP-SD-B were tested alongside its non-doxorubicin containing counterpart MIP-SN-A and free doxorubicin with vancomycin added to the inside and outside of the dialysis membrane to simulate interaction with the primary template alongside a control solution of doxorubicin with vancomycin present. The results are shown in Table 6 – 3 and figure 6 – 1.

Table 6 - 3: Table showing the release of doxorubicin from MIP-SD-B and MIP-SN-A in comparison to a control solution of doxorubicin with vancomycin present

Time (Mins)	Amount of doxorubicin released (mg mL^{-1}) Standard deviation = ± 0.001mg mL^{-1}		
	MIP-SD-B	MIP-SN-A	Doxorubicin Control Solution
0	0.000	0.000	0.000
5	0.072	0.073	0.109
10	0.127	0.124	0.193
15	0.168	0.164	0.261
20	0.204	0.198	0.318
25	0.235	0.229	0.369
30	0.261	0.257	0.414
35	0.284	0.284	0.455
40	0.306	0.309	0.494
45	0.327	0.334	0.529
50	0.346	0.358	0.564
55	0.364	0.382	0.596
60	0.382	0.405	0.624
90	0.482	0.539	0.754
120	0.573	0.647	0.847
180	0.727	0.793	0.987

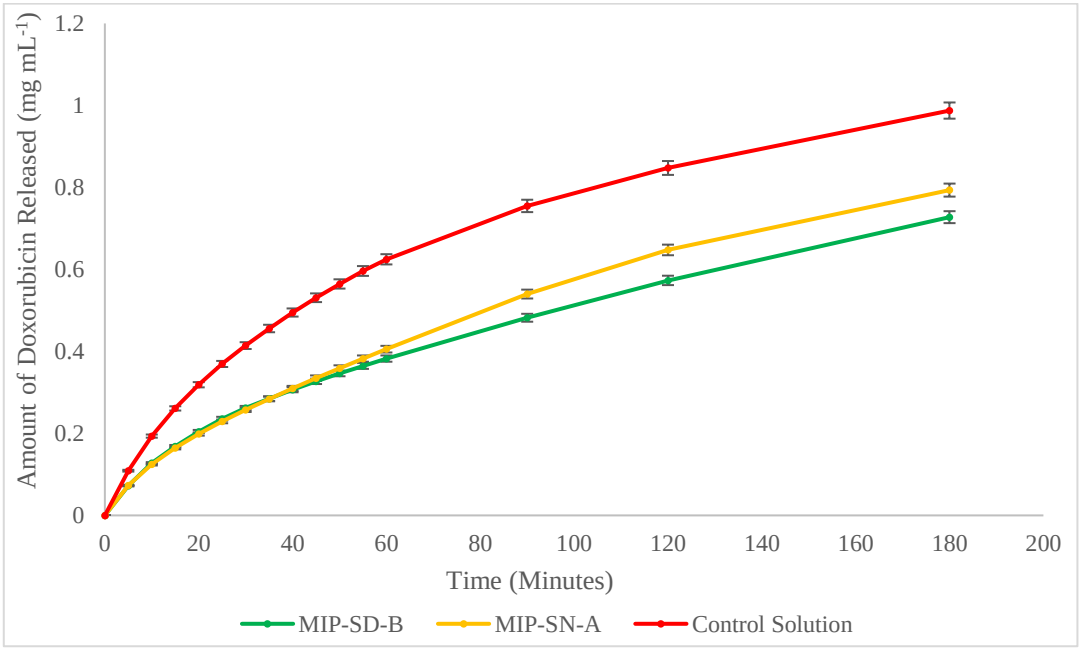

Figure 6 - 1: Graph showing a comparison of the release of doxorubicin from MIP-SD-B, MIP-SN-A and a doxorubicin control solution in the presence of vancomycin

During the initial 5 minutes of the experiments, the control solution of doxorubicin demonstrated an initial release of doxorubicin at a rate of 0.022 mg mL^{-1} min^{-1} whereas the MIP-SD-B and MIP-SN-A demonstrated a rate of 0.015 mg mL^{-1} min^{-1} and 0.014 mg mL^{-1} min^{-1} respectively.

The rate of release of the doxorubicin from the doxorubicin control solution decreased to 0.016 mg mL^{-1} min^{-1} at the 5-minute mark before decreasing to 0.011 mg mL^{-1} min^{-1} at the 20-minute mark. At the 30-minute mark, the rate decreased to 0.008 mg mL^{-1} min^{-1} before decreasing to 0.005 mg mL^{-1} min^{-1} at the 60-minute mark. The rate of release gradually decreased over the remainder of the experiment.

The rate of release of the doxorubicin from the MIP-SN-A decreased to 0.011 mg mL^{-1} min^{-1} at the 5-minute mark before decreasing to 0.006 mg mL^{-1} min^{-1} at the 20-minute mark. At the 30-minute mark, the rate decreased to 0.005 mg mL^{-1} min^{-1} before decreasing to 0.004 mg mL^{-1} min^{-1} at the 60-minute mark. The rate of release gradually decreased over the remainder of the experiment.

The rate of release of the doxorubicin from the MIP-SD-B decreased to 0.011 mg mL^{-1} min^{-1} at the 5-minute mark before decreasing to 0.006 mg mL^{-1} min^{-1} at the 20-minute mark. At the 30-minute mark, the rate decreased to 0.004 mg mL^{-1} min^{-1} before decreasing to 0.003 mg mL^{-1} min^{-1} at the 60-minute mark. The rate of release gradually decreased over the remainder of the experiment.

Overall the doxorubicin control solution containing vancomycin demonstrated the highest release of doxorubicin compared to both of the nanoparticle species, whereas MIP-SD-B demonstrated the lowest amount of doxorubicin release with 73.6% of the amount of doxorubicin from the control solution being released.

Secondly, the vancomycin templated species, MIP-SD-B nanoparticles were tested and compared with and without vancomycin being present in the solution. Also tested, were the MIP-SN-A nanoparticles with and without vancomycin being present in solution. From this, a comparison of the effect of template presence could be seen for both the doxorubicin-loaded and non-doxorubicin loaded nanoparticles. These nanoparticles were tested alongside a control solution of doxorubicin with vancomycin present. The results are shown in Table 6 – 4 and figure 6 – 2.

Table 6 - 4: Table showing the release of doxorubicin from MIP-SD-B and MIP-SN-A in comparison to a control solution of doxorubicin with and without vancomycin present

Time (Mins)	Amount of doxorubicin released (mg mL^{-1}) Standard deviation = ± 0.001mg mL^{-1}				
	No vancomycin added		Vancomycin added		Doxorubicin Control Solution
	MIP-SD-B	MIP-SN-A	MIP-SD-B	MIP-SN-A	
0	0.000	0.000	0.000	0.000	0.000
5	0.091	0.094	0.093	0.097	0.121
10	0.152	0.154	0.154	0.158	0.204
15	0.202	0.203	0.204	0.209	0.273
20	0.245	0.248	0.247	0.255	0.332
25	0.284	0.290	0.286	0.298	0.384
30	0.320	0.328	0.321	0.336	0.431
35	0.353	0.363	0.354	0.371	0.473
40	0.382	0.395	0.384	0.404	0.511
45	0.401	0.426	0.412	0.437	0.547
50	0.435	0.456	0.437	0.467	0.579
55	0.459	0.484	0.461	0.496	0.606
60	0.484	0.510	0.482	0.523	0.628
90	0.579	0.643	0.595	0.658	0.743
120	0.641	0.745	0.667	0.759	0.843
180	0.765	0.895	0.795	0.901	0.992

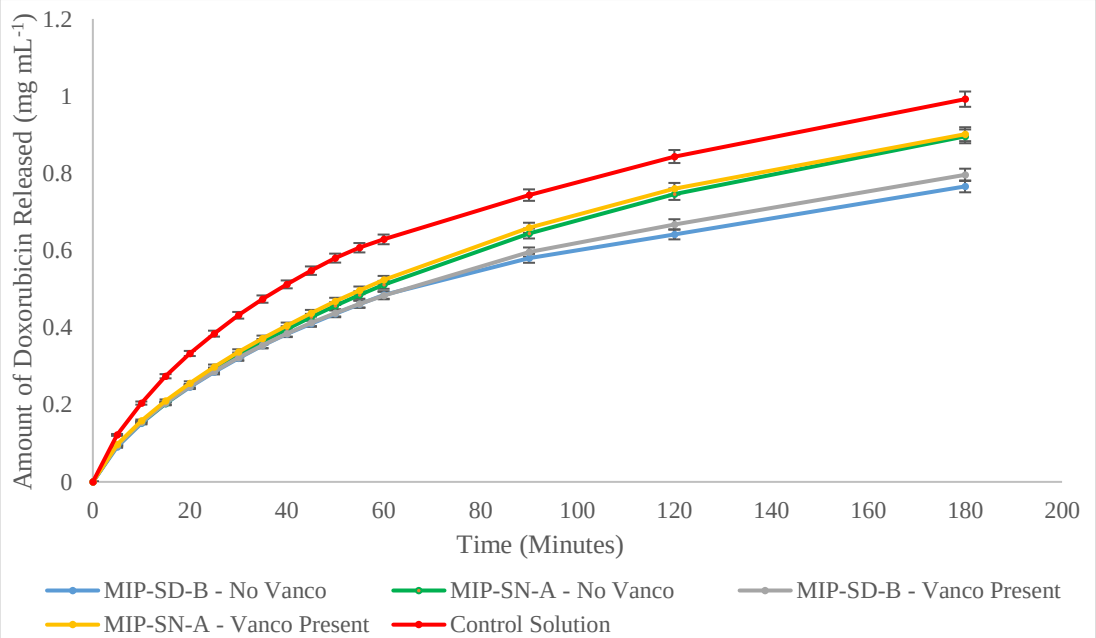

Figure 6 - 2: Graph showing a comparison of the release of doxorubicin from MIP-SD-A, MIP-SN-A and a doxorubicin control solution with and without vancomycin present

During the initial 5 minutes of the experiments, the control solution of doxorubicin-containing vancomycin demonstrated an initial release of doxorubicin at a rate of 0.024 mg mL^{-1} min^{-1} whereas the MIP-SD-B and MIP-SN-A in the presence of vancomycin demonstrated a rate of 0.018 mg mL^{-1} min^{-1} and 0.019 mg mL^{-1} min^{-1} respectively.

Whereas, without vancomycin present MIP-SD-B and MIP-SN-A demonstrated a rate of release of 0.018 mg mL^{-1} min^{-1} and 0.019 mg mL^{-1} min^{-1} respectively.

The rate of release of the doxorubicin from the doxorubicin control solution containing vancomycin decreased to 0.017 mg mL^{-1} min^{-1} at the 5-minute mark before decreasing to 0.011 mg mL^{-1} min^{-1} at the 20-minute mark. At the 30-minute mark, the rate decreased to 0.008 mg mL^{-1} min^{-1} before decreasing to 0.003 mg mL^{-1} min^{-1} at the 60-minute mark. The rate of release gradually decreased over the remainder of the experiment.

The rate of release of the doxorubicin from the MIP-SN-A in the presence of vancomycin decreased to 0.012 mg mL^{-1} min^{-1} at the 5-minute mark before decreasing to 0.009 mg mL^{-1} min^{-1} at the 20-minute mark. At the 30-minute mark, the rate decreased to 0.007 mg mL^{-1} min^{-1} before decreasing to 0.004 mg mL^{-1} min^{-1} at the 60-minute mark. The rate of release gradually decreased over the remainder of the experiment.

The rate of release of the doxorubicin from the MIP-SD-B in the presence of vancomycin decreased to 0.012 mg mL^{-1} min^{-1} at the 5-minute mark before decreasing to 0.007 mg mL^{-1} min^{-1} at the 20-minute mark. At the 30-minute mark, the rate decreased to 0.006 mg mL^{-1} min^{-1} before decreasing to 0.003 mg mL^{-1} min^{-1} at the 60-minute mark. The rate of release gradually decreased over the remainder of the experiment.

The rate of release of the doxorubicin from the MIP-SN-A without vancomycin present decreased to 0.012 mg mL^{-1} min^{-1} at the 5-minute mark before decreasing to 0.008 mg mL^{-1} min^{-1} at the 20-minute mark. At the 30-minute mark, the rate decreased to 0.007 mg mL^{-1} min^{-1} before decreasing to 0.004 mg mL^{-1} min^{-1} at the 60-minute mark. The rate of release gradually decreased over the remainder of the experiment.

The rate of release of the doxorubicin from the MIP-SD-B without vancomycin present decreased to 0.012 mg mL^{-1} min^{-1} at the 5-minute mark before decreasing to 0.007 mg mL^{-1} min^{-1} at the 20-minute mark. At the 30-minute mark, the rate decreased to 0.006 mg mL^{-1} min^{-1} before decreasing to 0.003 mg mL^{-1} min^{-1} at the 60-minute mark. The rate of release gradually decreased over the remainder of the experiment.

Overall the free doxorubicin solution demonstrated the highest release of doxorubicin compared to both of the nanoparticle species, whereas MIP-SD-B without vancomycin present demonstrated the lowest amount of doxorubicin release with 77.2% of the amount of doxorubicin from the control solution being released.

6.4.3. Effect of EGFR peptide presence on doxorubicin release

To determine if the presence and binding of the EGFR binding peptide affects the release profile of doxorubicin from the nanoparticles, EGFR binding peptide was added to the nanoparticle solution at the beginning of the experiment. As described in 6.4.2, the nanoparticles were tested by measuring the concentration on the inside of the membrane cell. By this method, the change in concentration is monitored by determining the decrease in doxorubicin fluorescence detected. From this, the rate of release of doxorubicin is determined.

6.4.3.1. Effect of EGFR peptide as a template on aqueous nanoparticles

Initially, the aqueous synthesised nanoparticles were tested with the EGFR binding peptide added to the solution on the inside and outside of the dialysis membrane to simulate the presence of primary template presence. The EGFR templated species, MIP-SD-D was tested alongside its non-doxorubicin containing counterpart MIP-SN-B and free doxorubicin with EGFR binding peptide added to the inside and outside of the dialysis membrane to simulate interaction with the primary template alongside a control solution of doxorubicin with EGFR peptide present. The results are shown in Table 6 – 5 and figure 6 – 3.

Table 6 - 5: Table showing the release of doxorubicin from MIP-SD-D and MIP-SN-B in comparison to a control solution of doxorubicin with EGFR peptide present

Time (Mins)	Amount of doxorubicin released (mg mL^{-1}) Standard deviation = ± 0.001mg mL^{-1}		
	MIP-SD-D	MIP-SN-B	Doxorubicin Control Solution
0	0.000	0.000	0.000
5	0.059	0.076	0.088
10	0.103	0.123	0.152
15	0.142	0.164	0.209
20	0.178	0.202	0.262
25	0.213	0.241	0.309
30	0.247	0.277	0.353
35	0.281	0.311	0.395
40	0.312	0.343	0.437
45	0.343	0.373	0.478
50	0.369	0.397	0.517
55	0.391	0.418	0.555
60	0.407	0.436	0.591
90	0.488	0.517	0.751
120	0.531	0.588	0.849
180	0.586	0.678	0.989

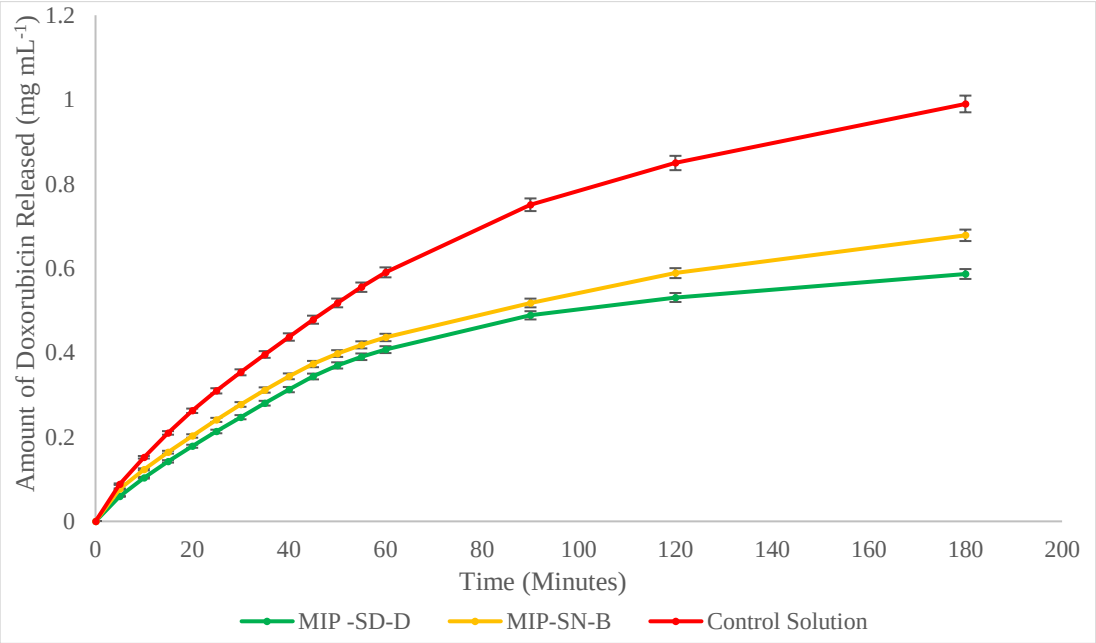

Figure 6 - 3: Graph showing a comparison of the release of doxorubicin from MIP-SD-D, MIP-SN-B and a doxorubicin control solution in the presence of EGFR peptide

During the initial 5 minutes of the experiments, the control solution of doxorubicin demonstrated an initial release of doxorubicin at a rate of 0.017 mg mL^{-1} min^{-1} whereas the MIP-SD-D and MIP-SN-B demonstrated a rate of 0.015 mg mL^{-1} min^{-1} and 0.012 mg mL^{-1} min^{-1} respectively.

The rate of release of the doxorubicin from the doxorubicin control solution decreased to 0.013 mg mL^{-1} min^{-1} at the 5-minute mark before decreasing to 0.009 mg mL^{-1} min^{-1} at the 20-minute mark. At the 30-minute mark, the rate decreased to 0.008 mg mL^{-1} min^{-1} before decreasing to 0.005 mg mL^{-1} min^{-1} at the 60-minute mark. The rate of release gradually decreased over the remainder of the experiment.

The rate of release of the doxorubicin from the MIP-SN-B decreased to 0.009 mg mL^{-1} min^{-1} at the 5-minute mark before decreasing to 0.008 mg mL^{-1} min^{-1} at the 20-minute mark. At the 30-minute mark, the rate decreased to 0.007 mg mL^{-1} min^{-1} before decreasing to 0.003 mg mL^{-1} min^{-1} at the 60-minute mark. The rate of release gradually decreased over the remainder of the experiment.

The rate of release of the doxorubicin from the MIP-SD-D decreased to 0.008 mg mL^{-1} min^{-1} at the 5-minute mark before decreasing to 0.007 mg mL^{-1} min^{-1} at the 20-minute mark. At the 30-minute mark, the rate decreased to 0.006 mg mL^{-1} min^{-1} before decreasing to 0.002 mg mL^{-1} min^{-1} at the 60-minute mark. The rate of release gradually decreased over the remainder of the experiment.

Overall the doxorubicin control solution demonstrated the highest release of doxorubicin compared to both of the nanoparticle species, whereas MIP-SD-D demonstrated the lowest amount of doxorubicin release with 59.2% of the amount of doxorubicin from the control solution being released.

Secondly, the EGFR templated species, MIP-SD-D nanoparticles were tested and compared with and without EGFR binding peptide present in the solution. Also tested, were the MIP-SN-B nanoparticles with and without EGFR binding peptide being present in solution. From this, a comparison of the effects of template presence could be seen for both the doxorubicin-loaded and non-doxorubicin loaded nanoparticles. These nanoparticles were also tested template alongside a control solution of doxorubicin with EGFR peptide present. The results are shown in Table 6 – 6 and figure 6 – 4.

Table 6 - 6: Table showing the release of doxorubicin from MIP-SD-D and MIP-SN-B in comparison to a control solution of doxorubicin with and without EGFR peptide present

Time (Mins)	Amount of doxorubicin released (mg mL^{-1}) Standard deviation = ± 0.001mg mL^{-1}				
	No EGFR peptide added		EGFR peptide added		Doxorubicin Control Solution
	MIP-SD-D	MIP-SN-B	MIP-SD-D	MIP-SN-B	
0	0.000	0.000	0.000	0.000	0.000
5	0.073	0.062	0.081	0.076	0.088
10	0.118	0.109	0.131	0.123	0.152
15	0.152	0.149	0.168	0.164	0.209
20	0.179	0.188	0.196	0.202	0.262
25	0.204	0.226	0.223	0.239	0.309
30	0.225	0.263	0.247	0.277	0.353
35	0.244	0.298	0.269	0.311	0.395
40	0.263	0.333	0.289	0.343	0.437
45	0.281	0.356	0.308	0.373	0.478
50	0.298	0.383	0.325	0.397	0.517
55	0.315	0.405	0.339	0.418	0.555
60	0.331	0.424	0.352	0.436	0.589
90	0.397	0.504	0.414	0.528	0.739
120	0.439	0.558	0.459	0.595	0.849
180	0.497	0.617	0.523	0.678	0.991

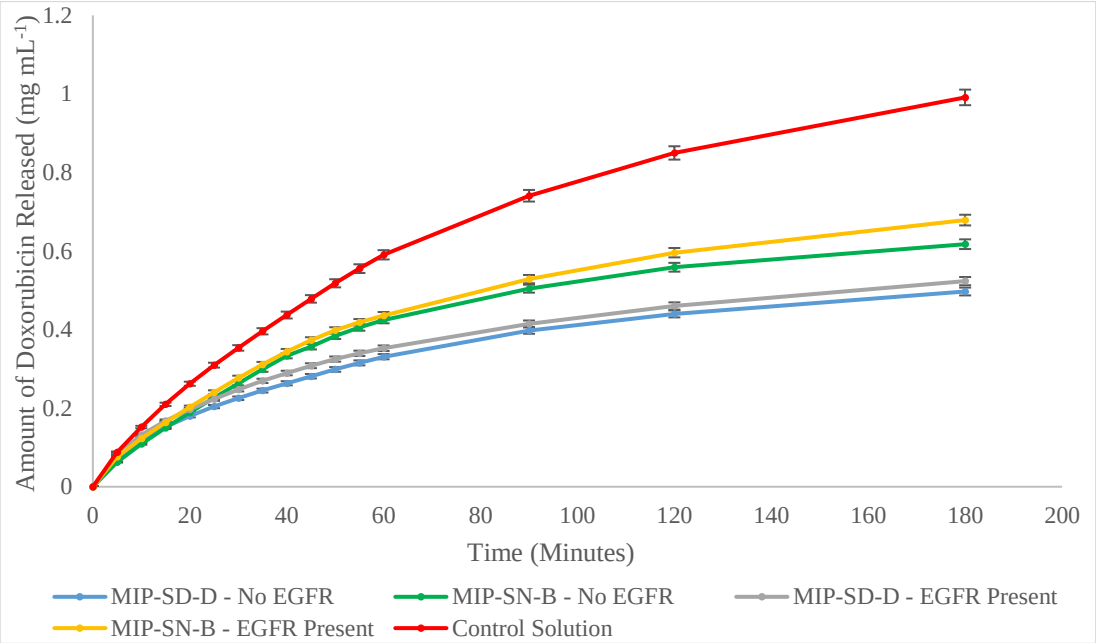

Figure 6 - 4: Graph showing a comparison of the release of doxorubicin from MIP-SD-D, MIP-SN-B and a doxorubicin control solution with and without EGFR peptide present

During the initial 5 minutes of the experiments, the control solution of doxorubicin-containing EGFR peptide demonstrated an initial release of doxorubicin at a rate of 0.017 mg mL^{-1} min^{-1} whereas the MIP-SD-D and MIP-SN-B in the presence of EGFR peptide demonstrated a rate of 0.016 mg mL^{-1} min^{-1} and 0.015 mg mL^{-1} min^{-1} respectively. Whereas, without EGFR peptide present MIP-SD-B and MIP-SN-A demonstrated a rate of release of 0.014 mg mL^{-1} min^{-1} and 0.012 mg mL^{-1} min^{-1} respectively.

The rate of release of the doxorubicin from the doxorubicin control solution containing EGFR peptide decreased to 0.012 mg mL^{-1} min^{-1} at the 5-minute mark before decreasing to 0.009 mg mL^{-1} min^{-1} at the 20-minute mark. At the 30-minute mark, the rate decreased to 0.008 mg mL^{-1} min^{-1} before decreasing to 0.005 mg mL^{-1} min^{-1} at the 60-minute mark. The rate of release gradually decreased over the remainder of the experiment.

The rate of release of the doxorubicin from the MIP-SN-B in the presence of EGFR peptide decreased to 0.009 mg mL^{-1} min^{-1} at the 5-minute mark before decreasing to 0.007 mg mL^{-1} min^{-1} at the 20-minute mark. At the 30-minute mark, the rate decreased to 0.006 mg mL^{-1} min^{-1} before decreasing to 0.003 mg mL^{-1} min^{-1} at the 60-minute mark. The rate of release gradually decreased over the remainder of the experiment.

The rate of release of the doxorubicin from the MIP-SD-D in the presence of EGFR peptide decreased to 0.010 mg mL^{-1} min^{-1} at the 5-minute mark before decreasing to 0.005 mg mL^{-1} min^{-1} at the 20-minute mark. At the 30-minute mark, the rate decreased to 0.004

mg mL^{-1} min^{-1} before decreasing to 0.002 mg mL^{-1} min^{-1} at the 60-minute mark. The rate of release gradually decreased over the remainder of the experiment.

The rate of release of the doxorubicin from the MIP-SN-B without EGFR peptide present decreased to 0.009 mg mL^{-1} min^{-1} at the 5-minute mark before decreasing to 0.008 mg mL^{-1} min^{-1} at the 20-minute mark. At the 30-minute mark, the rate decreased to 0.007 mg mL^{-1} min^{-1} before decreasing to 0.002 mg mL^{-1} min^{-1} at the 60-minute mark. The rate of release gradually decreased over the remainder of the experiment.

The rate of release of the doxorubicin from the MIP-SD-D without EGFR peptide present decreased to 0.009 mg mL^{-1} min^{-1} at the 5-minute mark before decreasing to 0.004 mg mL^{-1} min^{-1} at the 20-minute mark. At the 30-minute mark, the rate decreased to 0.003 mg mL^{-1} min^{-1} before decreasing to 0.002 mg mL^{-1} min^{-1} at the 60-minute mark. The rate of release gradually decreased over the remainder of the experiment.

Overall the doxorubicin control solution containing EGFR peptide demonstrated the highest release of doxorubicin compared to both of the nanoparticle species, whereas MIP-SD-B without EGFR peptide present demonstrated the lowest amount of doxorubicin release with 50.1% of the amount of doxorubicin from the control solution being released.

6.4.3.2. Effect of EGFR peptide as a template on organic nanoparticles

Secondly, the organic solvent synthesised nanoparticles were tested with the EGFR binding peptide added to the solution on the inside and outside of the dialysis membrane to simulate the presence of primary template presence. Initially, the EGFR templated species, MIP-OSD was tested alongside its non-doxorubicin containing counterpart MIP-OSN and free doxorubicin with EGFR binding peptide added to the inside and outside of the dialysis membrane to simulate interaction with the primary template alongside a control solution of doxorubicin with EGFR peptide present. The results are shown in Table 6 – 7 and figure 6 – 5.

Table 6 - 7: Table showing the release of doxorubicin from MIP-OSD and MIP-OSN in comparison to a control solution of doxorubicin with EGFR peptide present

Time (Mins)	Amount of doxorubicin released (mg mL^{-1}) Standard deviation = ± 0.001mg mL^{-1}		
	MIP-OSD	MIP-OSN	Doxorubicin Control Solution
0	0.000	0.000	0.000
5	0.055	0.081	0.133
10	0.097	0.148	0.231
15	0.128	0.204	0.307
20	0.154	0.251	0.369
25	0.177	0.287	0.426
30	0.199	0.334	0.478
35	0.219	0.361	0.527
40	0.237	0.391	0.569
45	0.253	0.409	0.607
50	0.267	0.437	0.639
55	0.279	0.459	0.666
60	0.289	0.481	0.687
90	0.336	0.545	0.789
120	0.372	0.579	0.869
180	0.426	0.625	0.989

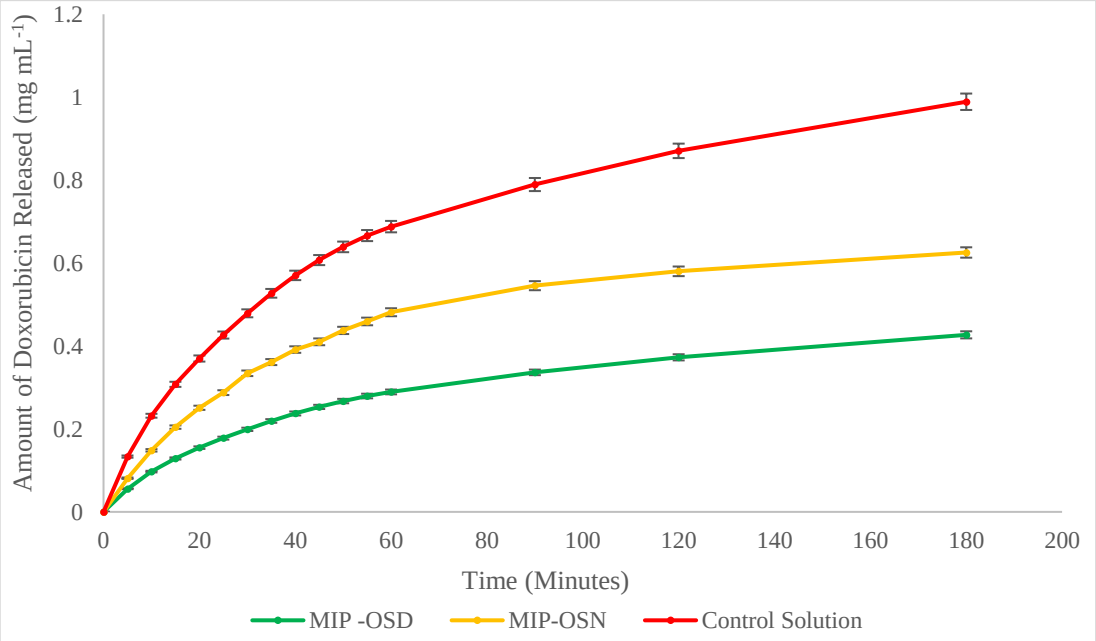

Figure 6 - 5: Graph showing a comparison of the release of doxorubicin from MIP-OSD, MIP-OSN and a doxorubicin control solution in the presence of EGFR peptide

During the initial 5 minutes of the experiments, the control solution of doxorubicin demonstrated an initial release of doxorubicin at a rate of 0.026 mg mL^{-1} min^{-1} whereas the MIP-OSD and MIP-OSN demonstrated a rate of 0.011 mg mL^{-1} min^{-1} and 0.016 mg mL^{-1} min^{-1} respectively.

The rate of release of the doxorubicin from the doxorubicin control solution decreased to 0.019 mg mL^{-1} min^{-1} at the 5-minute mark before decreasing to 0.011 mg mL^{-1} min^{-1} at the 20-minute mark. At the 30-minute mark, the rate decreased to 0.009 mg mL^{-1} min^{-1} before decreasing to 0.003 mg mL^{-1} min^{-1} at the 60-minute mark. The rate of release gradually decreased over the remainder of the experiment.

The rate of release of the doxorubicin from the MIP-OSN decreased to 0.013 mg mL^{-1} min^{-1} at the 5-minute mark before decreasing to 0.007 mg mL^{-1} min^{-1} at the 20-minute mark. At the 30-minute mark, the rate decreased to 0.005 mg mL^{-1} min^{-1} before decreasing to 0.002 mg mL^{-1} min^{-1} at the 60-minute mark. The rate of release gradually decreased over the remainder of the experiment.

The rate of release of the doxorubicin from the MIP-OSD decreased to 0.008 mg mL^{-1} min^{-1} at the 5-minute mark before decreasing to 0.005 mg mL^{-1} min^{-1} at the 20-minute mark. At the 30-minute mark, the rate decreased to 0.004 mg mL^{-1} min^{-1} before decreasing to 0.001 mg mL^{-1} min^{-1} at the 60-minute mark. The rate of release gradually decreased over the remainder of the experiment.

Overall the free doxorubicin solution demonstrated the highest release of doxorubicin compared to both of the nanoparticle species, whereas MIP-OSD demonstrated the lowest amount of doxorubicin release with 43.2% of the amount of doxorubicin from the control solution being released.

Secondly, the EGFR templated species, MIP-OSD nanoparticles were tested and compared with and without EGFR binding peptide present in the solution. Also tested, were the MIP-OSN nanoparticles with and without EGFR binding peptide present being present in solution. From this, a comparison of the effects of template presence could be seen for both the doxorubicin-loaded and non-doxorubicin loaded nanoparticles. These nanoparticles were tested alongside a control solution of doxorubicin with EGFR binding peptide present. The results are shown in Table 6 – 8 and figure 6 – 6.

Table 6 - 8: Table showing the release of doxorubicin from MIP-OSD and MIP-OSN in comparison to a control solution of doxorubicin with and without EGFR peptide present

Time (Mins)	Amount of doxorubicin released (mg mL^{-1}) Standard deviation = ± 0.001mg mL^{-1}				
	No EGFR peptide added		EGFR peptide added		Doxorubicin Control Solution
	MIP-OSD	MIP-OSN	MIP-OSD	MIP-OSN	
0	0.000	0.000	0.000	0.000	0.000
5	0.055	0.073	0.067	0.081	0.109
10	0.097	0.124	0.116	0.148	0.193
15	0.128	0.164	0.154	0.204	0.261
20	0.154	0.198	0.185	0.251	0.318
25	0.177	0.229	0.214	0.287	0.369
30	0.199	0.257	0.239	0.314	0.414
35	0.219	0.284	0.264	0.341	0.455
40	0.237	0.309	0.286	0.371	0.494
45	0.253	0.334	0.305	0.401	0.529
50	0.267	0.358	0.321	0.431	0.564
55	0.279	0.382	0.334	0.459	0.596
60	0.289	0.405	0.345	0.482	0.624
90	0.336	0.539	0.396	0.612	0.754
120	0.372	0.647	0.437	0.725	0.847
180	0.426	0.793	0.502	0.895	0.994

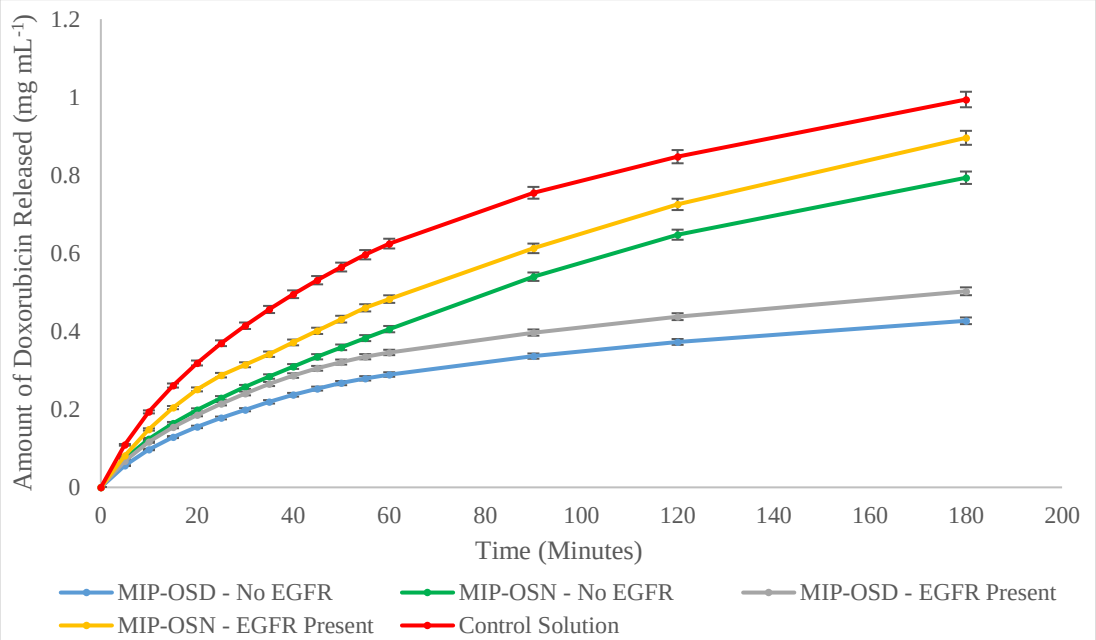

Figure 6 - 6: Graph showing a comparison of the release of doxorubicin from MIP-OSD, MIP-OSN and a doxorubicin control solution with and without EGFR peptide present

During the initial 5 minutes of the experiments, the control solution of doxorubicin-containing EGFR peptide demonstrated an initial release of doxorubicin at a rate of 0.021 mg mL^{-1} min^{-1} whereas the MIP-OSD and MIP-OSN in the presence of EGFR peptide demonstrated a rate of 0.013 mg mL^{-1} min^{-1} and 0.016 mg mL^{-1} min^{-1} respectively.

Whereas, without EGFR peptide present MIP-OSD and MIP-OSN demonstrated a rate of release of 0.011 mg mL^{-1} min^{-1} and 0.015 mg mL^{-1} min^{-1} respectively.

The rate of release of the doxorubicin from the doxorubicin control solution containing EGFR peptide decreased to 0.017 mg mL^{-1} min^{-1} at the 5-minute mark before decreasing to 0.011 mg mL^{-1} min^{-1} at the 20-minute mark. At the 30-minute mark, the rate decreased to 0.008 mg mL^{-1} min^{-1} before decreasing to 0.004 mg mL^{-1} min^{-1} at the 60-minute mark. The rate of release gradually decreased over the remainder of the experiment.

The rate of release of the doxorubicin from the MIP-OSN in the presence of EGFR peptide decreased to 0.013 mg mL^{-1} min^{-1} at the 5-minute mark before decreasing to 0.007 mg mL^{-1} min^{-1} at the 20-minute mark. At the 30-minute mark, the rate decreased to 0.005 mg mL^{-1} min^{-1} before decreasing to 0.004 mg mL^{-1} min^{-1} at the 60-minute mark. The rate of release gradually decreased over the remainder of the experiment.

The rate of release of the doxorubicin from the MIP-OSD in the presence of EGFR peptide decreased to 0.011 mg mL^{-1} min^{-1} at the 5-minute mark before decreasing to 0.005 mg mL^{-1} min^{-1} at the 20-minute mark. At the 30-minute mark, the rate decreased to 0.004 mg mL^{-1} min^{-1} before decreasing to 0.002 mg mL^{-1} min^{-1} at the 60-minute mark. The rate of release gradually decreased over the remainder of the experiment.

The rate of release of the doxorubicin from the MIP-OSN without EGFR peptide present decreased to 0.011 mg mL^{-1} min^{-1} at the 5-minute mark before decreasing to 0.006 mg mL^{-1} min^{-1} at the 20-minute mark. At the 30-minute mark, the rate decreased to 0.005 mg mL^{-1} min^{-1} before decreasing to 0.004 mg mL^{-1} min^{-1} at the 60-minute mark. The rate of release gradually decreased over the remainder of the experiment.

The rate of release of the doxorubicin from the MIP-OSD without EGFR peptide present decreased to 0.008 mg mL^{-1} min^{-1} at the 5-minute mark before decreasing to 0.005 mg mL^{-1} min^{-1} at the 20-minute mark. At the 30-minute mark, the rate decreased to 0.004 mg mL^{-1} min^{-1} before decreasing to 0.002 mg mL^{-1} min^{-1} at the 60-minute mark. The rate of release gradually decreased over the remainder of the experiment.

Overall the doxorubicin control solution demonstrated the highest release of doxorubicin compared to both of the nanoparticle species, whereas MIP-OSD without EGFR peptide present demonstrated the lowest amount of doxorubicin release with 42.9% of the amount of doxorubicin from the control solution being released.

6.4.3.3. Comparison of the release profile of doxorubicin from the organic and aqueous EGFR peptide-imprinted nanoparticles

To observe the effect of nanoparticle composition on the release of doxorubicin when the EGFR binding peptide is present, MIP-OSD and MIP-SD-D were compared alongside a control solution of doxorubicin. The results are shown in Table 6 – 9 and figure 6 – 7.

Table 6 - 9: Table showing the release of doxorubicin from MIP-SD-D and MIP-OSD in comparison to a control solution of doxorubicin with EGFR peptide present

Time (Mins)	Amount of doxorubicin released (mg mL^{-1}) Standard deviation = ± 0.001mg mL^{-1}		
	MIP-SD-D	MIP-OSD	Doxorubicin Control Solution
0	0.000	0.000	0.000
5	0.065	0.078	0.124
10	0.113	0.144	0.199
15	0.149	0.198	0.265
20	0.179	0.244	0.327
25	0.208	0.279	0.389
30	0.233	0.305	0.449
35	0.257	0.331	0.504
40	0.278	0.359	0.557
45	0.296	0.382	0.604
50	0.312	0.401	0.644
55	0.325	0.424	0.677
60	0.336	0.447	0.706
90	0.385	0.541	0.832
120	0.425	0.615	0.905
180	0.488	0.719	0.997

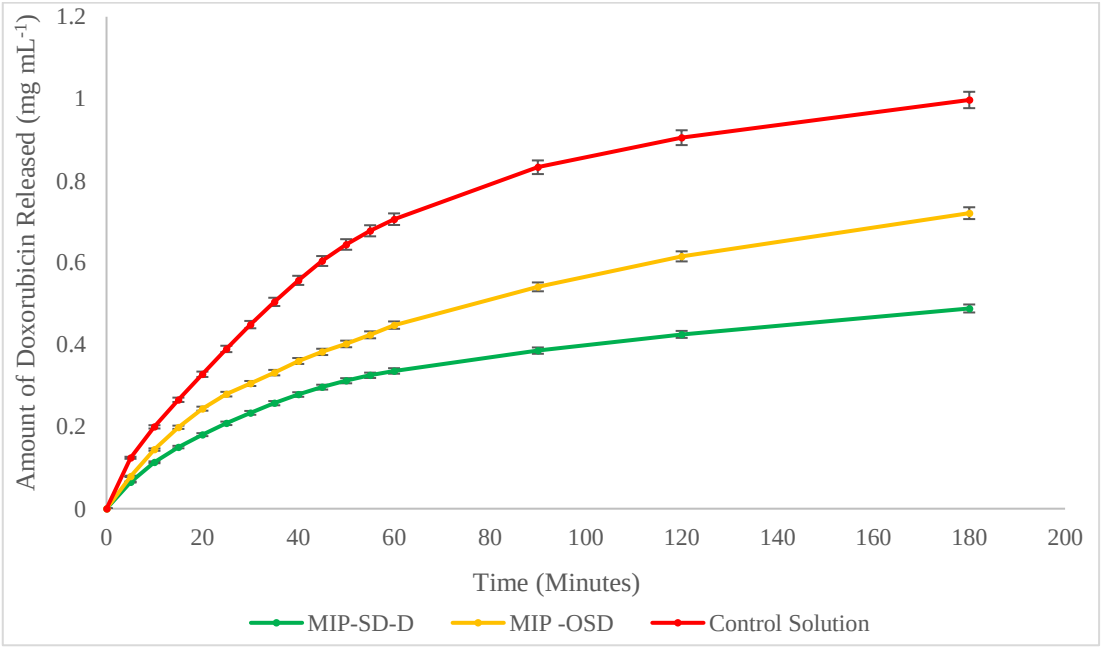

Figure 6 - 7: Graph showing a comparison of the release of doxorubicin from MIP-SD-D, MIP-OSD and a doxorubicin control solution in the presence of EGFR peptide

During the initial 5 minutes of the experiments, the control solution of doxorubicin demonstrated an initial release of doxorubicin at a rate of 0.024 mg mL^{-1} min^{-1} whereas the MIP-SD-D and MIP-OSD demonstrated a rate of 0.013 mg mL^{-1} min^{-1} and 0.016 mg mL^{-1} min^{-1} respectively.

The rate of release of the doxorubicin from the doxorubicin control solution decreased to 0.015 mg mL^{-1} min^{-1} at the 5-minute mark before decreasing to 0.013 mg mL^{-1} min^{-1} at the 20-minute mark. At the 30-minute mark, the rate decreased to 0.011 mg mL^{-1} min^{-1} before decreasing to 0.004 mg mL^{-1} min^{-1} at the 60-minute mark. The rate of release gradually decreased over the remainder of the experiment.

The rate of release of the doxorubicin from the MIP-OSD decreased to 0.013 mg mL^{-1} min^{-1} at the 5-minute mark before decreasing to 0.007 mg mL^{-1} min^{-1} at the 20-minute mark. At the 30-minute mark, the rate decreased to 0.005 mg mL^{-1} min^{-1} before decreasing to 0.003 mg mL^{-1} min^{-1} at the 60-minute mark. The rate of release gradually decreased over the remainder of the experiment.

The rate of release of the doxorubicin from the MIP-SD-D decreased to 0.009 mg mL^{-1} min^{-1} at the 5-minute mark before decreasing to 0.006 mg mL^{-1} min^{-1} at the 20-minute mark. At the 30-minute mark, the rate decreased to 0.005 mg mL^{-1} min^{-1} before decreasing to 0.002 mg mL^{-1} min^{-1} at the 60-minute mark. The rate of release gradually decreased over the remainder of the experiment.

Overall the free doxorubicin solution demonstrated the highest release of doxorubicin compared to both of the nanoparticle species, whereas MIP-SD-D demonstrated the lowest amount of doxorubicin release with 48.9% of the amount of doxorubicin from the control solution being released.

6.4.3.4. The conclusion of the effect of EGFR peptide presence on the release of doxorubicin

With the MIP-SD-D and MIP-OSD nanoparticles, the presence of the EGFR binding peptide had a small effect on the release of doxorubicin from the nanoparticles.

The MIP-SD-D nanoparticles were found to display an increase in the amount of doxorubicin released from both the doxorubicin imprinted and non-imprinted by small amounts in the presence of EGFR binding peptide. With the doxorubicin imprinted nanoparticles in the presence of the EGFR binding peptide, 0.076mg mL^{-1} more doxorubicin was released in comparison to the doxorubicin imprinted nanoparticles without the EGFR binding peptide present. However, with the non-doxorubicin imprinted nanoparticles in the presence of the EGFR binding peptide, 0.102mg mL^{-1} more doxorubicin was released in comparison to the doxorubicin imprinted nanoparticles without the EGFR binding peptide present. The MIP-OSD nanoparticles were also found to display an increase in the amount of doxorubicin released from both the doxorubicin imprinted and non-imprinted by a small degree in the presence of EGFR binding peptide. With the doxorubicin imprinted nanoparticles in the presence of the EGFR binding peptide, 0.026mg mL^{-1} more doxorubicin was released in comparison to the doxorubicin imprinted nanoparticles without the EGFR binding peptide present. However, with the non-doxorubicin imprinted nanoparticles in the presence of the EGFR binding peptide, 0.061mg mL^{-1} more doxorubicin was released in comparison to the doxorubicin imprinted nanoparticles without the EGFR binding peptide present.

6.5 Conclusions

With the addition of the primary template to the nanoparticle solution in the experiments, there is an increase in the rate and amount of doxorubicin released. This increase is caused by the interaction of the primary template with the nanoparticles causing a more significant amount of doxorubicin release. However, if the primary template is large enough, the template can cause the doxorubicin to be pushed out into the dialysis membrane due to the greater molecule concentration inside the membrane. With the vancomycin templated nanoparticles, the doxorubicin imprinted nanoparticles displayed a more significant increase in the amount of doxorubicin released in comparison to the non-imprinted nanoparticles. This increase is most likely due to the presence of the vancomycin, causing a small amount of doxorubicin to release from the nanoparticles in addition to the standard doxorubicin release. However, the vancomycin presence may cause more doxorubicin to be released due to the increased concentration of molecules inside the dialysis tubing.

In contrast, the EGFR binding peptide templated nanoparticles the non-imprinted nanoparticles demonstrated a higher level of release compared to the doxorubicin imprinted nanoparticles. This increase is most likely due to the presence of the EGFR binding peptide, causing a small amount of doxorubicin to release from the nanoparticles in addition to the standard doxorubicin release. However, the EGFR binding presence may cause more doxorubicin to release due to the increased concentration of molecules inside the dialysis tubing.

Chapter 7: Investigation of the effect of altering the cross-linking degree on the release of doxorubicin.

7.1. Introduction

With molecularly imprinted nanoparticles, the functional monomers used to create binding sites are held in place around the template using cross-linking monomers. These cross-linking chains affect the size and density of binding sites on molecularly imprinted nanoparticles. Altering the level of cross-linking of a molecularly imprinted nanoparticle can affect how well nanoparticles bind to the imprinted template. With drug loading, the cross-linking degree can affect how well the drug is retained by the nanoparticles and the rate at which the payload is released.

To determine whether this influences doxorubicin release from the nanoparticles tested. A series of nanoparticles with different levels of cross-linking were synthesised to see if the release rate of doxorubicin is affected. The following cross-linking levels were tested, 1x, 5x, 10x and 25x. The cross-linking level was altered by changing the amount of N, N′- methylene-bis-acrylamide used in the nanoparticle synthesis as this was the primary cross-linking monomer used. The doxorubicin release profiles of the nanoparticles were determined initially as previously tested. Also, the presence of the solid-phase template, vancomycin was tested to determine if the presence had any effect on the doxorubicin release profile.

7.1.1. Aim and objectives

Aim of the chapter:

- Synthesis and testing of vancomycin imprinted nanoparticles with different amounts of cross-linking monomer present for the controlled release of doxorubicin over time.

Objectives for this chapter:

- Synthesis of solid phase nanoparticles using aqueous solvent templated to vancomycin as the primary template with and without doxorubicin imprinted with different amounts of cross-linking monomer present.
- Testing of the release of doxorubicin from the nanoparticles without vancomycin present.
- Comparing the doxorubicin imprinted nanoparticles against the non-imprinted nanoparticles.
- Testing of the release of doxorubicin from the nanoparticles with vancomycin present in solution.
- Comparing the doxorubicin imprinted nanoparticles against the non-imprinted nanoparticles with vancomycin present.

7.2. Chemicals

Glass beads SPHERIGLASS® A-Glass 2429 (70 – 100 µm diameter) obtained from Potters Industries LLC. A dialysis membrane (Spectra/Por, MWCO = 10 kDa) was purchased from Spectrum Laboratories Inc. Acrylic acid, ammonium persulfate, 1,2-bis(trimethoxysilyl)ethane, glutaraldehyde, phosphate buffered saline tablets, N-isopropylacrylamide, N′-methylene-bisacrylamide, N-tert-butylacrylamide, N, N, N′, N′-tetramethylethylenediamine, vancomycin hydrochloride, acetone, ethanol, methanol and toluene were purchased from Sigma-Aldrich, UK. (3-Aminopropyl) trimethoxysilane and sodium cyanoborohydride were obtained from Acros Organics. N-(3-Aminopropyl) methacrylamide hydrochloride was purchased from PolySciences Inc., UK. Amicon Ultra-15 Centrifugal Filter Units (MWCO 30 kDa), Acetonitrile, sodium hydroxide and sulphuric acid were obtained from Fisher Scientific (UK). Doxorubicin Hydrochloride was purchased from Cambridge Bioscience, UK. Ultrapure water was produced by a Millipore Milli-Q system (Millipore, Bedford, MA, USA), Double-distilled ultrapure water (Millipore) was used for analysis. All chemicals and solvents were analytical or HPLC grade and were used without further purification. Phosphate buffered saline was prepared as directed from PBS buffer tablets (Sigma-Aldrich, Gillingham, UK).

7.3. Methods

7.3.1. Preparation of the nanoparticles

7.3.1.1 Templated solid phase glass beads.

Templated beads for vancomycin were synthesised as described in 2.3.1.1.

7.3.1.2. Increased cross-linking nanoparticles synthesis

Nanoparticles imprinted with for vancomycin were synthesised *via* the method described in 2.3.1.2 using vancomycin templated glass beads. Half of the polymerisations utilised the standard composition used in 2.3.1.2 with alterations to the amount of N, N′-methylene bis(acrylamide) to form the MIP-SNX series of nanoparticles, whereas, the other half incorporated doxorubicin (1mg) to produce the MIP-SDX series of nanoparticles with alterations to the amount of N, N′-methylene bisacrylamide. List of species produced listed in Table 7 – 1.

Table 7 - 1: List of nanoparticle species tested and the amount of cross-linker used in the synthesis

Species	**Mass**	**Moles**	**Cross-linking degree compared to the original composition**	**Doxorubicin present in the polymerisation**
MIP-SDX-A	2mg	12.9µmol	1x	Yes
MIP-SDX-B	10mg	64.8µmol	5x	Yes
MIP-SDX-C	20mg	129.7µmol	10x	Yes
MIP-SDX-D	50mg	324.3µmol	25x	Yes
MIP-SNX-A	2mg	12.9µmol	1x	No
MIP-SNX-B	10mg	64.8µmol	5x	No
MIP-SNX-C	20mg	129.7µmol	10x	No
MIP-SNX-D	50mg	324.3µmol	25x	No

7.3.1.3. Nanoparticle collection

All nanoparticle species were all collected *via* the procedure was carried out in 2.3.1.3.

7.3.1.4. Nanoparticle purification

All nanoparticle species were all purified *via* the procedure was carried out in 2.3.1.4.

7.3.2. Effect of the level of cross-linking on doxorubicin release.

Carried out as in 5.3.2 with the vancomycin imprinted nanoparticles containing alternate amounts of cross-linking monomer within the nanoparticles. A series of nanoparticles species were polymerised in the presence of doxorubicin (MIP-SDX series of nanoparticles) and compared against the control nanoparticles with alternate amounts of cross-linking monomer (MIP-SNX series of nanoparticles).

7.3.3. Effect of the level of cross-linking on doxorubicin release with primary template present.

This was carried out as described in 6.3.2 on the MIP-SDX and MIP-SNX species of nanoparticles. However, Vancomycin (10mg) was added at the start of the experiment to the solution on both the inside and outside of the dialysis membrane.

7.4. Analysis and discussion

7.4.1. Nanoparticle synthesis

The solid phase was prepared successfully, as described in 5.3.1. While the APS-TEMED initiated polymerisation successfully synthesised all the nanoparticles as described in 2.3.1.2 with the modifications outlined in 7.3.2, 7.3.3. and 6.3.1. The nanoparticles were successfully collected and washed as described in 2.3.1.3 and 2.3.1.4.

7.4.2. Effect of an increased level of crosslinking on doxorubicin release

MIP-SDX series of nanoparticles was tested to determine the effect of changing the level of cross-linking on the release profile of doxorubicin from the nanoparticles. The nanoparticles were pre-incubated with doxorubicin (1.mg, 1.84µmol) for the release testing. The release of doxorubicin was monitored as described in 5.3.2. The molecularly imprinted nanoparticles were compared against the MIP-SNX control series of nanoparticles prepared without doxorubicin present, they underwent incubation with a doxorubicin solution at the same concentration. Initially, the doxorubicin imprinted nanoparticles were compared to see if there was a difference when the level of cross-linking was changed, followed by the non-imprinted nanoparticles. Following this, each cross-linking degree was investigated for the effect of doxorubicin being present in the initial polymerisation mixture. This was done by comparing the doxorubicin imprinted nanoparticles with the non-imprinted nanoparticles. List of species produced listed in Table 7 – 2.

Table 7 - 2: List of species tested

Species	**Doxorubicin present**	**Cross-linking degree**
MIP-SDX-A	Yes	1 x Cross-linking
MIP-SDX-B	Yes	5 x Cross-linking
MIP-SDX-C	Yes	10 x Cross-linking
MIP-SDX-D	Yes	25 x Cross-linking
MIP-SNX-A	No	1 x Cross-linking
MIP-SNX-B	No	5 x Cross-linking
MIP-SNX-C	No	10 x Cross-linking
MIP-SNX-D	No	25 x Cross-linking

7.4.2.1. Comparison of the doxorubicin imprinted nanoparticles at increased levels of cross-linking.

Initially, the nanoparticles which were loaded with doxorubicin were tested first to determine the overall effect of the increasing levels of cross-linking. All the nanoparticles underwent incubation with the same amount of doxorubicin before being tested alongside a control solution of doxorubicin. The results are shown in Table 7 – 3 and figure 7 – 1.

Table 7 - 3: Table showing the comparison of the release of doxorubicin from vancomycin imprinted nanoparticles with different levels of cross-linking against a control solution of doxorubicin

Time (Mins)	Amount of doxorubicin released (mg mL^{-1}) Standard deviation = ± 0.001mg mL^{-1}				
	MIP-SDX-A	MIP-SDX-B	MIP-SDX-C	MIP-SDX-D	Doxorubicin Control Solution
0	0.000	0.000	0.000	0.000	0.000
5	0.078	0.068	0.038	0.032	0.128
10	0.139	0.129	0.101	0.062	0.175
15	0.192	0.182	0.152	0.091	0.231
20	0.239	0.229	0.199	0.119	0.281
25	0.282	0.272	0.242	0.144	0.324
30	0.321	0.311	0.281	0.169	0.359
35	0.356	0.346	0.316	0.192	0.391
40	0.385	0.375	0.345	0.214	0.421
45	0.408	0.398	0.368	0.236	0.449
50	0.426	0.416	0.386	0.256	0.476
55	0.443	0.433	0.403	0.276	0.501
60	0.468	0.449	0.419	0.294	0.525
75	0.515	0.494	0.464	0.348	0.593
90	0.569	0.541	0.511	0.398	0.662
120	0.655	0.609	0.579	0.467	0.787
180	0.805	0.719	0.689	0.557	0.991

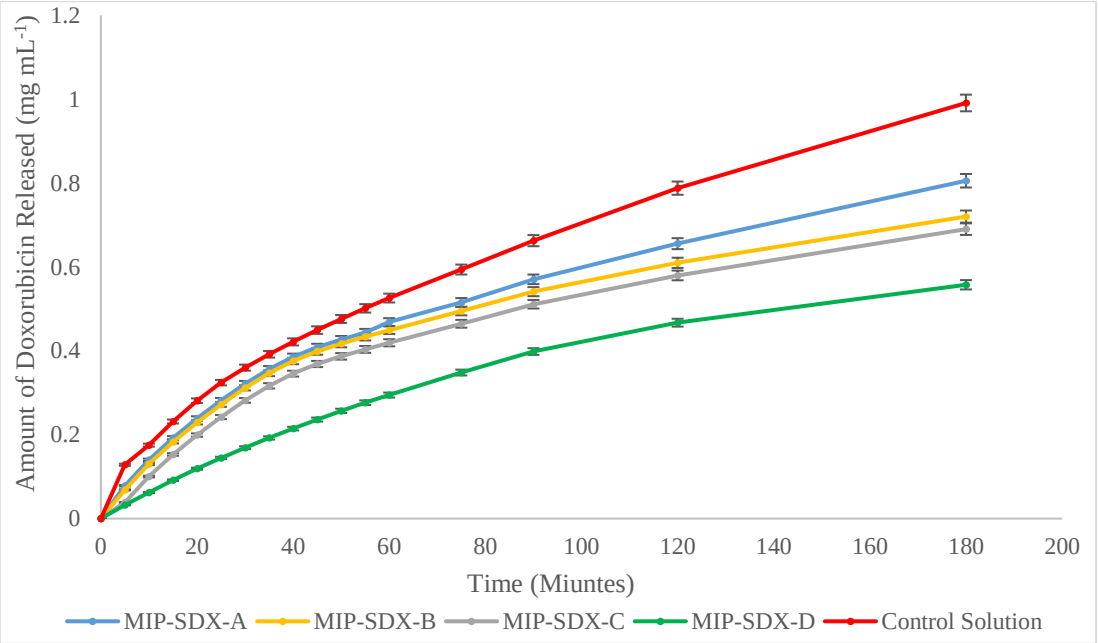

Figure 7 - 1: Graph showing the comparison of the release of doxorubicin from vancomycin imprinted nanoparticles with different levels of cross-linking against a control solution of doxorubicin

During the initial 5 minutes of the experiments the control solution of doxorubicin demonstrated an initial release of doxorubicin at a rate of 0.025 mg mL^{-1} min^{-1} whereas the MIP-SX-A, MIP-SX-B, MIP-SX-C and MIP-SX-D demonstrated a rate of 0.015 mg mL^{-1} min^{-1}, 0.013 mg mL^{-1} min^{-1}, 0.012 mg mL^{-1} min^{-1} and 0.008 mg mL^{-1} min^{-1} respectively.

The rate of release of the doxorubicin from the doxorubicin control solution decreased to 0.009 mg mL^{-1} min^{-1} at the 5-minute mark before decreasing to 0.008 mg mL^{-1} min^{-1} at the 20-minute mark. At the 30-minute mark, the rate decreased to 0.006 mg mL^{-1} min^{-1} before decreasing to 0.004 mg mL^{-1} min^{-1} at the 60-minute mark. The rate of release gradually decreased over the remainder of the experiment.

The rate of release of the doxorubicin from the MIP-SDX-A decreased to 0.012 mg mL^{-1} min^{-1} at the 5-minute mark before decreasing to 0.008 mg mL^{-1} min^{-1} at the 20-minute mark. At the 30-minute mark, the rate decreased to 0.006 mg mL^{-1} min^{-1} before decreasing to 0.003 mg mL^{-1} min^{-1} at the 60-minute mark. The rate of release gradually decreased over the remainder of the experiment.

The rate of release of the doxorubicin from the MIP-SDX-B decreased to 0.012 mg mL^{-1} min^{-1} at the 5-minute mark before decreasing to 0.008 mg mL^{-1} min^{-1} at the 20-minute mark. At the 30-minute mark, the rate decreased to 0.007 mg mL^{-1} min^{-1} before decreasing to 0.003 mg mL^{-1} min^{-1} at the 60-minute mark. The rate of release gradually decreased over the remainder of the experiment.

The rate of release of the doxorubicin from the MIP-SDX-C decreased to 0.011 mg mL^{-1} min^{-1} at the 5-minute mark before decreasing to 0.009 mg mL^{-1} min^{-1} at the 20-minute mark. At the 30-minute mark, the rate decreased to 0.007 mg mL^{-1} min^{-1} before decreasing to 0.003 mg mL^{-1} min^{-1} at the 60-minute mark. The rate of release gradually decreased over the remainder of the experiment.

The rate of release of the doxorubicin from the MIP-SDX-D decreased to 0.006 mg mL^{-1} min^{-1} at the 5-minute mark before decreasing to 0.005 mg mL^{-1} min^{-1} at the 20-minute mark. At the 30-minute mark, the rate decreased to 0.004 mg mL^{-1} min^{-1} before decreasing to 0.003 mg mL^{-1} min^{-1} at the 60-minute mark. The rate of release gradually decreased over the remainder of the experiment.

Overall the doxorubicin control solution demonstrated the highest release of doxorubicin compared to both of the nanoparticle species, whereas MIP-SDX-D demonstrated the lowest amount of doxorubicin release with 56.2% of the amount of doxorubicin from the control solution being released.

7.4.2.2. Effect of doxorubicin incorporation on the release from the nanoparticles with the original level of cross-linking.

Initially, the original composition of the nanoparticles was tested. The doxorubicin incorporated nanoparticles, MIP-SDX-A were pre-incubated with doxorubicin (1mg, 1.84μmol) for the release testing. The MIP-SDX-A nanoparticles were compared against the non-doxorubicin incorporated MIP-SNX-A nanoparticles. These were compared alongside a control solution of doxorubicin. The results are shown in Table 7 – 4 and figure 7 – 2.

Table 7 - 4: Table showing the comparison of the release of doxorubicin from MIP-SDX-A and MIP-SNX-A against a control solution of doxorubicin

Time (Mins)	Amount of doxorubicin released (mg mL^{-1}) Standard deviation = ± 0.001mg mL^{-1}		
	MIP-SDX-A	MIP-SNX-A	Doxorubicin Control Solution
0	0	0	0
5	0.0861	0.0913	0.1016
10	0.1376	0.146	0.1624
15	0.2072	0.2199	0.2446
20	0.2682	0.2847	0.3167
25	0.3215	0.3413	0.3796
30	0.3656	0.3881	0.4317
35	0.4049	0.4297	0.478
40	0.4415	0.4686	0.5212
45	0.4762	0.5054	0.5622
50	0.509	0.5402	0.6009
55	0.5401	0.5733	0.6377
60	0.5632	0.5977	0.6649
75	0.623	0.6612	0.7355
90	0.6686	0.7097	0.7894
120	0.7348	0.7799	0.8675
180	0.847	0.899	0.9971

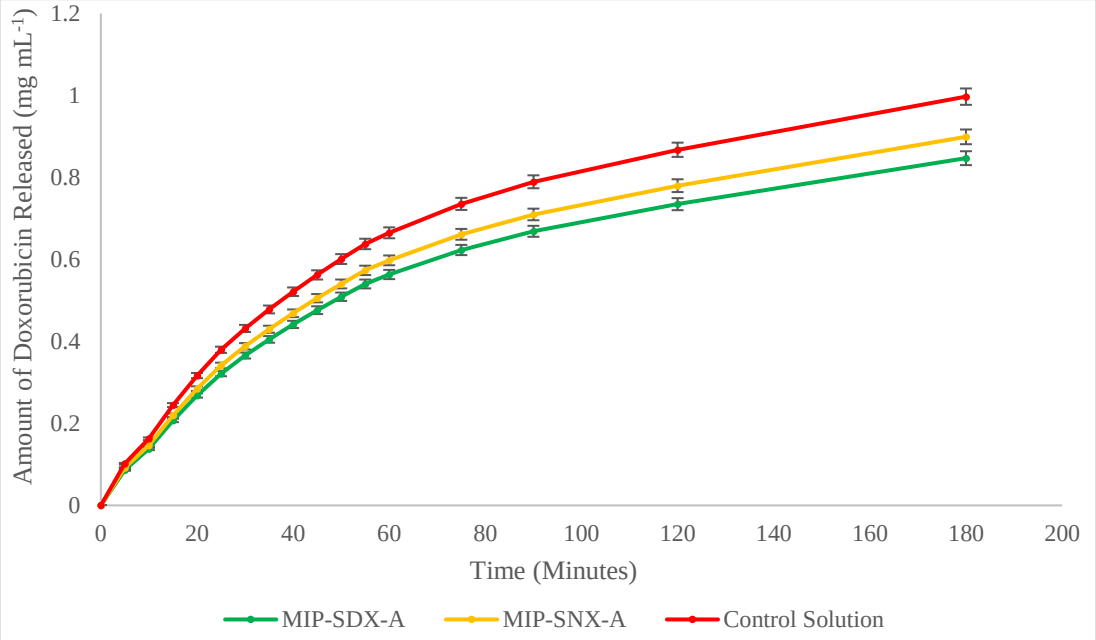

Figure 7 - 2: Graph showing the comparison of the release of doxorubicin from MIP-SDX-A and MIP-SNX-A against a control solution of doxorubicin

During the initial 5 minutes of the experiments, the control solution of doxorubicin demonstrated an initial release of doxorubicin at a rate of 0.021 mg mL^{-1} min^{-1} whereas the MIP-SDX-A and MIP-SNX-A demonstrated a rate of 0.018 mg mL^{-1} min^{-1} and 0.017 mg mL^{-1} min^{-1} respectively.

The rate of release of the doxorubicin from the doxorubicin control solution decreased to 0.013 mg mL^{-1} min^{-1} at the 5-minute mark before decreasing to 0.012 mg mL^{-1} min^{-1} at the 20-minute mark. At the 30-minute mark, the rate decreased to 0.009 mg mL^{-1} min^{-1} before decreasing to 0.005 mg mL^{-1} min^{-1} at the 60-minute mark. The rate of release gradually decreased over the remainder of the experiment.

The rate of release of the doxorubicin from the MIP-SNX-A decreased to 0.012 mg mL^{-1} min^{-1} at the 5-minute mark before decreasing to 0.011 mg mL^{-1} min^{-1} at the 20-minute mark. At the 30-minute mark, the rate decreased to 0.008 mg mL^{-1} min^{-1} before decreasing to 0.004 mg mL^{-1} min^{-1} at the 60-minute mark. The rate of release gradually decreased over the remainder of the experiment.

The rate of release of the doxorubicin from the MIP-SDX-A decreased to 0.011 mg mL^{-1} min^{-1} at the 5-minute mark before decreasing to 0.009 mg mL^{-1} min^{-1} at the 20-minute mark. At the 30-minute mark, the rate decreased to 0.007 mg mL^{-1} min^{-1} before decreasing to 0.004 mg mL^{-1} min^{-1} at the 60-minute mark. The rate of release gradually decreased over the remainder of the experiment.

Overall the free doxorubicin solution demonstrated the highest release of doxorubicin compared to both of the nanoparticle species, whereas MIP-SDX-A demonstrated the lowest amount of doxorubicin release with 84.9% of the amount of doxorubicin from the control solution being released.

7.4.2.3. Effect of doxorubicin incorporation on the release from the nanoparticles with the 5x the original level of cross-linking.

Secondly, the nanoparticles with a level of cross-linking 5x higher than the original were tested. The doxorubicin incorporated nanoparticles, MIP-SDX-B were pre-incubated with doxorubicin (1mg, 1.84µmol) for the release testing. The MIP-SDX-B nanoparticles were compared against the non-doxorubicin incorporated MIP-SNX-B nanoparticles. These were compared alongside a control solution of doxorubicin. The results are shown in Table 7 – 5 and figure 7 – 3.

Table 7 - 5: Table showing the comparison of the release of doxorubicin from MIP-SDX-B and MIP-SNX-B against a control solution of doxorubicin

Time (Mins)	Amount of doxorubicin released (mg mL^{-1}) Standard deviation = ± 0.001mg mL^{-1}		
	MIP-SDX-B	MIP-SNX-B	Doxorubicin Control Solution
0	0.000	0.000	0.000
5	0.075	0.089	0.101
10	0.121	0.142	0.162
15	0.182	0.214	0.244
20	0.236	0.277	0.316
25	0.283	0.332	0.379
30	0.322	0.378	0.431
35	0.357	0.419	0.478
40	0.389	0.457	0.521
45	0.419	0.493	0.562
50	0.448	0.526	0.659
55	0.476	0.559	0.637
60	0.496	0.583	0.664
75	0.549	0.645	0.735
90	0.589	0.692	0.789
120	0.648	0.759	0.867
180	0.747	0.876	0.989

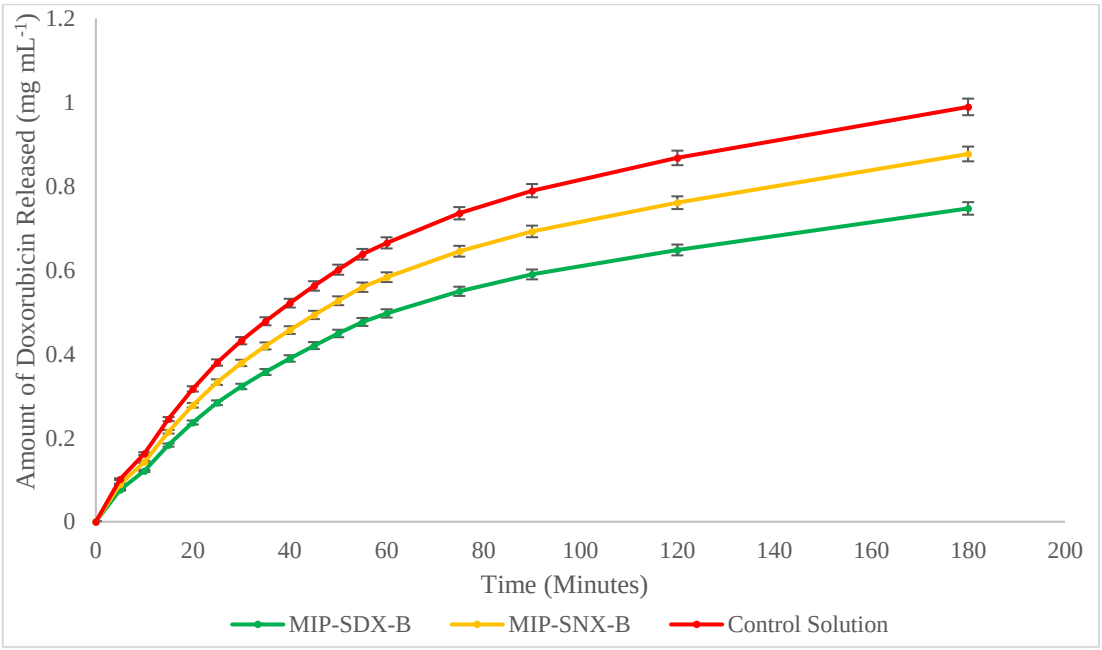

Figure 7 - 3: Graph showing the comparison of the release of doxorubicin from MIP-SDX-B and MIP-SNX-B against a control solution of doxorubicin

During the initial 5 minutes of the experiments, the control solution of doxorubicin demonstrated an initial release of doxorubicin at a rate of 0.021 mg mL^{-1} min^{-1} whereas the MIP-SDX-B and MIP-SNX-B demonstrated a rate of 0.015 mg mL^{-1} min^{-1} and 0.017 mg mL^{-1} min^{-1} respectively.

The rate of release of the doxorubicin from the doxorubicin control solution decreased to 0.013 mg mL^{-1} min^{-1} at the 5-minute mark before decreasing to 0.012 mg mL^{-1} min^{-1} at the 20-minute mark. At the 30-minute mark, the rate decreased to 0.009 mg mL^{-1} min^{-1} before decreasing to 0.004 mg mL^{-1} min^{-1} at the 60-minute mark. The rate of release gradually decreased over the remainder of the experiment.

The rate of release of the doxorubicin from the MIP-SNX-B decreased to 0.012 mg mL^{-1} min^{-1} at the 5-minute mark before decreasing to 0.011 mg mL^{-1} min^{-1} at the 20-minute mark. At the 30-minute mark, the rate decreased to 0.008 mg mL^{-1} min^{-1} before decreasing to 0.004 mg mL^{-1} min^{-1} at the 60-minute mark. The rate of release gradually decreased over the remainder of the experiment.

The rate of release of the doxorubicin from the MIP-SDX-B decreased to 0.009 mg mL^{-1} min^{-1} at the 5-minute mark before decreasing to 0.008 mg mL^{-1} min^{-1} at the 20-minute mark. At the 30-minute mark, the rate decreased to 0.007 mg mL^{-1} min^{-1} before decreasing to 0.003 mg mL^{-1} min^{-1} at the 60-minute mark. The rate of release gradually decreased over the remainder of the experiment.

Overall the free doxorubicin solution demonstrated the highest release of doxorubicin compared to both of the nanoparticle species, whereas MIP-SDX-B demonstrated the lowest amount of doxorubicin release with 75.5% of the amount of doxorubicin from the control solution being released.

7.4.2.4. Effect of doxorubicin incorporation on the release from the nanoparticles with the 10x the original level of cross-linking.

Secondly, the nanoparticles with a level of cross-linking 10x higher than the original were tested. The doxorubicin incorporated nanoparticles, MIP-SDX-C were pre-incubated with doxorubicin (1mg, 1.84µmol) for the release testing. The MIP-SDX-C nanoparticles were compared against the non-doxorubicin incorporated MIP-SNX-C nanoparticles. These were compared alongside a control solution of doxorubicin. The results are shown in Table 7 – 6 and figure 7 – 4.

Table 7 - 6: Table showing the comparison of the release of doxorubicin from MIP-SDX-C and MIP-SNX-C against a control solution of doxorubicin

Time (Mins)	Amount of doxorubicin released (mg mL^{-1}) Standard deviation = ± 0.001mg mL^{-1}		
	MIP-SDX-C	MIP-SNX-C	Doxorubicin Control Solution
0	0.000	0.000	0.000
5	0.071	0.086	0.101
10	0.114	0.137	0.162
15	0.172	0.207	0.244
20	0.223	0.268	0.316
25	0.268	0.321	0.379
30	0.304	0.365	0.431
35	0.337	0.405	0.478
40	0.368	0.441	0.521
45	0.397	0.476	0.562
50	0.424	0.509	0.599
55	0.449	0.539	0.637
60	0.469	0.563	0.664
75	0.519	0.623	0.735
90	0.557	0.669	0.789
120	0.612	0.735	0.867
180	0.706	0.847	0.987

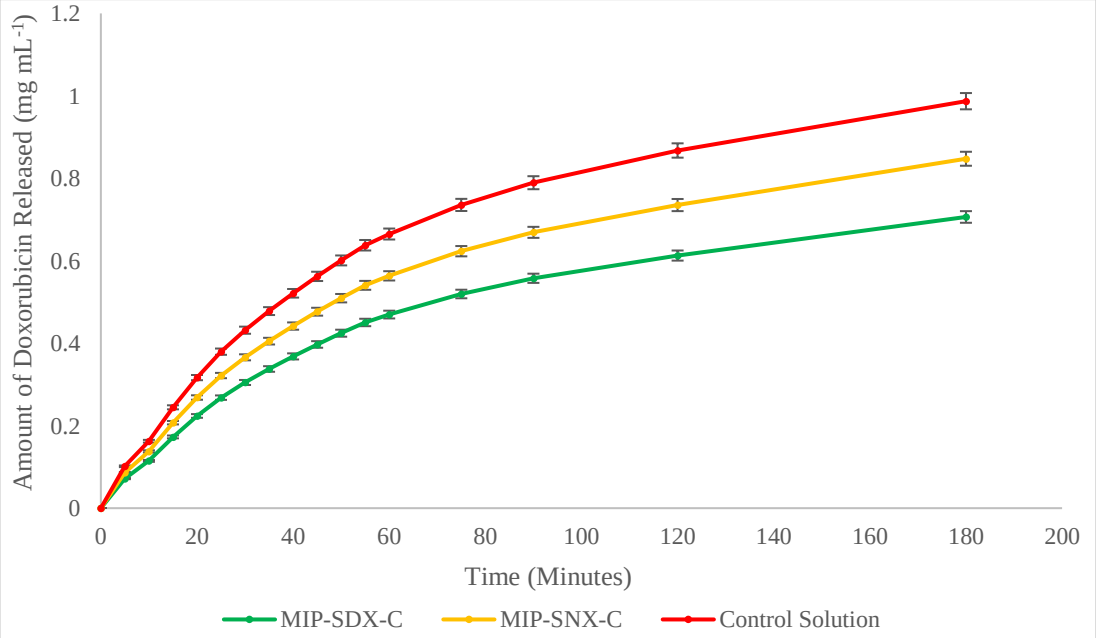

Figure 7 - 4: Graph showing the comparison of the release of doxorubicin from MIP-SDX-C and MIP-SNX-C against a control solution of doxorubicin

During the initial 5 minutes of the experiments, the control solution of doxorubicin demonstrated an initial release of doxorubicin at a rate of 0.021 mg mL^{-1} min^{-1} whereas the MIP-SDX-C and MIP-SNX-C demonstrated a rate of 0.014 mg mL^{-1} min^{-1} and 0.017 mg mL^{-1} min^{-1} respectively.

The rate of release of the doxorubicin from the doxorubicin control solution decreased to 0.013 mg mL^{-1} min^{-1} at the 5-minute mark before decreasing to 0.012 mg mL^{-1} min^{-1} at the 20-minute mark. At the 30-minute mark, the rate decreased to 0.009 mg mL^{-1} min^{-1} before decreasing to 0.004 mg mL^{-1} min^{-1} at the 60-minute mark. The rate of release gradually decreased over the remainder of the experiment.

The rate of release of the doxorubicin from the MIP-SNX-C decreased to 0.011 mg mL^{-1} min^{-1} at the 5-minute mark before decreasing to 0.010 mg mL^{-1} min^{-1} at the 20-minute mark. At the 30-minute mark, the rate decreased to 0.007 mg mL^{-1} min^{-1} before decreasing to 0.004 mg mL^{-1} min^{-1} at the 60-minute mark. The rate of release gradually decreased over the remainder of the experiment.

The rate of release of the doxorubicin from the MIP-SDX-C decreased to 0.009 mg mL^{-1} min^{-1} at the 5-minute mark before decreasing to 0.008 mg mL^{-1} min^{-1} at the 20-minute mark. At the 30-minute mark, the rate decreased to 0.006 mg mL^{-1} min^{-1} before decreasing to 0.003 mg mL^{-1} min^{-1} at the 60-minute mark. The rate of release gradually decreased over the remainder of the experiment.

Overall the free doxorubicin solution demonstrated the highest release of doxorubicin compared to both of the nanoparticle species, whereas MIP-SDX-C demonstrated the lowest amount of doxorubicin release with 71.5% of the amount of doxorubicin from the control solution being released.

7.4.2.5. Effect of doxorubicin incorporation on the release from the nanoparticles with the 25x the original level of cross-linking.

Fourthly, the nanoparticles with a level of cross-linking 25x higher than the original were tested. The doxorubicin incorporated nanoparticles, MIP-SDX-D were pre-incubated with doxorubicin (1mg, 1.84µmol) for the release testing. The MIP-SDX-D nanoparticles were compared against the non-doxorubicin incorporated MIP-SNX-D nanoparticles. These were compared alongside a control solution of doxorubicin. The results are shown in Table 7 – 7 and figure 7 – 5.

Table 7 - 7: Table showing the comparison of the release of doxorubicin from MIP-SDX-D and MIP-SNX-D against a control solution of doxorubicin

Time (Mins)	Amount of doxorubicin released (mg mL^{-1}) Standard deviation = ± 0.001mg mL^{-1}		
	MIP-SDX-D	MIP-SNX-D	Doxorubicin Control Solution
0	0.000	0.000	0.000
5	0.065	0.081	0.101
10	0.104	0.129	0.162
15	0.157	0.195	0.244
20	0.204	0.253	0.316
25	0.245	0.304	0.379
30	0.278	0.345	0.431
35	0.308	0.382	0.478
40	0.336	0.417	0.521
45	0.363	0.449	0.562
50	0.388	0.481	0.599
55	0.411	0.509	0.637
60	0.429	0.532	0.664
75	0.474	0.589	0.735
90	0.509	0.632	0.789
120	0.559	0.694	0.867
180	0.645	0.799	0.987

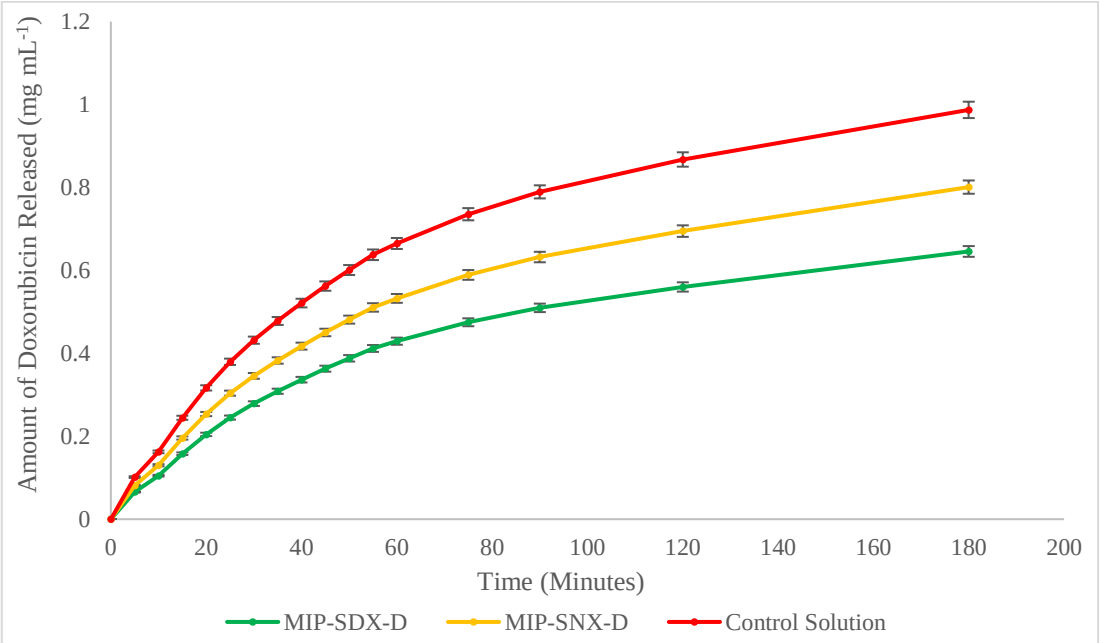

Figure 7 - 5: Graph showing the comparison of the release of doxorubicin from MIP-SDX-D and MIP-SNX-D against a control solution of doxorubicin

During the initial 5 minutes of the experiments, the control solution of doxorubicin demonstrated an initial release of doxorubicin at a rate of 0.021 mg mL^{-1} min^{-1} whereas

the MIP-SDX-D and MIP-SNX-D demonstrated a rate of 0.013 mg mL^{-1} min^{-1} and 0.016 mg mL^{-1} min^{-1} respectively.

The rate of release of the doxorubicin from the doxorubicin control solution decreased to 0.013 mg mL^{-1} min^{-1} at the 5-minute mark before decreasing to 0.012 mg mL^{-1} min^{-1} at the 20-minute mark. At the 30-minute mark, the rate decreased to 0.007 mg mL^{-1} min^{-1} before decreasing to 0.004 mg mL^{-1} min^{-1} at the 60-minute mark. The rate of release gradually decreased over the remainder of the experiment.

The rate of release of the doxorubicin from the MIP-SNX-D decreased to 0.009 mg mL^{-1} min^{-1} at the 5-minute mark before decreasing to 0.008 mg mL^{-1} min^{-1} at the 20-minute mark. At the 30-minute mark, the rate decreased to 0.005 mg mL^{-1} min^{-1} before decreasing to 0.003 mg mL^{-1} min^{-1} at the 60-minute mark. The rate of release gradually decreased over the remainder of the experiment.

The rate of release of the doxorubicin from the MIP-SDX-D decreased to 0.008 mg mL^{-1} min^{-1} at the 5-minute mark before decreasing to 0.007 mg mL^{-1} min^{-1} at the 20-minute mark. At the 30-minute mark, the rate decreased to 0.006 mg mL^{-1} min^{-1} before decreasing to 0.003 mg mL^{-1} min^{-1} at the 60-minute mark. The rate of release gradually decreased over the remainder of the experiment.

Overall the free doxorubicin solution demonstrated the highest release of doxorubicin compared to both of the nanoparticle species, whereas MIP-SDX-D demonstrated the lowest amount of doxorubicin release with 65.4% of the amount of doxorubicin from the control solution being released.

7.4.2.6. Summary of the effect of cross-linking degree on doxorubicin release.

With the alteration of the cross-linking degree, the release rate of doxorubicin is altered. When the cross-linking degree is increased, the rate of doxorubicin release decreases. All the doxorubicin imprinted nanoparticles demonstrated a lower rate of release in comparison to their non-imprinted counterparts.

7.4.3. Effect of an increased level of crosslinking on doxorubicin release combined with primary template addition.

To determine if the presence of vancomycin affects the release profile of doxorubicin from the different level of cross-linking in the nanoparticles. The vancomycin was added to the nanoparticle solution at the beginning of the experiment. As described in 6.4.2, the nanoparticles were tested by measuring the concentration on the inside of the membrane cell. By this method, the change in concentration is monitored by determining the decrease in doxorubicin fluorescence detected. From this, the rate of release of doxorubicin is determined. The amount of doxorubicin release was measured alongside a control solution of doxorubicin. List of species used listed in Table 7 – 8.

Table 7 - 8: List of the nanoparticle species tested

Species	**Doxorubicin present**	**Cross-linking degree**
MIP-SDX-A	Yes	1 x Cross-linking
MIP-SDX-B	Yes	5 x Cross-linking
MIP-SDX-C	Yes	10 x Cross-linking
MIP-SDX-D	Yes	25 x Cross-linking
MIP-SNX-A	No	1 x Cross-linking
MIP-SNX-B	No	5 x Cross-linking
MIP-SNX-C	No	10 x Cross-linking
MIP-SNX-D	No	25 x Cross-linking

7.4.3.1. Effect of vancomycin presence on the release of doxorubicin from the nanoparticles with the original level of cross-linking.

Firstly, the nanoparticles with the original level of cross-linking, MIP-SDX-A were tested and compared with and without vancomycin being present in the solution. Also tested, were the MIP-SNX-A nanoparticles with and without vancomycin being present in solution. From this, a comparison of the effects of template presence could be seen for both the doxorubicin-loaded and non-doxorubicin loaded nanoparticles alongside a control solution of doxorubicin with vancomycin present. The results are shown in Table 7 – 9 and figure 7 – 6.

Table 7 - 9: Table showing the comparison of the release of doxorubicin from MIP-SDX-A and MIP-SNX-A against a control solution of doxorubicin with and without vancomycin present

Time (Mins)	Amount of doxorubicin released (mg mL^{-1}) Standard deviation = ± 0.001mg mL^{-1}				
	No vancomycin added		Vancomycin added		Doxorubicin Control Solution
	0MIP-SDX-A	MIP-SNX-A	MIP-SDX-A	MIP-SNX-A	
0	0.000	0.000	0.000	0.000	0.000
5	0.069	0.083	0.074	0.089	0.099
10	0.124	0.148	0.131	0.157	0.175
15	0.163	0.195	0.173	0.207	0.231
20	0.199	0.237	0.209	0.252	0.281
25	0.229	0.274	0.242	0.291	0.324
30	0.254	0.304	0.269	0.323	0.359
35	0.277	0.331	0.293	0.351	0.391
40	0.298	0.356	0.315	0.378	0.421
45	0.318	0.379	0.336	0.403	0.449
50	0.337	0.402	0.356	0.427	0.476
55	0.354	0.424	0.375	0.449	0.501
60	0.372	0.444	0.393	0.472	0.525
75	0.419	0.502	0.444	0.533	0.593
90	0.469	0.559	0.495	0.595	0.662
120	0.557	0.666	0.589	0.707	0.787
180	0.708	0.845	0.748	0.898	0.996

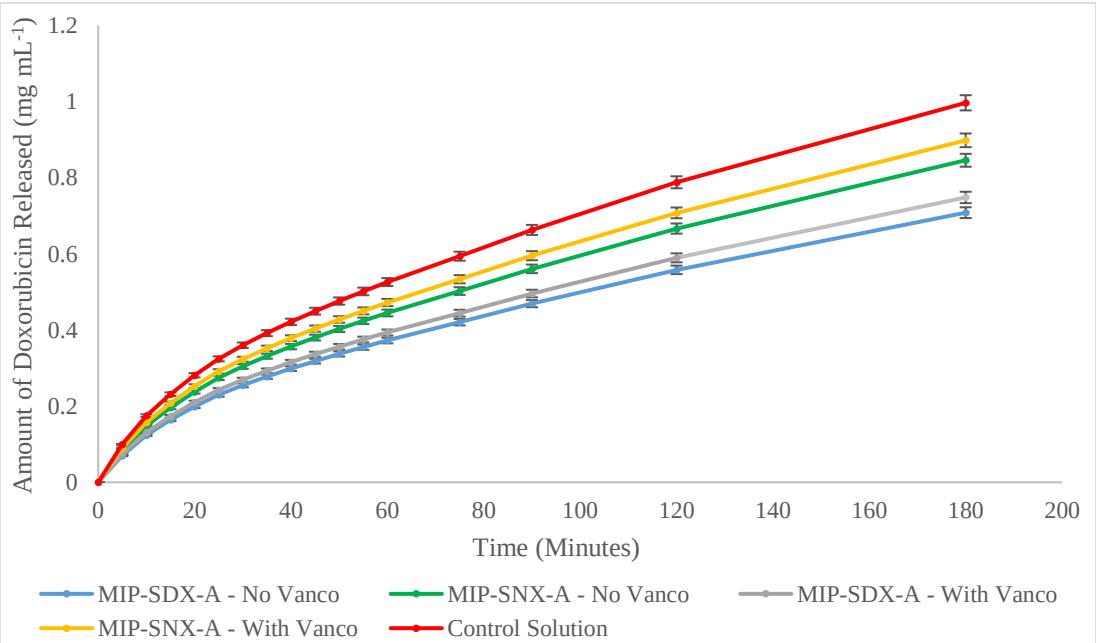

Figure 7 - 6: Graph showing the comparison of the release of doxorubicin from MIP-SDX-A and MIP-SNX-A against a control solution of doxorubicin with and without vancomycin present

During the initial 5 minutes of the experiments, the control solution of doxorubicin-containing vancomycin demonstrated an initial release of doxorubicin at a rate of 0.019

mg mL^{-1} min^{-1} whereas the MIP- SDX-A and MIP-SNX-A in the presence of vancomycin demonstrated a rate of 0.015 mg mL^{-1} min^{-1} and 0.018 mg mL^{-1} min^{-1} respectively. Whereas, without vancomycin present MIP-SDX-A and MIP-SNX-A demonstrated a rate of release of 0.014 mg mL^{-1} min^{-1} and 0.017 mg mL^{-1} min^{-1} respectively.

The rate of release of the doxorubicin from the doxorubicin control solution containing vancomycin decreased to 0.015 mg mL^{-1} min^{-1} at the 5-minute mark before decreasing to 0.009 mg mL^{-1} min^{-1} at the 20-minute mark. At the 30-minute mark, the rate decreased to 0.006 mg mL^{-1} min^{-1} before decreasing to 0.004 mg mL^{-1} min^{-1} at the 60-minute mark. The rate of release gradually decreased over the remainder of the experiment.

The rate of release of the doxorubicin from the MIP-OSN in the presence of vancomycin decreased to 0.014 mg mL^{-1} min^{-1} at the 5-minute mark before decreasing to 0.008 mg mL^{-1} min^{-1} at the 20-minute mark. At the 30-minute mark, the rate decreased to 0.006 mg mL^{-1} min^{-1} before decreasing to 0.004 mg mL^{-1} min^{-1} at the 60-minute mark. The rate of release gradually decreased over the remainder of the experiment.

The rate of release of the doxorubicin from the MIP-OSD in the presence of vancomycin decreased to 0.012 mg mL^{-1} min^{-1} at the 5-minute mark before decreasing to 0.007 mg mL^{-1} min^{-1} at the 20-minute mark. At the 30-minute mark, the rate decreased to 0.005 mg mL^{-1} min^{-1} before decreasing to 0.003 mg mL^{-1} min^{-1} at the 60-minute mark. The rate of release gradually decreased over the remainder of the experiment.

The rate of release of the doxorubicin from the MIP-OSN without vancomycin present decreased to 0.013 mg mL^{-1} min^{-1} at the 5-minute mark before decreasing to 0.007 mg mL^{-1} min^{-1} at the 20-minute mark. At the 30-minute mark, the rate decreased to 0.005 mg mL^{-1} min^{-1} before decreasing to 0.004 mg mL^{-1} min^{-1} at the 60-minute mark. The rate of release gradually decreased over the remainder of the experiment.

The rate of release of the doxorubicin from the MIP-OSD without vancomycin present decreased to 0.011 mg mL^{-1} min^{-1} at the 5-minute mark before decreasing to 0.006 mg mL^{-1} min^{-1} at the 20-minute mark. At the 30-minute mark, the rate decreased to 0.005 mg mL^{-1} min^{-1} before decreasing to 0.003 mg mL^{-1} min^{-1} at the 60-minute mark. The rate of release gradually decreased over the remainder of the experiment.

Overall the doxorubicin control solution demonstrated the highest release of doxorubicin compared to both of the nanoparticle species, whereas MIP-OSD without vancomycin present demonstrated the lowest amount of doxorubicin release with 71.1% of the amount of doxorubicin from the control solution being released.

7.4.3.2. Effect of vancomycin presence on the release of doxorubicin from the nanoparticles with 5x the original level of cross-linking.

Secondly, the nanoparticles with a level of cross-linking 5x higher than the original, MIP-SDX-B were tested and compared with and without vancomycin being present in the solution. Also tested, were the MIP-SNX-B nanoparticles with and without vancomycin being present in solution. From this, a comparison of the effects of template presence could be seen for both the doxorubicin-loaded and non-doxorubicin loaded nanoparticles alongside a control solution of doxorubicin with vancomycin present. The results are shown in Table 7 – 10 and figure 7 – 7.

Table 7 - 10: Table showing the comparison of the release of doxorubicin from MIP-SDX-B and MIP-SNX-B against a control solution of doxorubicin with and without vancomycin present

Time (Mins)	Amount of doxorubicin released (mg mL^{-1}) Standard deviation = ± 0.001mg mL^{-1}				
	No vancomycin added		Vancomycin added		Doxorubicin Control Solution
	MIP-SDX-B	MIP-SNX-B	MIP-SDX-B	MIP-SNX-B	
0	0.000	0.000	0.000	0.000	0.000
5	0.067	0.081	0.072	0.087	0.099
10	0.118	0.144	0.127	0.153	0.175
15	0.157	0.191	0.168	0.203	0.231
20	0.189	0.232	0.204	0.246	0.281
25	0.219	0.267	0.236	0.284	0.324
30	0.244	0.297	0.262	0.316	0.359
35	0.265	0.323	0.285	0.344	0.391
40	0.285	0.347	0.306	0.369	0.421
45	0.304	0.371	0.327	0.394	0.449
50	0.322	0.393	0.346	0.418	0.476
55	0.339	0.414	0.365	0.439	0.501
60	0.356	0.434	0.382	0.461	0.525
75	0.402	0.490	0.432	0.521	0.593
90	0.449	0.547	0.482	0.581	0.662
120	0.534	0.649	0.573	0.691	0.787
180	0.678	0.825	0.728	0.878	0.997

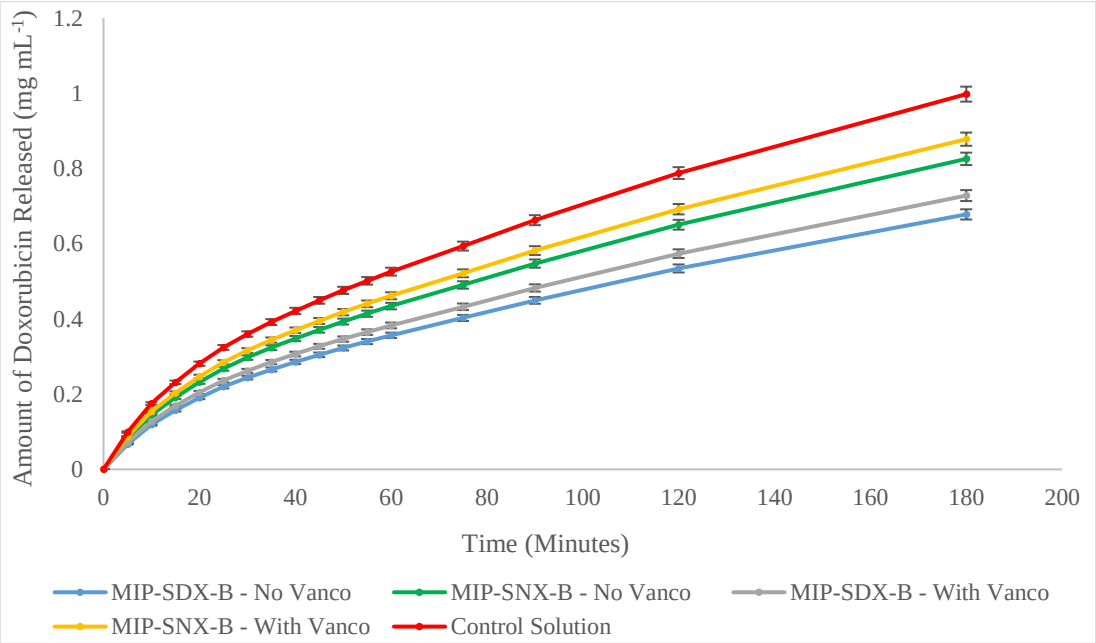

Figure 7 - 7: Graph showing the comparison of the release of doxorubicin from MIP-SDX-B and MIP-SNX-B against a control solution of doxorubicin with and without vancomycin present

During the initial 5 minutes of the experiments, the control solution of doxorubicin-containing vancomycin demonstrated an initial release of doxorubicin at a rate of 0.019 mg mL^{-1} min^{-1} whereas the MIP- SDX-B and MIP-SNX-B in the presence of vancomycin demonstrated a rate of 0.014 mg mL^{-1} min^{-1} and 0.017 mg mL^{-1} min^{-1} respectively. Whereas, without vancomycin present MIP-SDX-B and MIP-SNX-B demonstrated a rate of release of 0.013 mg mL^{-1} min^{-1} and 0.016 mg mL^{-1} min^{-1} respectively.

The rate of release of the doxorubicin from the doxorubicin control solution containing vancomycin decreased to 0.015 mg mL^{-1} min^{-1} at the 5-minute mark before decreasing to 0.008 mg mL^{-1} min^{-1} at the 20-minute mark. At the 30-minute mark, the rate decreased to 0.006 mg mL^{-1} min^{-1} before decreasing to 0.004 mg mL^{-1} min^{-1} at the 60-minute mark. The rate of release gradually decreased over the remainder of the experiment.

The rate of release of the doxorubicin from the MIP-SNX-B in the presence of vancomycin decreased to 0.013 mg mL^{-1} min^{-1} at the 5-minute mark before decreasing to 0.007 mg mL^{-1} min^{-1} at the 20-minute mark. At the 30-minute mark, the rate decreased to 0.005 mg mL^{-1} min^{-1} before decreasing to 0.004 mg mL^{-1} min^{-1} at the 60-minute mark. The rate of release gradually decreased over the remainder of the experiment.

The rate of release of the doxorubicin from the MIP-SDX-B in the presence of vancomycin decreased to 0.011 mg mL^{-1} min^{-1} at the 5-minute mark before decreasing to 0.006 mg mL^{-1} min^{-1} at the 20-minute mark. At the 30-minute mark, the rate decreased to

0.005 mg mL^{-1} min^{-1} before decreasing to 0.003 mg mL^{-1} min^{-1} at the 60-minute mark. The rate of release gradually decreased over the remainder of the experiment.

The rate of release of the doxorubicin from the MIP-SNX-B without vancomycin present decreased to 0.013 mg mL^{-1} min^{-1} at the 5-minute mark before decreasing to 0.007 mg mL^{-1} min^{-1} at the 20-minute mark. At the 30-minute mark, the rate decreased to 0.005 mg mL^{-1} min^{-1} before decreasing to 0.004 mg mL^{-1} min^{-1} at the 60-minute mark. The rate of release gradually decreased over the remainder of the experiment.

The rate of release of the doxorubicin from the MIP-SDX-B without vancomycin present decreased to 0.011 mg mL^{-1} min^{-1} at the 5-minute mark before decreasing to 0.006 mg mL^{-1} min^{-1} at the 20-minute mark. At the 30-minute mark, the rate decreased to 0.004 mg mL^{-1} min^{-1} before decreasing to 0.003 mg mL^{-1} min^{-1} at the 60-minute mark. The rate of release gradually decreased over the remainder of the experiment.

Overall the doxorubicin control solution demonstrated the highest release of doxorubicin compared to both of the nanoparticle species, whereas MIP-SDX-B without vancomycin present demonstrated the lowest amount of doxorubicin release with 67.9% of the amount of doxorubicin from the control solution being released.

7.4.3.3. Effect of vancomycin presence on the release of doxorubicin from the nanoparticles with 10x the original level of cross-linking.

Thirdly, the nanoparticles with a level of cross-linking 10x higher than the original, MIP-SDX-C were tested and compared with and without vancomycin being present in the solution. Also tested, were the MIP-SNX-C nanoparticles with and without vancomycin being present in solution. From this, a comparison of the effects of template presence could be seen for both the doxorubicin-loaded and non-doxorubicin loaded nanoparticles alongside a control solution of doxorubicin with vancomycin present. The results are shown in Table 7 – 11 and figure 7 – 8.

Table 7 - 11: Table showing the comparison of the release of doxorubicin from MIP-SDX-C and MIP-SNX-C against a control solution of doxorubicin with and without vancomycin present

Time (Mins)	Amount of doxorubicin released (mg mL^{-1}) Standard deviation = ± 0.001mg mL^{-1}				
	No vancomycin added		Vancomycin added		Doxorubicin Control Solution
	MIP-SDX-C	MIP-SNX-C	MIP-SDX-C	MIP-SNX-C	
0	0.000	0.000	0.000	0.000	0.000
5	0.062	0.079	0.069	0.084	0.099
10	0.109	0.141	0.123	0.148	0.175
15	0.146	0.187	0.163	0.196	0.231
20	0.177	0.227	0.198	0.238	0.281
25	0.204	0.262	0.229	0.275	0.324
30	0.227	0.291	0.254	0.305	0.359
35	0.247	0.317	0.277	0.332	0.391
40	0.265	0.341	0.297	0.358	0.421
45	0.283	0.364	0.317	0.381	0.449
50	0.299	0.385	0.336	0.404	0.476
55	0.316	0.406	0.354	0.426	0.501
60	0.331	0.426	0.371	0.446	0.525
75	0.374	0.481	0.419	0.504	0.593
90	0.418	0.536	0.468	0.563	0.662
120	0.497	0.638	0.557	0.669	0.787
180	0.629	0.809	0.707	0.849	0.996

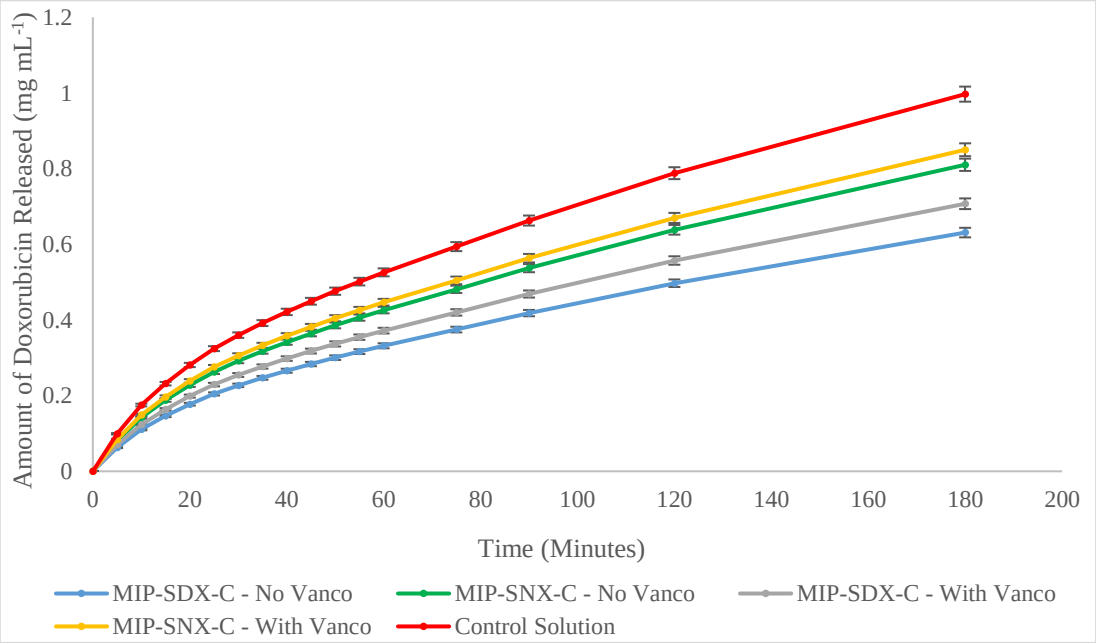

Figure 7 - 8: Graph showing the comparison of the release of doxorubicin from MIP-SDX-C and MIP-SNX-C against a control solution of doxorubicin with and without vancomycin present

During the initial 5 minutes of the experiments, the control solution of doxorubicin-containing vancomycin demonstrated an initial release of doxorubicin at a rate of 0.019

mg mL^{-1} min^{-1} whereas the MIP-SDX-C and MIP-SNX-C in the presence of vancomycin demonstrated a rate of 0.014 mg mL^{-1} min^{-1} and 0.017 mg mL^{-1} min^{-1} respectively. Whereas, without EGFR peptide present MIP-SDX-C and MIP-SNX-C demonstrated a rate of release of 0.013 mg mL^{-1} min^{-1} and 0.016 mg mL^{-1} min^{-1} respectively.

The rate of release of the doxorubicin from the doxorubicin control solution containing vancomycin decreased to 0.015 mg mL^{-1} min^{-1} at the 5-minute mark before decreasing to 0.008 mg mL^{-1} min^{-1} at the 20-minute mark. At the 30-minute mark, the rate decreased to 0.006 mg mL^{-1} min^{-1} before decreasing to 0.004 mg mL^{-1} min^{-1} at the 60-minute mark. The rate of release gradually decreased over the remainder of the experiment.

The rate of release of the doxorubicin from the MIP-SNX-C in the presence of vancomycin decreased to 0.013 mg mL^{-1} min^{-1} at the 5-minute mark before decreasing to 0.007 mg mL^{-1} min^{-1} at the 20-minute mark. At the 30-minute mark, the rate decreased to 0.005 mg mL^{-1} min^{-1} before decreasing to 0.004 mg mL^{-1} min^{-1} at the 60-minute mark. The rate of release gradually decreased over the remainder of the experiment.

The rate of release of the doxorubicin from the MIP-SDX-C in the presence of vancomycin decreased to 0.011 mg mL^{-1} min^{-1} at the 5-minute mark before decreasing to 0.006 mg mL^{-1} min^{-1} at the 20-minute mark. At the 30-minute mark, the rate decreased to 0.004 mg mL^{-1} min^{-1} before decreasing to 0.003 mg mL^{-1} min^{-1} at the 60-minute mark. The rate of release gradually decreased over the remainder of the experiment.

The rate of release of the doxorubicin from the MIP-SNX-C without vancomycin present decreased to 0.012 mg mL^{-1} min^{-1} at the 5-minute mark before decreasing to 0.007 mg mL^{-1} min^{-1} at the 20-minute mark. At the 30-minute mark, the rate decreased to 0.005 mg mL^{-1} min^{-1} before decreasing to 0.004 mg mL^{-1} min^{-1} at the 60-minute mark. The rate of release gradually decreased over the remainder of the experiment.

The rate of release of the doxorubicin from the MIP-SDX-C without vancomycin present decreased to 0.009 mg mL^{-1} min^{-1} at the 5-minute mark before decreasing to 0.005 mg mL^{-1} min^{-1} at the 20-minute mark. At the 30-minute mark, the rate decreased to 0.004 mg mL^{-1} min^{-1} before decreasing to 0.003 mg mL^{-1} min^{-1} at the 60-minute mark. The rate of release gradually decreased over the remainder of the experiment.

Overall the doxorubicin control solution demonstrated the highest release of doxorubicin compared to both of the nanoparticle species, whereas MIP-OSD without vancomycin present demonstrated the lowest amount of doxorubicin release with 63.2% of the amount of doxorubicin from the control solution being released.

7.4.3.4. Effect of vancomycin presence on the release of doxorubicin from the nanoparticles with 25x the original level of cross-linking.

Fourthly, the nanoparticles with a level of cross-linking 25x higher than the original, MIP-SDX-D were tested and compared with and without vancomycin being present in the solution. Also tested, were the MIP-SNX-D nanoparticles with and without vancomycin being present in solution. From this, a comparison of the effects of template presence could be seen for both the doxorubicin-loaded and non-doxorubicin loaded nanoparticles alongside a control solution of doxorubicin with vancomycin present. The results are shown in Table 7 – 12 and figure 7 – 9.

Table 7 - 12: Table showing the comparison of the release of doxorubicin from MIP-SDX-D and MIP-SNX-D against a control solution of doxorubicin with and without vancomycin present

Time (Mins)	Amount of doxorubicin released (mg mL^{-1}) Standard deviation = ± 0.001mg mL^{-1}				
	No vancomycin added		Vancomycin added		Doxorubicin Control Solution
	MIP-SDX-D	MIP-SNX-D	MIP-SDX-D	MIP-SNX-D	
0	0.000	0.000	0.000	0.000	0.000
5	0.058	0.078	0.067	0.079	0.099
10	0.103	0.138	0.118	0.141	0.175
15	0.136	0.182	0.156	0.187	0.231
20	0.166	0.222	0.189	0.227	0.281
25	0.191	0.256	0.219	0.262	0.324
30	0.212	0.284	0.243	0.291	0.359
35	0.231	0.309	0.265	0.317	0.391
40	0.248	0.332	0.285	0.341	0.421
45	0.265	0.355	0.304	0.363	0.449
50	0.281	0.376	0.322	0.385	0.476
55	0.296	0.396	0.339	0.406	0.501
60	0.309	0.415	0.356	0.425	0.525
75	0.349	0.469	0.402	0.479	0.593
90	0.391	0.523	0.448	0.536	0.662
120	0.465	0.622	0.533	0.638	0.787
180	0.589	0.789	0.677	0.809	0.999

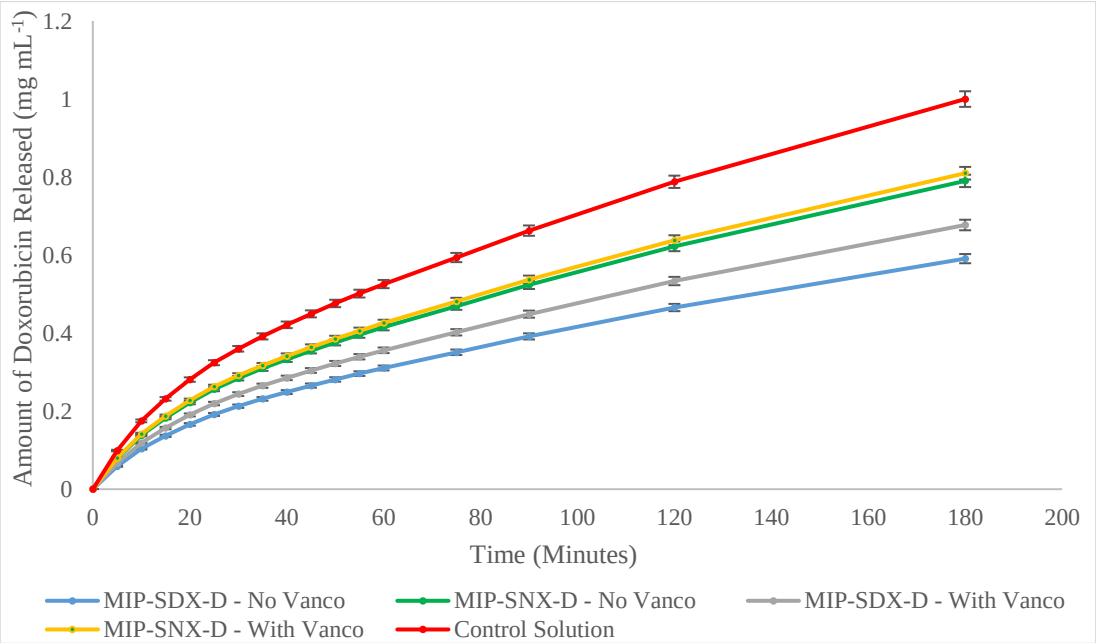

Figure 7 - 9: Graph showing the comparison of the release of doxorubicin from MIP-SDX-D and MIP-SNX-D against a control solution of doxorubicin with and without vancomycin present

During the initial 5 minutes of the experiments, the control solution of doxorubicin-containing vancomycin demonstrated an initial release of doxorubicin at a rate of 0.019 mg mL^{-1} min^{-1} whereas the MIP-SDX-D and MIP-SNX-D in the presence of vancomycin demonstrated a rate of 0.013 mg mL^{-1} min^{-1} and 0.016 mg mL^{-1} min^{-1} respectively. Whereas, without vancomycin present MIP-SDX-D and MIP-SNX-D demonstrated a rate of release of 0.012 mg mL^{-1} min^{-1} and 0.016 mg mL^{-1} min^{-1} respectively.

The rate of release of the doxorubicin from the doxorubicin control solution containing vancomycin decreased to 0.015 mg mL^{-1} min^{-1} at the 5-minute mark before decreasing to 0.008 mg mL^{-1} min^{-1} at the 20-minute mark. At the 30-minute mark, the rate decreased to 0.006 mg mL^{-1} min^{-1} before decreasing to 0.004 mg mL^{-1} min^{-1} at the 60-minute mark. The rate of release gradually decreased over the remainder of the experiment.

The rate of release of the doxorubicin from the MIP-SNX-D in the presence of vancomycin decreased to 0.012 mg mL^{-1} min^{-1} at the 5-minute mark before decreasing to 0.007 mg mL^{-1} min^{-1} at the 20-minute mark. At the 30-minute mark, the rate decreased to 0.005 mg mL^{-1} min^{-1} before decreasing to 0.004 mg mL^{-1} min^{-1} at the 60-minute mark. The rate of release gradually decreased over the remainder of the experiment.

The rate of release of the doxorubicin from the MIP-SDX-D in the presence of vancomycin decreased to 0.011 mg mL^{-1} min^{-1} at the 5-minute mark before decreasing to 0.006 mg mL^{-1} min^{-1} at the 20-minute mark. At the 30-minute mark, the rate decreased to

0.004 mg mL^{-1} min^{-1} before decreasing to 0.003 mg mL^{-1} min^{-1} at the 60-minute mark. The rate of release gradually decreased over the remainder of the experiment.

The rate of release of the doxorubicin from the MIP-SNX-D without vancomycin present decreased to 0.012 mg mL^{-1} min^{-1} at the 5-minute mark before decreasing to 0.007 mg mL^{-1} min^{-1} at the 20-minute mark. At the 30-minute mark, the rate decreased to 0.005 mg mL^{-1} min^{-1} before decreasing to 0.004 mg mL^{-1} min^{-1} at the 60-minute mark. The rate of release gradually decreased over the remainder of the experiment.

The rate of release of the doxorubicin from the MIP-SDX-D without vancomycin present decreased to 0.009 mg mL^{-1} min^{-1} at the 5-minute mark before decreasing to 0.005 mg mL^{-1} min^{-1} at the 20-minute mark. At the 30-minute mark, the rate decreased to 0.004 mg mL^{-1} min^{-1} before decreasing to 0.003 mg mL^{-1} min^{-1} at the 60-minute mark. The rate of release gradually decreased over the remainder of the experiment.

Overall the doxorubicin control solution demonstrated the highest release of doxorubicin compared to both of the nanoparticle species, whereas MIP-SDX-D without vancomycin present demonstrated the lowest amount of doxorubicin release with 59.1% of the amount of doxorubicin from the control solution being released.

7.4.3.5. Summary of the effect of cross-linking degree on doxorubicin release in the presence of the primary template.

With the alteration of the cross-linking degree, the release rate of doxorubicin is altered. When the cross-linking degree is increased, the rate of doxorubicin release decreases. All the doxorubicin imprinted nanoparticles demonstrated a lower rate of release in comparison to their non-imprinted counterparts. When the primary template was added to the nanoparticles both the doxorubicin imprinted and non-imprinted nanoparticles, there was a slight increase in the rate and amount of doxorubicin released.

7.5 Conclusions

With the increase in the level of cross-linking, the release rate of doxorubicin decreases. This change is evident with when the level of cross-linking increases to 5x the original level of cross-linking the rate of doxorubicin release decreases by 8% when increased to 10x the original level of cross-linking the rate of doxorubicin release decreases by 11% from the original. However, when this increases to 25x the original level of cross-linking, the rate of doxorubicin release is decreased by 25% from the original, demonstrating a significant increase in the retention of doxorubicin by the nanoparticles.

When the primary template, vancomycin is added to the nanoparticle solution, there is an increase in the amount of doxorubicin released from the nanoparticles. The change in doxorubicin release between the solution with and without doxorubicin increases as the level of cross-linking increases. This change in doxorubicin release is most likely by the presence of the vancomycin, causing a small amount of doxorubicin to be released from the nanoparticles in addition to the standard doxorubicin release. However, the vancomycin presence may cause more doxorubicin to be released due to the increased concentration of molecules inside the dialysis tubing.

Chapter 8. Concluding remarks

Drug-loaded MIP nanoparticles demonstrate significant potential for the controlled delivery of therapeutic agents such as doxorubicin or other chemotherapeutic drugs. This usage is beneficial as it facilitates the delivery of a therapeutic agent over an extended period at a sustained concentration. This is instead of oversaturating the target with a massive singular burst, exposing the target cell to a more considerable amount of drug with a smaller dosage. This dosing is beneficial as the use of a lower dosage reduces the side effects of any therapeutic agent used.

In this work, nanoparticles were investigated for their potential as a doxorubicin delivery system. Firstly, the storage of nanoparticles was optimised, initially testing the use of lyophilisation to see how this process affects the properties of the nanoparticles. To protect the nanoparticles during this lyophilisation, four different cryoprotectants based from the literature were tested, glucose, glycine, sorbitol and trehalose. From this trehalose was tested then optimised to find the ideal amount to protect the nanoparticles while undergoing lyophilisation without affecting the nanoparticle properties. The most effective amount was found to be 10mg mL-1 of trehalose added to the nanoparticles as this had the least significant effect on the nanoparticle properties. Secondly, the nanoparticles underwent autoclaving to see what effect this had on the nanoparticles. Both methods show potential for storing nanoparticles preventing biological contamination of the nanoparticle solution, for use in live cells.

In the initial testing of the nanoparticles for therapeutic delivery, nanoparticles loaded with Caspase-3 siRNA attached was *via* a charge based interaction. The nanoparticles were found to interact with the siRNA successfully, creating a nanoparticle-RNA complex; however, this complex was found to be double the size of the nanoparticles. When testing the nanoparticles, two of the organic nanoparticle species were found to kill off the cells with the remaining neutral organic species giving the lowest caspase-3 level of the nanoparticles tested. When this species was tested and compared to the liposomal transfection reagent used as a control, it was found to be less effective. With consideration to the process of transfection, the nanoparticles performed as well as expected primarily due to the uncertainties surrounding the suitable amount of siRNA to use and insufficiently optimised control delivery system.

Following on from this, the focus turned to the use of doxorubicin as a chemotherapeutic drug and how to deliver this to cells *via* a controlled release and *via* targeted delivery.

The first step in this was the testing use of magnetic core nanoparticles imprinted to carry doxorubicin within the polymeric structure. This work is developed from research carried out by Piletska et al. for the controlled delivery and release of curcumin.[113] Based on these five nanoparticle compositions were tested to determine the best functional monomer to use for the imprinting of doxorubicin for loading into the nanoparticle. Of the functional monomers tested, 2-hydroxymethyl acrylate was found to retain the highest amount of doxorubicin with the lowest amount released. These nanoparticles show the potential of being a multi-functional drug delivery system in that a drug payload can be administered alongside the magnetic core being used as a contrasting agent for MRI or being subjected to an alternating magnetic field to cause a temperature increase in the tissue surrounding the nanoparticles causing the cellular death of the afflicted cells.

Following on from the magnetic nanoparticles, a more targeted delivery system for doxorubicin was investigated. For this work, two different solid phase templates were used, vancomycin and an EGFR binding peptide. Vancomycin was used initially due to previous work by the group using vancomycin as a template.[117] The nanoparticles were found to release doxorubicin fairly quickly during the initial minutes of the experiment before slowing down by the 180-minute mark. Initially of different amounts of doxorubicin were incorporated into the nanoparticles, this was followed by changing the template to a cancer-specific target, an EGFR binding peptide. The nanoparticles for this were synthesised in both aqueous and organic solvents to observe the effect of different compositions on doxorubicin release, resulting in the aqueous synthesis showing greater retention of doxorubicin compared to its organic counterpart. To further investigate the effect of nanoparticle composition, the level of cross-linking in the nanoparticles was increased to see what effect this would have on the release profile of doxorubicin. It was observed that as the level of cross-linking increased, the rate of release decreased.

The final investigation conducted was into the addition of the primary template to the nanoparticle solution when the release profile was determined. This addition was carried out to simulate the effect of the MIP nanoparticles binding to the complementary target when injected into cells. The results of this showed that with the addition of the template, there was a small increase in the amount of doxorubicin release from the nanoparticles compared to the nanoparticles without the template present in the solution. This increase is likely caused by the template molecules increasing the concentration gradient inside the dialysis membrane causing more doxorubicin to be released.

Overall the work carried out has shown that the use of MIP nanoparticles for the controlled delivery of doxorubicin is possible and can allow a sustained release over time. However, loading doxorubicin in this matter is not suitable for a specific cell-targeted delivery due to the doxorubicin's ability to diffuse out of the nanoparticles. To achieve this, a trigger mechanism would be required to ensure that the drug payload only releases in a specific cellular environment or condition. The best way of achieving this would be with the use of a cleavable linker such as hydrazone or an enzyme-cleavable peptide. Hydrazone can be used for delivery into cells which possess a slightly acidic pH.[118] When the nanoparticles enter the cells, the hydrazone will cleave releasing the drug payload into the target cell while remaining attached in normal physiological pH. An enzyme-susceptible peptide is an alternative way of using a cleavable linker as the peptide should only be broken down inside a cell by an enzyme specific to that species of the cell. In cancer cells, the enzyme cathepsin B is over-expressed so a peptide that is cleavable by this enzyme would be ideal for attaching a drug payload to a nanoparticle. An example of a peptide that is cleavable by cathepsin B is the tetrapeptide Alanine-Leucine-Alanine-Leucine (Ala-Leu-Ala-Leu) which was found to be cleaved by cathepsin-B by Schmid et al.[119] Use of either of these would make for an ideal target specific drug delivery system.

References

1. S.-O. Ralph, *Current Radiopharmaceuticals*, 2011, **4**, 140-143.
2. X. Cun, S. Ruan, J. Chen, L. Zhang, J. Li, Q. He and H. Gao, *Acta Biomaterialia*, 2016, **31**, 186-196.
3. A. Sarafraz-Yazdi and N. Razavi, *TrAC Trends in Analytical Chemistry*, 2015, **73**, 81-90.
4. M. Mohammed, J. Syeda, K. Wasan and E. Wasan, *Pharmaceutics*, 2017, **9**, 53.
5. J. Emami, M. S. S. Boushehri and J. Varshosaz, *Res Pharm Sci*, 2014, **9**, 301-314.
6. X. Huang, T. Zhang, A. Goswami, F. Luo and T. Asefa, *RSC Advances*, 2015, **5**, 28836-28839.
7. U. Grether and H. Waldmann, *Chemistry (Weinheim an der Bergstrasse, Germany)*, 2001, **7**, 959-971.
8. C. J. Sunderland, M. Steiert, J. E. Talmadge, A. M. Derfus and S. E. Barry, *Drug Development Research*, 2006, **67**, 70-93.
9. C. d. Santos Giuberti, E. C. de Oliveira Reis, T. G. Ribeiro Rocha, E. A. Leite, R. G. Lacerda, G. A. Ramaldes and M. C. de Oliveira, *Journal of Liposome Research*, 2011, **21**, 60-69.
10. T. Davis and S. S Farag, *Treating relapsed or refractory Philadelphia chromosome-negative acute lymphoblastic leukemia: Liposome-encapsulated vincristine*, 2013.
11. J.-S. An, J.-E. Kim, D.-H. Lee, B.-Y. Kim, S. Cho, I.-H. Kwon, W.-W. Choi, S.-M. Kang, C.-H. Won, S.-E. Chang, M.-W. Lee, J.-H. Choi and K.-C. Moon, *Journal of Cosmetic and Laser Therapy*, 2011, **13**, 28-32.
12. S. Biswas, N. S. Dodwadkar, P. P. Deshpande and V. P. Torchilin, *Journal of Controlled Release*, 2012, **159**, 393-402.
13. C.-H. Lin, C.-H. Chen, Z.-C. Lin and J.-Y. Fang, *Journal of Food and Drug Analysis*, 2017, **25**, 219-234.
14. J. Liu, T. Gong, H. Fu, C. Wang, X. Wang, Q. Chen, Q. Zhang, Q. He and Z. Zhang, *International Journal of Pharmaceutics*, 2008, **356**, 333-344.
15. M. M. A. Abdel-Mottaleb, D. Neumann and A. Lamprecht, *European Journal of Pharmaceutics and Biopharmaceutics*, 2011, **79**, 36-42.
16. A. P. Nayak, W. Tiyaboonchai, S. Patankar, B. Madhusudhan and E. B. Souto, *Colloids and Surfaces B: Biointerfaces*, 2010, **81**, 263-273.
17. T. Abboud, H. Andresen, J. Koeppen, P. Czorlich, L. Duehrsen, J. Stenzig, M. Westphal and J. Regelsberger, *Acta Neurochirurgica*, 2015, **157**, 763-767.
18. R. V. J. Chari, B. A. Martell, J. L. Gross, S. B. Cook, S. A. Shah, W. A. Blättler, S. J. McKenzie and V. S. Goldmacher, *Cancer Research*, 1992, **52**, 127-131.

19. J. F. A. DiJoseph, Douglas C. Boghaert, Erwin R. Khandke, Kiran Dougher, Maureen M. Sridharan, Latha Kunz, Arthur Hamann, Philip R. Gorovits, Boris Udata, Chandrasekhar Moran, Justin K. Popplewell, Andrew G. Stephens, Sue Frost, Philip Damle, Nitin K., *Blood*, 2004, **103**, 1807-1814.
20. A. Mullard, *Nature Reviews Drug Discovery*, 2013, **12**, 329.
21. R. A. Firestone, D. Willner, S. J. Hofstead, H. D. King, T. Kaneko, G. R. Braslawsky, R. S. Greenfield, P. A. Trail, S. J. Lasch, A. J. Henderson, A. M. Casazza, I. Hellström and K. E. Hellström, *Journal of Controlled Release*, 1996, **39**, 251-259.
22. M. Murphy, S. Phinney, O. Ab, M. Mayo, K. Whiteman, R. Lutz and G. Payne, *Cancer Research*, 2008, **68**, 4898-4898.
23. J. Conde, J. Dias, V. Grazu, M. Moros, P. Baptista and J. Fuente, *Revisiting 30 years of Biofunctionalization and Surface Chemistry of Inorganic Nanoparticles for Nanomedicine*, 2014.
24. G. M. Dubowchik, R. A. Firestone, L. Padilla, D. Willner, S. J. Hofstead, K. Mosure, J. O. Knipe, S. J. Lasch and P. A. Trail, *Bioconjugate Chemistry*, 2002, **13**, 855-869.
25. S. C. Jeffrey, M. T. Nguyen, R. F. Moser, D. L. Meyer, J. B. Miyamoto and P. D. Senter, *Bioorganic & Medicinal Chemistry Letters*, 2007, **17**, 2278-2280.
26. S. Moktan, C. Ryppa, F. Kratz and D. Raucher, *Investigational New Drugs*, 2012, **30**, 236-248.
27. P. Swietach, R. D. Vaughan-Jones, A. L. Harris and A. Hulikova, *Philosophical Transactions of the Royal Society B: Biological Sciences*, 2014, **369**.
28. P. Zhang and J. Kong, *Talanta*, 2015, **134**, 501-507.
29. G. Amato, *Nanoscale Research Letters*, 2010, **5**, 1156-1160.
30. I. I. Slowing, B. G. Trewyn, S. Giri and V. S. Y. Lin, *Advanced Functional Materials*, 2007, **17**, 1225-1236.
31. J. C. Echeverría, J. Estella, V. Barbería, J. Musgo and J. J. Garrido, *Journal of Non-Crystalline Solids*, 2010, **356**, 378-382.
32. K. Czarnobaj, *Drug Delivery*, 2008, **15**, 485-492.
33. U. Maver, A. Godec, M. Bele, O. Planinšek, M. Gaberšček, S. Srčič and J. Jamnik, *International Journal of Pharmaceutics*, 2007, **330**, 164-174.
34. M. Ahmad, T. Ahmad, R. A. Sultan and G. Murtaza, *Trop. J. Pharm. Res.*, 2009, **8**, 385-391.
35. B. J. Melde, B. J. Johnson and P. T. Charles, *Sensors (Basel, Switzerland)*, 2008, **8**, 5202-5228.
36. K. Czarnobaj and J. Łukasiak, *Journal of Materials Science: Materials in Medicine*, 2007, **18**, 2041-2044.
37. M. Prokopowicz, *Journal of Sol-Gel Science and Technology*, 2010, **53**, 525-533.

38. L. Wei, N. Hu and Y. Zhang, *Materials*, 2010, **3**, 4066.
39. A. J. Di Pasqua, S. Wallner, D. J. Kerwood and J. C. Dabrowiak, *Chemistry and Biodiversity*, 2009, **6**, 1343-1349.
40. W. Lin, Y. w. Huang, X. D. Zhou and Y. Ma, *Toxicology and Applied Pharmacology*, 2006, **217**, 252-259.
41. M. Cho, W. S. Cho, M. Choi, S. J. Kim, B. S. Han, S. H. Kim, H. O. Kim, Y. Y. Sheen and J. Jeong, *Toxicology Letters*, 2009, **189**, 177-183.
42. M. Vallet-Regí, M. Colilla, I. Izquierdo-Barba and M. Manzano, *Molecules*, 2018, **23**, 47.
43. Z. Li, K. Su, B. Cheng and Y. Deng, *Journal of Colloid and Interface Science*, 2010, **342**, 607-613.
44. C. Llor, J. Arranz, R. Morros, A. Garcia-Sangenis, H. Pera, J. Llobera, M. Guillen-Sola, E. Carandell, J. Ortega, S. Hernandez and M. Miravitlles, *BMC Fam. Pract.*, 2013, **14**, 7.
45. G. Martínez-Edo, A. Balmori, I. Pontón, A. Martí del Rio and D. Sánchez-García, *Catalysts*, 2018, **8**, 617.
46. Q. He, Y. Gao, L. Zhang, Z. Zhang, F. Gao, X. Ji, Y. Li and J. Shi, *Biomaterials*, 2011, **32**, 7711-7720.
47. A. Fahr and X. Liu, *Expert Opinion on Drug Delivery*, 2007, **4**, 403-416.
48. R. F. Popovici, E. M. Seftel, G. D. Mihai, E. Popovici and V. A. Voicu, *Journal of Pharmaceutical Sciences*, 2011, **100**, 704-714.
49. S. Bangalore, R. Fakheri, S. Wandel, B. Toklu, J. Wandel and F. H. Messerli, *BMJ*, 2017, **356**.
50. W.-Y. Qian, D.-M. Sun, R.-R. Zhu, X.-L. Du, H. Liu and S.-L. Wang, *International Journal of Nanomedicine*, 2012, **7**, 5781-5792.
51. J.-E. Kim, H.-T. Lim, A. Minai-Tehrani, J.-T. Kwon, J.-Y. Shin, C.-G. Woo, M. Choi, J. Baek, D. H. Jeong, Y.-C. Ha, C.-H. Chae, K.-S. Song, K.-H. Ahn, J.-H. Lee, H.-J. Sung, I.-J. Yu, G. R. Beck and M.-H. Cho, *Journal of Toxicology and Environmental Health, Part A*, 2010, **73**, 1530-1543.
52. Z. Li, L. Chen, S. Meng, L. Guo, J. Huang, Y. Liu, W. Wang and X. Chen, *Physical Review B*, 2015, **91**, 094429.
53. S. Hu, T. Wang, X. Pei, H. Cai, J. Chen, X. Zhang, Q. Wan and J. Wang, *Nanoscale Research Letters*, 2016, **11**, 452.
54. N. Ma, B. Zhang, J. Liu, P. Zhang, Z. Li and Y. Luan, *International Journal of Pharmaceutics*, 2015, **496**, 984-992.
55. R. Imani, S. H. Emami and S. Faghihi, *Physical Chemistry Chemical Physics*, 2015, **17**, 6328-6339.

56. M. Arruebo, R. Fernández-Pacheco, M. R. Ibarra and J. Santamaría, *Nano Today*, 2007, **2**, 22-32.
57. S. Louguet, B. Rousseau, R. Epherre, N. Guidolin, G. Goglio, S. Mornet, E. Duguet, S. Lecommandoux and C. Schatz, *Polymer Chemistry*, 2012, **3**, 1408-1417.
58. X. Wang, A. Deng, W. Cao, Q. Li, L. Wang, J. Zhou, B. Hu and X. Xing, *Journal of Materials Science*, 2018, **53**, 6433-6449.
59. J. M. Lopez-Novoa, Y. Quiros, L. Vicente, A. I. Morales and F. J. Lopez-Hernandez, *Kidney International*, 2011, **79**, 33-45.
60. Q. F. Meng, L. Rao, M. Zan, M. Chen, G. T. Yu, X. Wei, Z. Wu, Y. Sun, S. S. Guo, X. Z. Zhao, F. B. Wang and W. Liu, *Nanotechnology*, 2018, **29**, 134004.
61. D. A. Ovchinnikov, *genesis*, 2008, **46**, 447-462.
62. S. Mizrahy and D. Peer, *Chemical Society Reviews*, 2012, **41**, 2623-2640.
63. J. Zhang and R. D. K. Misra, *Acta Biomaterialia*, 2007, **3**, 838-850.
64. X. Yang, J. J. Grailer, I. J. Rowland, A. Javadi, S. A. Hurley, V. Z. Matson, D. A. Steeber and S. Gong, *ACS Nano*, 2010, **4**, 6805-6817.
65. C. Qian, J. Yu, Y. Chen, Q. Hu, X. Xiao, W. Sun, C. Wang, P. Feng, Q. D. Shen and Z. Gu, *Advanced Materials*, 2016, **28**, 3313-3320.
66. M. R. Juchau, *Annual Review of Pharmacology and Toxicology*, 1989, **29**, 165-187.
67. Y. Garcia, K. Smolinska-Kempisty, E. Pereira, E. Piletska and S. Piletsky, *Analytical Methods*, 2017, **9**, 4592-4598.
68. N. B. D. Turkmen, M. E. Corman, H. Shaikh, S. Akgol and A. Denizli, *Artificial cells, nanomedicine, and biotechnology*, 2014, **42**, 316-322.
69. M. Tomasz, *Chemistry & Biology*, 1995, **2**, 575-579.
70. J. O. S. Peltier, F. Lagarce, W. Couet, J. Benoît, *Pharmaceutical Research*, 2006, **23**, 1243-1250.
71. F. A. Ishkuh, M. Javanbakht, M. Esfandyari-Manesh, R. Dinarvand and F. Atyabi, *Journal of Materials Science*, 2014, **49**, 6343-6352.
72. H. Zhang, *Controlled/"living" radical precipitation polymerization: A versatile polymerization technique for advanced functional polymers*, 2013.
73. K. Cetin and A. Denizli, *Colloids and Surfaces B-Biointerfaces*, 2015, **126**, 401-406.
74. S. D. Baker, J. Verweij, E. K. Rowinsky, R. C. Donehower, J. H. M. Schellens, L. B. Grochow and A. Sparreboom, *JNCI: Journal of the National Cancer Institute*, 2002, **94**, 1883-1888.
75. K. Çetin, H. Alkan, N. Bereli and A. Denizli, *Journal of Macromolecular Science, Part A*, 2017, **54**, 502-508.
76. T. Gillich, C. Acikgöz, L. Isa, A. D. Schlüter, N. D. Spencer and M. Textor, *ACS Nano*, 2013, **7**, 316-329.

77. Z. Dai, J. Ronholm, Y. Tian, B. Sethi and X. Cao, *Journal of Tissue Engineering*, 2016, **7**, 2041731416648810.
78. W. H. Morrison and S. M. Truhlsen, *American Journal of Ophthalmology*, 1950, **33**, 357-367.
79. Y. Darwis and I. W. Kellaway, *The lyophilisation and aerosolisation of liposomes for pulmonary drug administration*, 2002.
80. N. S. El-Salamouni, R. M. Farid, A. H. El-Kamel and S. S. El-Gamal, *International Journal of Pharmaceutics*, 2015, **496**, 976-983.
81. M. Siri, M. Grasselli and S. d. V. Alonso, *Journal of Pharmaceutical and Biomedical Analysis*, 2016, **126**, 66-74.
82. J. Boerio-Goates, *The Journal of Chemical Thermodynamics*, 1991, **23**, 403-409.
83. I. Amelio, F. Cutruzzolá, A. Antonov, M. Agostini and G. Melino, *Trends in Biochemical Sciences*, 2014, **39**, 191-198.
84. J. R. Medina and R. L. Garrote, *Brazilian Journal of Chemical Engineering*, 2002, **19**, 419-424.
85. A. Saleh, K. McGarry, C. S. Chaw and A. A. Elkordy, *Pharmaceutics*, 2018, **10**, 22.
86. C. Urban and P. Schurtenberger, *Journal of Colloid and Interface Science*, 1998, **207**, 150-158.
87. E. S. Alnemri, D. J. Livingston, D. W. Nicholson, G. Salvesen, N. A. Thornberry, W. W. Wong and J. Yuan, *Cell*, 1996, **87**, 171.
88. A. G. Porter and R. U. Jänicke, *Cell Death And Differentiation*, 1999, **6**, 99.
89. S. Ghavami, M. Hashemi, S. R. Ande, B. Yeganeh, W. Xiao, M. Eshraghi, C. J. Bus, K. Kadkhoda, E. Wiechec, A. J. Halayko and M. Los, *Journal of Medical Genetics*, 2009, **46**, 497.
90. F. G. Gervais, D. Xu, G. S. Robertson, J. P. Vaillancourt, Y. Zhu, J. Huang, A. LeBlanc, D. Smith, M. Rigby, M. S. Shearman, E. E. Clarke, H. Zheng, L. H. T. Van Der Ploeg, S. C. Ruffolo, N. A. Thornberry, S. Xanthoudakis, R. J. Zamboni, S. Roy and D. W. Nicholson, *Cell*, 1999, **97**, 395-406.
91. A. Nikolaev, T. McLaughlin, D. D. M. O'Leary and M. Tessier-Lavigne, *Nature*, 2009, **457**, 981.
92. N. Agrawal, P. V. N. Dasaradhi, A. Mohmmed, P. Malhotra, R. K. Bhatnagar and S. K. Mukherjee, *Microbiology and Molecular Biology Reviews*, 2003, **67**, 657-685.
93. A. J. C. Quaresma, R. Sievert, J. A. Nickerson and A. G. Matera, *Molecular Biology of the Cell*, 2013, **24**, 1208-1221.
94. S. J. Sharp, J. Schaack, L. Cooley, D. J. Burke and D. Soil, *Critical Reviews in Biochemistry*, 1985, **19**, 107-144.
95. H. Siomi and M. C. Siomi, *Nature*, 2009, **457**, 396.

96. P. D. Zamore, T. Tuschl, P. A. Sharp and D. P. Bartel, *Cell*, 2000, **101**, 25-33.
97. G. L. Sen and H. M. Blau, *Nature Cell Biology*, 2005, **7**, 633.
98. G. S. Mack, *Nature Biotechnology*, 2007, **25**, 631.
99. W. Rychlik, W. J. Spencer and R. E. Rhoads, *Nucleic Acids Res.*, 1990, **18**, 6409-6412.
100. P. S. a. C. R. D. O. Tacar, *Journal of Pharmacy and Pharmacology*, 2013, **65**, 157-170.
101. L. Xiao, S. Q. Hu, L. Y. Wang, J. X. Liu and X. Y. Li, *Eur Rev Med Pharmacol Sci*, 2015, **19**, 3763-3769.
102. K. Chatterjee, J. Zhang, N. Honbo and J. S. Karliner, *Cardiology*, 2010, **115**, 155-162.
103. K. Agnieszka, B. B. M, H. Liesbeth, V. Peter and K. D. V, *The Journal of Pathology*, 2012, **226**, 598-608.
104. A. M. Lopez, L. Wallace, R. T. Dorr, M. Koff, E. M. Hersh and D. S. Alberts, *Cancer Chemother Pharmacol*, 1999, **44**, 303-306.
105. G. E. Kellogg, J. N. Scarsdale and F. A. Fornari, *Nucleic Acids Res.*, 1998, **26**, 4721-4732.
106. F. Yang, S. S. Teves, C. J. Kemp and S. Henikoff, *Biochimica et Biophysica Acta (BBA) - Reviews on Cancer*, 2014, **1845**, 84-89.
107. A. Bodley, L. F. Liu, M. Israel, R. Seshadri, Y. Koseki, F. C. Giuliani, S. Kirschenbaum, R. Silber and M. Potmesil, *Cancer Research*, 1989, **49**, 5969-5978.
108. T. Geninatti, E. Small and A. Grattoni, *Meas. Sci. Technol.*, 2014, **25**, 6.
109. J. M. Pallicer and S. D. Kramer, *Journal of Pharmaceutical and Biomedical Analysis*, 2012, **71**, 219-227.
110. S. Basak and K. Chattopadhyay, *Physical Chemistry Chemical Physics*, 2014, **16**, 11139-11149.
111. G. Such, R. A Evans, L. Yee and T. Davis, *Factors influencing photochromism of spiro–compounds within polymeric matrices*, 2003.
112. F. L. Zu, F. Y. Yan, Z. J. Bai, J. X. Xu, Y. Y. Wang, Y. C. Huang and X. G. Zhou, *Microchim. Acta*, 2017, **184**, 1899-1914.
113. E. V. Piletska, B. H. Abd, A. S. Krakowiak, A. Parmar, D. L. Pink, K. S. Wall, L. Wharton, E. Moczko, M. J. Whitcombe, K. Karim and S. A. Piletsky, *Analyst*, 2015, **140**, 3113-3120.
114. Y. Manolova, V. Deneva, L. Antonov, E. Drakalska, D. Momekova and N. Lambov, *Spectrochimica Acta Part A: Molecular and Biomolecular Spectroscopy*, 2014, **132**, 815-820.
115. I. Chianella, A. Guerreiro, E. Moczko, J. S. Caygill, E. V. Piletska, I. M. P. De Vargas Sansalvador, M. J. Whitcombe and S. A. Piletsky, *Analytical Chemistry*, 2013, **85**, 8462-8468.

116. F. Canfarotta, L. Lezina, A. Guerreiro, J. Czulak, A. Petukhov, A. Daks, K. Smolinska-Kempisty, A. Poma, S. Piletsky and N. A. Barlev, *Nano Letters*, 2018, **18**, 4641-4646.
117. I. Chianella, A. Guerreiro, E. Moczko, J. S. Caygill, E. V. Piletska, I. Sansalvador, M. J. Whitcombe and S. A. Piletsky, *Analytical Chemistry*, 2013, **85**, 8462-8468.
118. Y. Nakajima and H. Suzuki, *Organometallics*, 2003, **22**, 959-969.
119. B. Schmid, D. E. Chung, A. Warnecke, I. Fichtner and F. Kratz, *Bioconjugate Chemistry*, 2007, **18**, 702-716.

Appendix

Appendix 1 - Dynamic Light Scattering Data - Initial cryoprotect screening

Appendix 1.1. - Control Screening – No Cryoprotectant – Pre-Lyophilisation

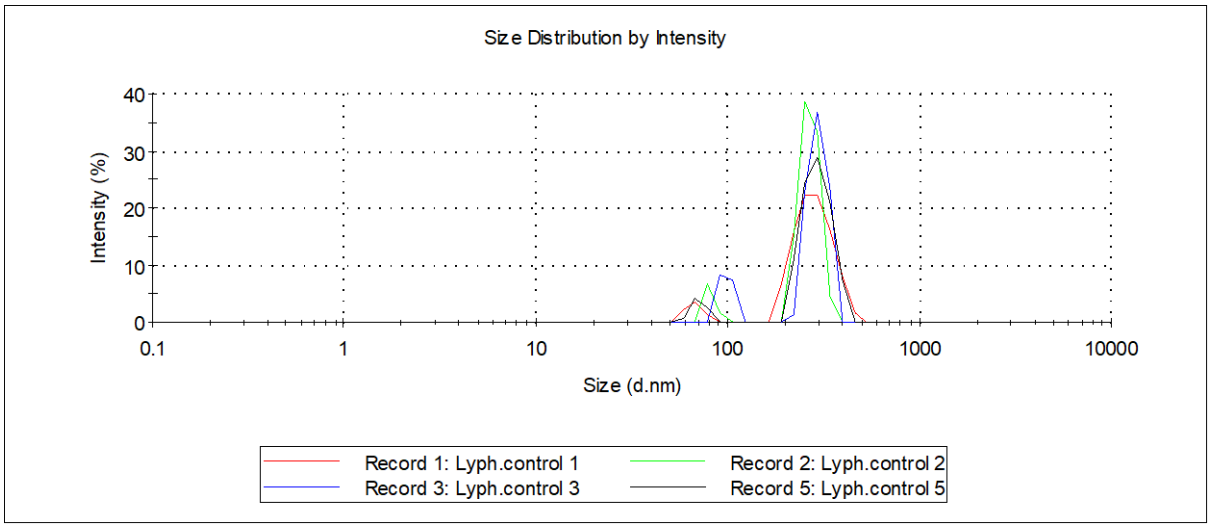

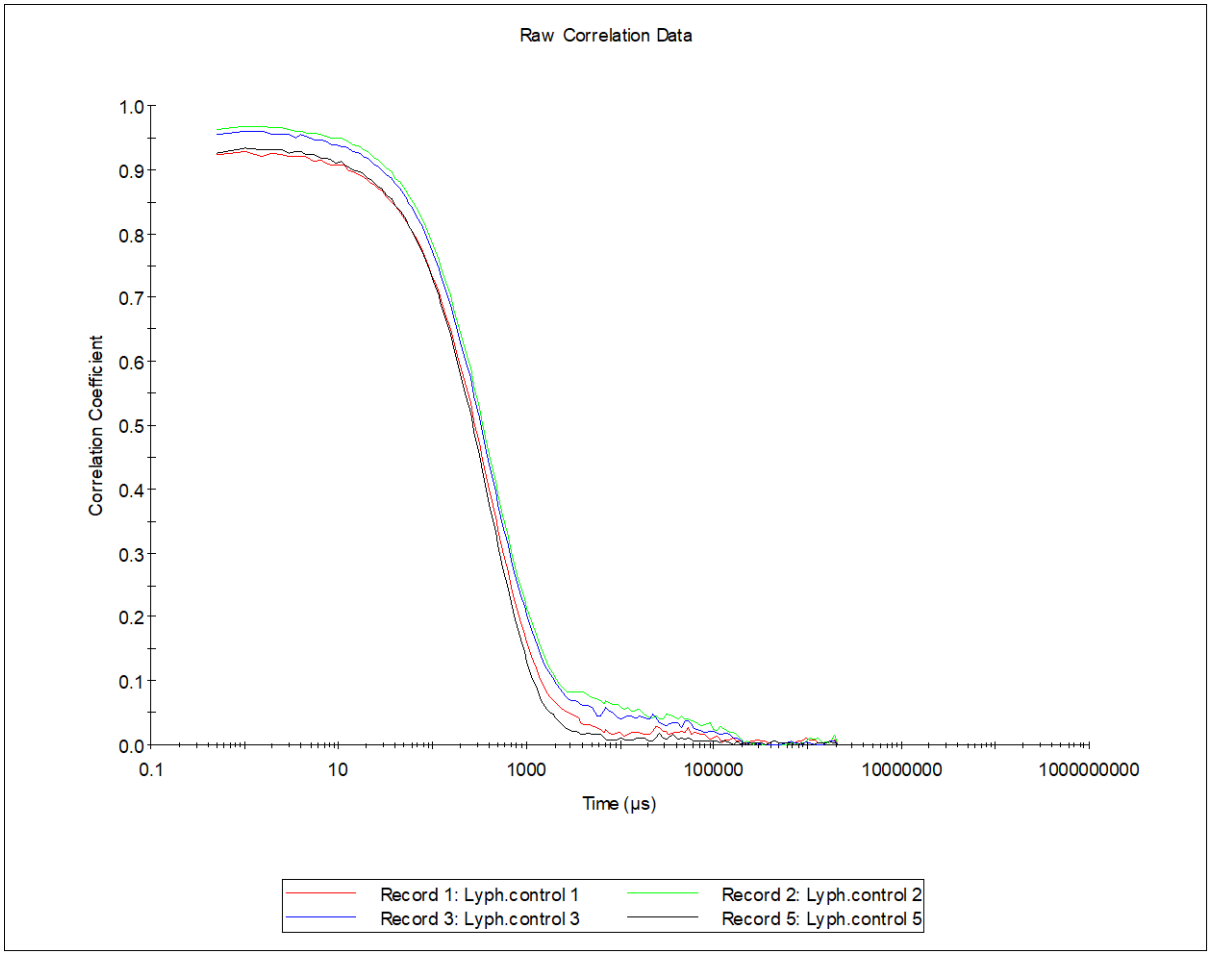

Appendix 1.2. - Control Screening – No Cryoprotectant – Post-Lyophilisation

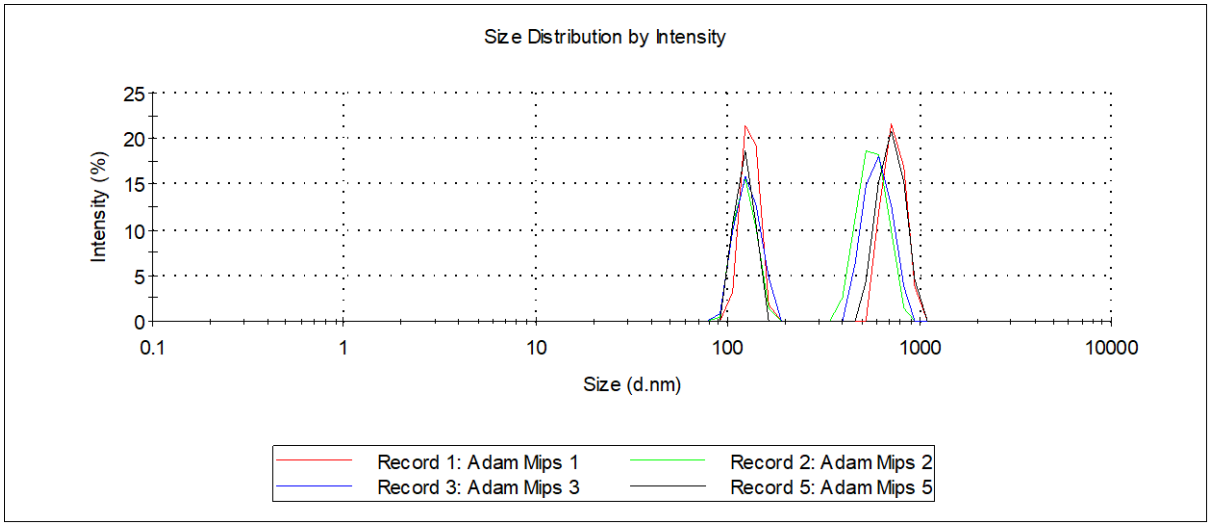

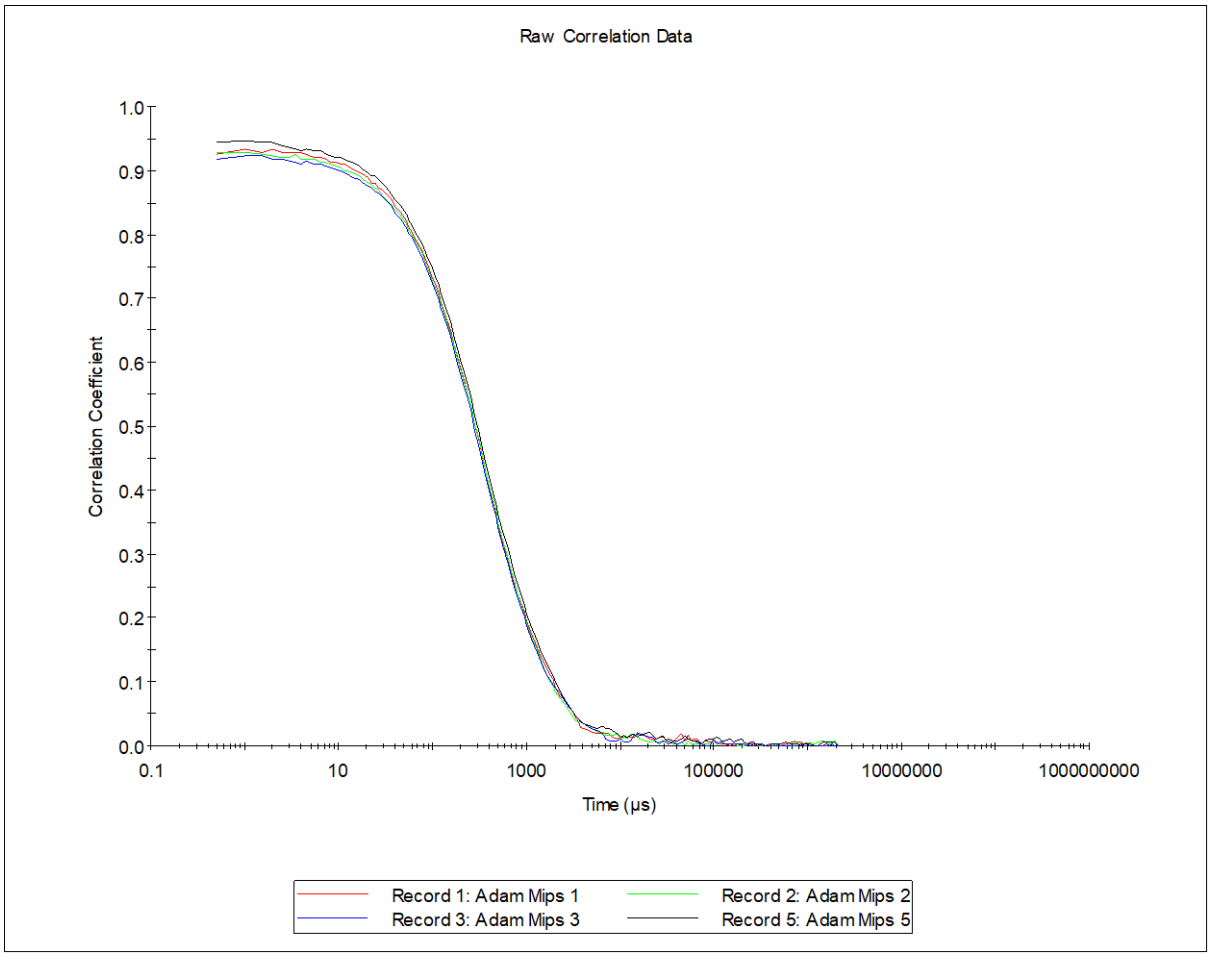

Appendix 1.3. - Glucose Screening – 25mg Glucose – Pre-Lyophilisation

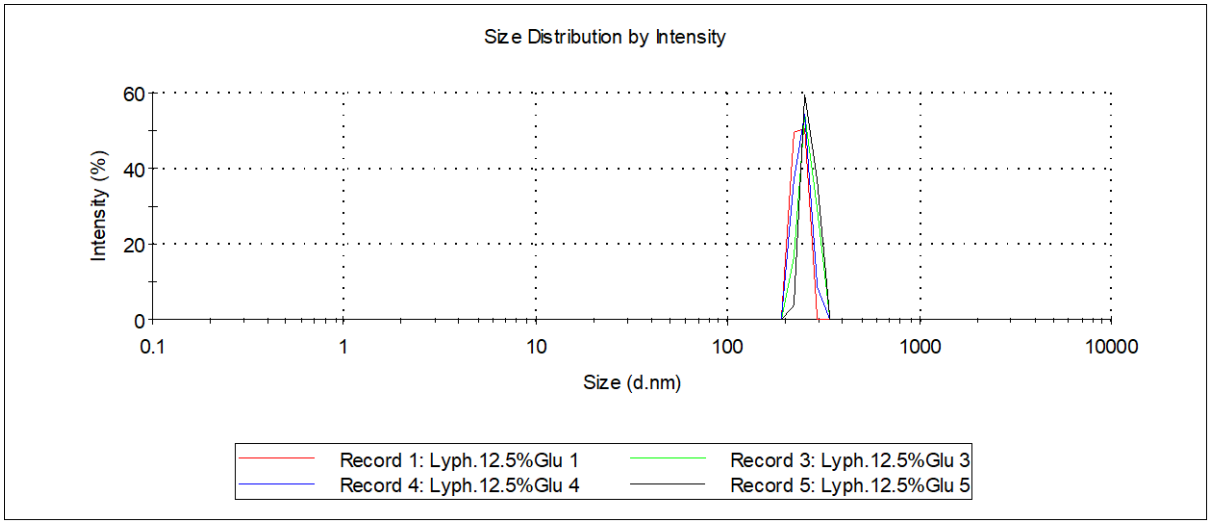

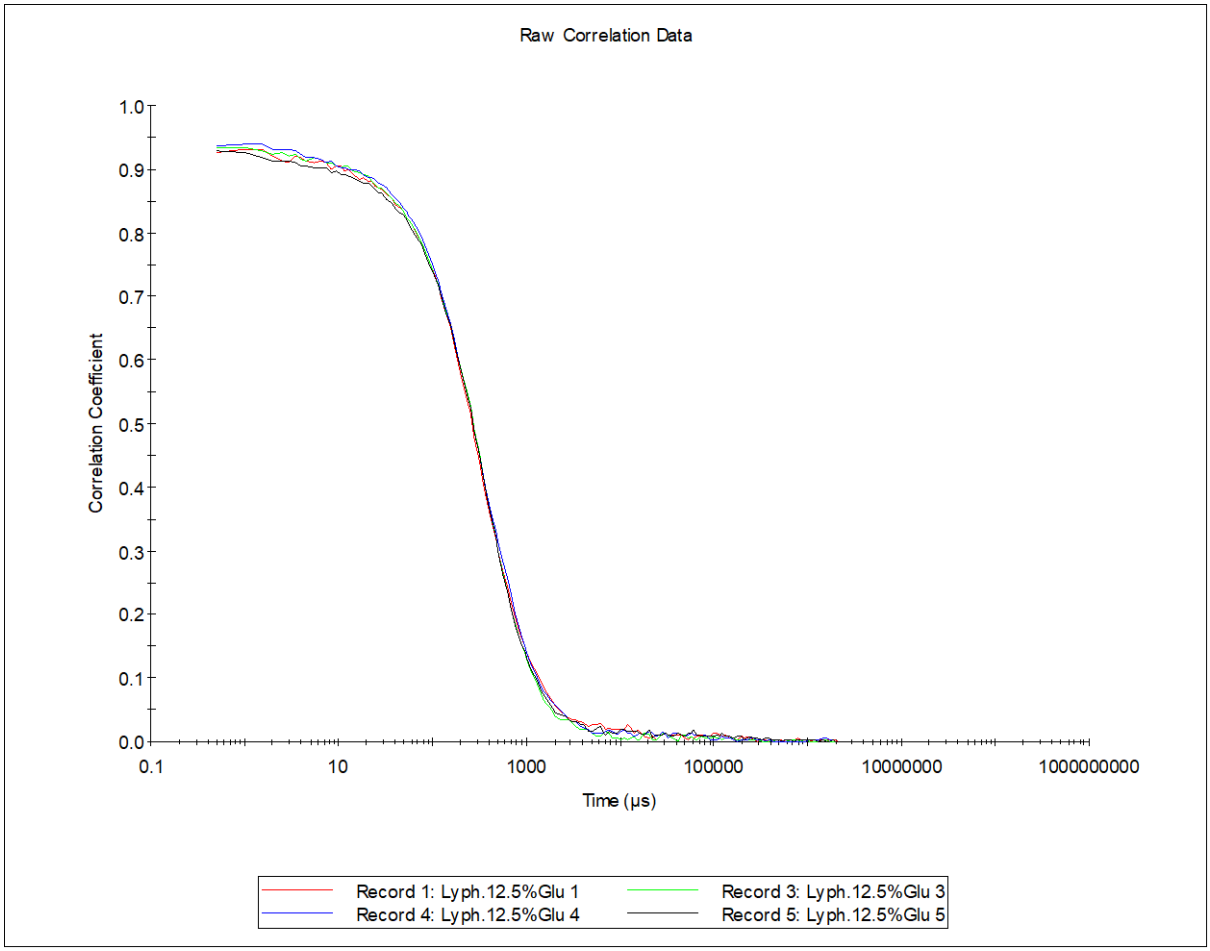

Appendix 1.4. - Glucose Screening – 25mg Glucose – Post-Lyophilisation

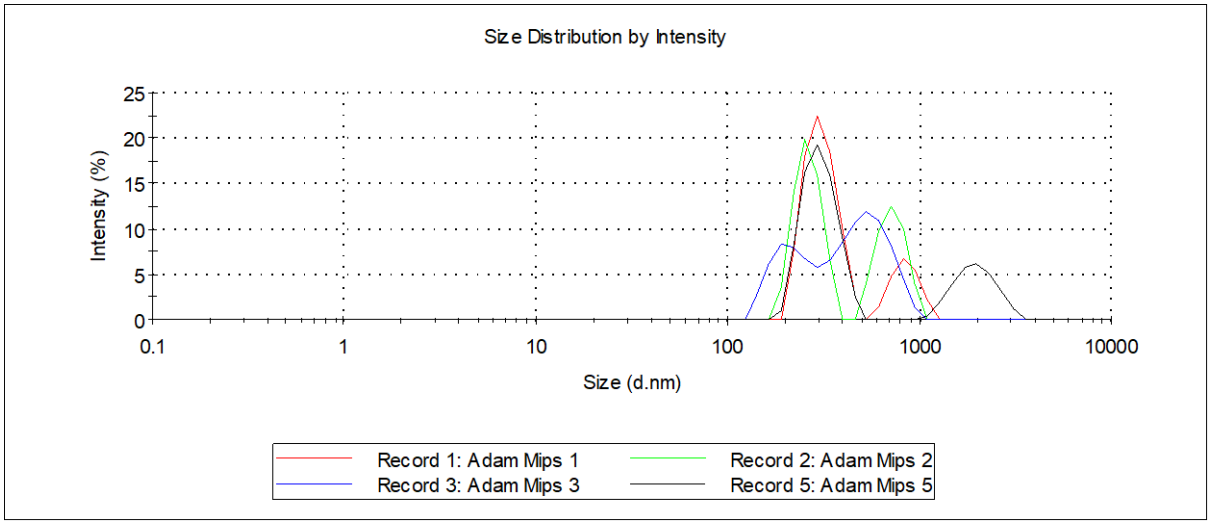

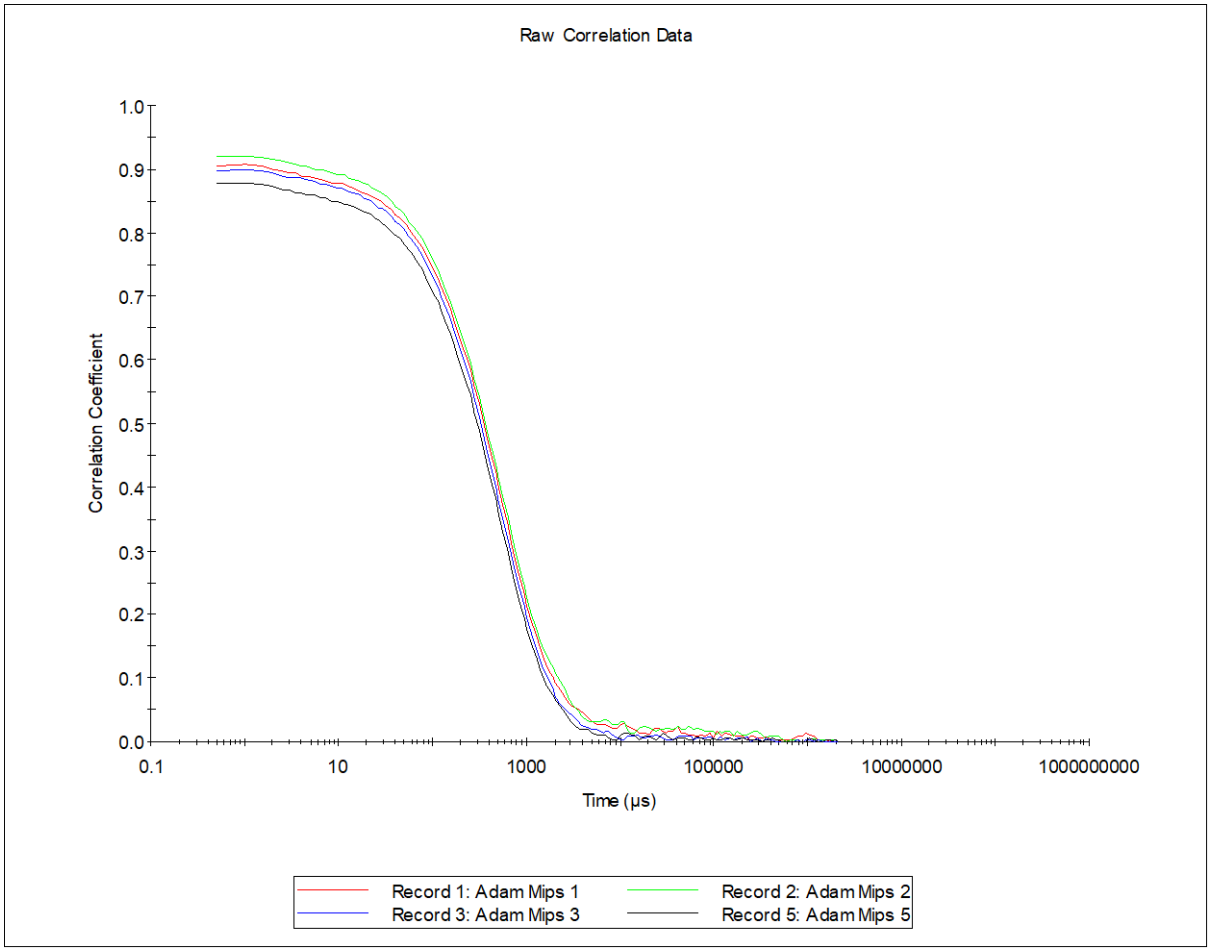

Appendix 1.5. - Glucose Screening – 50mg Glucose – Pre-Lyophilisation

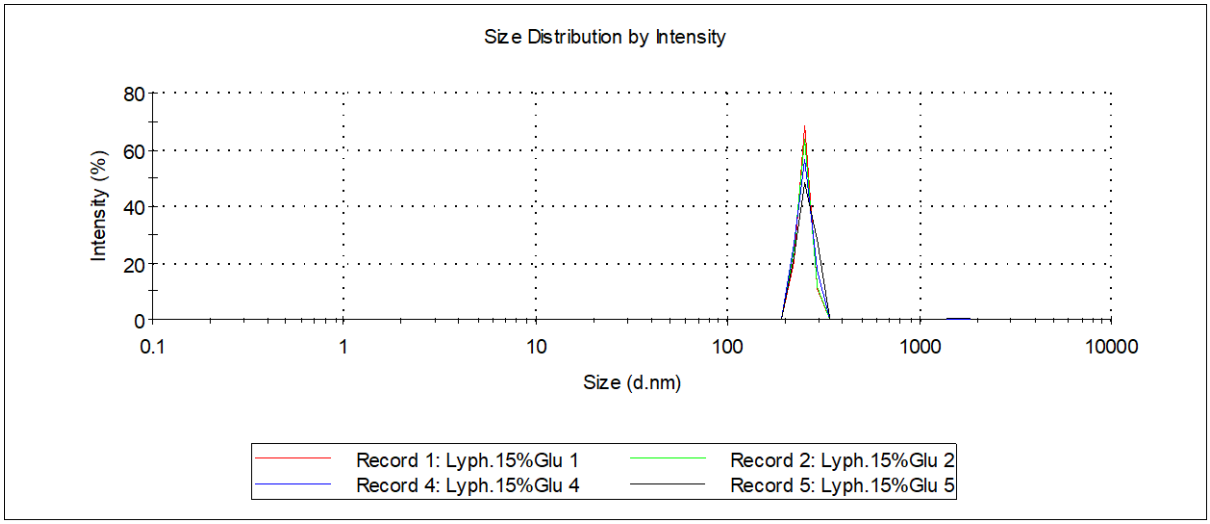

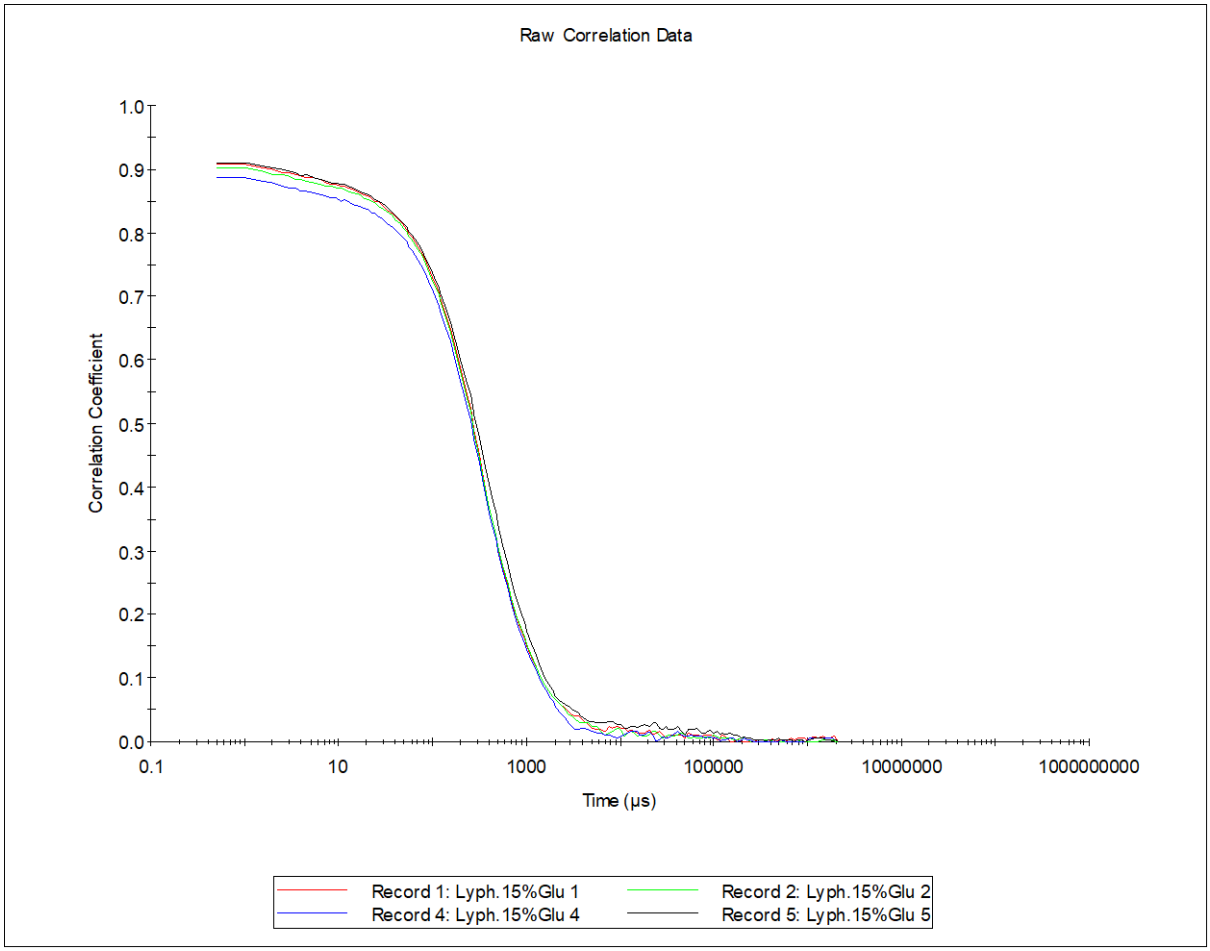

Appendix 1.6. - Glucose Screening – 50mg Glucose – Post-Lyophilisation

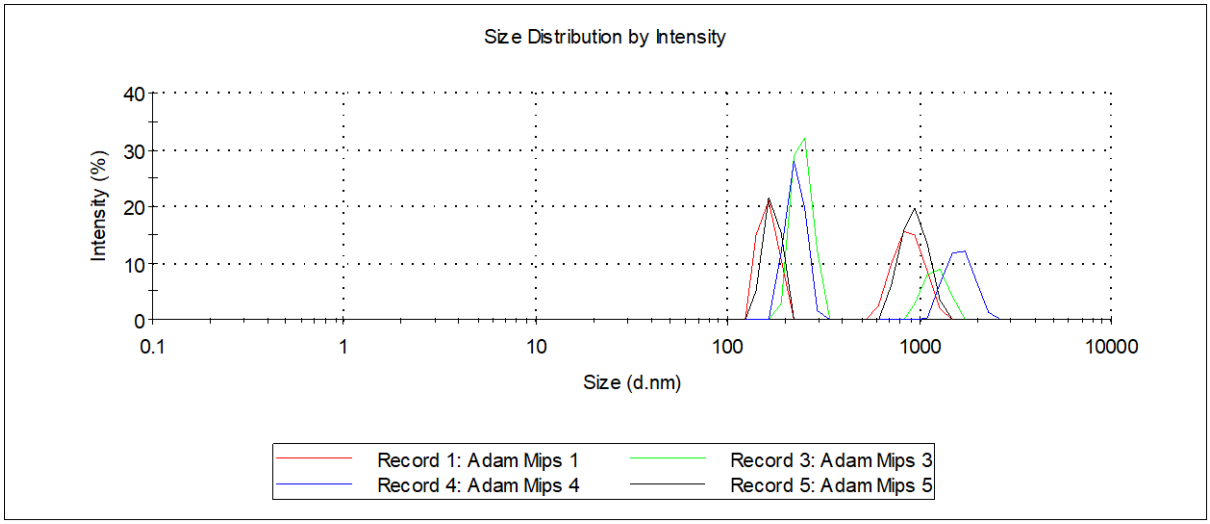

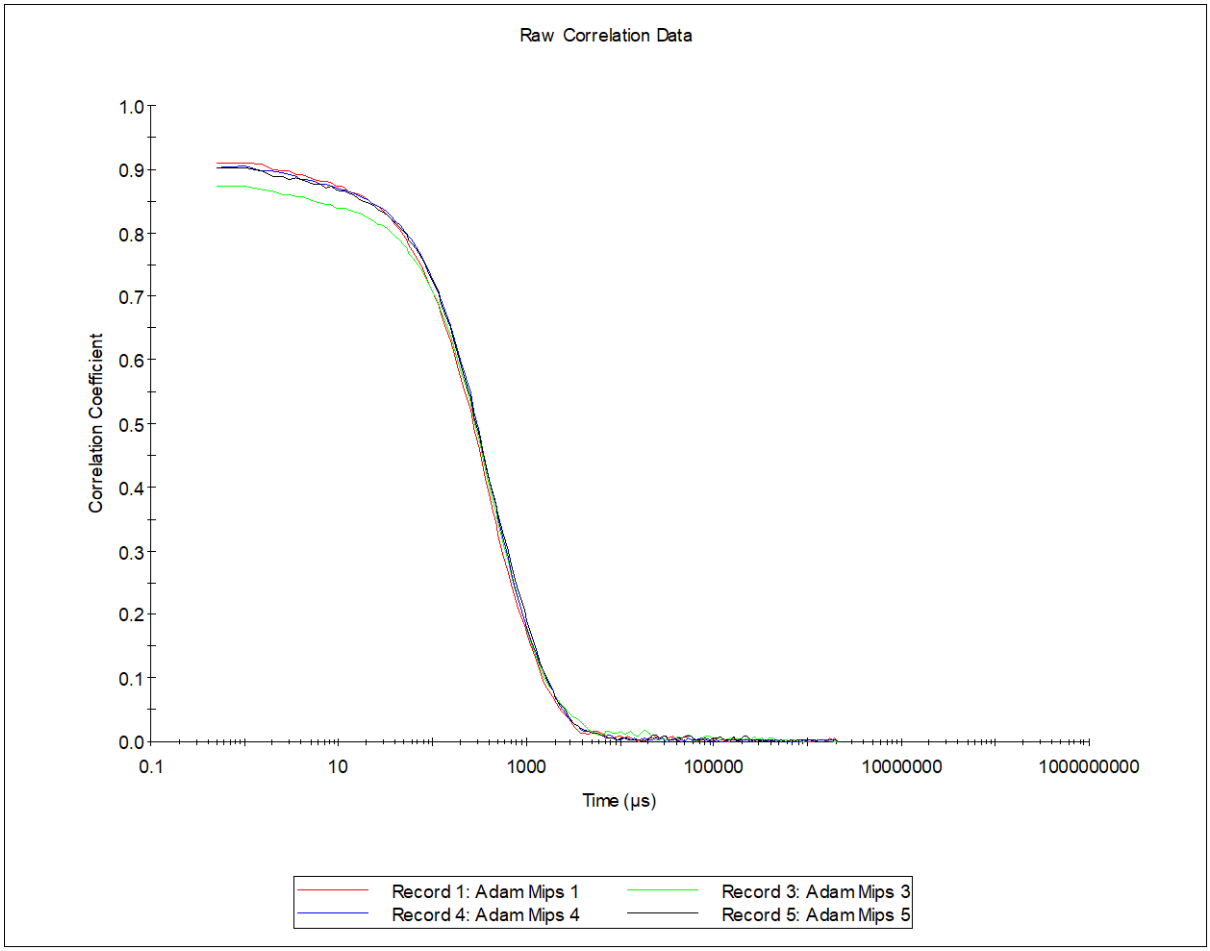

Appendix 1.7. - Glucose Screening – 25mg Glycine – Pre-Lyophilisation

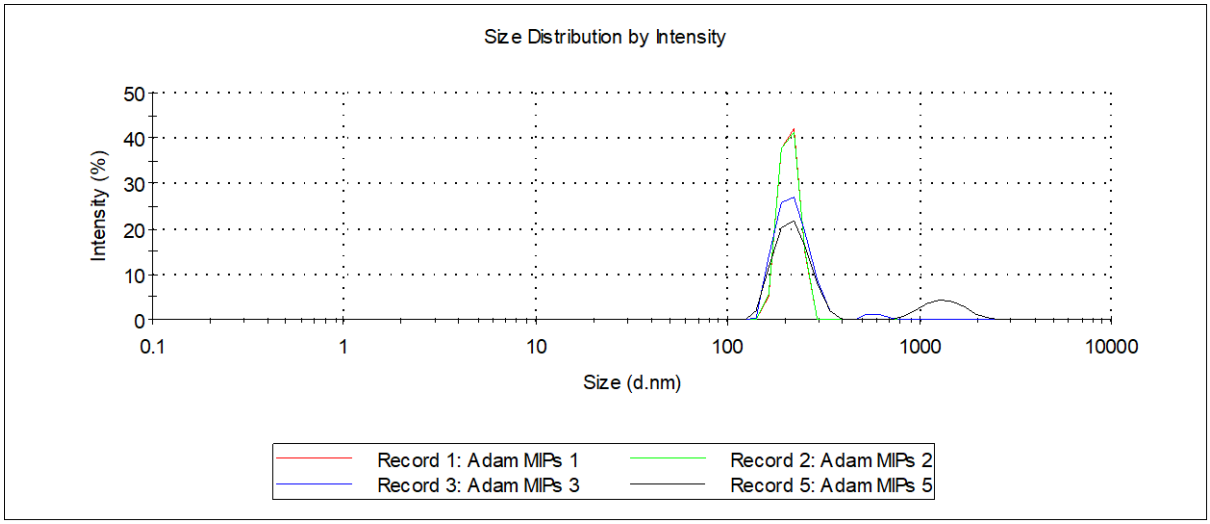

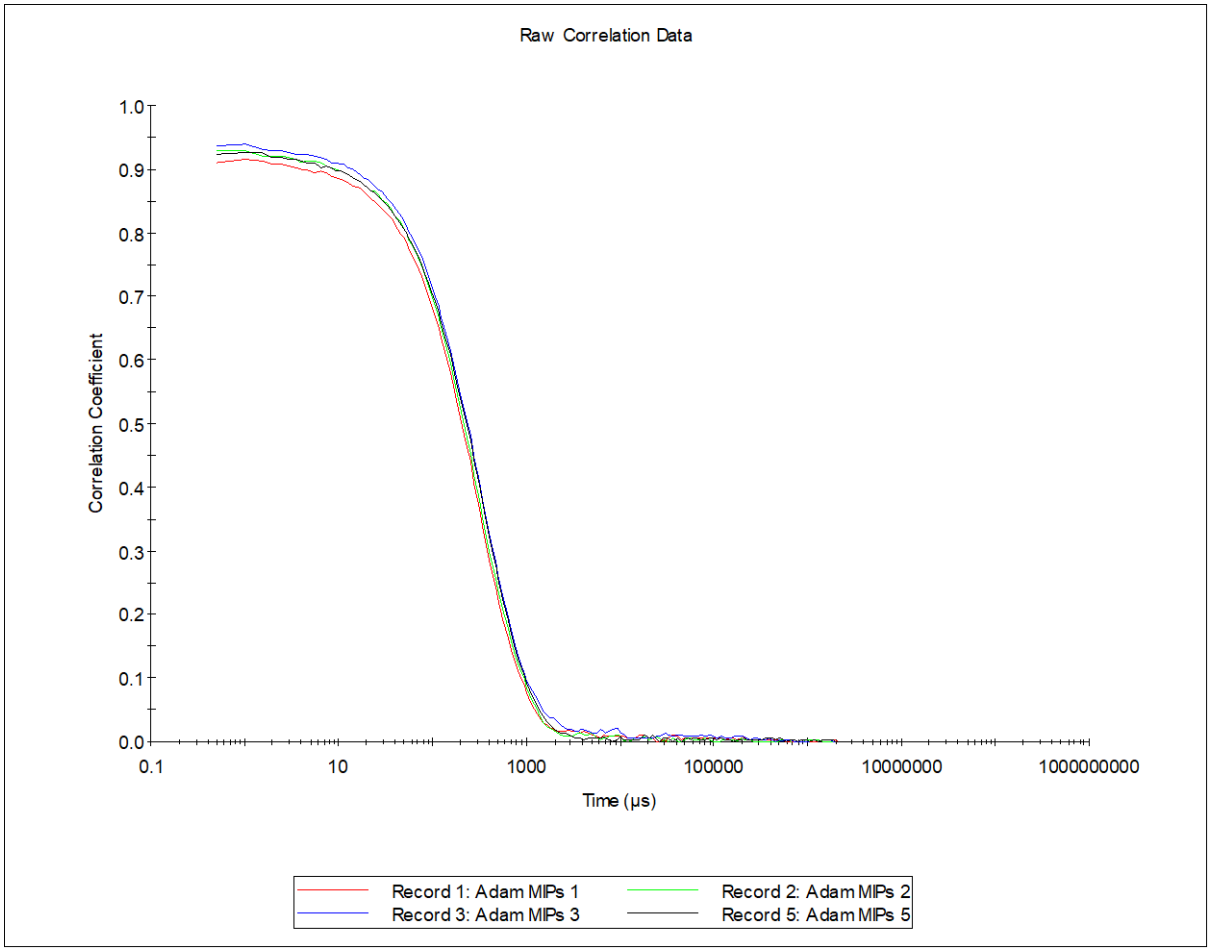

Appendix 1.8. - Glycine Screening – 25mg Glycine – Post-Lyophilisation

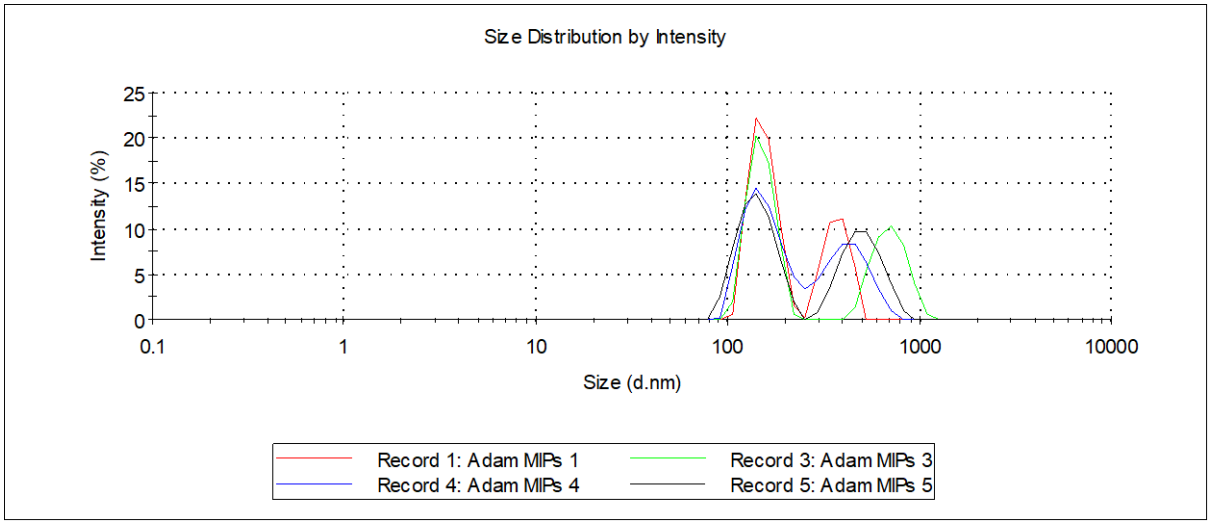

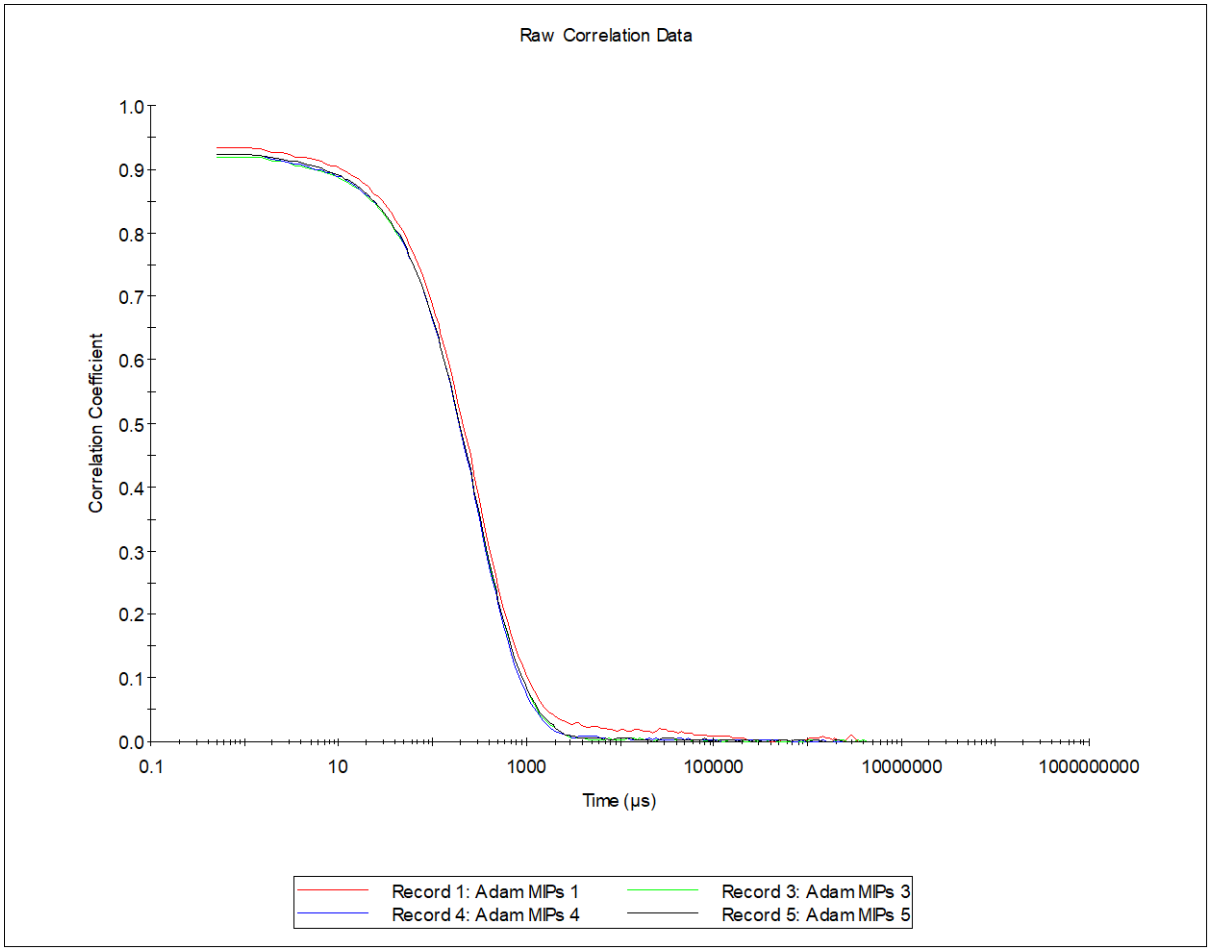

Appendix 1.9. - Glycine Screening – 50mg Glycine – Pre-Lyophilisation

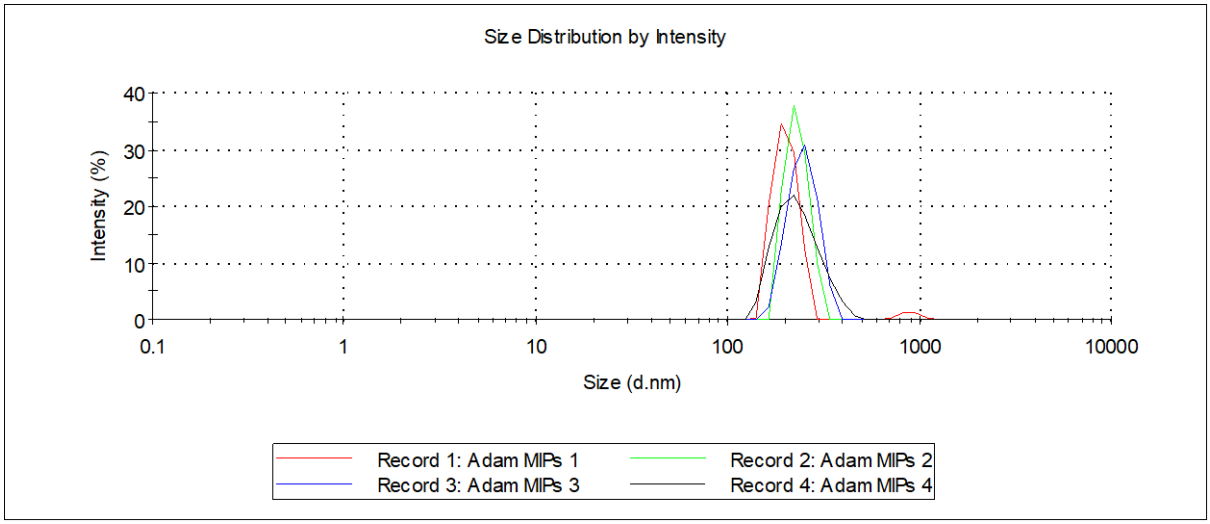

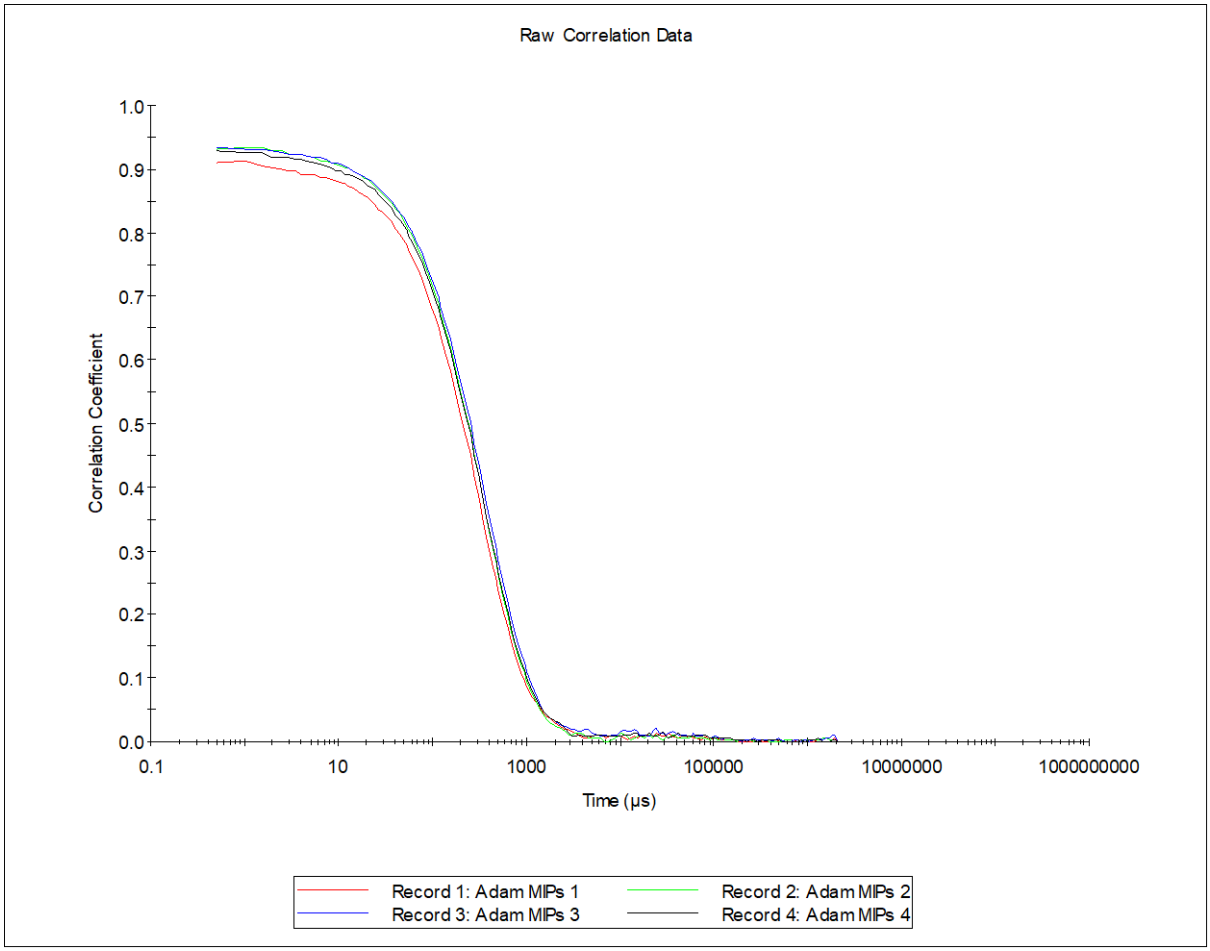

Appendix 1.10. - Glycine Screening – 50mg Glycine – Post-Lyophilisation

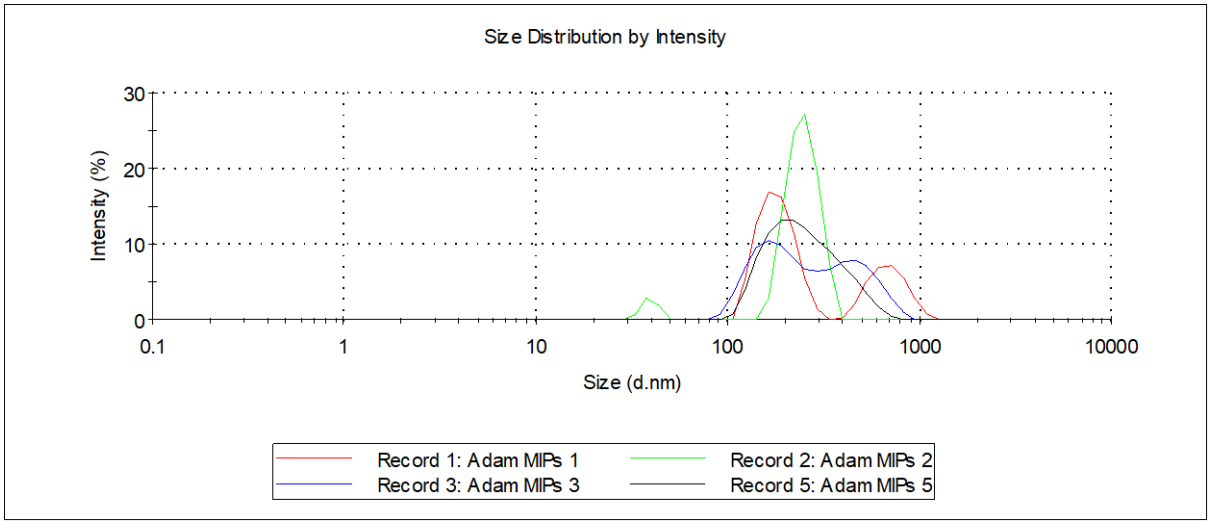

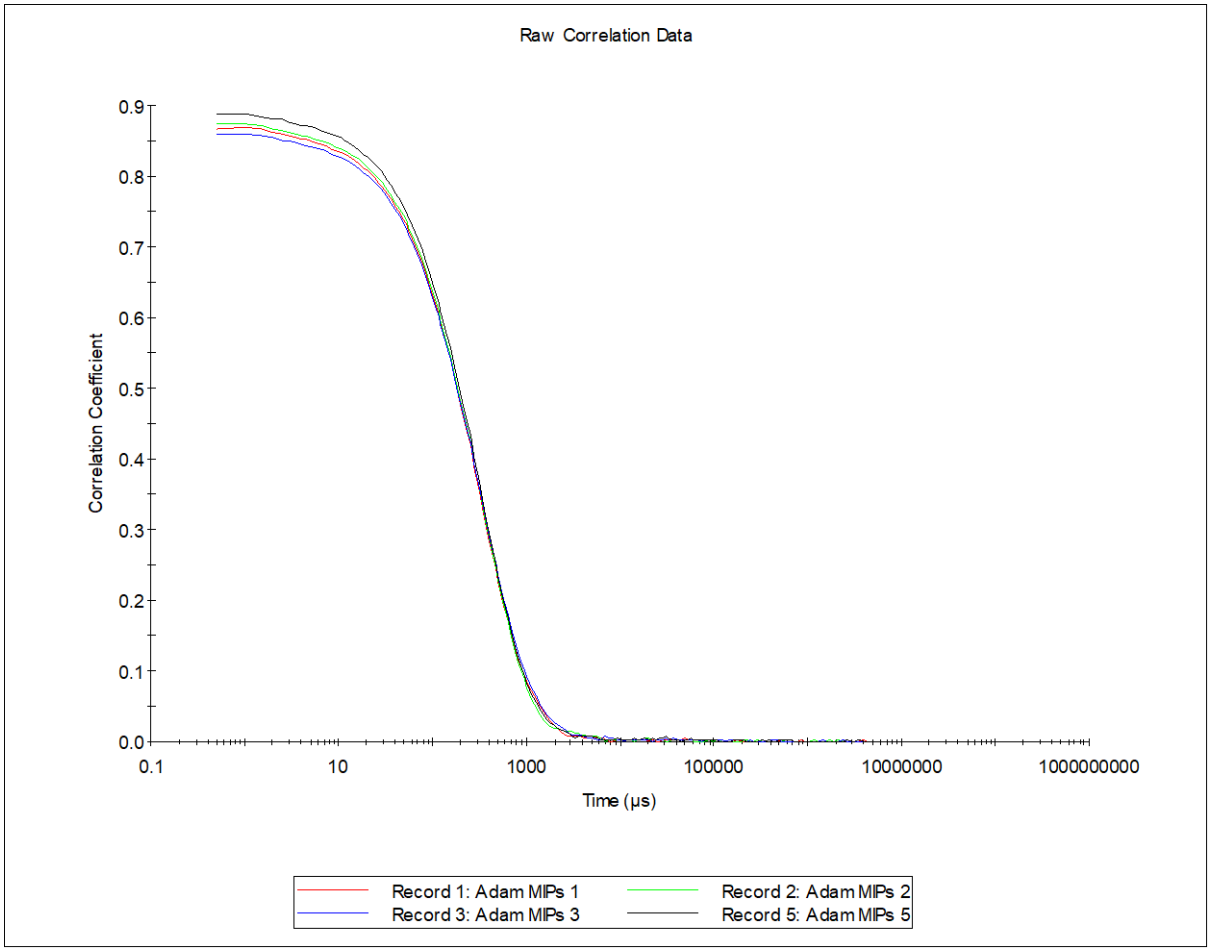

Appendix 1.11. - Sorbitol Screening – 25mg Sorbitol – Pre-Lyophilisation

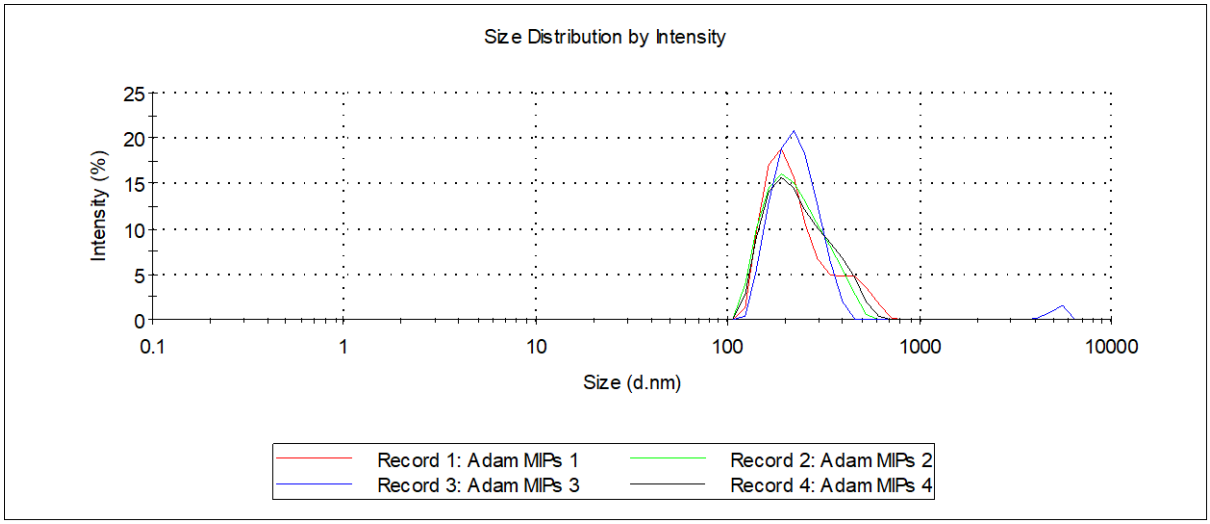

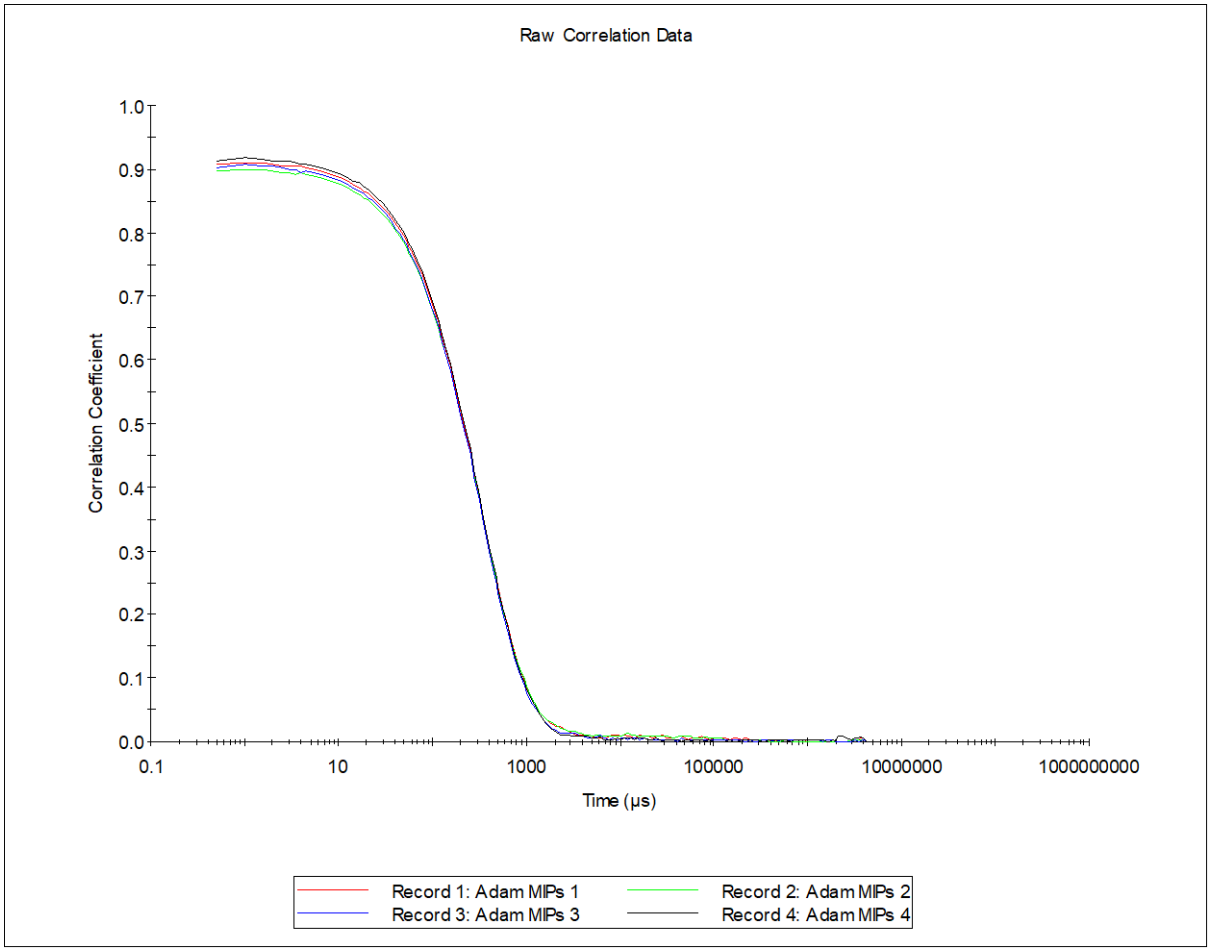

Appendix 1.12. - Sorbitol Screening – 25mg Sorbitol – Post-Lyophilisation

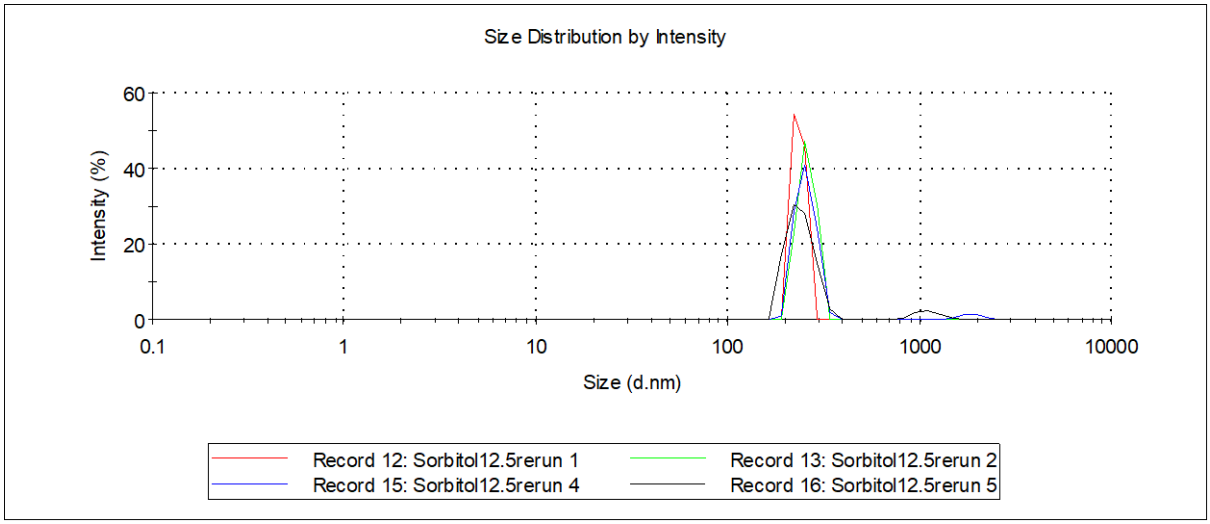

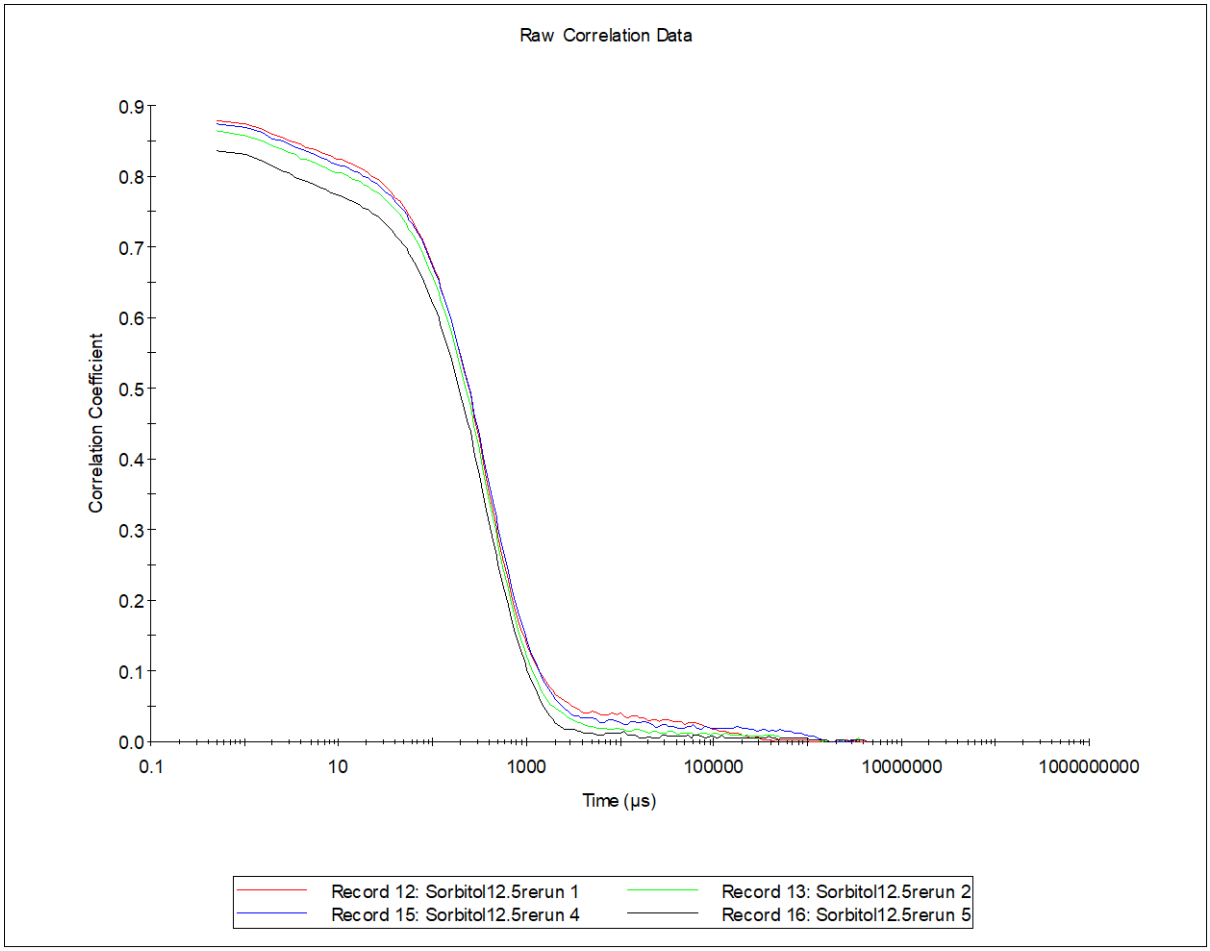

Appendix 1.13. - Sorbitol Screening – 50mg Sorbitol – Pre-Lyophilisation

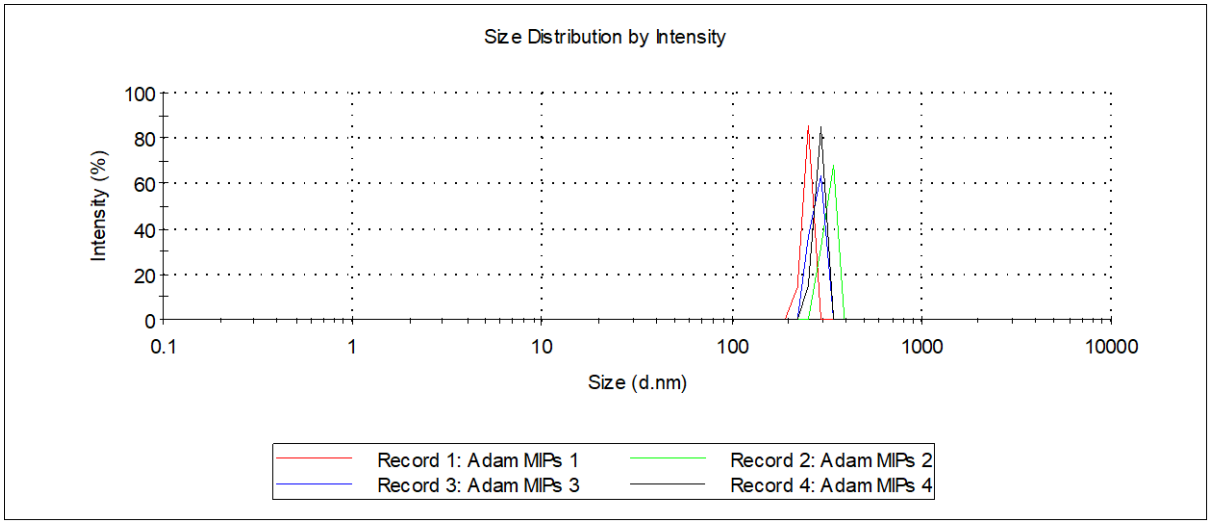

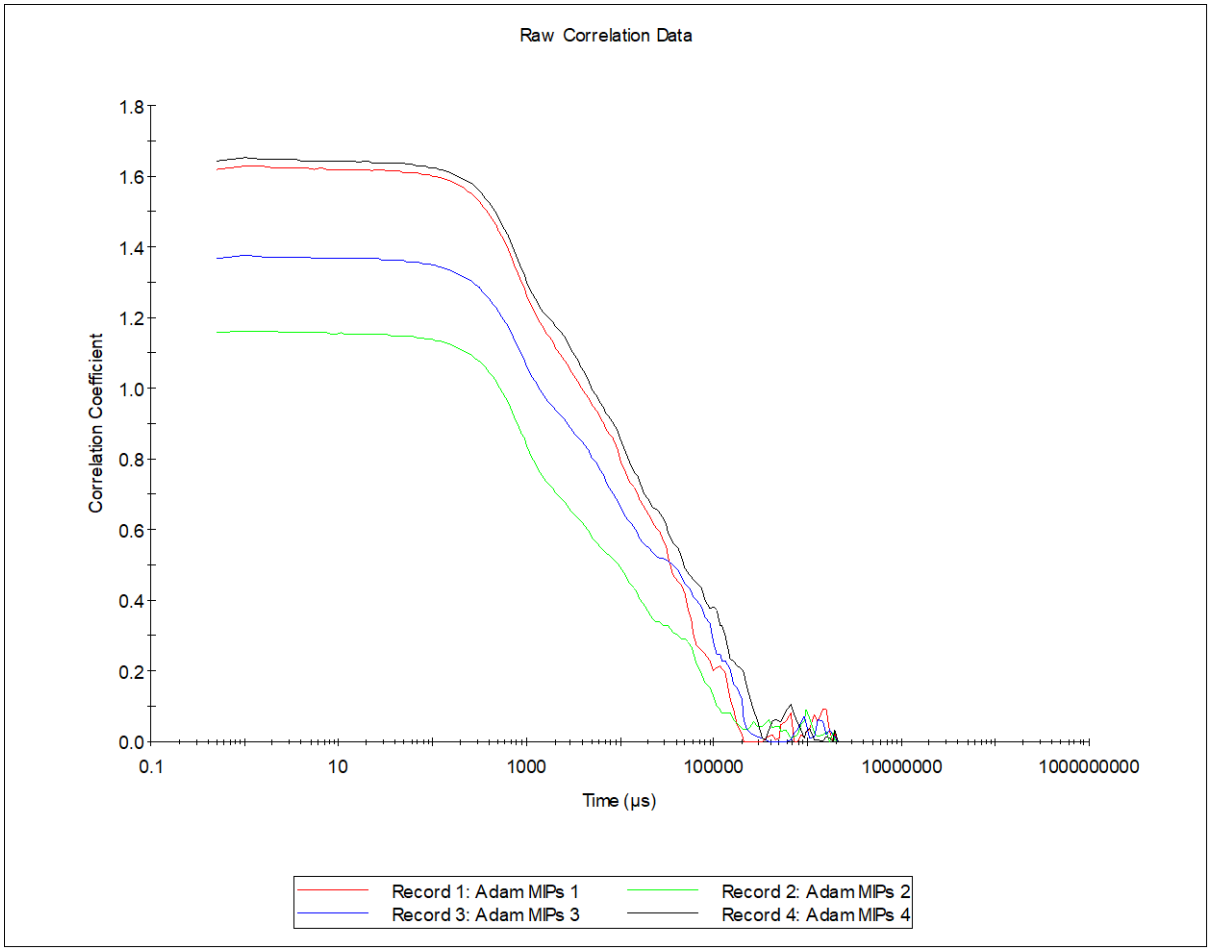

Appendix 1.14. - Sorbitol Screening – 50mg Sorbitol – Post-Lyophilisation

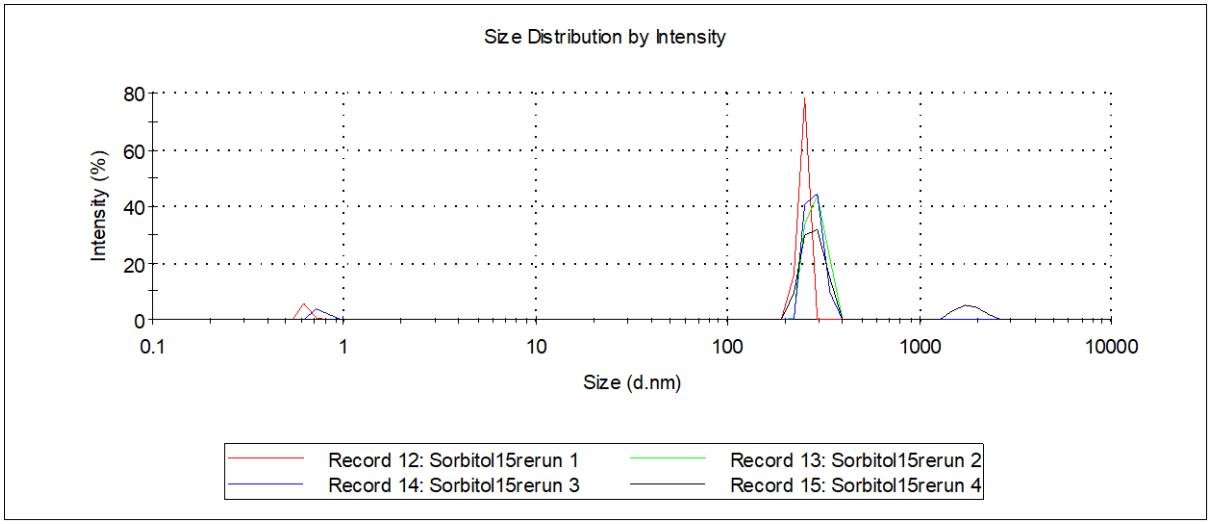

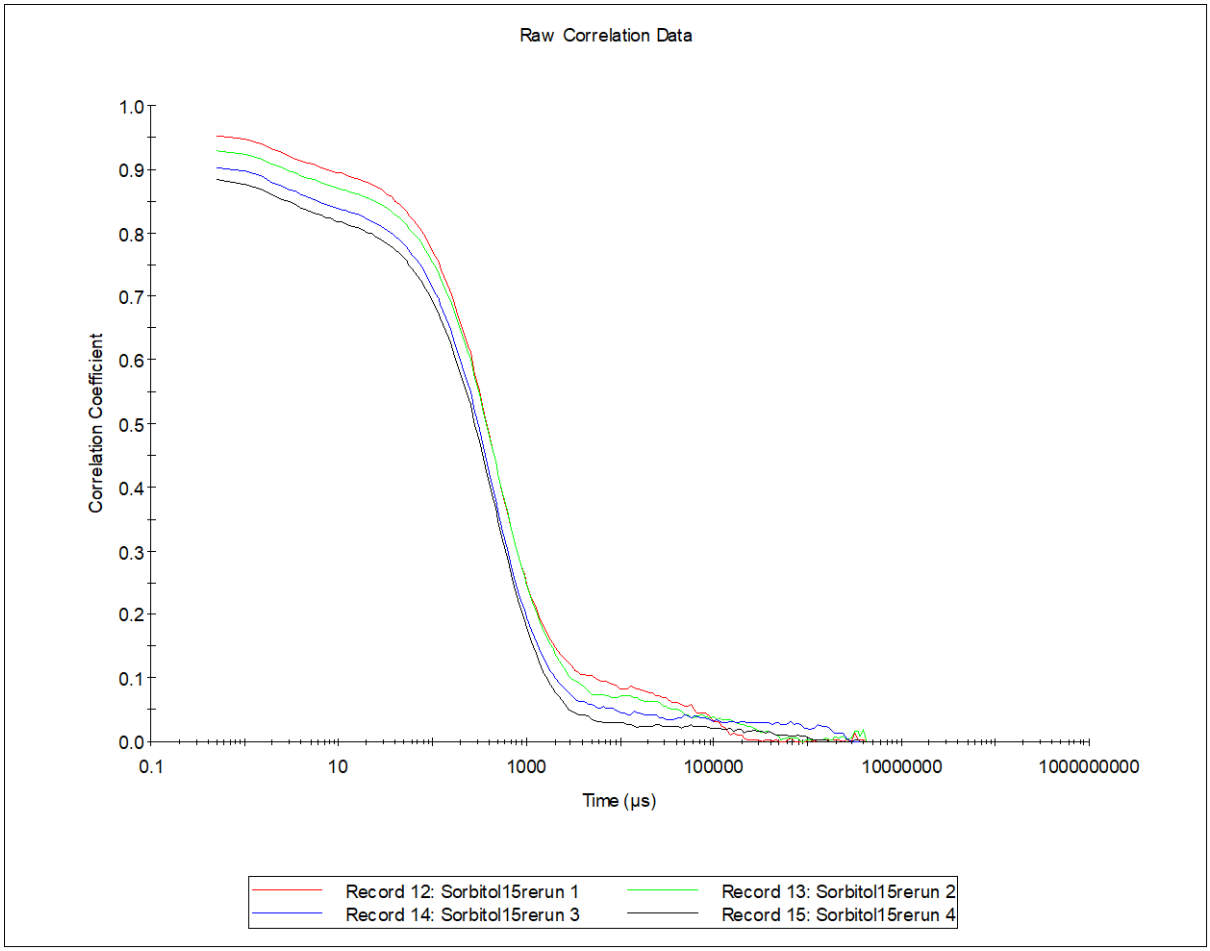

Appendix 1.15. - Trehalose Screening – 25mg Trehalose – Pre-Lyophilisation

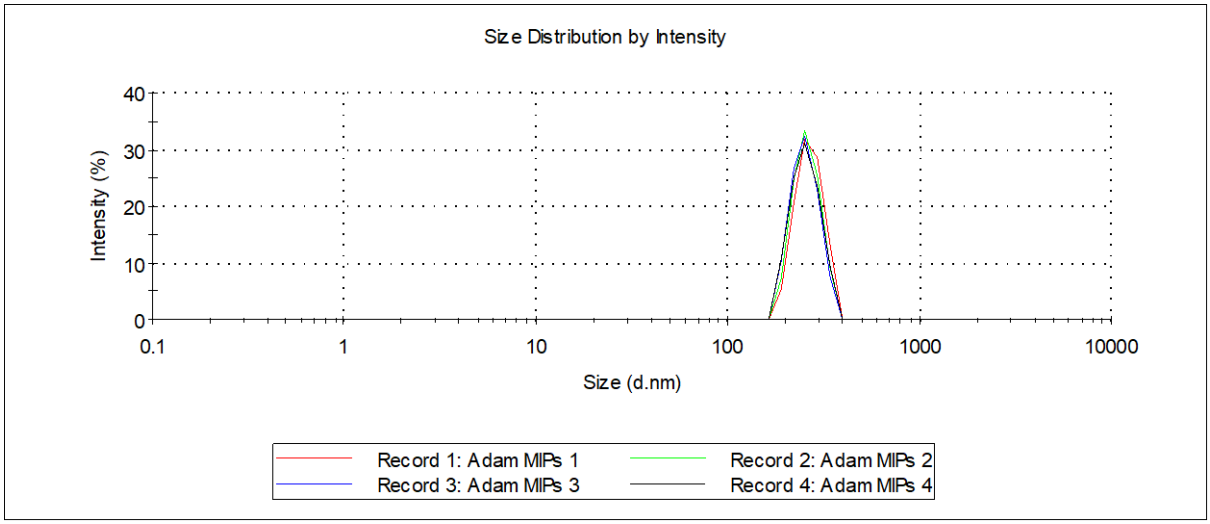

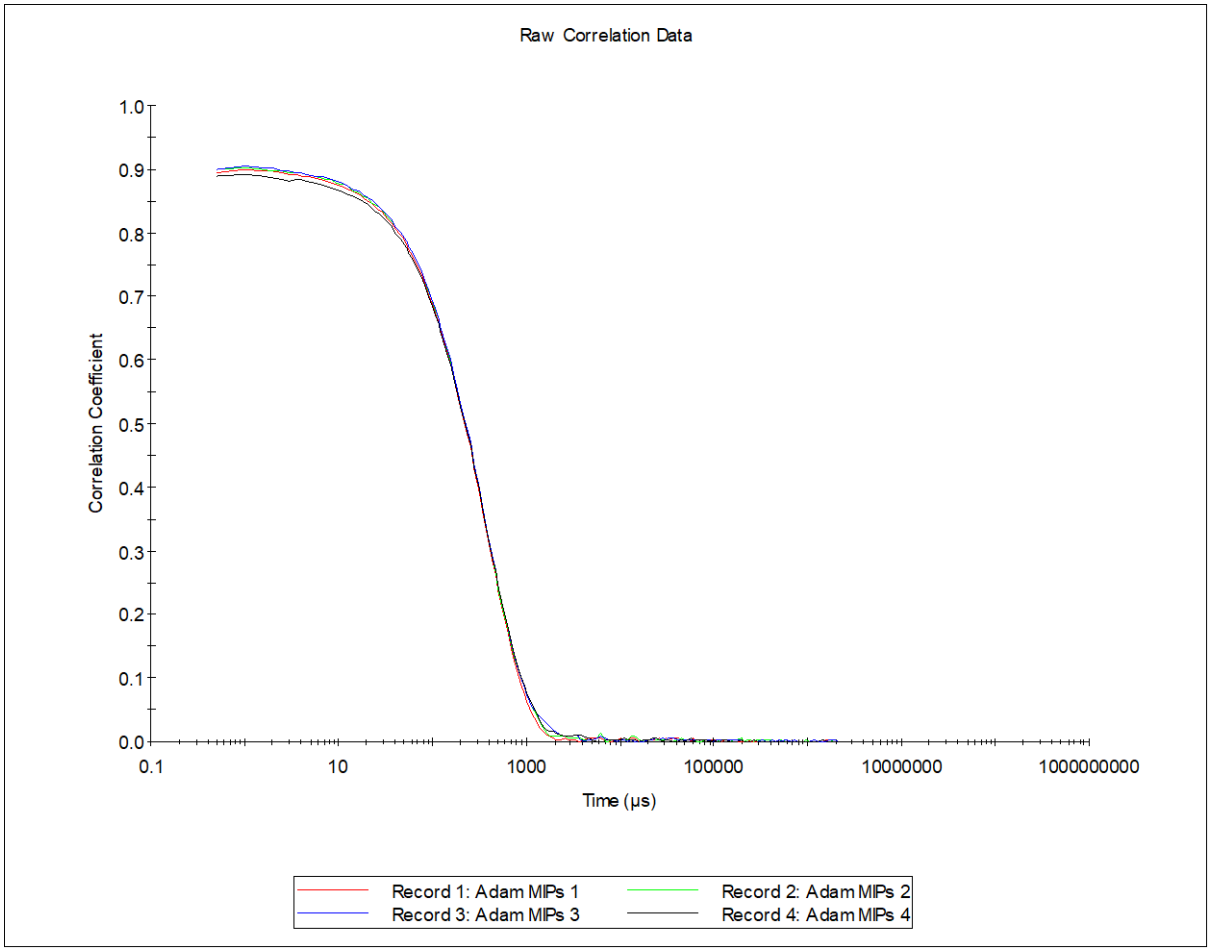

Appendix 1.16. - Trehalose Screening – 25mg Trehalose – Post-Lyophilisation

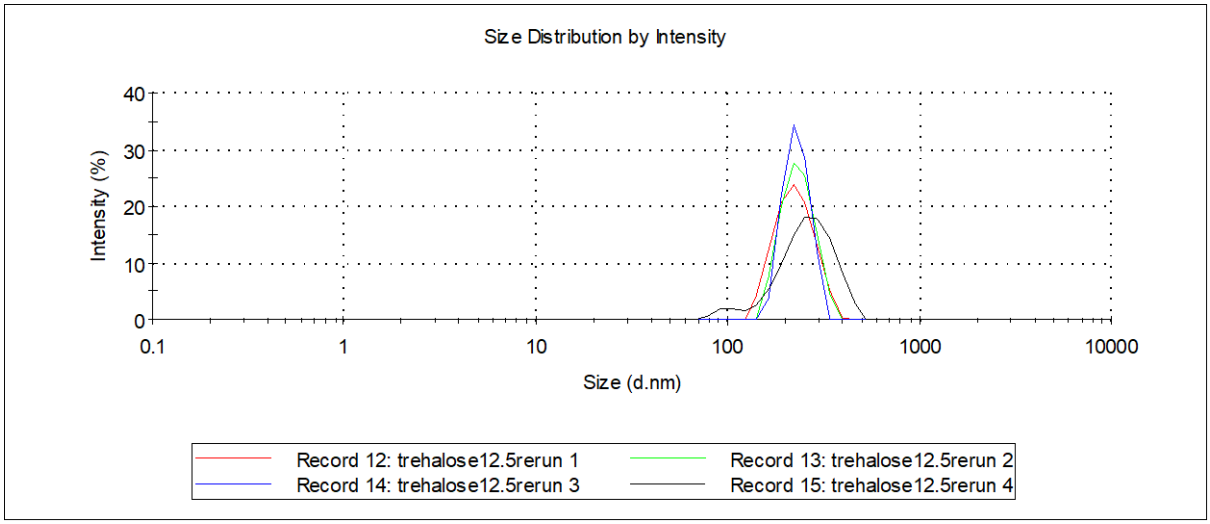

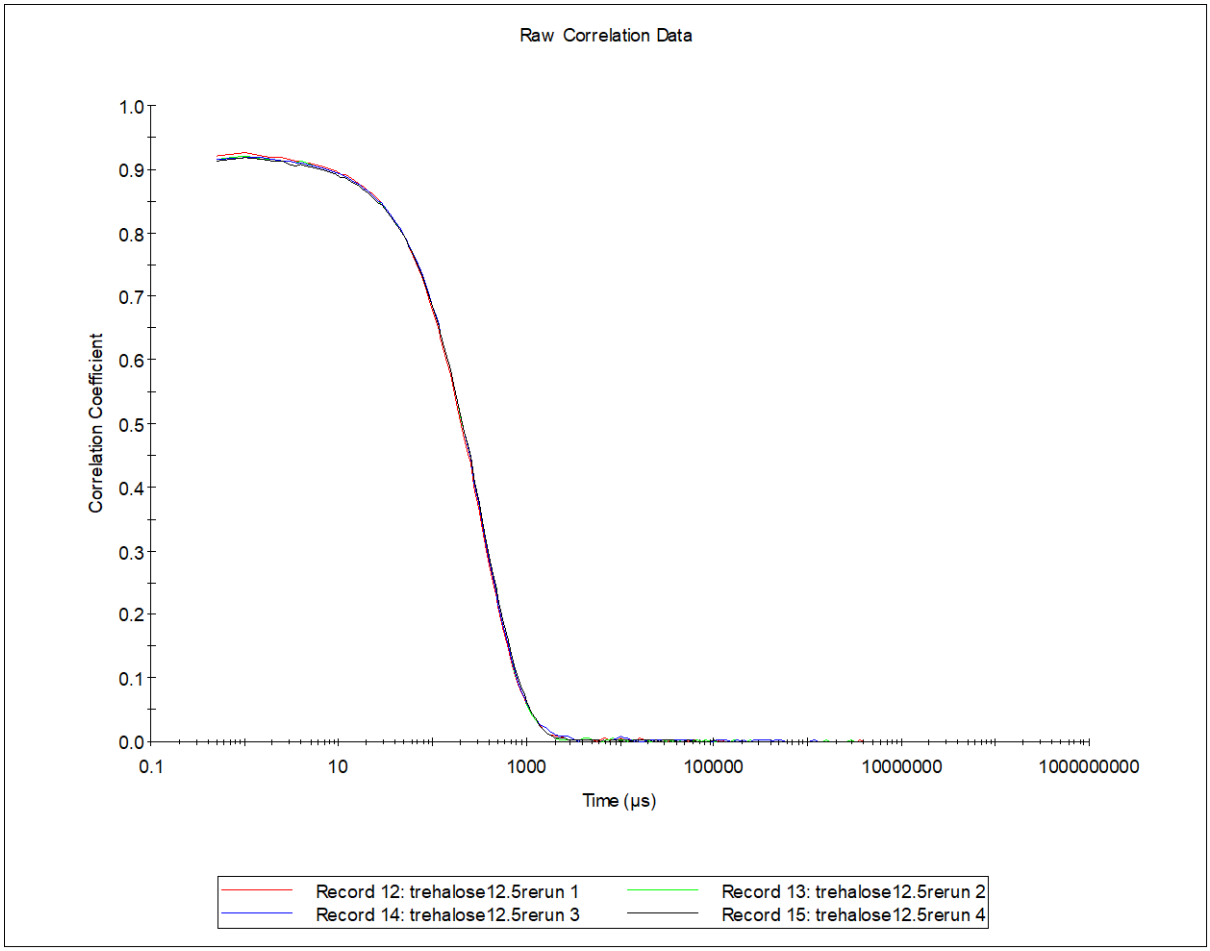

Appendix 1.17. - Trehalose Screening – 50mg Trehalose – Pre-Lyophilisation

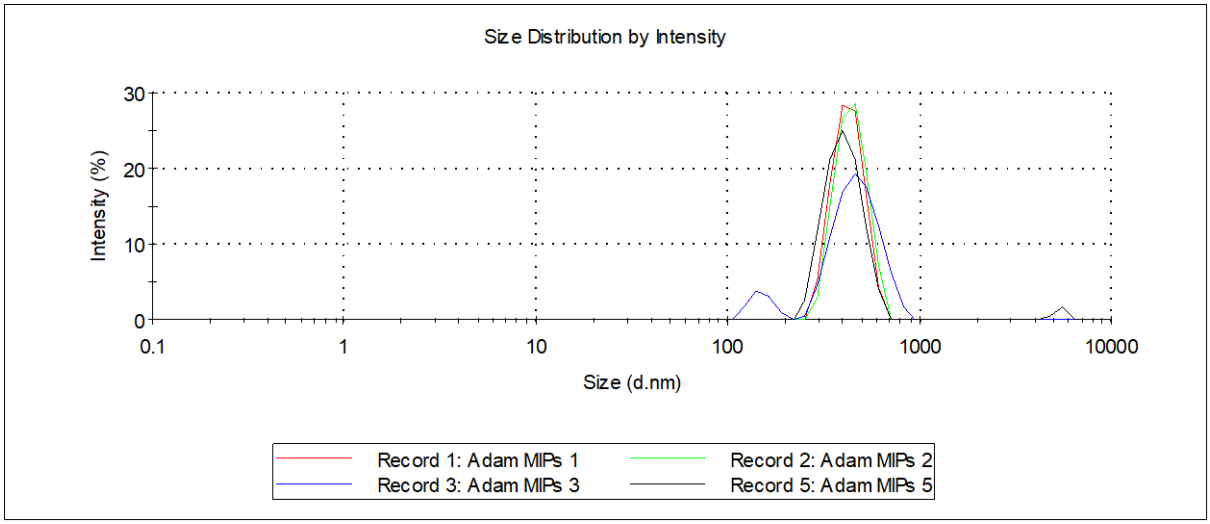

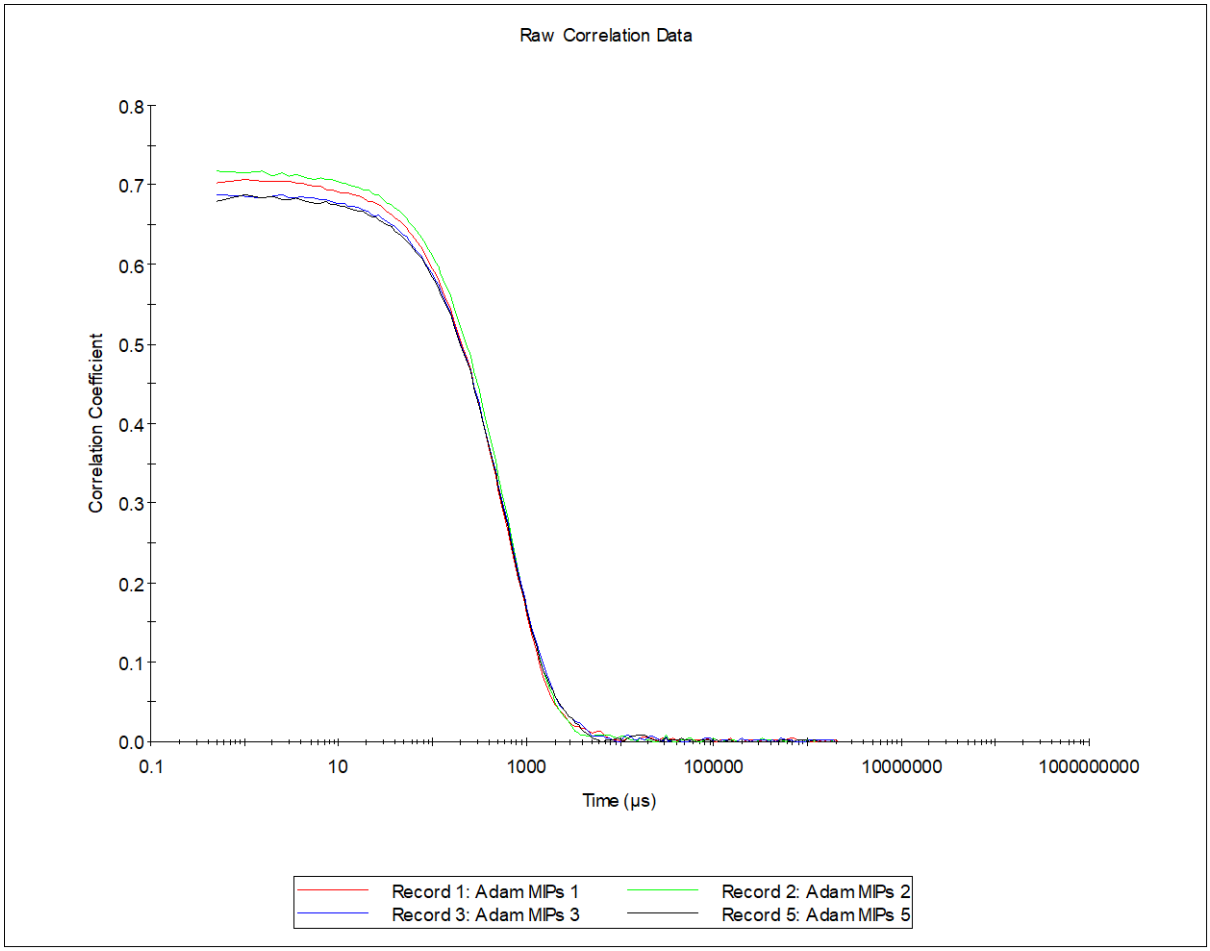

Appendix 1.18. - Trehalose Screening – 50mg Trehalose – Post-Lyophilisation

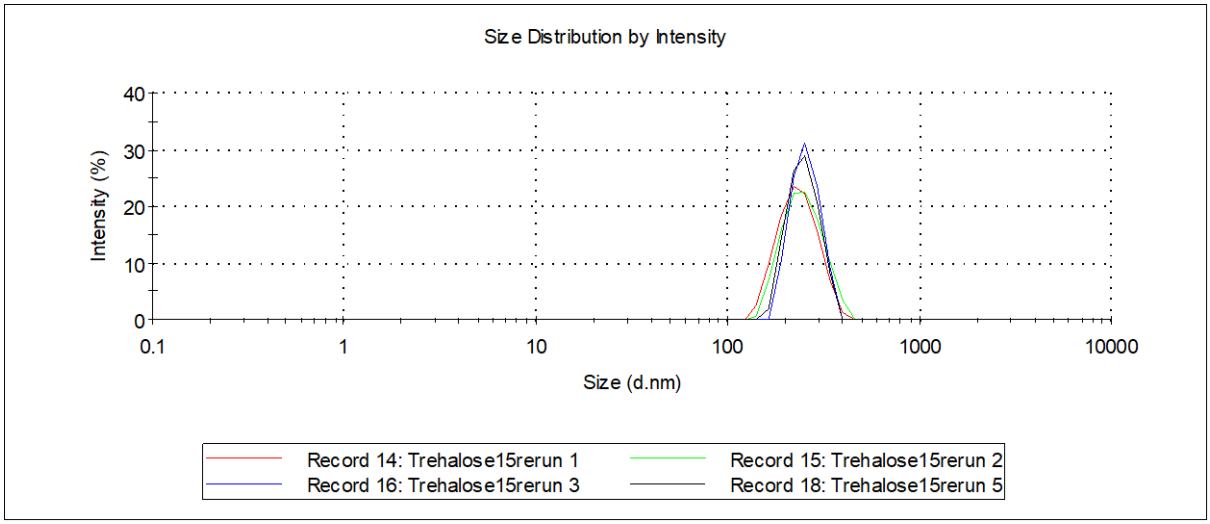

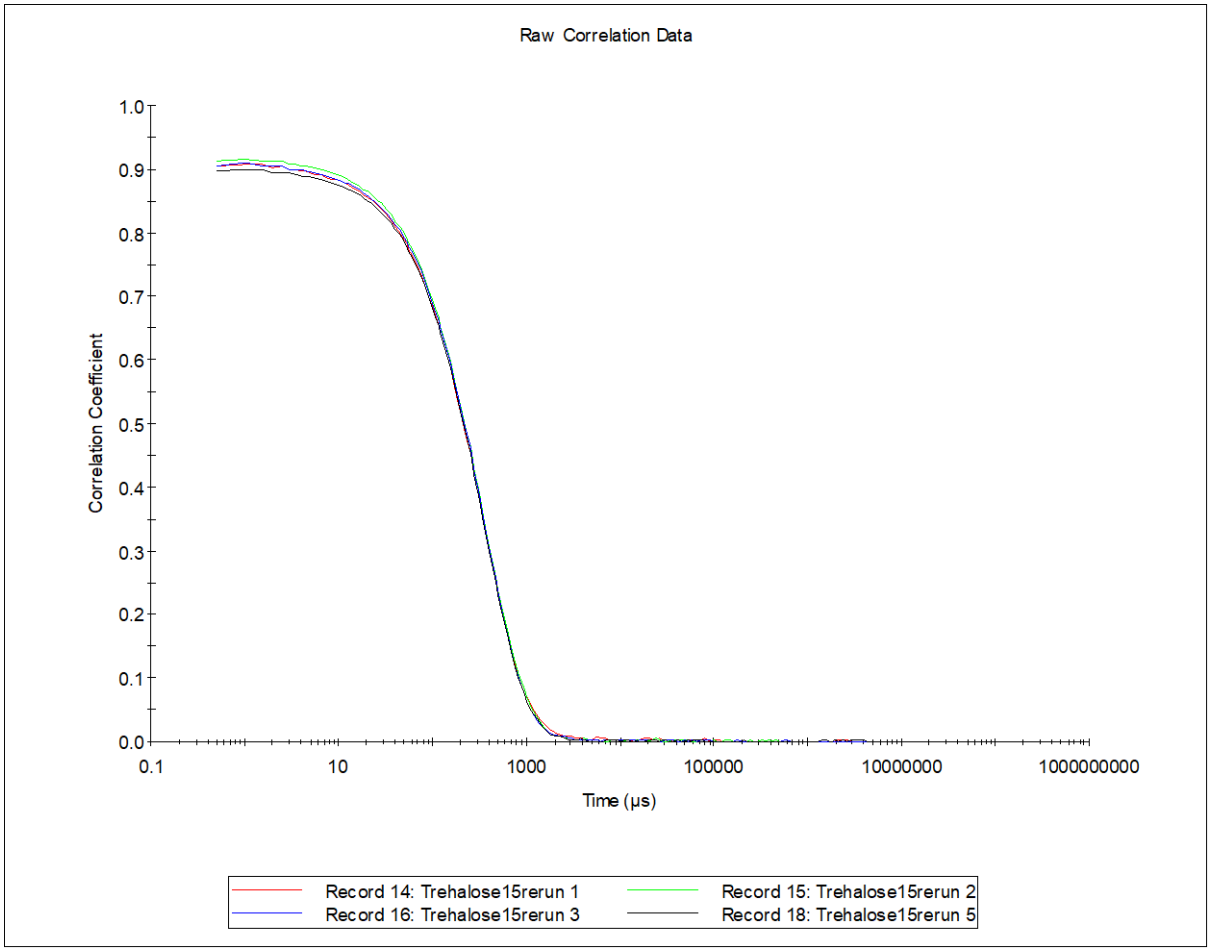

Appendix 2 - Dynamic Light Scattering Data – Trehalose Concentration Screening

Appendix 2.1. - Trehalose Optimisation – 0mg Trehalose – Control – Pre-Lyophilisation

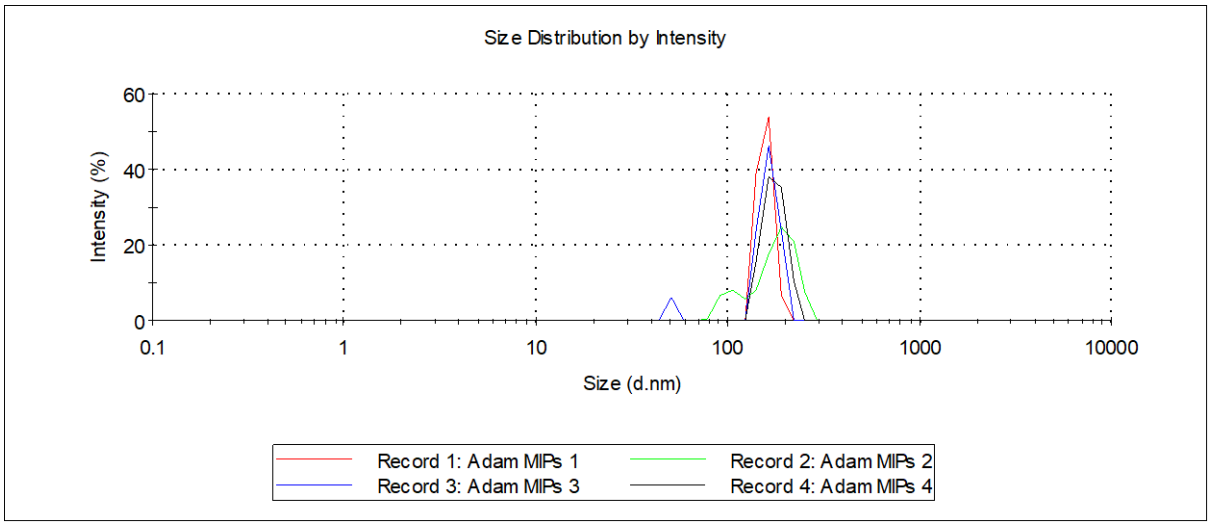

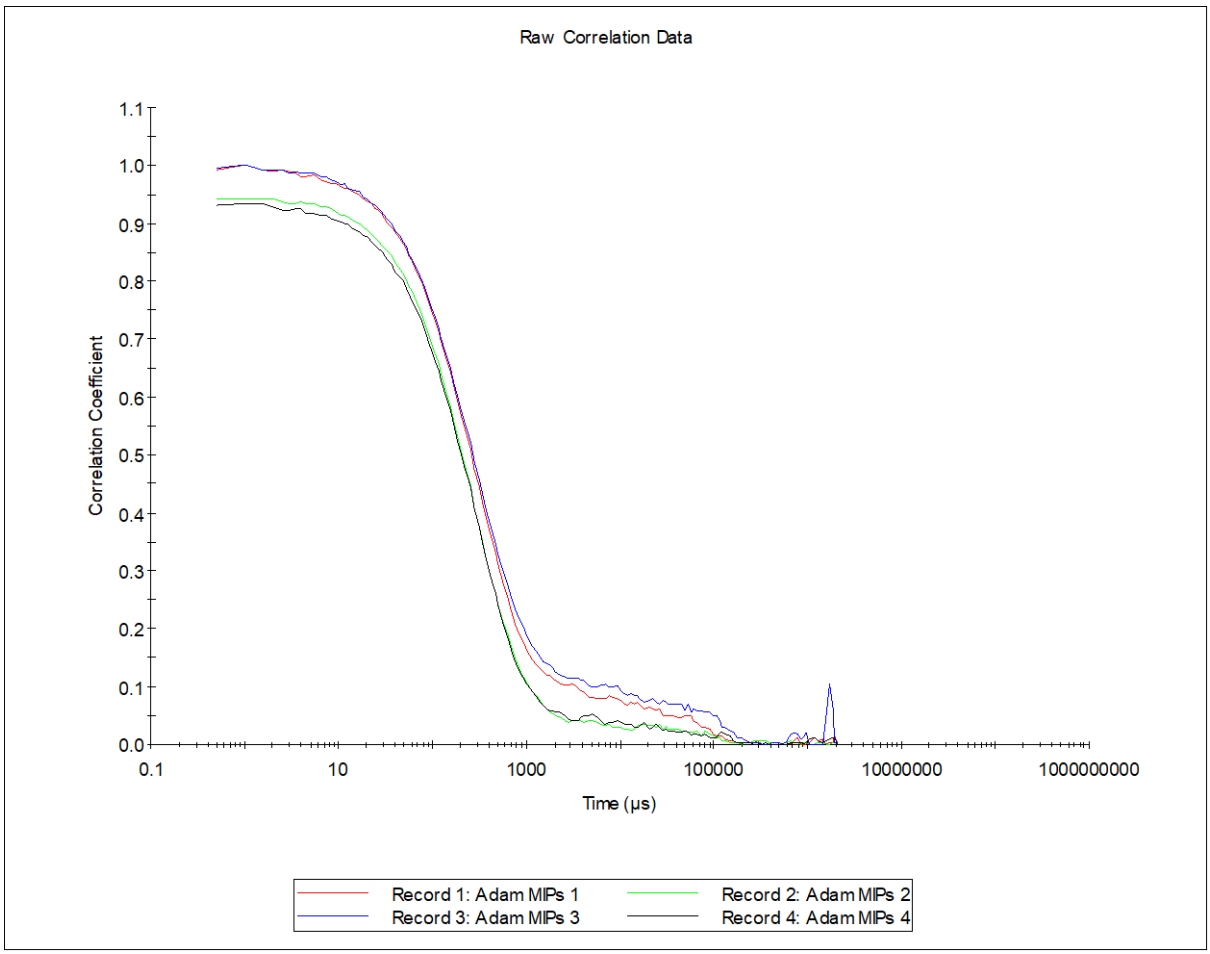

Appendix 2.2. - Trehalose Optimisation – 0mg Trehalose – Control – Post-Lyophilisation

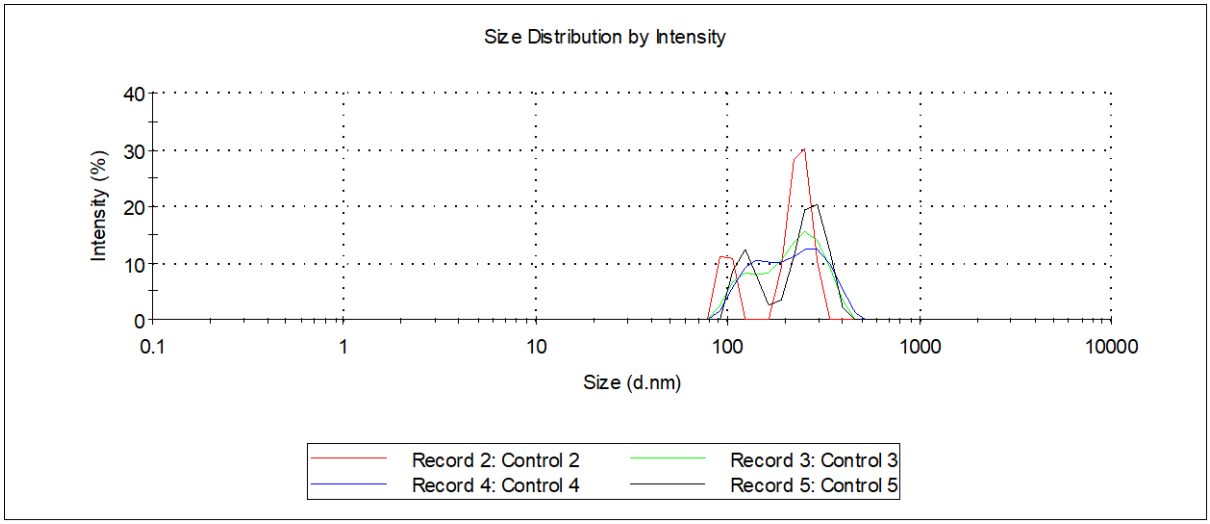

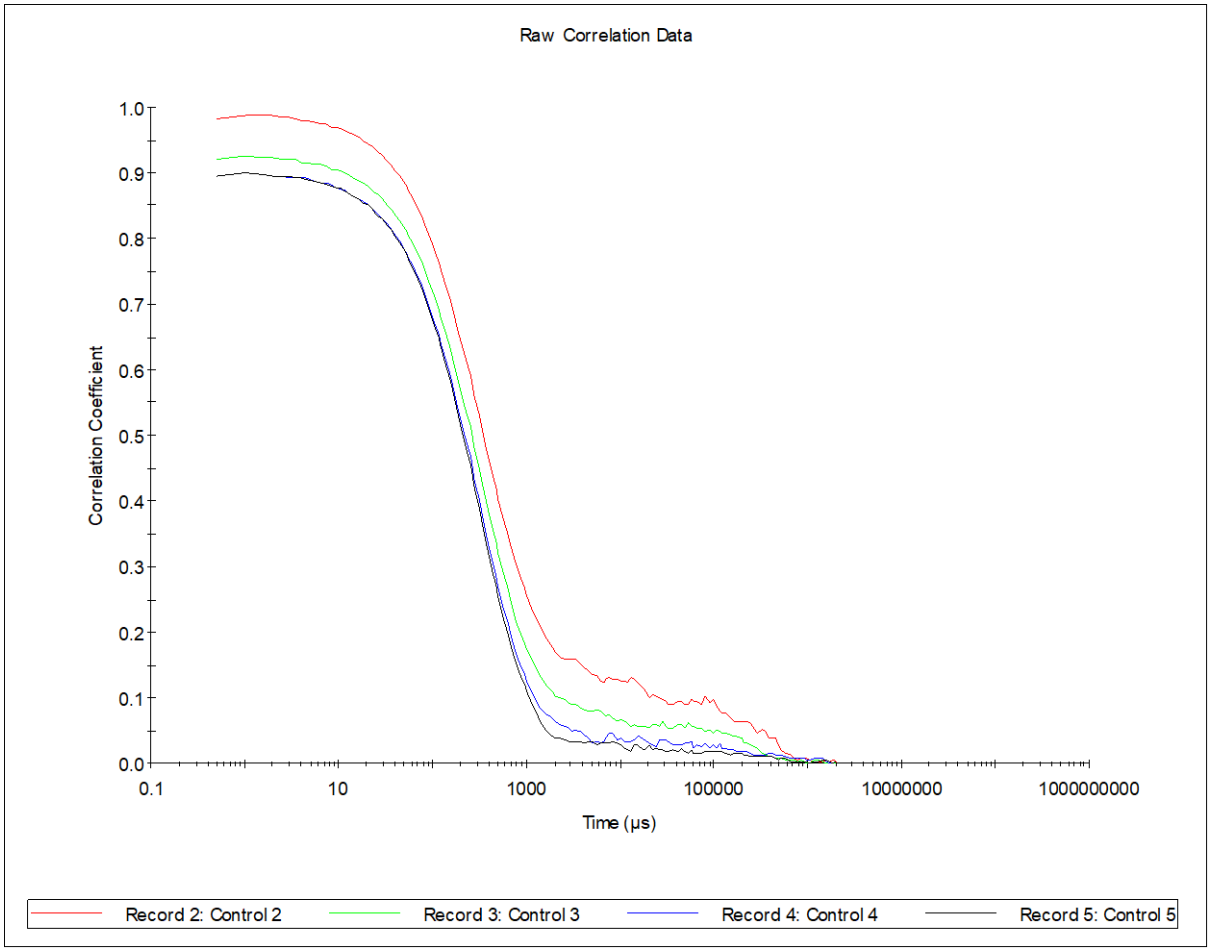

Appendix 2.3. - Trehalose Optimisation – 5mg Trehalose – Pre-Lyophilisation

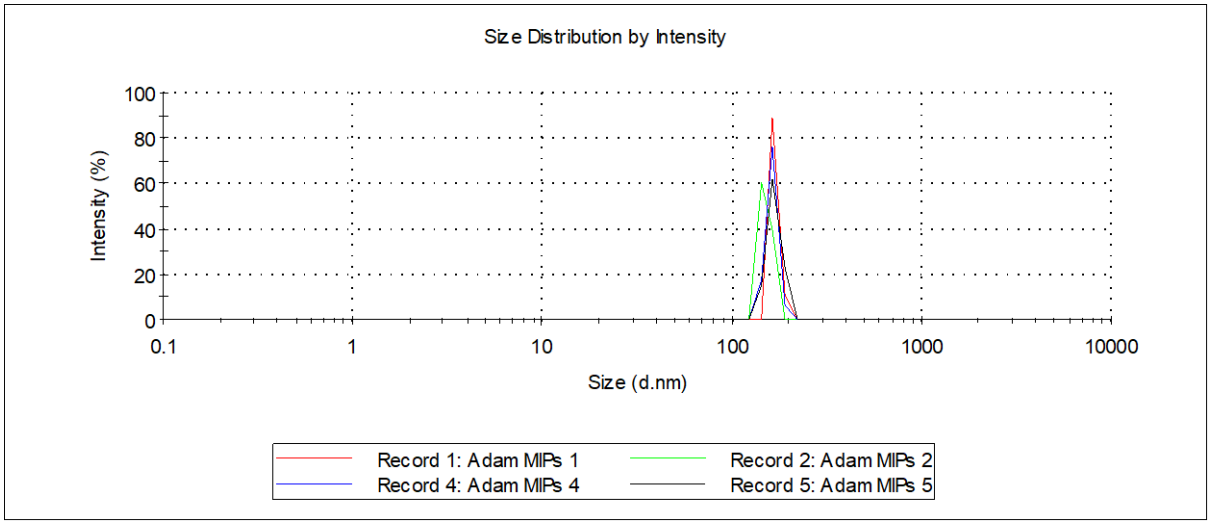

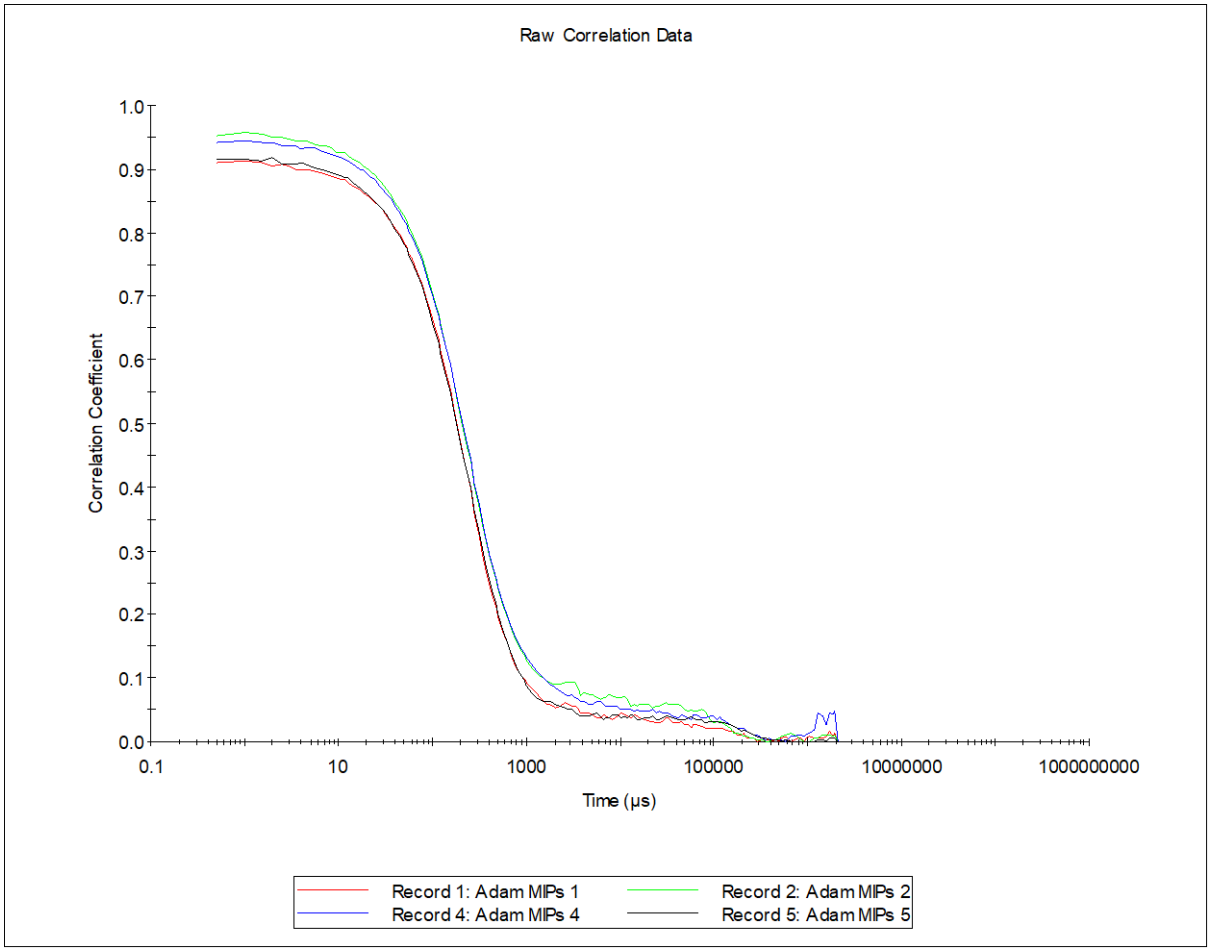

Appendix 2.4. Trehalose Optimisation – 5mg Trehalose – Post-Lyophilisation

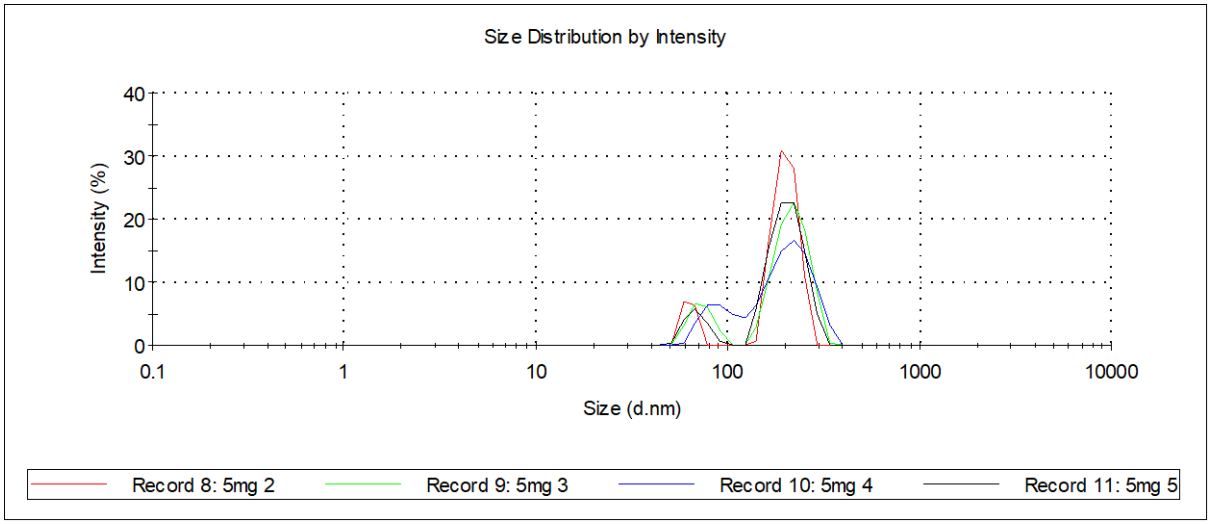

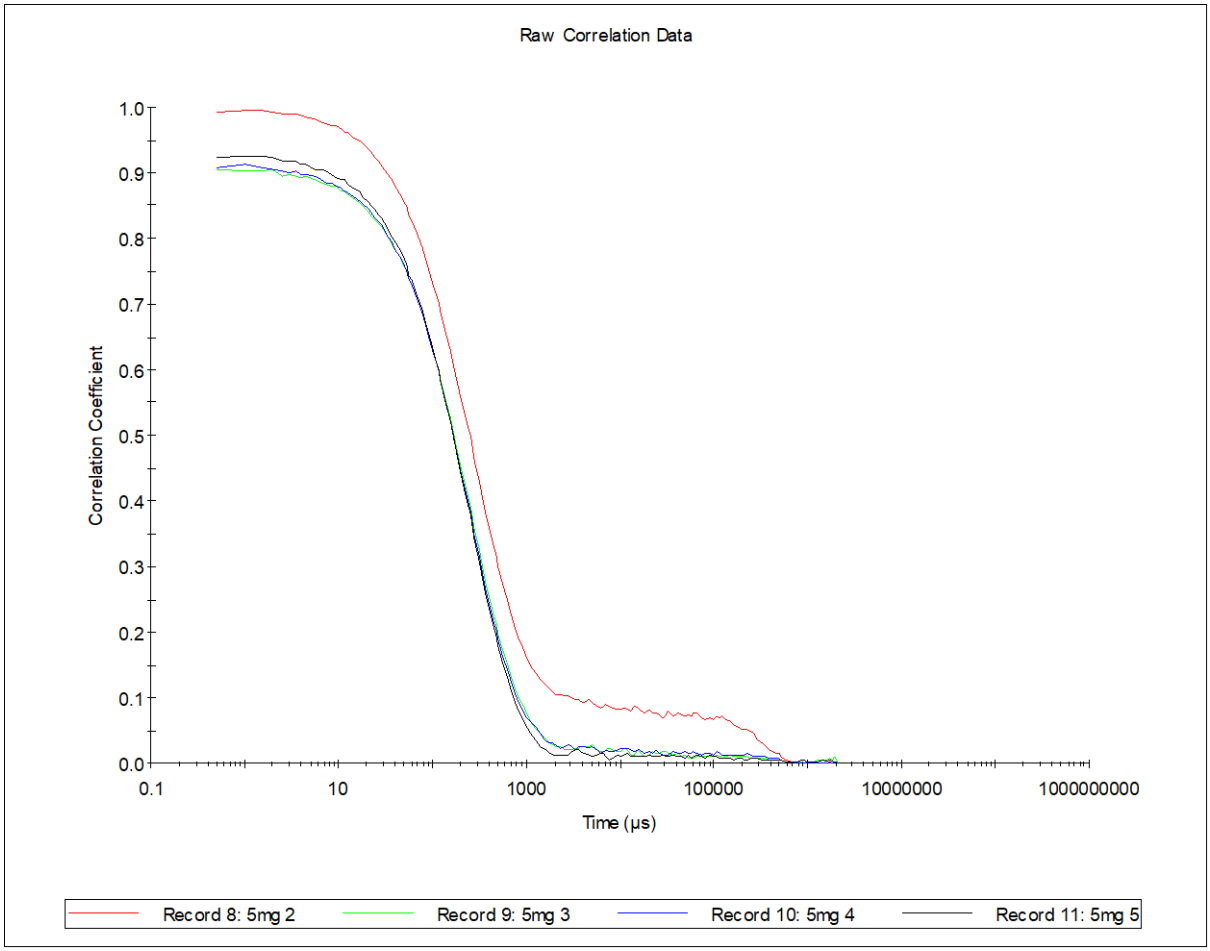

Appendix 2.5. Trehalose Optimisation – 10mg Trehalose – Pre-Lyophilisation

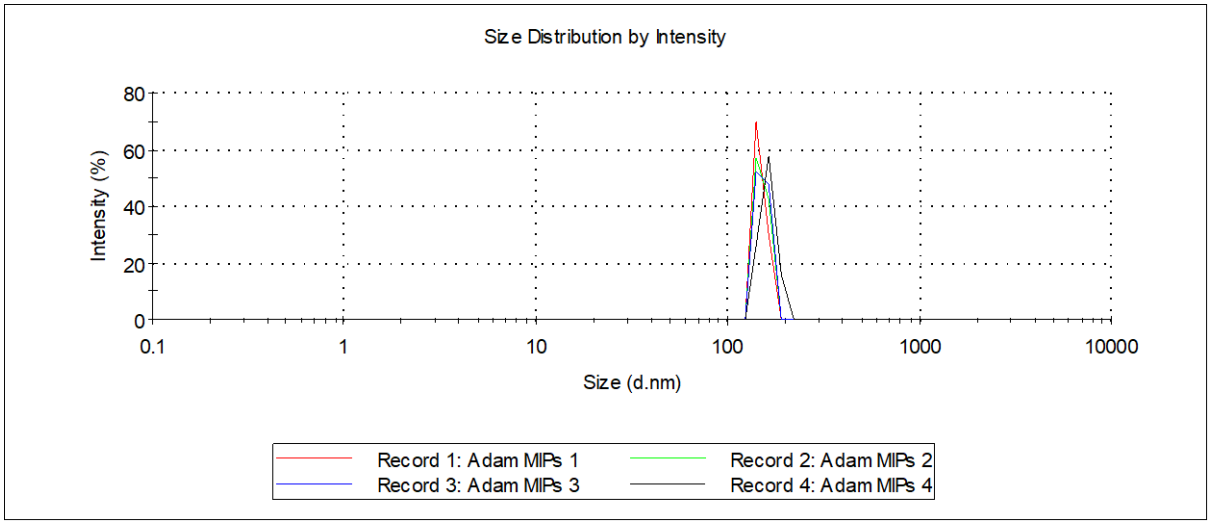

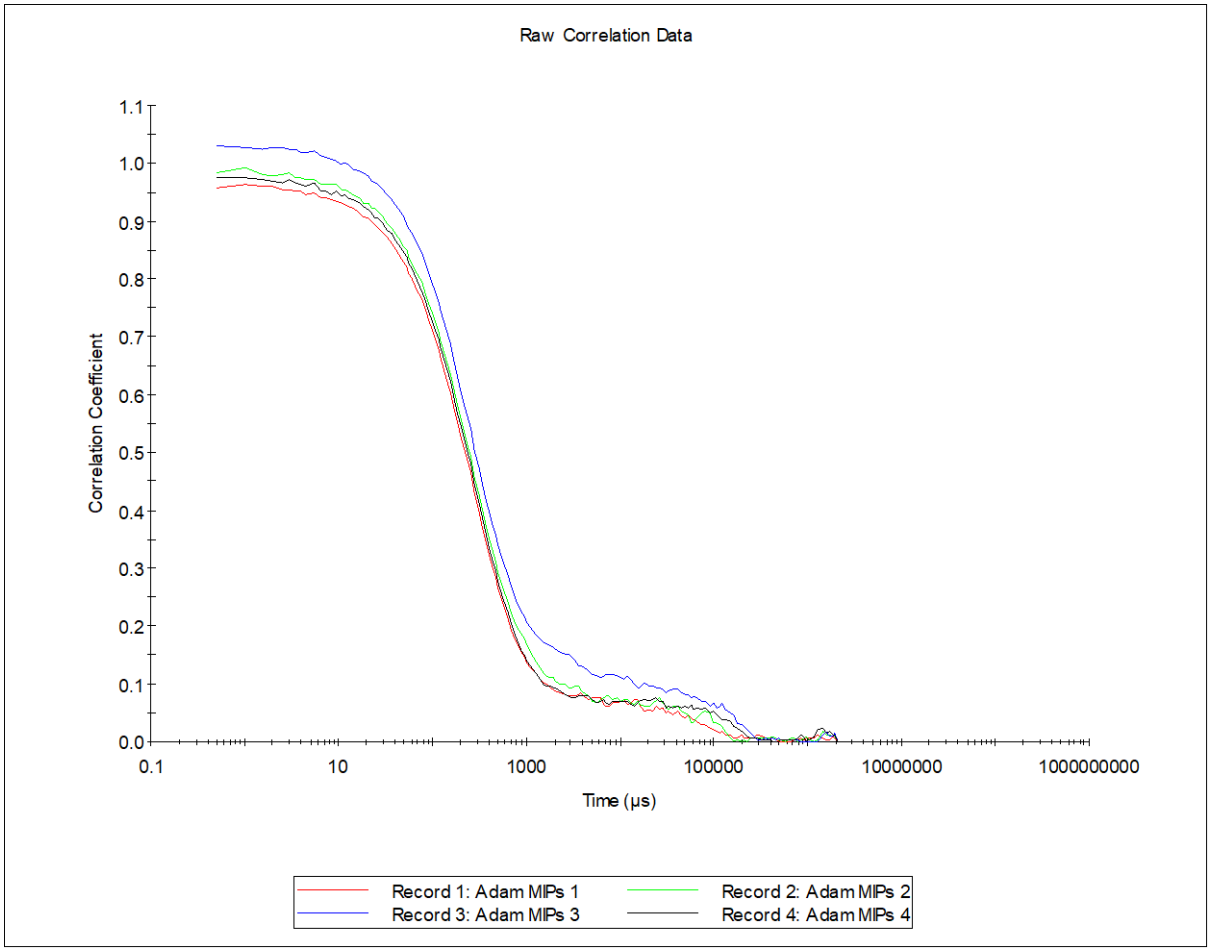

Appendix 2.6. Trehalose Optimisation – 10mg Trehalose – Post-Lyophilisation

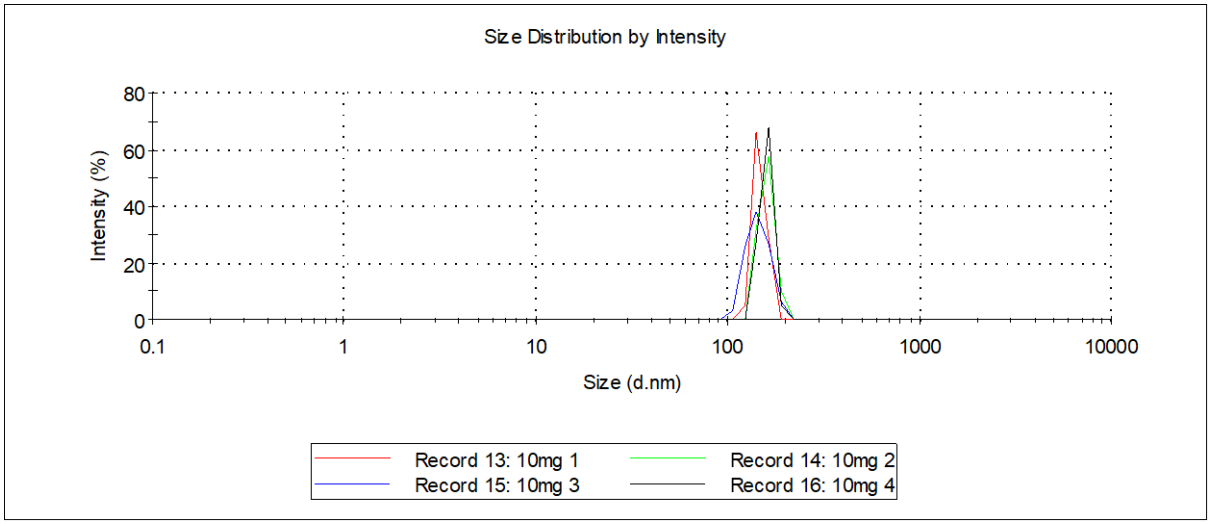

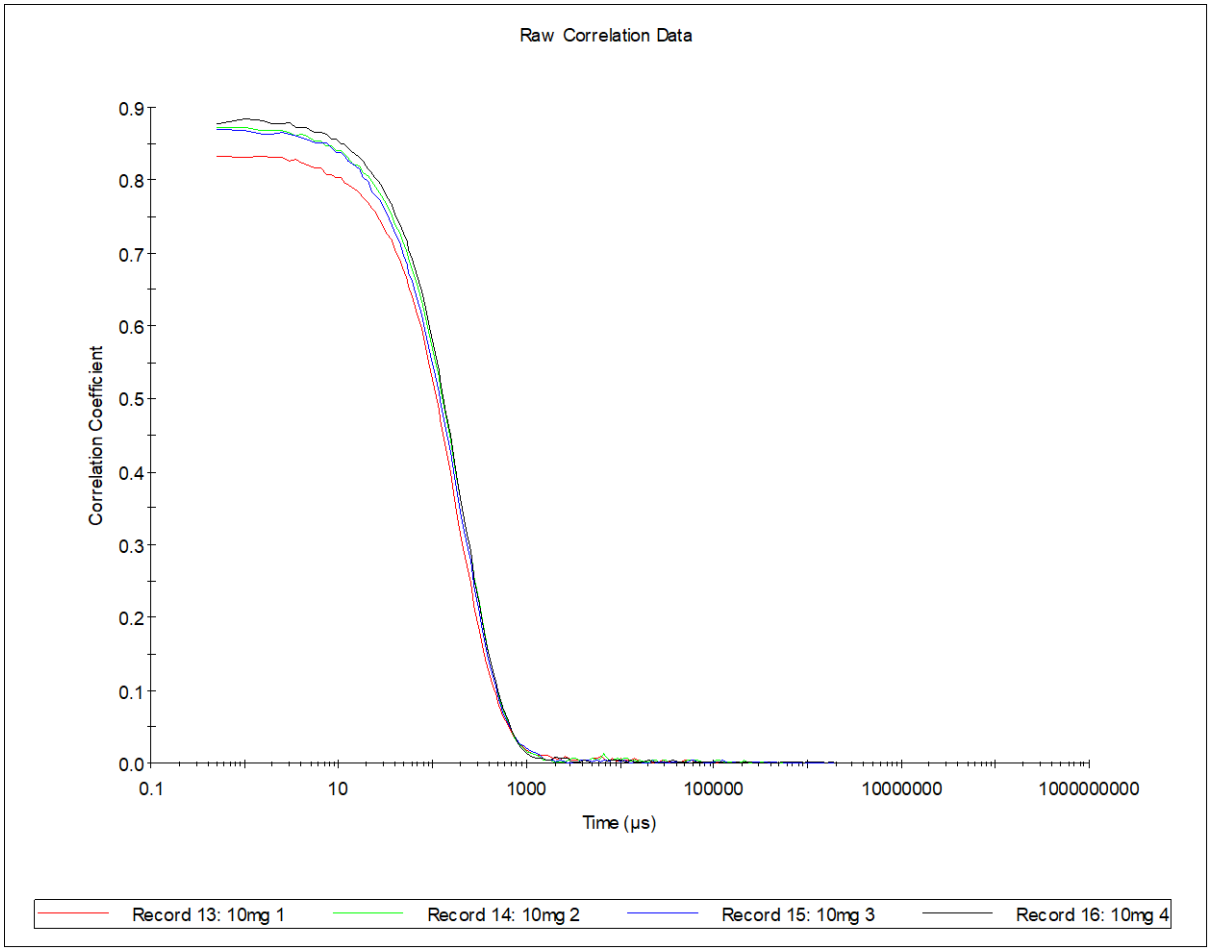

Appendix 2.7. Trehalose Optimisation – 15mg Trehalose – Pre-Lyophilisation

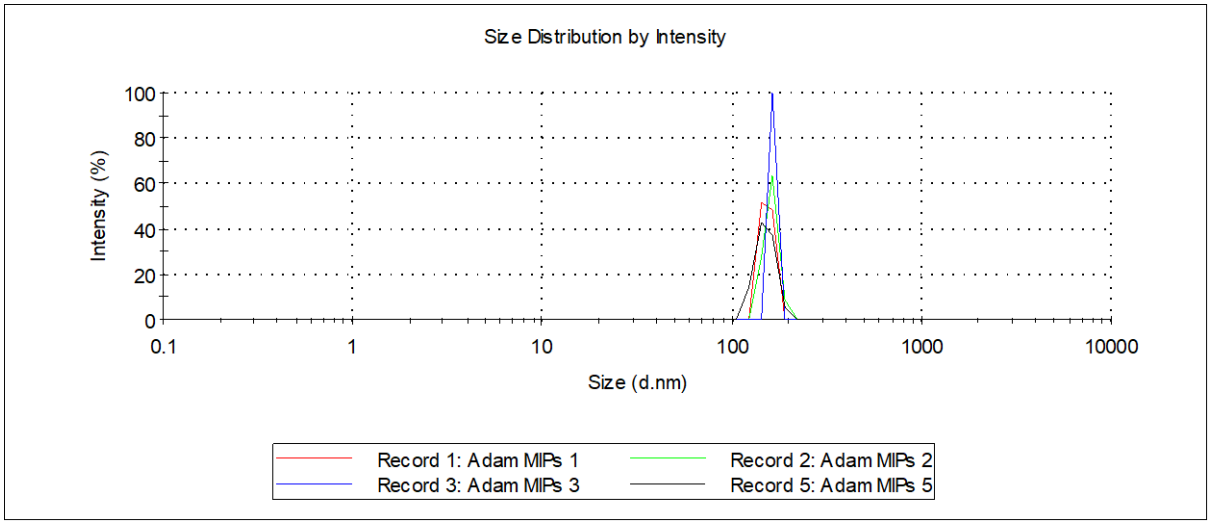

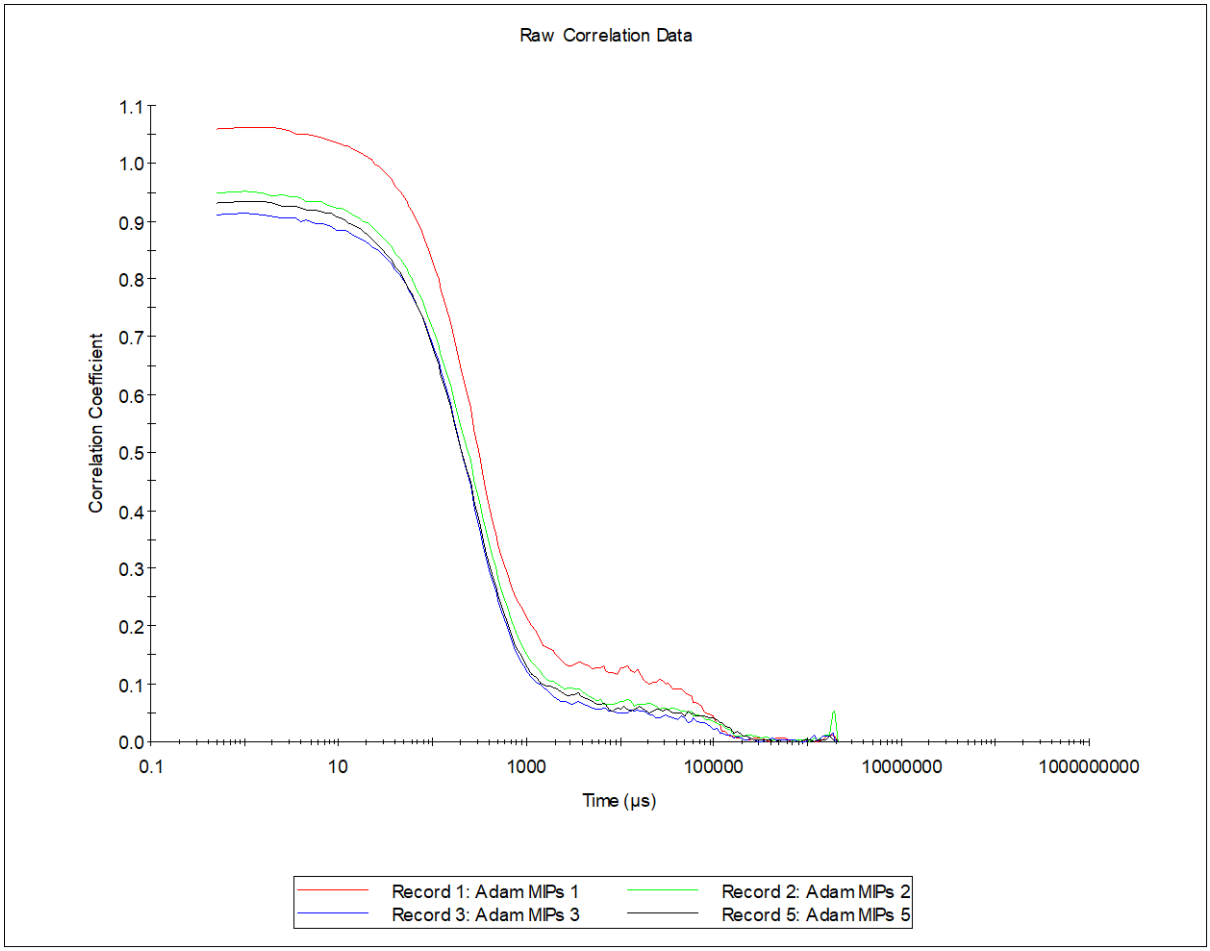

Appendix 2.8. Trehalose Optimisation – 15mg Trehalose – Post-Lyophilisation

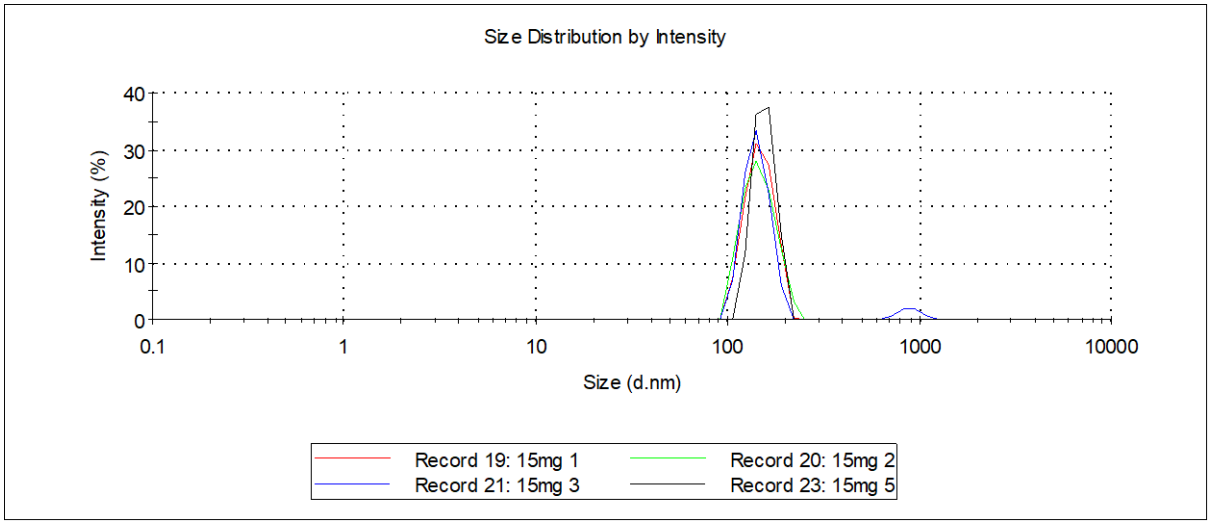

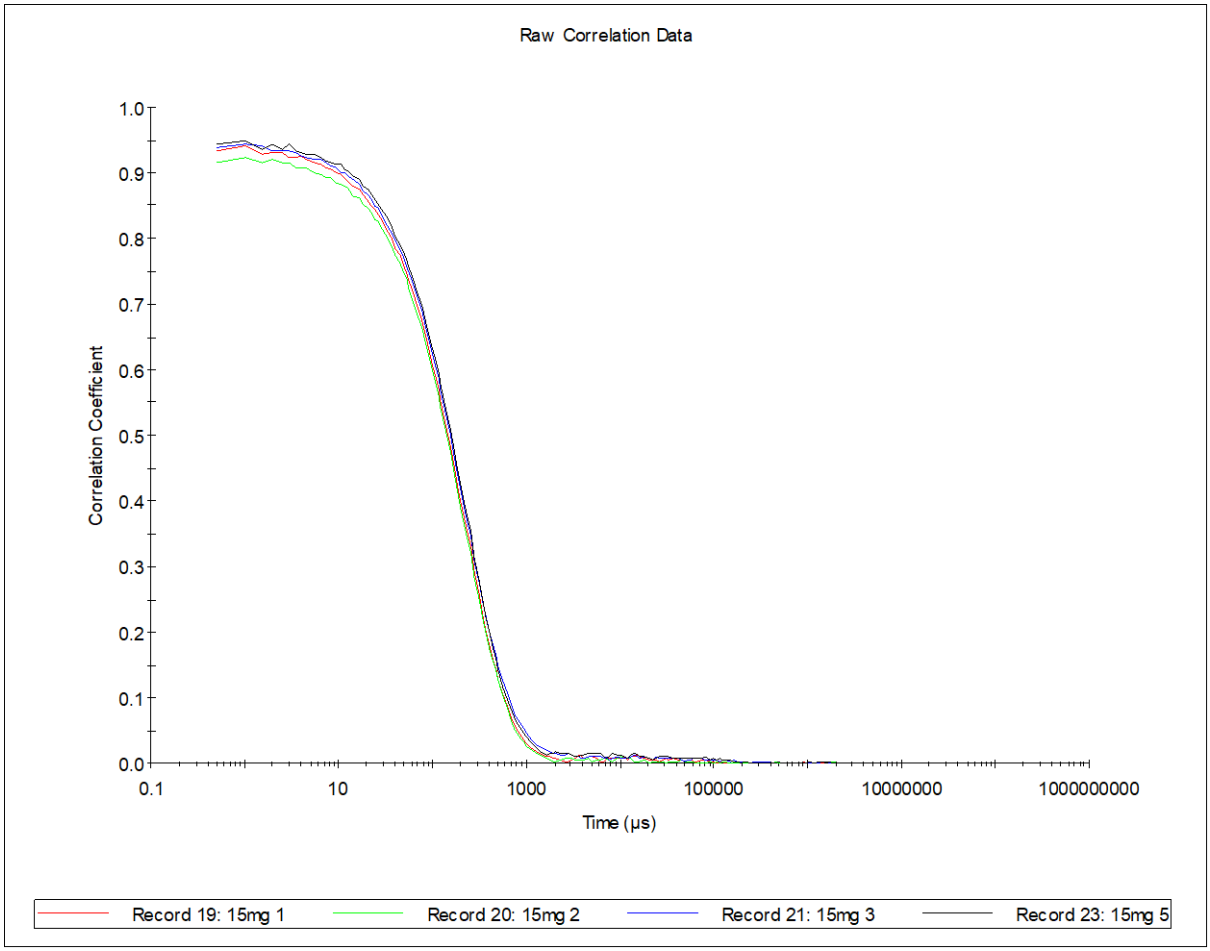

Appendix 2.9. Trehalose Optimisation – 20mg Trehalose – Pre-Lyophilisation

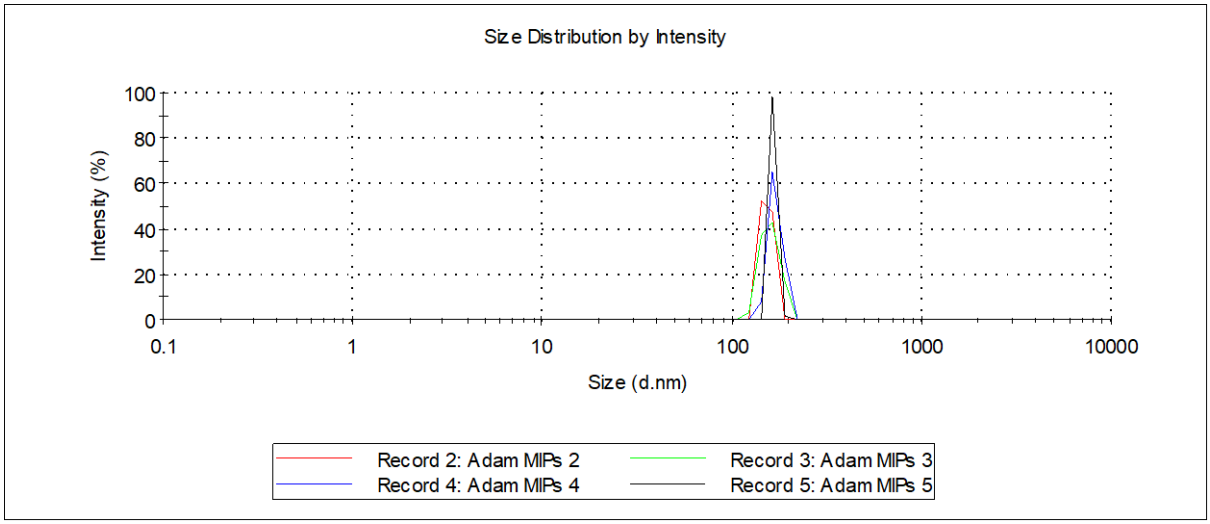

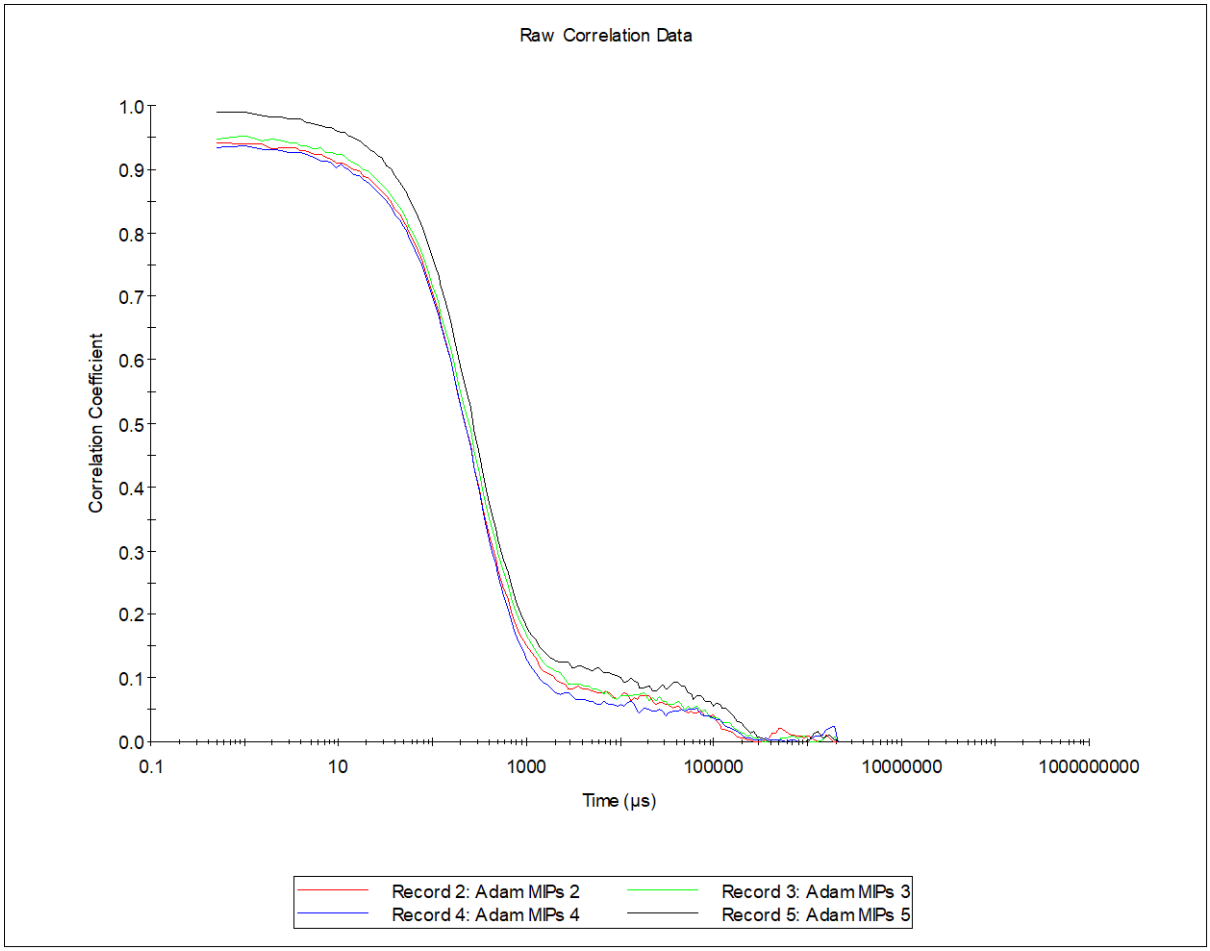

Appendix 2.10. Trehalose Optimisation – 20mg Trehalose – Post-Lyophilisation

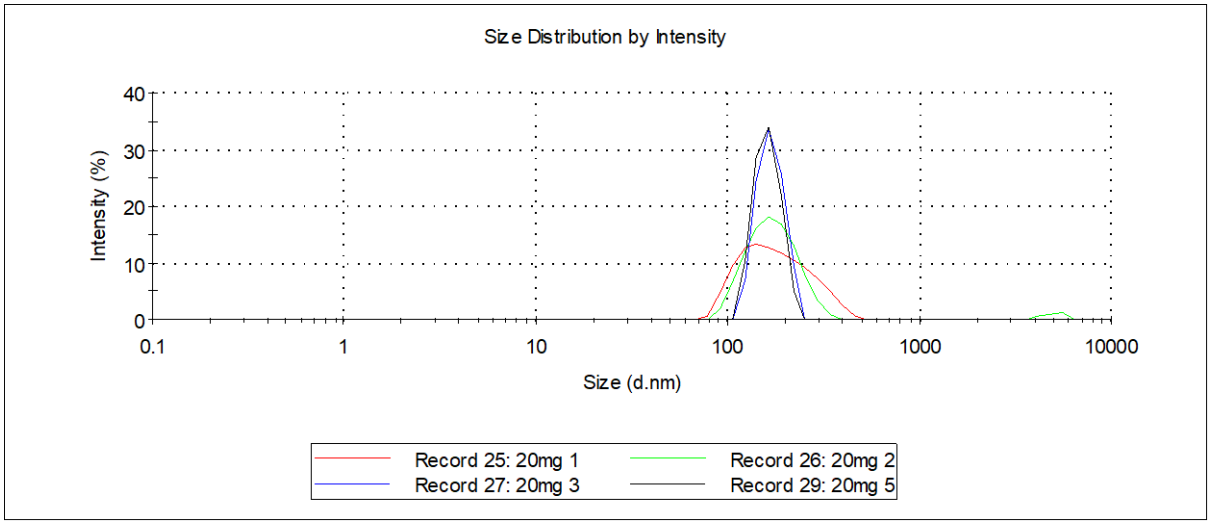

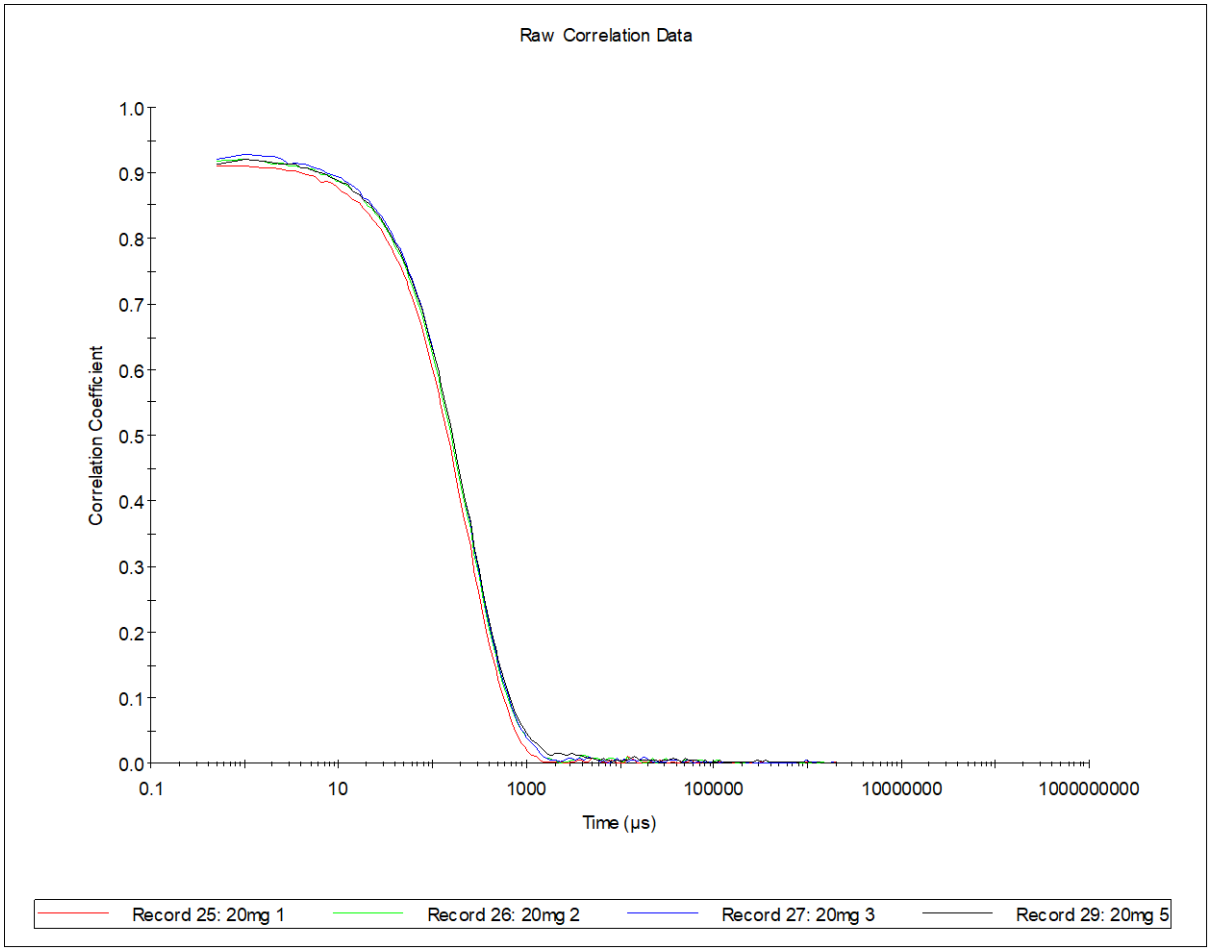

Appendix 2.11. Trehalose Optimisation – 25mg Trehalose – Pre-Lyophilisation

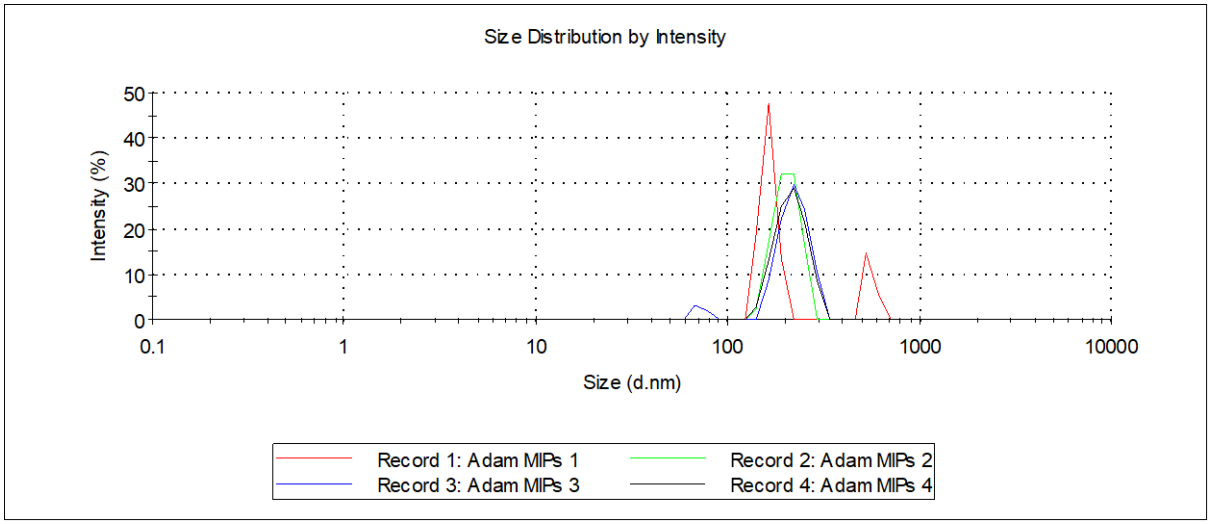

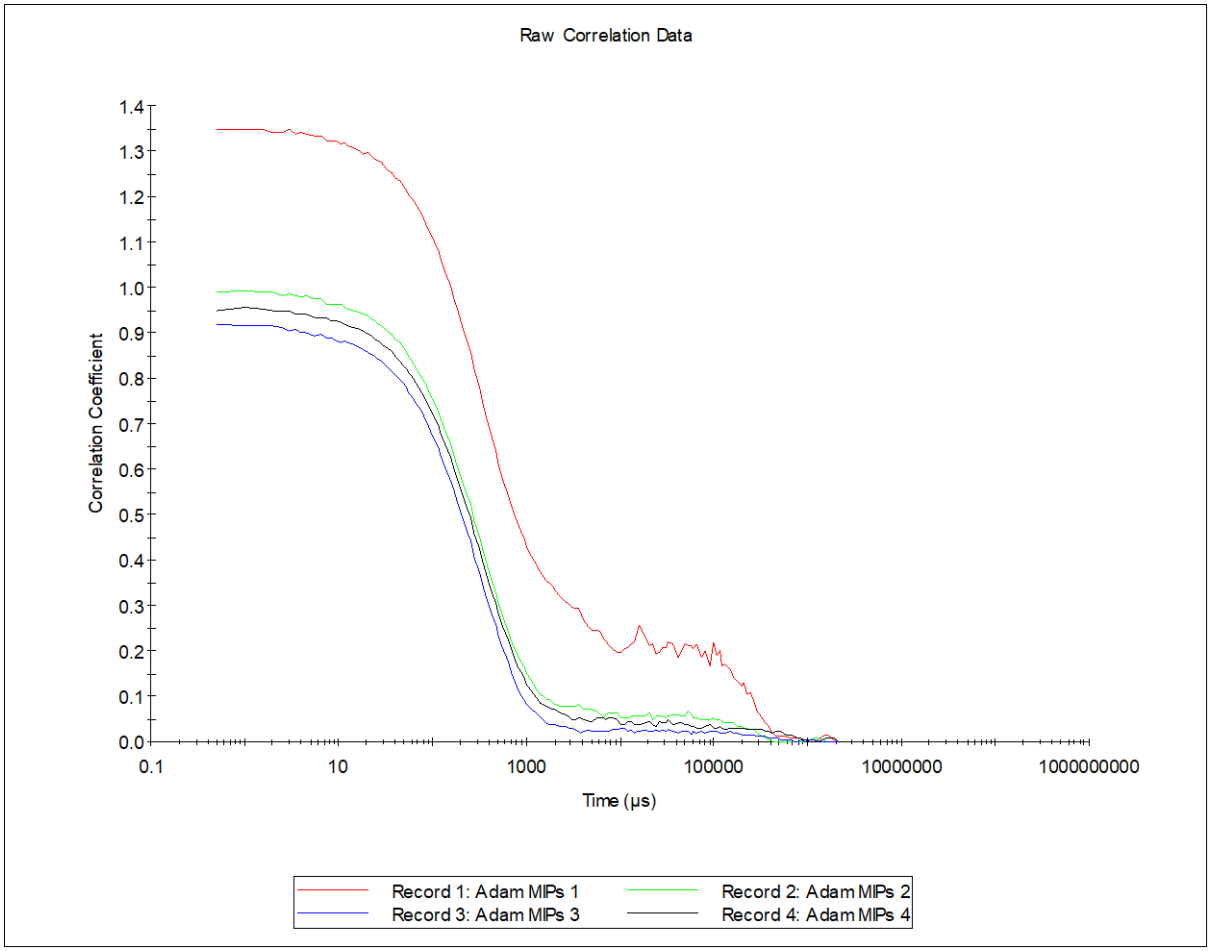

Appendix 2.12. Trehalose Optimisation – 25mg Trehalose – Post-Lyophilisation

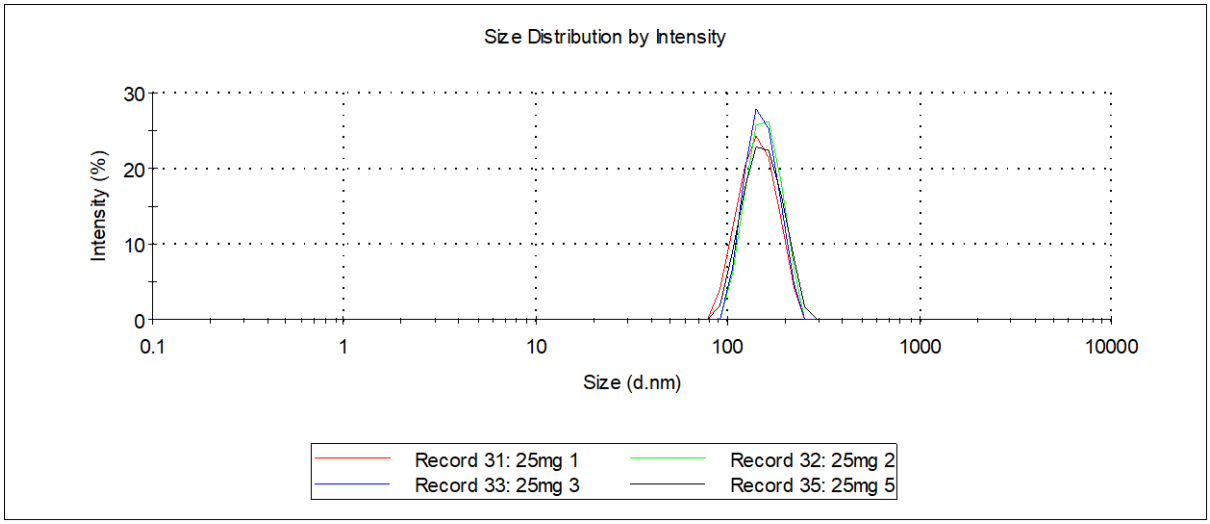

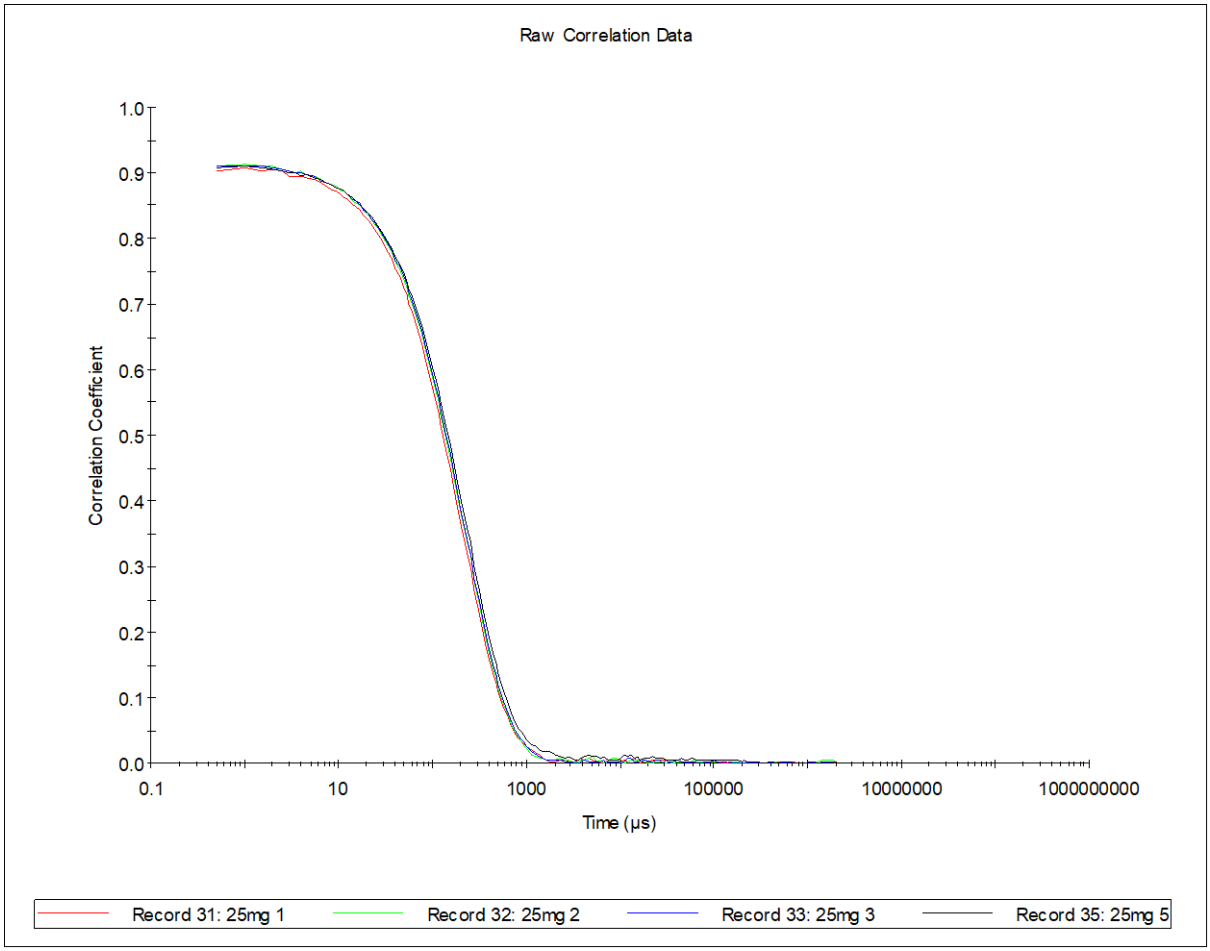

Appendix 2.13. Trehalose Optimisation – 50mg Trehalose – Pre-Lyophilisation

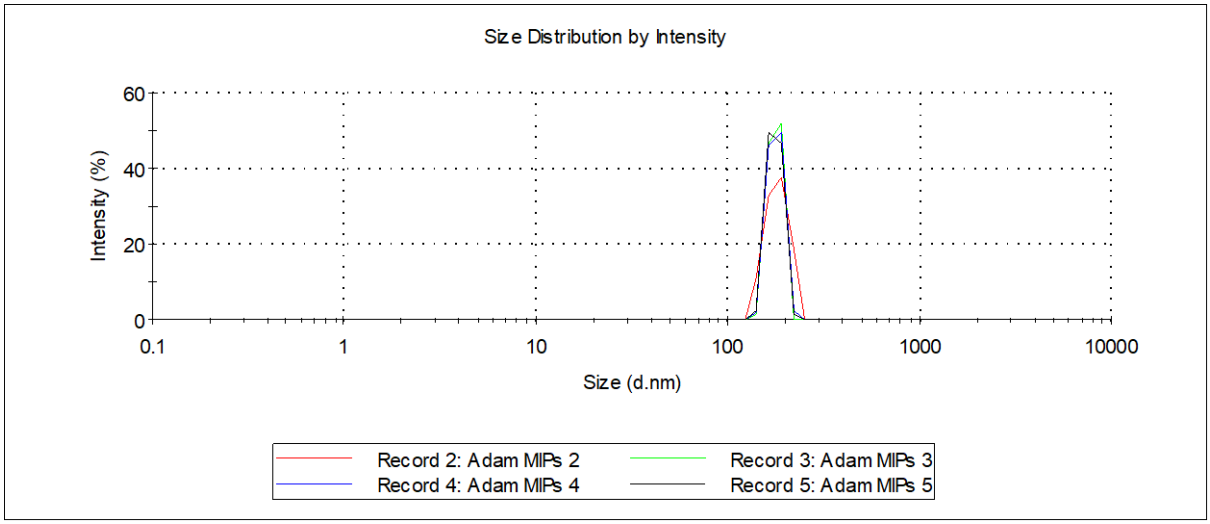

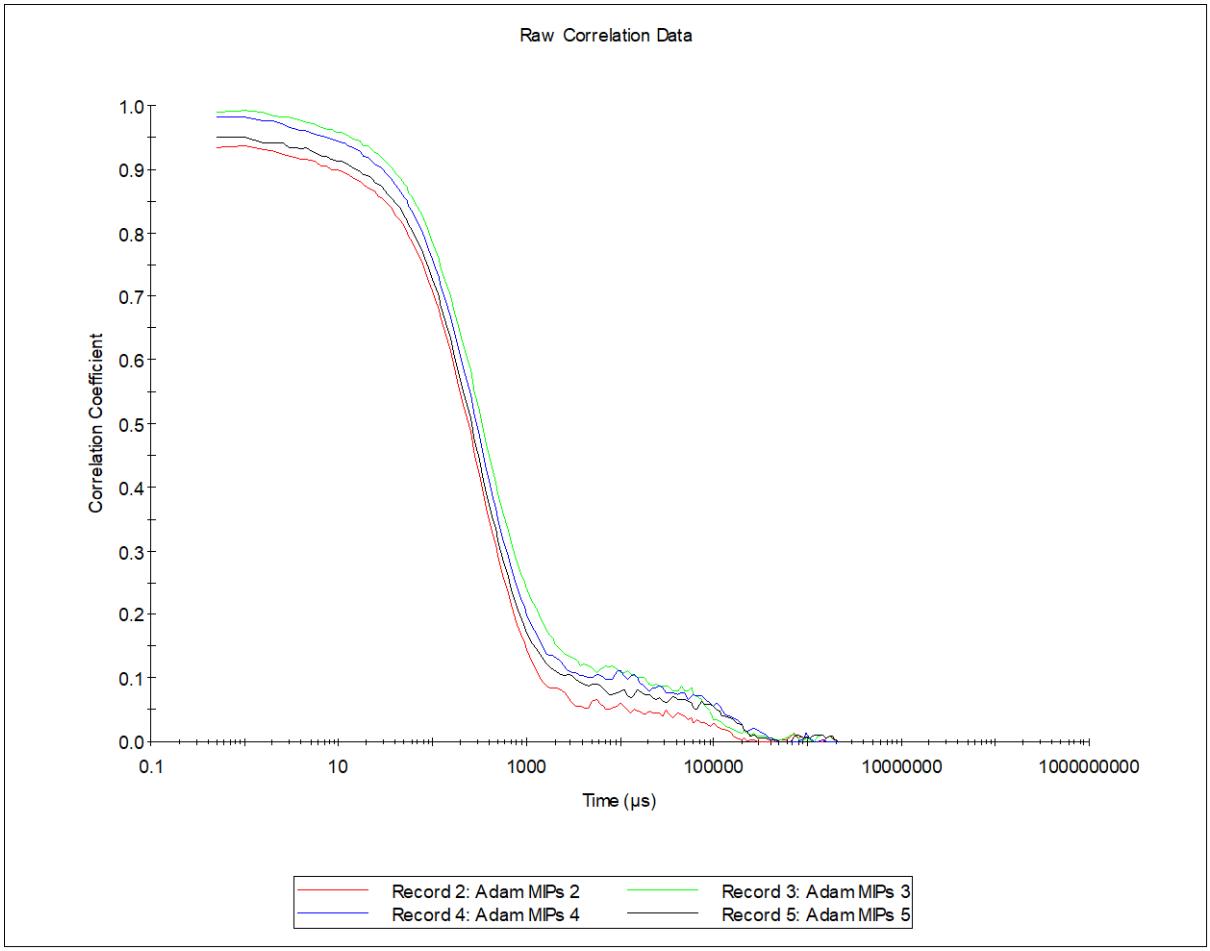

Appendix 2.14. Trehalose Optimisation – 50mg Trehalose – Post-Lyophilisation

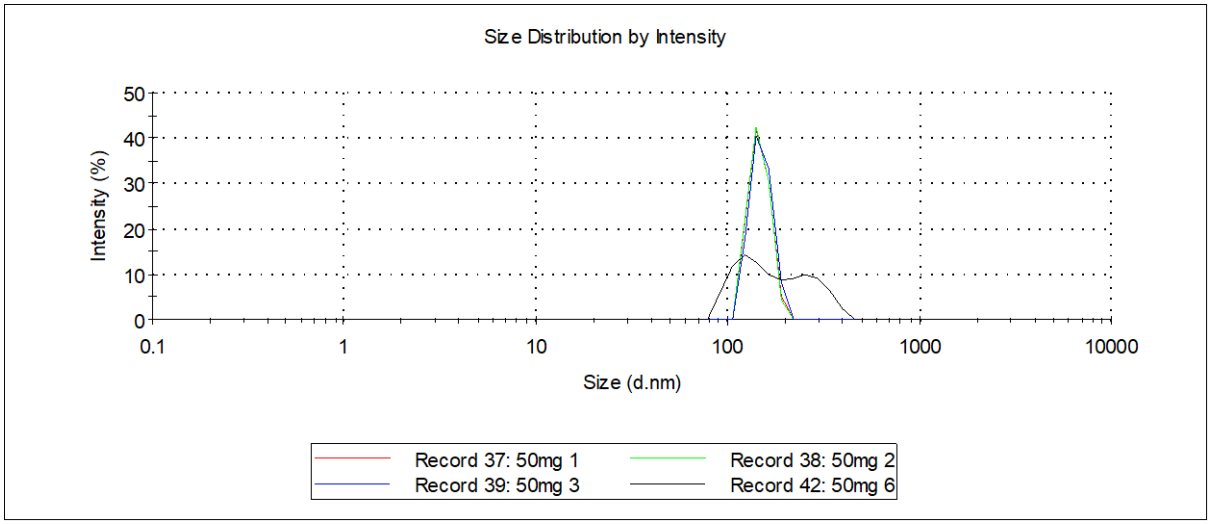

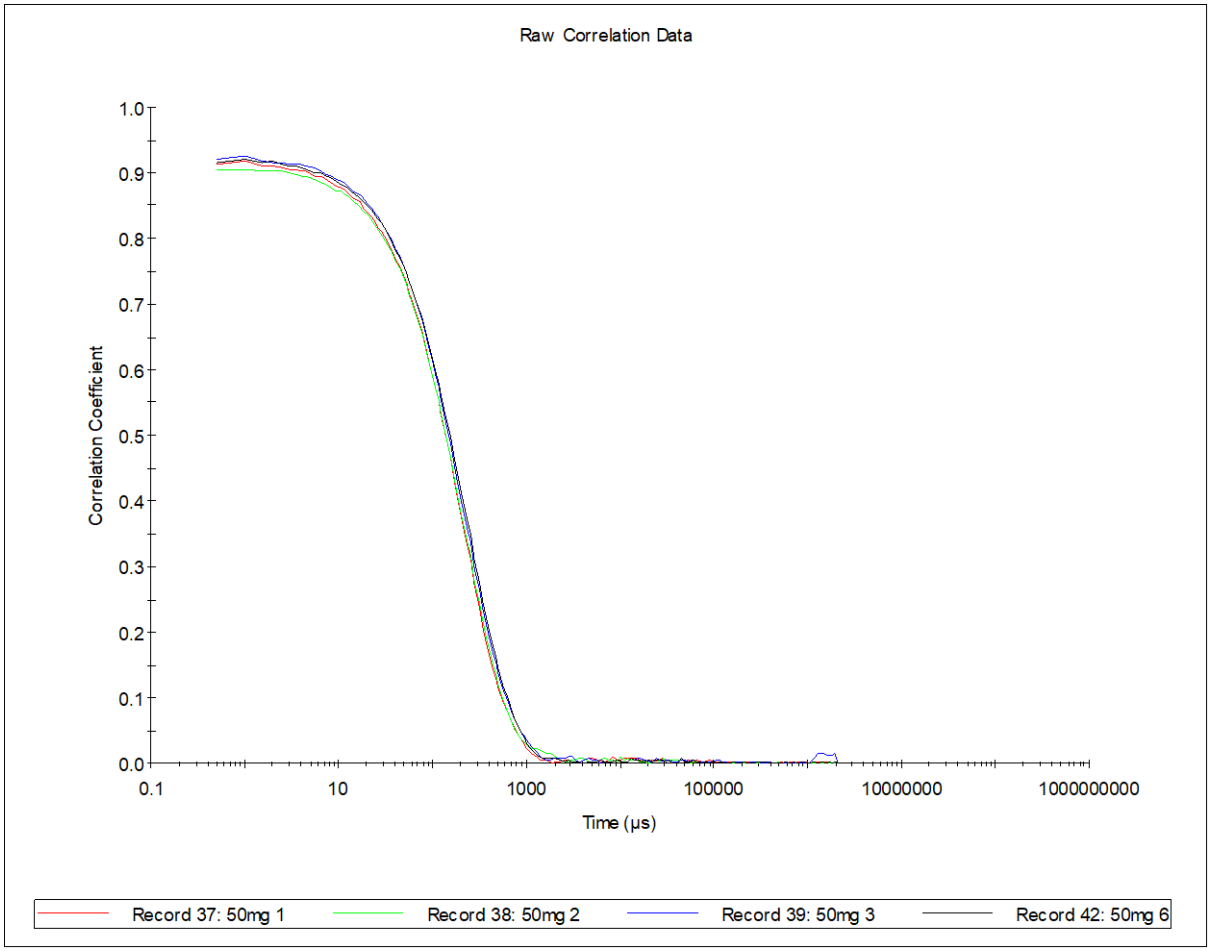

Appendix 2.15. Trehalose Optimisation – 100mg Trehalose – Pre-Lyophilisation

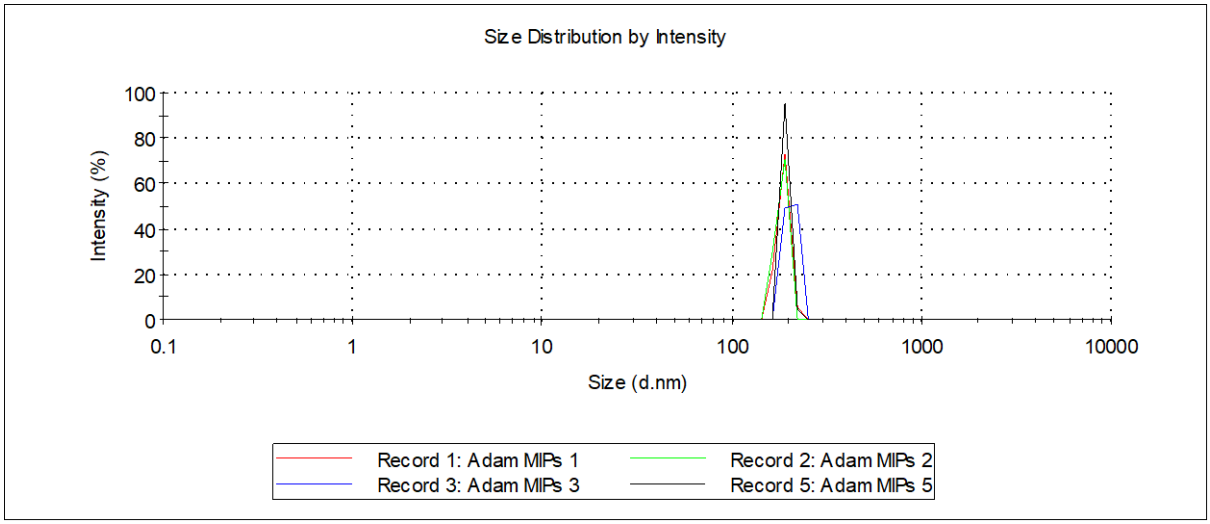

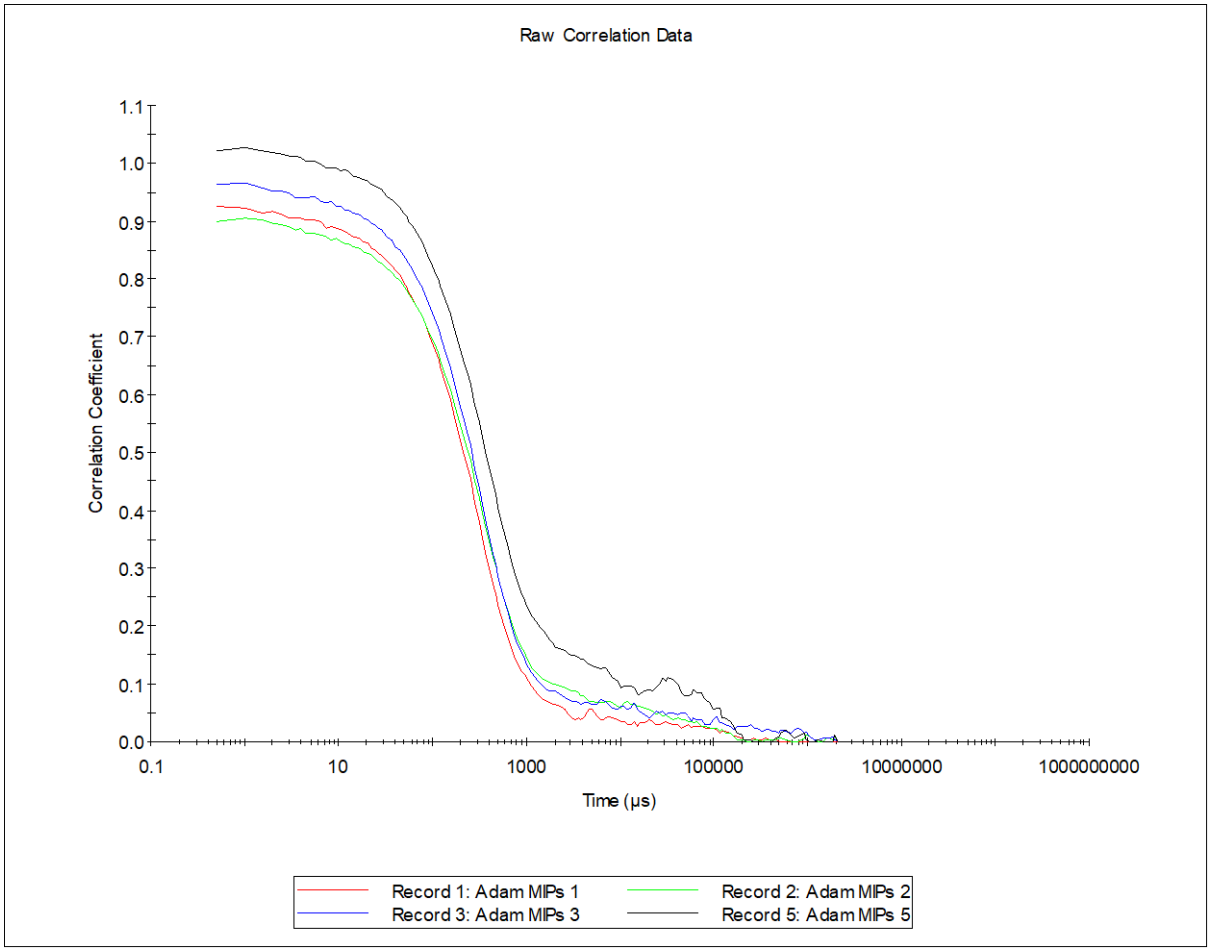

Appendix 2.16. Trehalose Optimisation – 100mg Trehalose – Post-Lyophilisation

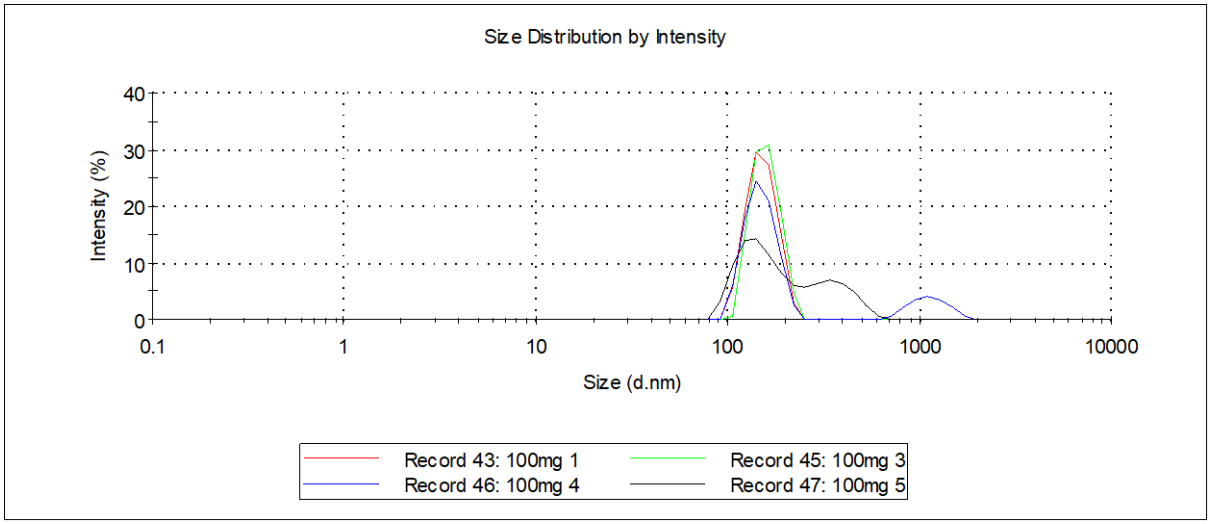

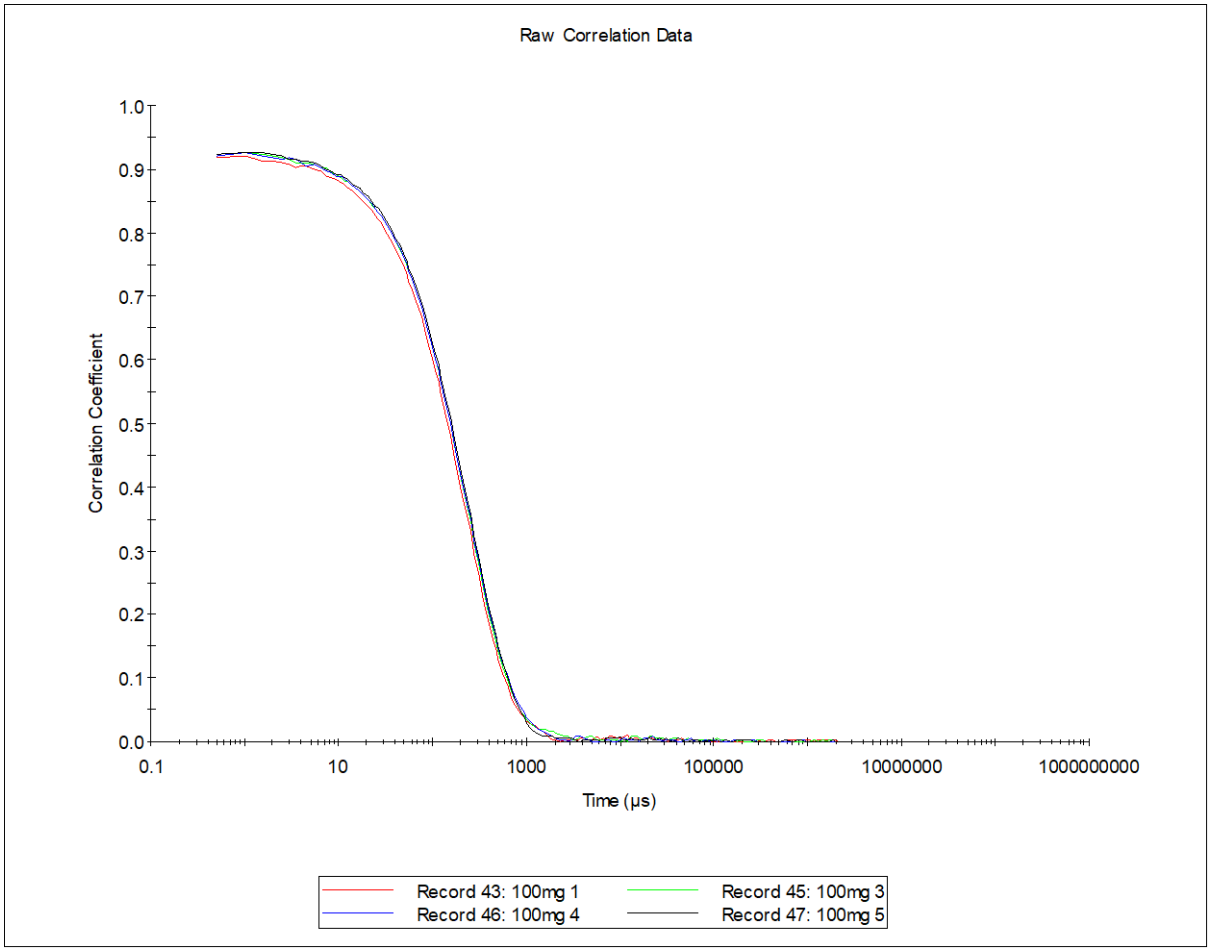

Appendix 3 - Dynamic Light Scattering Data – Nanoparticle post-synthesis sizing with no RNA

Appendix 3.1. - MIP 1 Positive Aqueous Nanoparticles

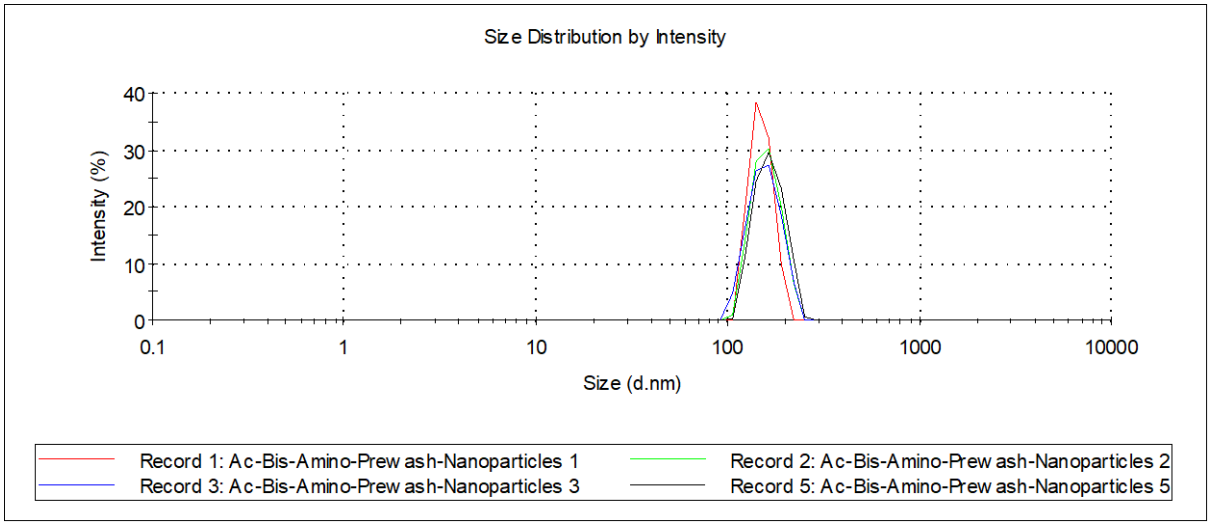

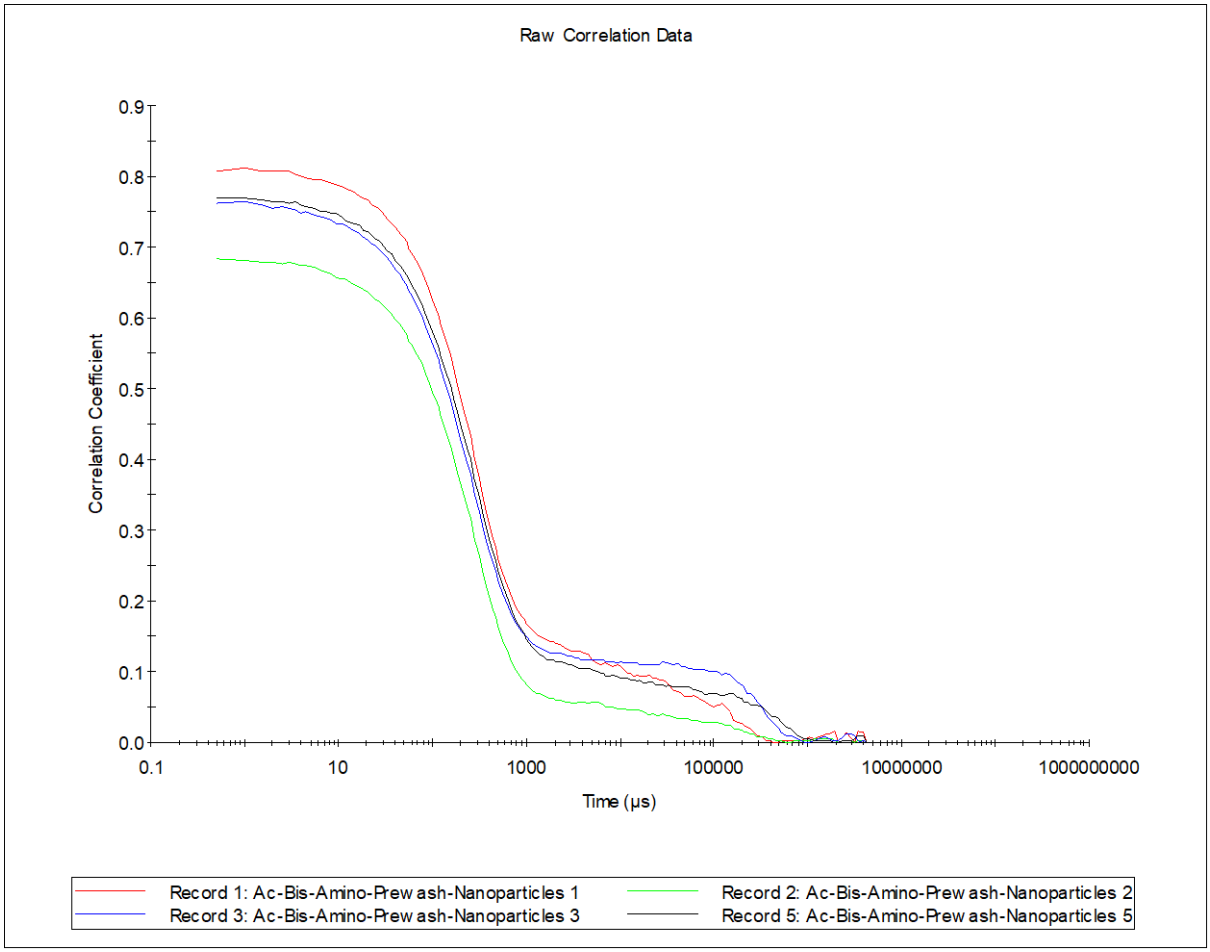

Appendix 3.2. - MIP 2 Negative Aqueous Nanoparticles

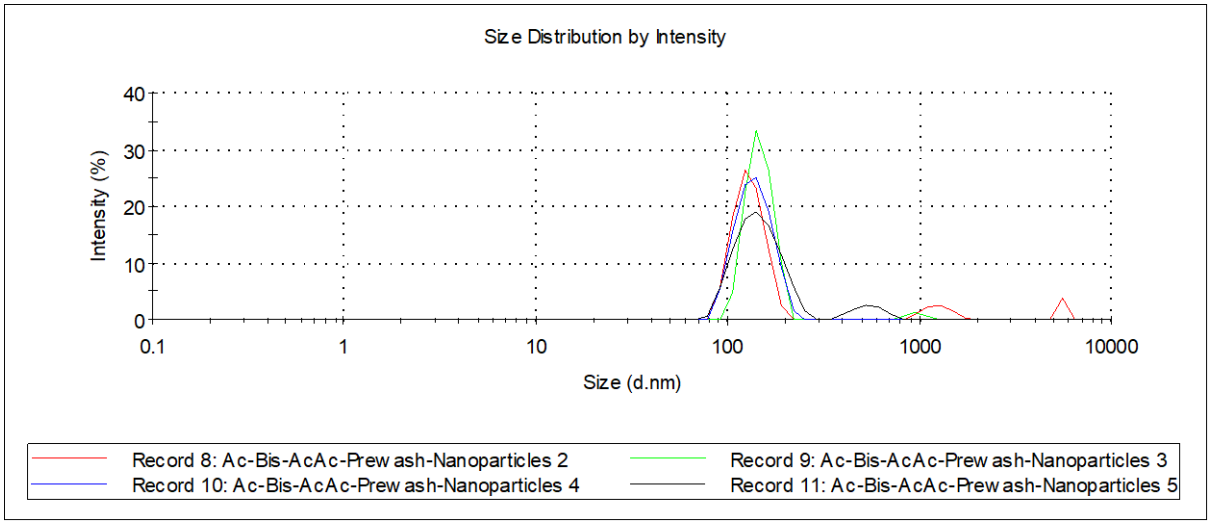

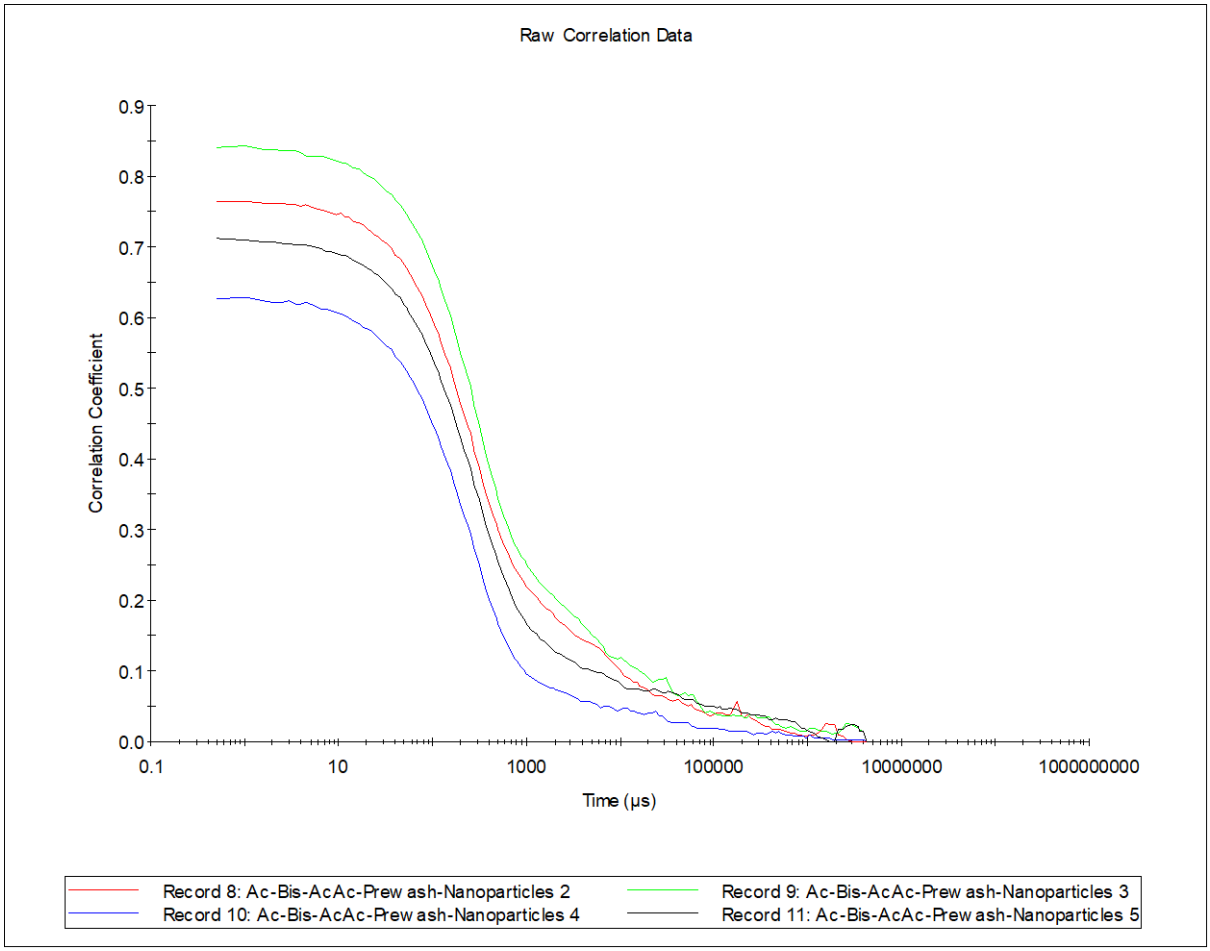

Appendix 3.3. - MIP 3 Neutral Aqueous Nanoparticles

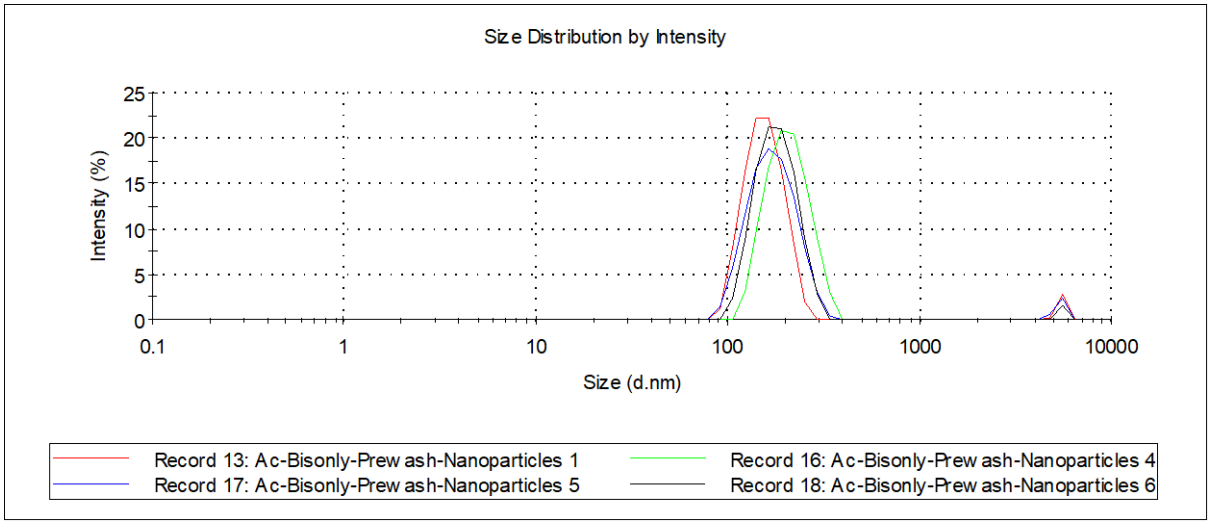

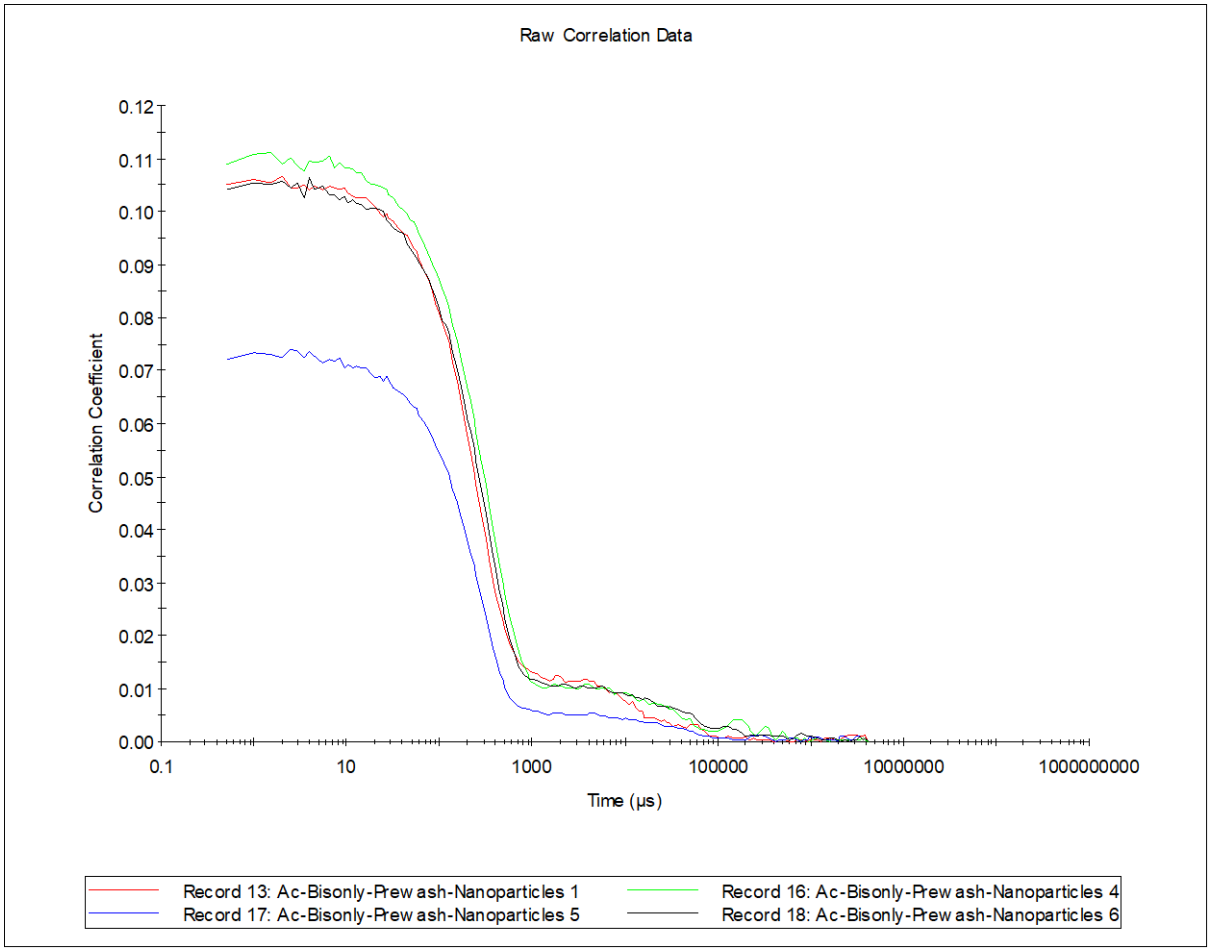

Appendix 3.4. - MIP 4 Positive Organic Nanoparticles

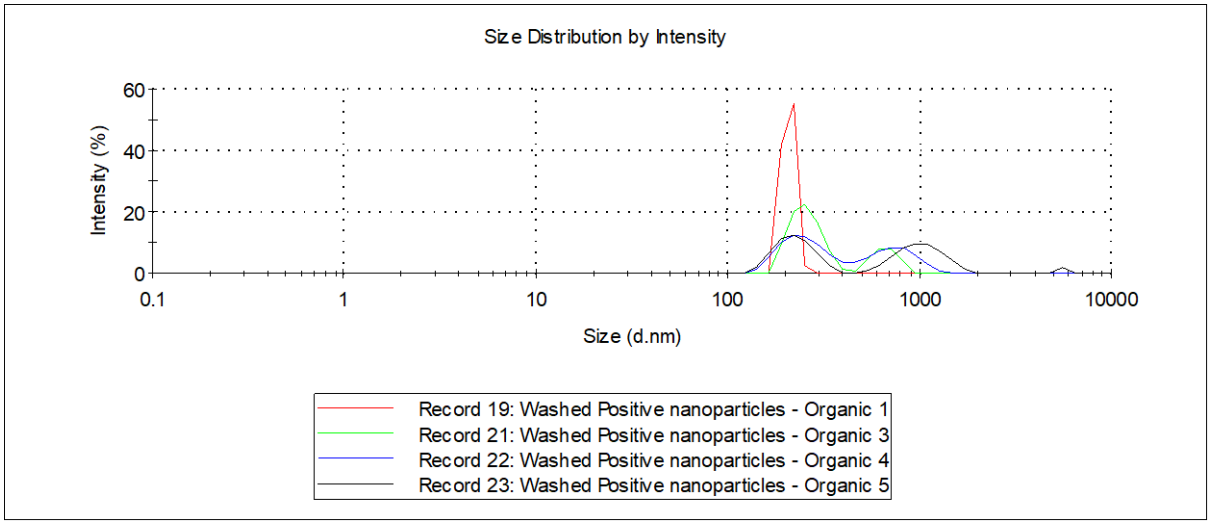

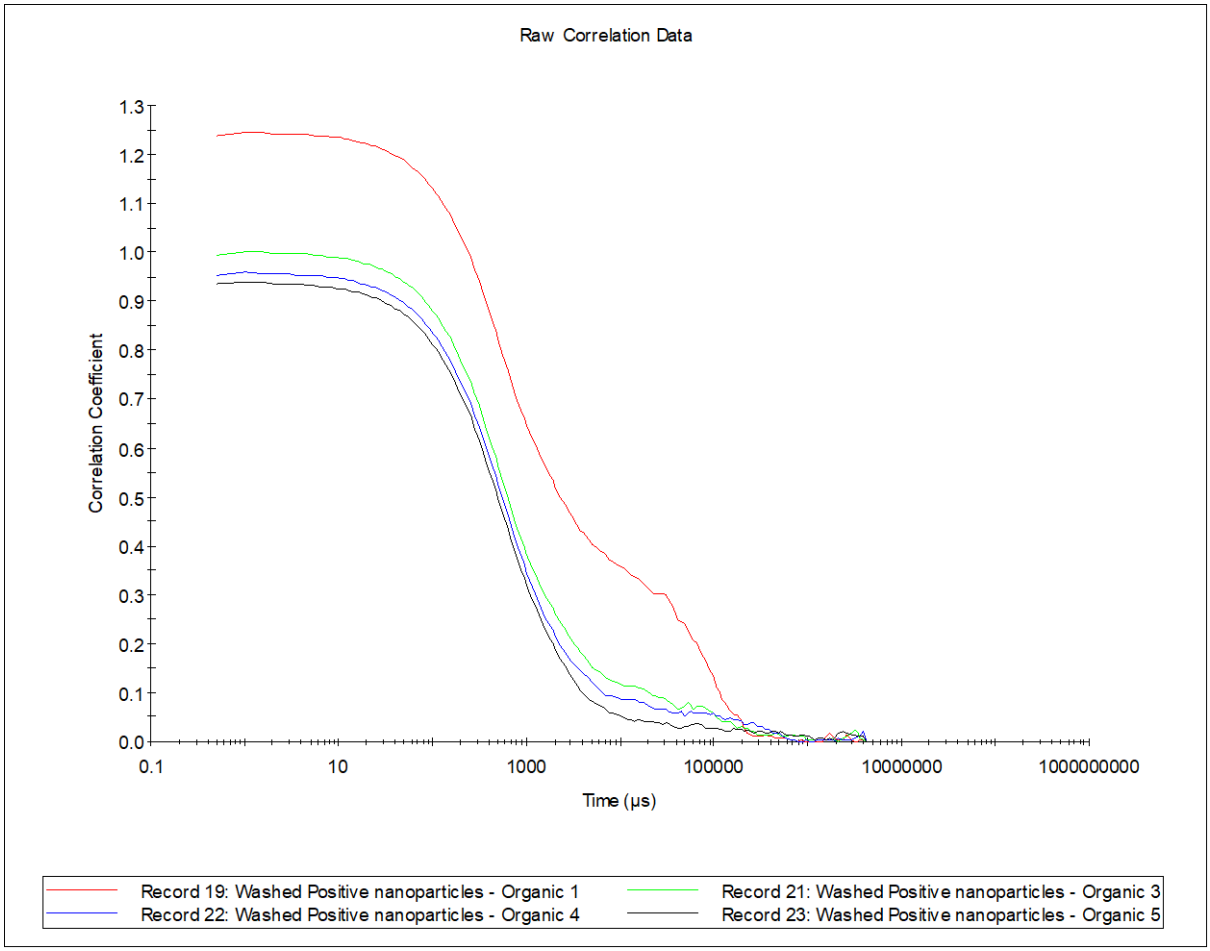

Appendix 3.5. - MIP 5 Negative Organic Nanoparticles

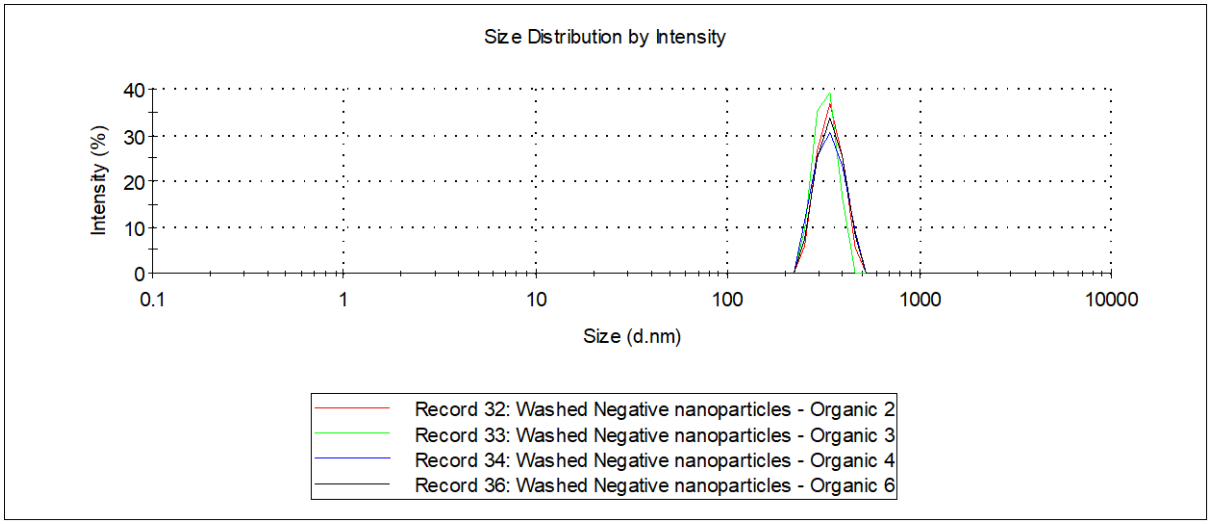

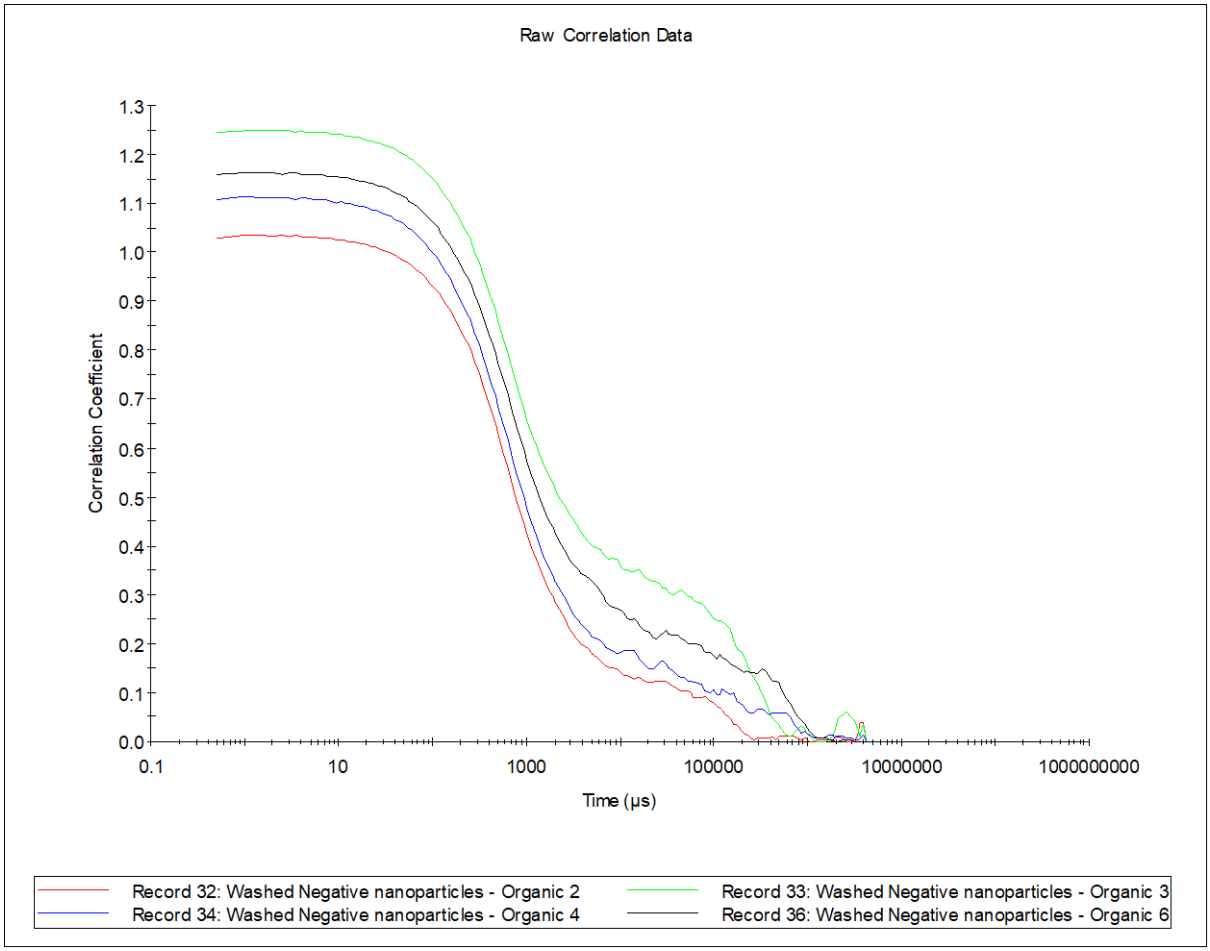

Appendix 3.6. - MIP 6 Neutral Organic Nanoparticles

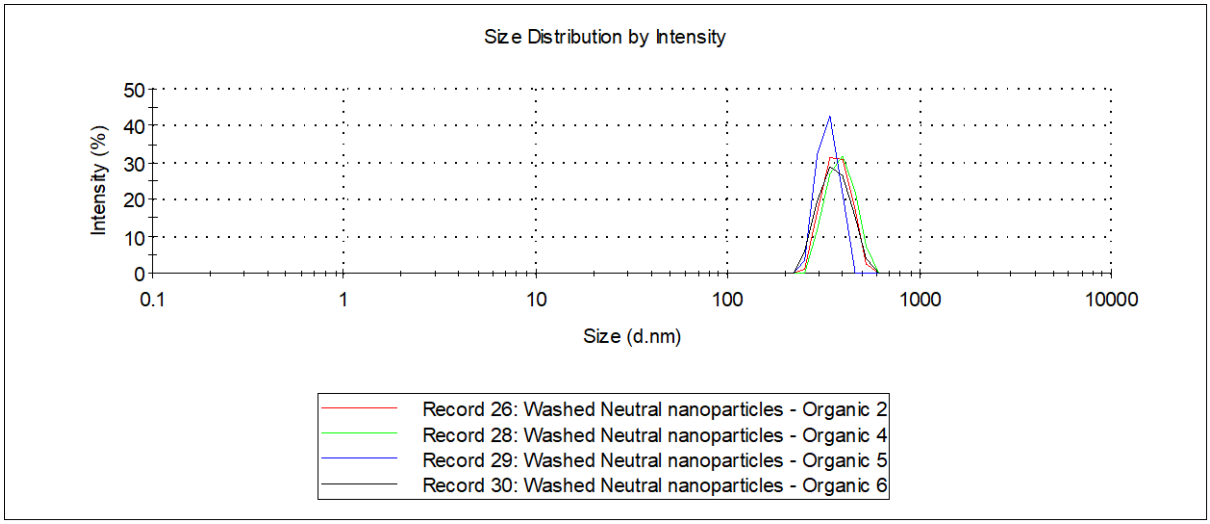

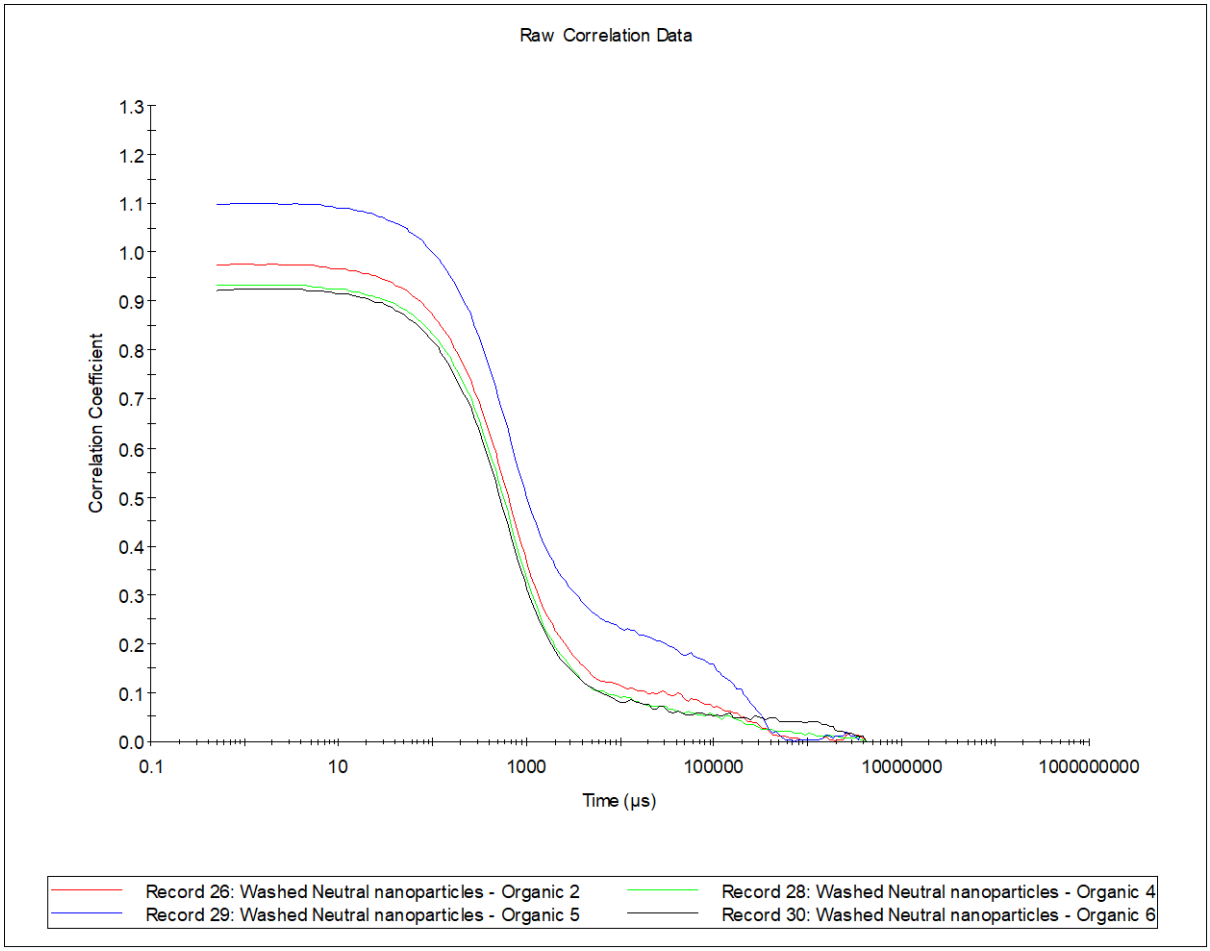

Appendix 4 - Dynamic Light Scattering Data – Nanoparticle-RNA complex size

Appendix 4.1. - MIP 1 nanoparticle-RNA complex

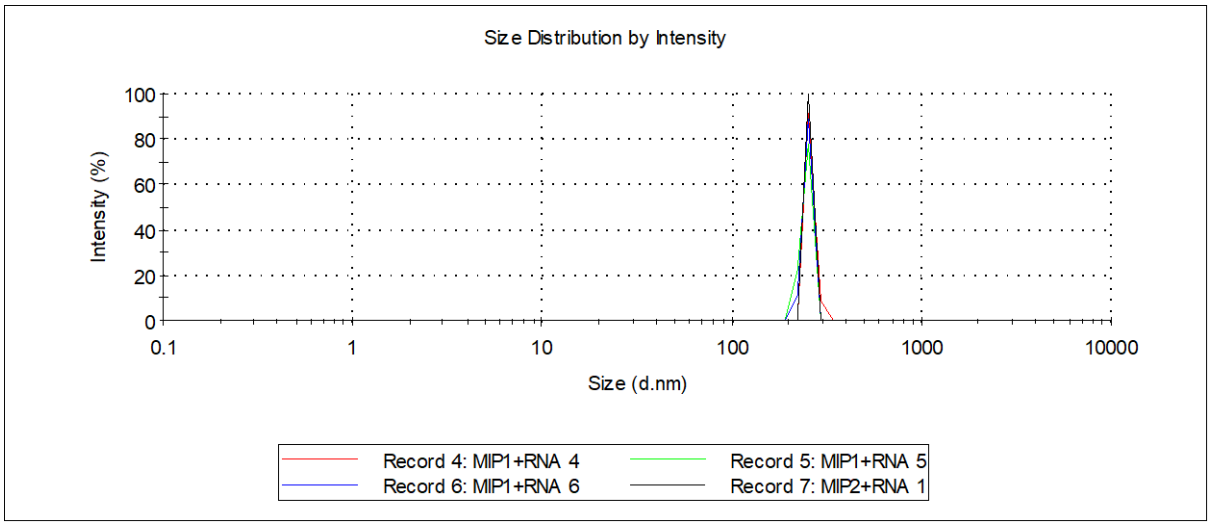

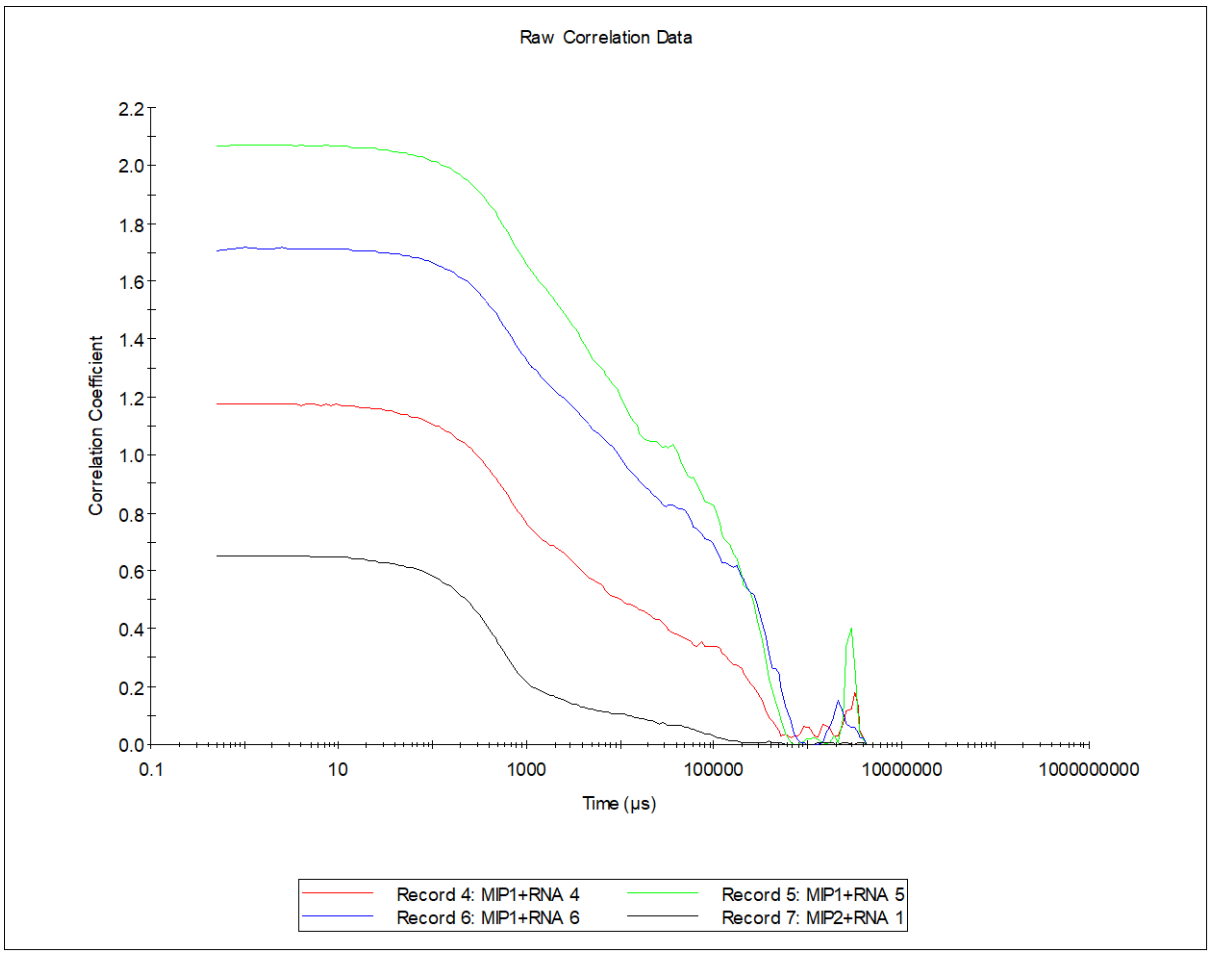

Appendix 4.2. - MIP 2 nanoparticle-RNA complex

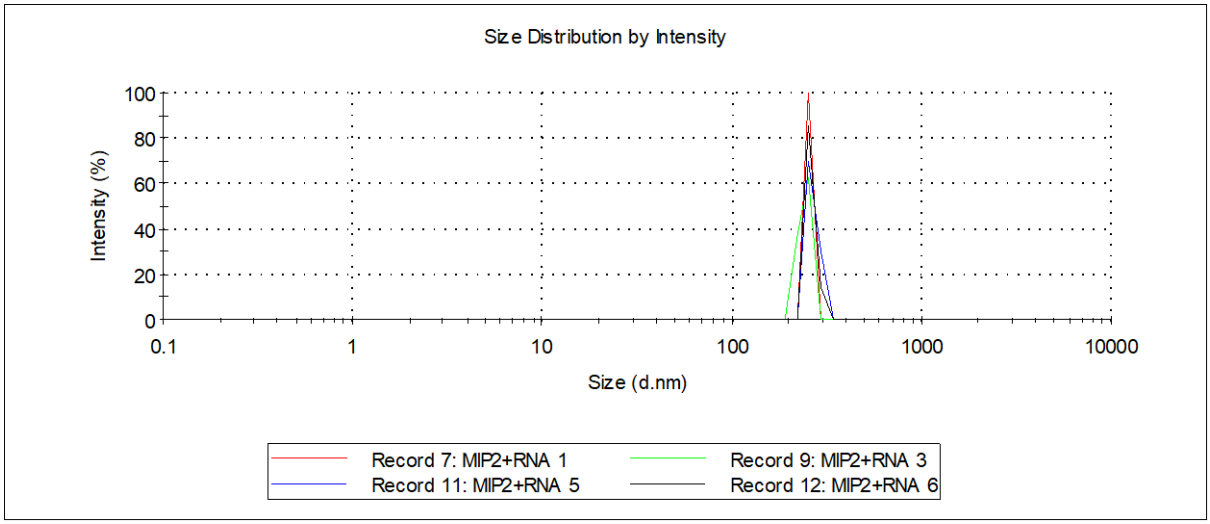

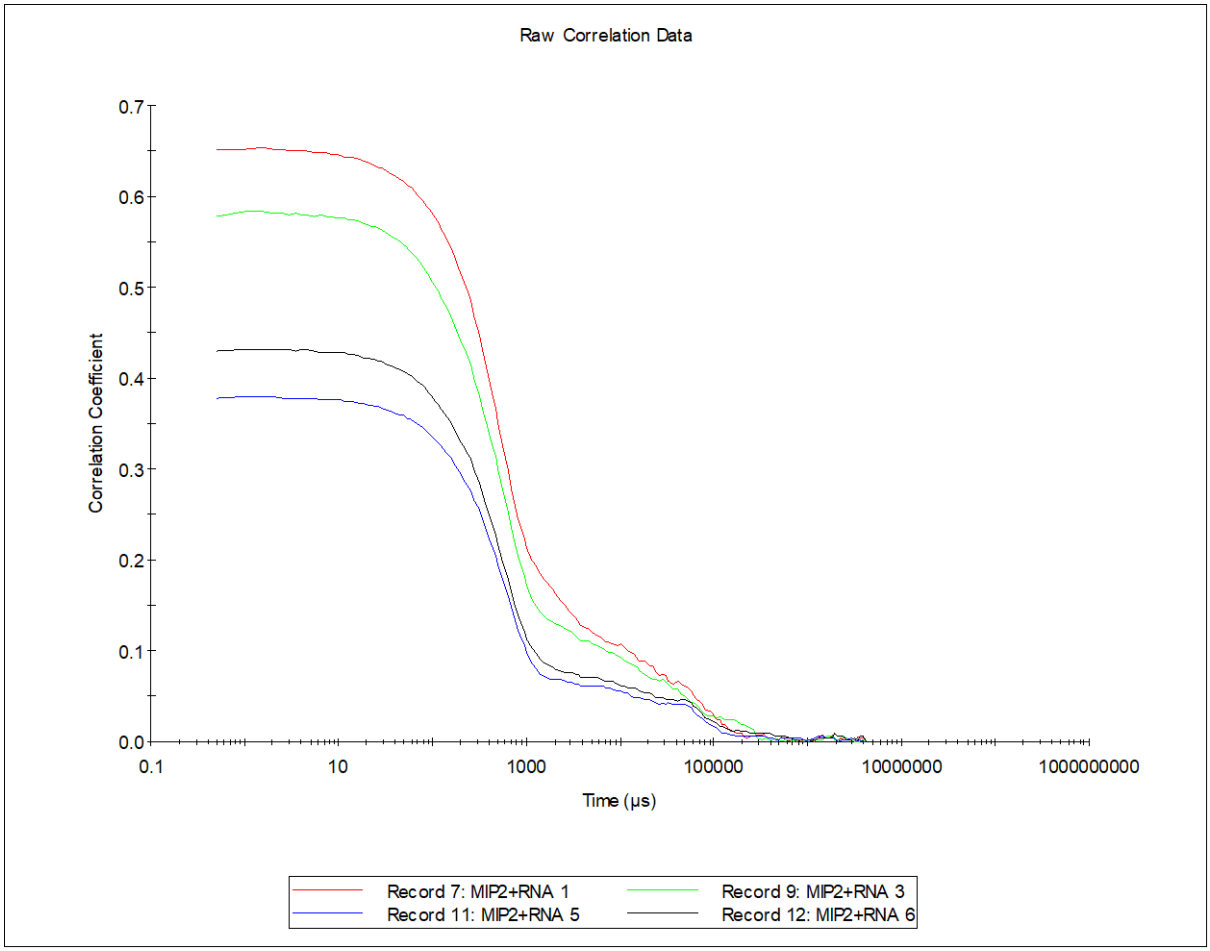

Appendix 4.3. - MIP 3 nanoparticle-RNA complex

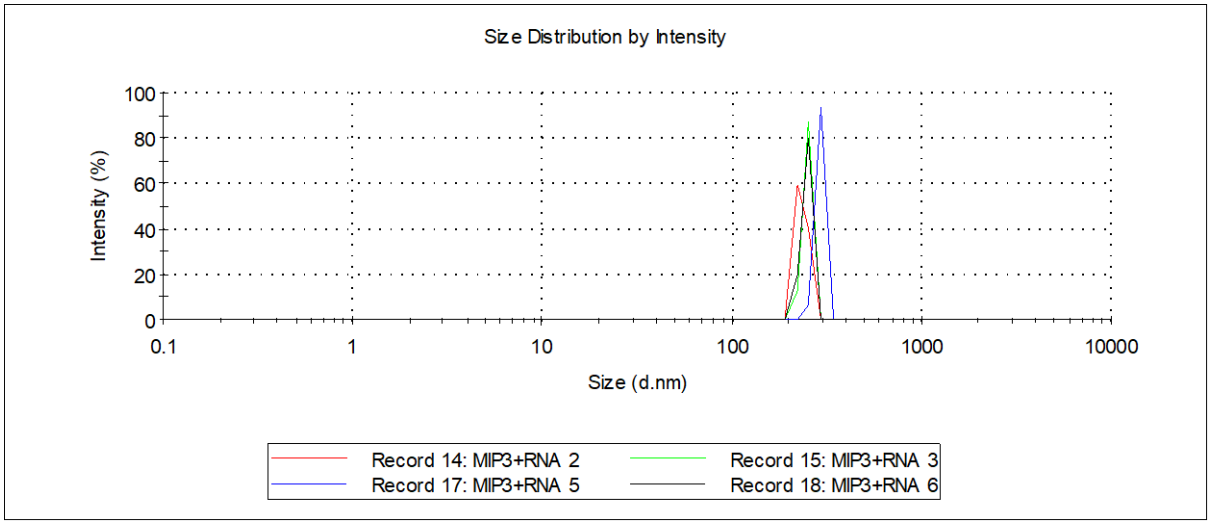

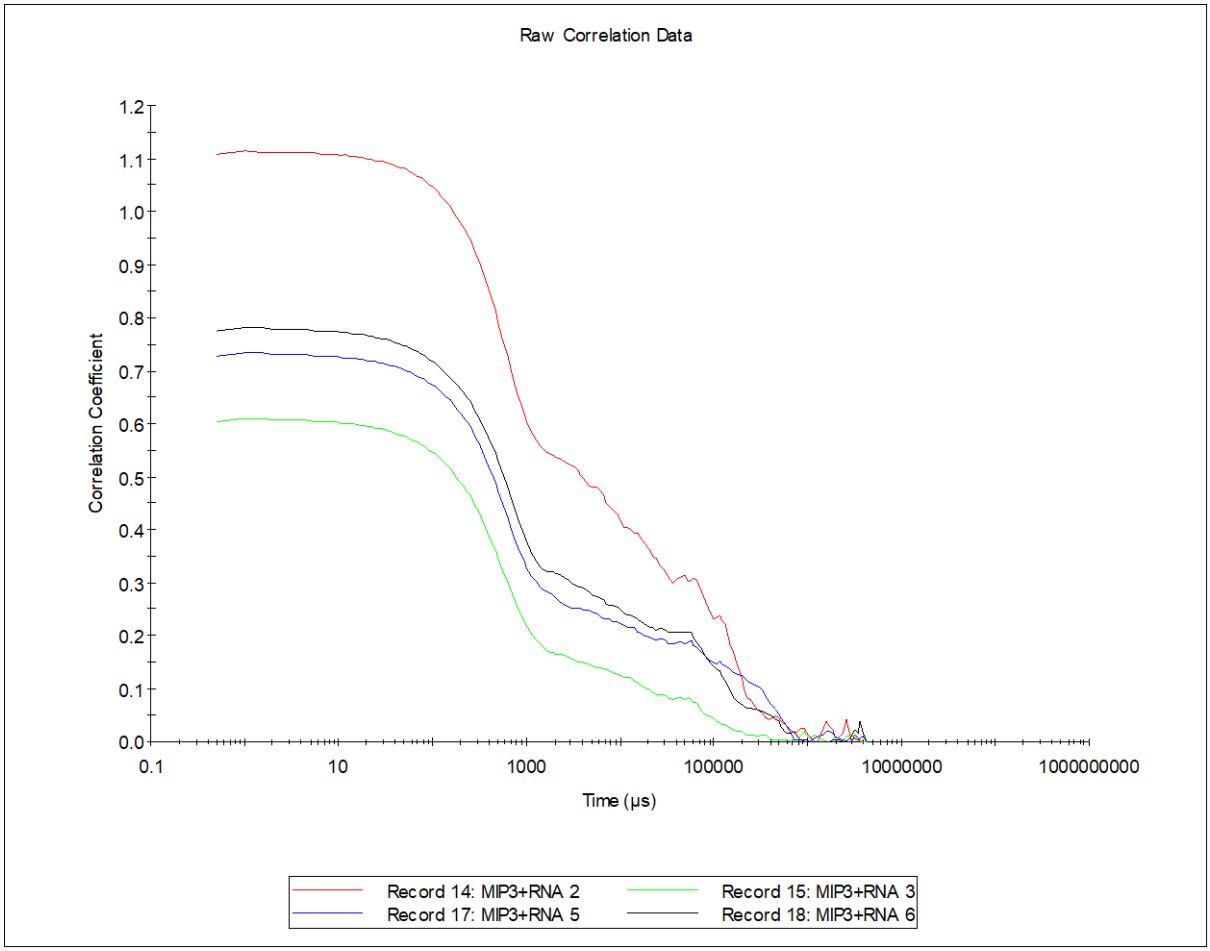

Appendix 4.4. - MIP 4 nanoparticle-RNA complex

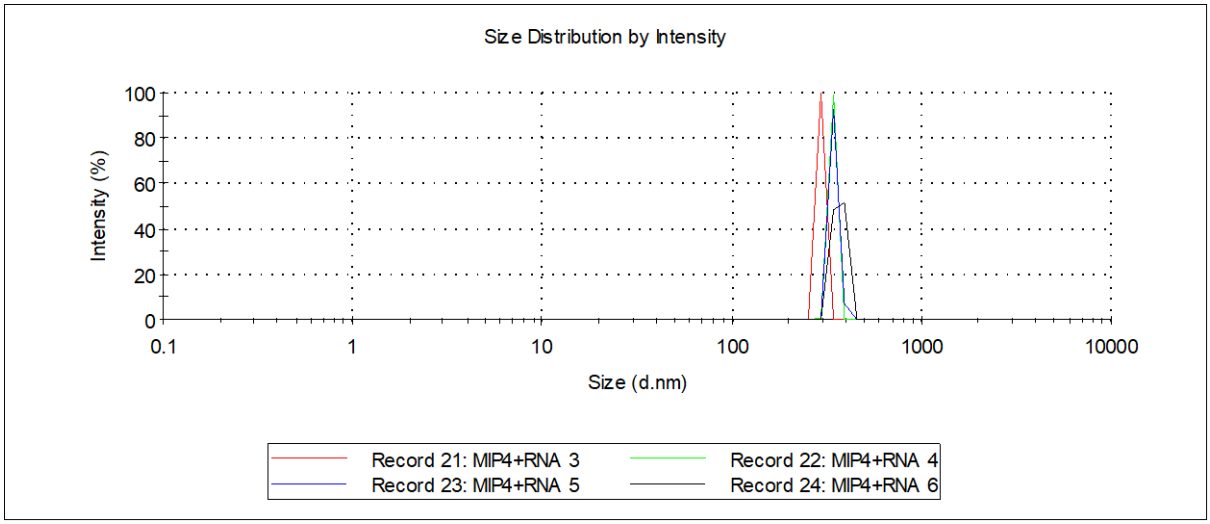

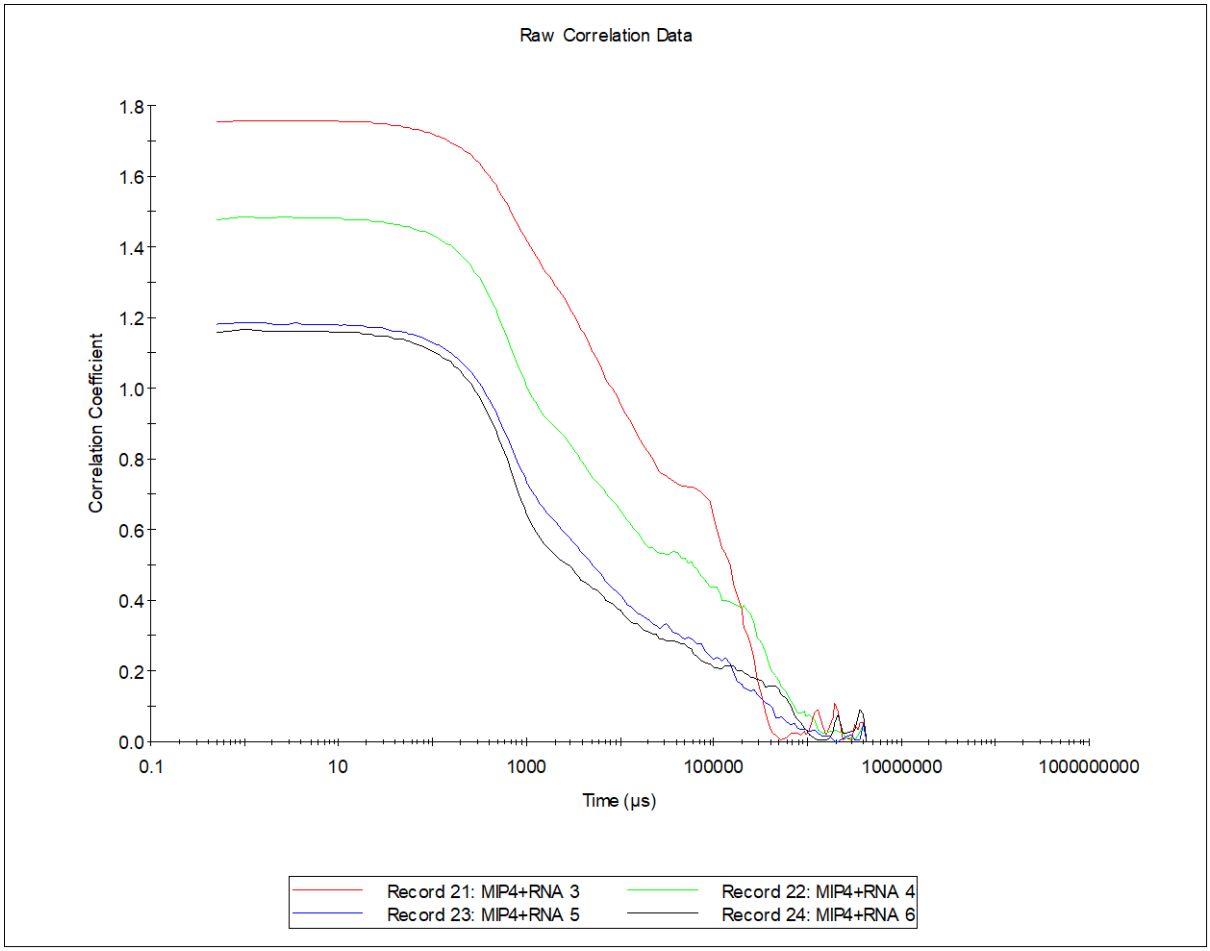

Appendix 4.5. - MIP 5 nanoparticle-RNA complex

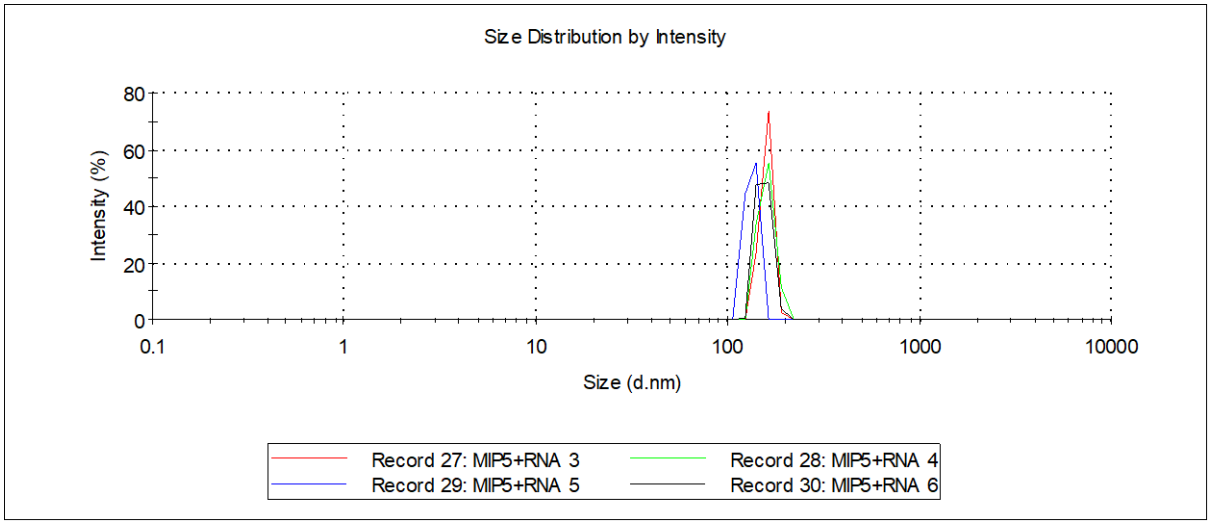

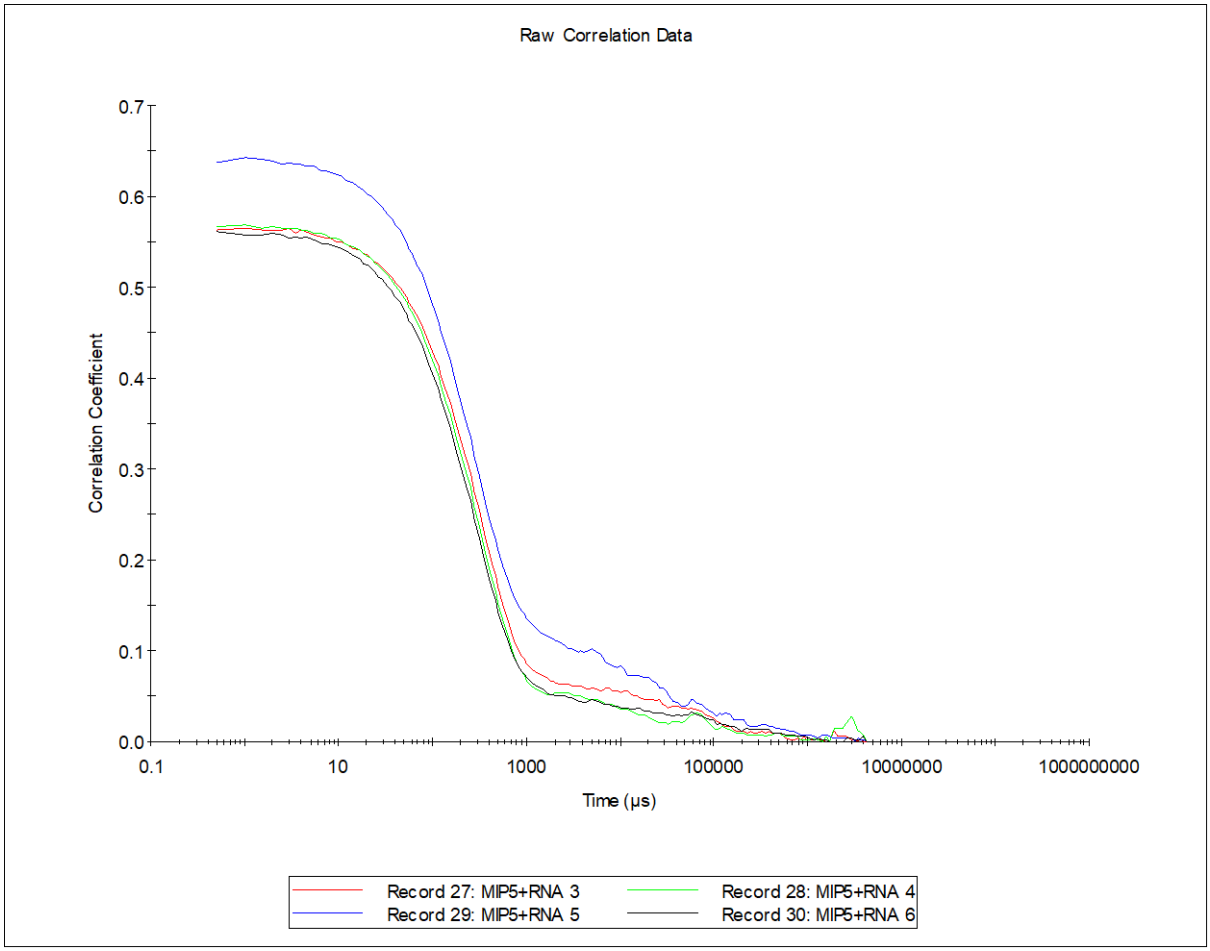

Appendix 4.6. - MIP 6 nanoparticle-RNA complex